ORS 47th International Musculoskeletal Biology Workshop at Sun Valley

Abstract Book

August 6 – 9, 2017

Sun Valley, Idaho

The ORS 47th International Musculoskeletal Biology Workshop appreciates the generous contributions from the following supporters:

Platinum

National Science Foundation
WHERE DISCOVERIES BEGIN

NIH
National Institutes of Health

REGENERON
SCIENCE TO MEDICINE®

Gold

ORTHOFIX®

Silver

AAA American Association of Anatomists

NOVARTIS

OsteoMetrics

Bronze

BIOQUANT®
image analysis corporation

Micro Photonics Inc.
Instrumental to your success

SCANCO MEDICAL

ultragenyx
pharmaceutical

The ORS would like to recognize all participants of the Mentor Program and thank

BIOQUANT®
image analysis corporation

for their generous support.

Mentees	Mentors
Claire Acevedo	Teresita Bellido
Cleo Bonnet	Susan Bloomfield
Beth Bragdon	Alison Boyce
Whitney Bullock	David Burr
Chike Cao	Michael Collins
Erica Clinkenbeard	Matthew Drake
Jesus Delgado-Calle	Aris Economides
Neha Dole	Roger Fielding
Michael Duffy	Christopher Hernandez
Pablo Florenzano	Ed Hsiao
Jaime Fornetti	Christopher Jacobs
Anyonya Guntur	Ivo Kalajzic
Sri Harsha Tella	James Kang
Paula Hernandez	Michaela Kneissel
Mavis Irwin	Nancy Lane
Rachelle Johnson	Ben Leder
Mariana Kersh	Gayle Lester
Anthony Le	Bob Majeska
Mengxi Lv	Gloria Mathews
Maleeha Mashiatulla	Scott Miller
Elsa Mevel	Corey Neu
Michael Mosca	Jeffry Nyman
Zeynep Seref-Ferlengez	Charles O'Brien
Milos Spasic	Munro Peacock
Lance Stechschulte	Hollis Potter
Nicholas Theilen	Makarand Risbud
Trupti Trivedi	Alex Robling
Mustafa Unal	Rick Sumner
Megan Weivoda	Simon Tang
Kelly Wentworth	Marjolein van der Meulen
Biming Wu	Andre van Wijnen
Chaofan Zhang	Felix Wherli

Schedule-At-A-Glance

Saturday, August 5, 2017

3:00 PM – 5:30 PM	Registration Open	Continental Promenade

7:00 PM – 10:00 PM	Welcome Reception *Sponsored by* Micro Photonics Inc. *Instrumental to your success*	Dr. Burr's Lodge Apartment (inquire at the Lodge Reception Desk)

Sunday, August 6, 2017 — Continental Room

General Contributions provided to the workshop by:	National Science Foundation WHERE DISCOVERIES BEGIN; NIH National Institutes of Health; NOVARTIS; ORTHOFIX; REGENERON SCIENCE TO MEDICINE

7:00 AM – 8:00 AM	**Breakfast & Registration**

8:00 AM - 9:15 AM	**Welcome & The RIB Award/Plenary Session** Rib Awardee: Michaela Kneissel, PhD *(Novartis)* Targeting Musculoskeletal Disease to Restore Mobility in Disease and Old Age *Sponsored by* AAA American Association of Anatomists

9:30 AM - 10:00 AM	**Blue Ribbon Sun Valley Posters** Chair: Teresita Bellido, PhD *(Indiana University)*
	COL11A1 Expression is Required for Normal Chondrocyte Behavior during Skeletal Development Jonathon Reeck, PhD *(Boise State University)*
	Chondro-Protective Function of Statin Is Related to the Inhibition of Small GTPase Activities Mengxi Lv *(University of Delaware)*
	Fatty Acid Binding Protein 4 (FABP4) As A Biomarker for Knee Osteoarthritis Chaofan Zhang, MD, MS *(The University of Hong Kong)*
	Histopathological Analysis of Healing Responses to a Novel Tendon Transfer Surgery in a Chicken Model Anthony Le, BS *(Oregon State University)*
	RON Kinase: A New Target for Treatment of Cancer-induced Bone Destruction and Osteoporosis Jaime Fornetti, PhD *(Huntsman Cancer Institute)*

10:15 AM - 12:00 PM	**Major Methodologies: The Essentials of Finite Element Analysis for Basic and Clinical Studies** Chair: Christopher Jacobs, PhD *(Columbia University)*
	Introduction: The Pros and Cons of FEA Christopher Jacobs, PhD *(Columbia University)*
	Cell Mechanics: The Role of Simulation Christopher Jacobs, PhD *(Columbia University)*
	Finite Element Analysis for Clinical Assessment of Whole-Bone Strength David Kopperdahl, PhD *(O.N. Diagnostics, LLC)*

2:00 PM – 4:00 PM	Volleyball *Sponsored by* ultragenyx pharmaceutical	Volleyball Court

7:30 PM - 8:00 PM	**Blue Ribbon Sun Valley Posters** Chair: Alexander Robling, PhD *(Indiana University)*
	Prx-1 Embryonic Specification Is Retained in a Postnatal Regenerative Stem Cell Population that Gives Rise to Skeletal, Fat, and Vascular Tissues Beth Bragdon, PhD *(Boston University School of Medicine)*
	Improved Fracture Risk Assessment via Bound/Pore Water MRI Jeffry Nyman, PhD *(Vanderbilt University Medical Center)*
	Anabolic PTH Signaling Activates the Canonical Notch Pathway in Osteocytes to Restrain Bone Resorption and Facilitate Bone Gain Jesus Delgado-Calle, PhD *(Indiana University School of Medicine)*
	Characterization of Fibroblast Growth Factor 23 (FGF23) Levels in Patients with Fanconi Syndrome due to Nephropathic Cystinosis Pablo Florenzano, MD *(NIDCR, National Institutes of Health)*
	PPARϒ and PPARα Regulate Osteocyte Activity by Controlling Expression of Sclerostin and DKK1 Proteins Lance Stechschulte, PhD *(University of Toledo)*

8:00 PM - 10:00 PM	**Poster Session with wine and cheese**
	Alice L. Jee Award Winners
	Prx-1 Embryonic Specification Is Retained in a Postnatal Regenerative Stem Cell Population that Gives Rise to Skeletal, Fat, and Vascular Tissues Beth Bragdon, PhD *(Boston University School of Medicine)*
	Anabolic PTH Signaling Activates the Canonical Notch Pathway in Osteocytes to Restrain Bone Resorption and Facilitate Bone Gain Jesus Delgado-Calle, PhD *(Indiana University School of Medicine)*
	Characterization of Fibroblast Growth Factor 23 (FGF23) Levels in Patients with Fanconi Syndrome due to Nephropathic Cystinosis Pablo Florenzano, MD *(NIDCR, National Institutes of Health)*
	RON Kinase: A New Target for Treatment of Cancer-induced Bone Destruction and Osteoporosis Jaime Fornetti, PhD *(Huntsman Cancer Institute)*
	Deletion of CaMKK2 in Osteocytes Elicits Gender-Specific Effects on Bone Mass Mavis Irwin, PhD *(Indiana University / Purdue University)*
	Linking Cortical Bone Mechanics, Structure and Remodeling in the Fibula Mariana Kersh, PhD *(University of Illinois at Urbana-Champaign)*
	Chondro-Protective Function of Statin Is Related to the Inhibition of Small GTPase Activities Mengxi Lv *(University of Delaware)*
	Early Subchondral Bone and Articular Cartilage Compositional Changes in the Medial Compartment after DMM Surgery Quantified by μCT Maleeha Mashiatulla, PhD *(Rush University Medical Center)*
	Inhibition of CaMKK2 Attenuates Subchondral Bone Remodeling in Post-traumatic Osteoarthritis Model Elsa Mevel, PhD *(Indiana University School of Medicine)*
	Promoting Load-induced Bone Formation by Manipulating Primary Cilia Mechanobiology Milos Spasic, MS *(Columbia University)*

8:00 PM - 10:00 PM	PPARϒ and PPARα Regulate Osteocyte Activity by Controlling Expression of Sclerostin and DKK1 Proteins Lance Stechschulte, PhD *(University of Toledo)*
	Mechanism of Exercise in Preventing Skeletal Muscle Atrophy Nicholas Theilen, MS (*University of Louisville School of Medicine)*
	Raman Spectroscopic Parameters Correlates with the Fracture Toughness of Human Cortical Bone Mustafa Unal, PhD *(Vanderbilt University Medical Center)*
	Fatty Acid Binding Protein 4 (FABP4) As A Biomarker for Knee Osteoarthritis Chaofan Zhang, MD, MS *(The University of Hong Kong)*
	Osteoarthritis Award Winner
	Repurposing Glutamate Receptor Antagonists for the Prevention of Post-traumatic Osteoarthritis Cleo Bonnet, PhD *(Cardiff University)*
	Charles H. Turner Young Investigator Bone Research Award Winner
	Impact of High Bone Turnover on Skeletal Muscle Weakness in a Mouse Model of Camurati-Engelmann Disease Trupti Trivedi *(Indiana University)*
	Submitted Poster Presenters
	Positive Adaptations in Cancellous Microarchitecture with Moderate Iron Overload, Even in Hindlimb Unloaded Mice, Are Associated with Elevated Serum Hepcidin Susan Bloomfield, PhD *(Texas A&M University)*
	Point Mutation in Lrp4 Sost Binding Pocket Increases Bone Mass in Mice Whitney Bullock, BS *(Indiana University)*
	Actin Organization and Response to Fluid Flow are Influenced by the Osteocyte Primary Cilium Michael Duffy, MPh (*Columbia University)*
	TGFβ Regulation of Osteocytic Perilacunar Remodeling is Crucial for Maintaining Bone Quality Neha Dole, PhD *(University of California San Francisco)*
	Severe Burn-Induced Inflammation and Remodeling of Achilles Tendon in a Rat Model Paula Hernandez, PhD *(University of Texas Southwestern)*
	The Expansion of Heterotopic Bone in Fibrodysplasia Ossificans Progressiva is Activin A-Dependent Lily Huang, MS *(Regeneron)*
	Trends in the Theory that Inflammation Plays a Causal Role in Tendon Disease: A Systematic Review and Quantitative Analysis of Published Mechanistic Reviews Michael Mosca, MSc *(Columbia University)*
	Mesenchymal Stem Cells Differentiation into Nucleus Pulposus-Like Cells Based On the New Phenotype of Young Healthy Nucleus Pulposus Cells Arjun Sinkemani *(Southeast University School of Medicine)*
	Cell-Free Biomimetic Scaffolds Lead to Non-Unions in Critical Sized Defect Repair as Compared to Identically Structured Stem Cell Infiltrated Scaffolds that Induce Rapid Bone Growth John Szivek, PhD *(University of Arizona)*
	Changes in Intervertebral Disc Structure and Morphology in Back-healthy Humans During Standing Simon Tang, PhD *(Washington University in Saint Louis)*
	Scoliosis in Fibrous Dysplasia/McCune-Albright Syndrome Sri Harsha Tella, MD *(National Institute of Health)*
	The Biphasic Response to Phosphate During Chondrogenic Differentiation Biming Wu, MS *(University of Michigan)*
	LaminA/C Knock Down Enhances Adipogenesis but does not Eliminate Mechanical Response in MSCs Gunes Uzer, PhD *(Boise State University)*

Monday, August 7, 2017 — Continental Room

7:00 AM – 8:00 AM	Breakfast & Registration

8:00 AM – 9:00 AM	ASBMR/Harold M. Frost Young Investigator Award Presentations Chair: Teresita Bellido, PhD *(Indiana University)*
	Increased Ca2+ Signaling Through Altered CaV1.2 L-type Ca2+ Channel Activity Promotes Bone Formation and Prevents Estrogen Deficiency-induced Bone Loss Chike Cao, PhD *(Duke University Medical Center)*
	A Human Induced Pluripotent Stem Cell Model for Elucidating Cell Fate Defects in McCune-Albright Syndrome Kelly Wentworth, MD *(University of California San Francisco)*
	Identification of Osteoclast-Derived Factors And Target Pathways that Couple Bone Resorption to Bone Formation Megan Weivoda, PhD *(Mayo Clinic)*

9:15 AM - 12:00 PM	Problems in Endocrinology: Rare Bone Diseases - Fibrous Dysplasia Chair: Michael Collins, MD *(NIDCR, NIH)*
	Overview of Fibrous Dysplasia. A Complex Mosaic of Dease of Activated Gαs Michael Collins, MD *(NIDCR, NIH)*
	Clinical Perspectives of Fibrous Dysplasia/McCune-Albright Syndrome Alison Boyce, MD *(NIDCR, NIH)*
	Challenges and Approcahes for Fibrous Dysplasia Research Ed Hsiao, MD, PhD *(University of California San Francisco)*

1:30 PM - 4:00 PM	Career Development Workshop: Research Funding Chair: Marjolein van der Meulen, PhD *(Cornell University)* *Sponsored by* SCANCO MEDICAL

7:30 PM - 9:30 PM	New Progress in Imaging Musculoskeletal Tissues Chair: Felix Wehrli, PHD *(University of Pennsylvania)*
	Quantitative MRI of Cortical and Trabecular Bone Felix Wehrli, PhD *(University of Pennsylvania)*
	Using MRI to Detect Cartilage Damage Corey Neu, PhD *(University of Colorado)*
	In Vivo MRI Hollis Potter, MD *(Hospital for Special Surgery)*

Tuesday, August 8, 2017 — Continental Room

7:00 AM – 8:00 AM	Breakfast & Registration
7:00 AM – 7:30 AM	Industry Breakfast Session presented by: REGENERON SCIENCE TO MEDICINE
	Lessons from Rare Genetic Diseases: From Novel Biology to Drug Discovery *Presenter: Aris N. Economides, PhD*

8:00 AM – 9:00 AM	**ASBMR/Harold M. Frost Young Investigator Award Presentations** Chair: Alexander Robling, PhD *(Indiana University)*
	TGFβ Regulation of Osteocytic Perilacunar Remodeling is Crucial Neha Dole, PhD *(University of California San Francisco)*
	Role of Panx1-P2X7R Signaling in Anabolic Bone Response of Type 1 Diabetic Mice Zeynep Seref-Ferlengez, PhD *(Albert Einstein College of Medicine)*
	Overexpression of MitoNEET in Osteoblasts Leads to Impaired Bone Mass and Energy Metabolism in Mice Anyonya Guntur, PhD *(Maine Medical Center Research Institute)*

9:15 AM - 12:00 PM	**Using Genetically Engineered Animal Models to Solve Problems in Musculoskeletal Disease: State of the Art and Application** Chair: Charles O'Brien, PhD *(University of Arkansas)*
	Validating Cre Driver Models: Where are we Cutting and How Do We Know? Ivo Kalajzic, MD, PhD *(University of Connecticut Health Center)*
	How Can We Improve CRE Driver Models? Charles O'Brien, PhD *(University of Arkansas)*
	Modeling Human Disease in Mice Aris Economides, PhD *(Regeneron Pharmaceuticals, NY)*

4:30 PM – 8:00 PM	Banquet & Symphony	Lodge Terrace

Wednesday, August 9, 2017 — Continental Room

7:00 AM – 8:00 AM	Breakfast & Registration

8:00 AM - 9:00 AM	**ASBMR/Harold M. Frost Young Investigator Award Presentations** Chair: David Burr, PhD *(Indiana University)*
	The Connection Between Fatigue and Fragility Fracture In Bone Claire Acevedo, PhD *(University of California San Francisco)*
	Regulation of Leukemia Inhibitory Factor Receptor (LIFR) in Bone Disseminated Dormant Tumor Cells Rachelle Johnson, PhD *(Vanderbilt University)*
	CKD-MBD in a Model of Targeted FGF23 Deletion Erica Clinkenbeard, PhD *(Indiana University School of Medicine)*

9:15 AM - 12:00 PM	**Problems in Orthopaedics: Degenerative Disk Disease** Chair: James Iatridis, PhD *(Icahn School of Medicine at Mount Sinai)*
	Introduction James Iatridis, PhD *(Icahn School of Medicine at Mount Sinai)*
	Intervertebral Disc Biology: An Enigma Machine Makarand Risbud, PhD *(Thomas Jefferson University)*
	Clinical Perspective of Low Back Pain: Still a Black Box James Kang, MD *(Brigham and Women's Hopsital)*

12:30 PM – 5:00 PM	**Guided Hikes** *Sponsored by* OsteoMetrics **Pioneer Cabin** *(rigorous, 8 miles round-trip, led by David Burr)* **TBD Location** *(shorter and easy, led by Sue Bloomfield)* Attendees meet at the back door of the Sun Valley Resort Inn at 12:30 PM

7:30 PM - 9:30 PM	**Next Generation Therapies** Chair: David Burr, PhD *(Indiana University)*
	New Approaches to Anabolic Therapy Ben Leder, MD *(Harvard University)*
	Treatment of Osteoarthritis: New Horizons Nancy Lane, MD *(UC Davis)*
	Novel/Potential Therapies for Age-Related Sarcopenia Roger Fielding, PhD *(Tufts University)*

7:00 AM – 8:00 AM	**Breakfast & Registration**

8:00 AM - 9:15 AM	**Welcome & The RIB Award/Plenary Session** Rib Awardee: Michaela Kneissel, PhD *(Novartis)* Targeting Musculoskeletal Disease to Restore Mobility in Disease and Old Age *Sponsored by* American Association of Anatomists

9:30 AM - 10:00 AM	**Blue Ribbon Sun Valley Posters** Chair: Teresita Bellido, PhD *(Indiana University)*
	COL11A1 Expression is Required for Normal Chondrocyte Behavior during Skeletal Development Jonathon Reeck, PhD *(Boise State University)*
	Chondro-Protective Function of Statin Is Related to the Inhibition of Small GTPase Activities Mengxi Lv *(University of Delaware)*
	Fatty Acid Binding Protein 4 (FABP4) As A Biomarker for Knee Osteoarthritis Chaofan Zhang, MD, MS *(The University of Hong Kong)*
	Histopathological Analysis of Healing Responses to a Novel Tendon Transfer Surgery in a Chicken Model Anthony Le, BS *(Oregon State University)*
	RON Kinase: A New Target for Treatment of Cancer-induced Bone Destruction and Osteoporosis Jaime Fornetti, PhD *(Huntsman Cancer Institute)*

10:15 AM - 12:00 PM	**Major Methodologies: The Essentials of Finite Element Analysis for Basic and Clinical Studies** Chair: Christopher Jacobs, PhD *(Columbia University)*
	Introduction: The Pros and Cons of FEA Christopher Jacobs, PhD *(Columbia University)*
	Cell Mechanics: The Role of Simulation Christopher Jacobs, PhD *(Columbia University)*
	Finite Element Analysis for Clinical Assessment of Whole-Bone Strength David Kopperdahl, PhD *(O.N. Diagnostics, LLC)*

2:00 PM – 4:00 PM	**Volleyball** *Sponsored by* ultragenyx pharmaceutical	Volleyball Court

7:30 PM - 8:00 PM	**Blue Ribbon Sun Valley Posters** Chair: Alexander Robling, PhD *(Indiana University)*
	Prx-1 Embryonic Specification Is Retained in a Postnatal Regenerative Stem Cell Population that Gives Rise to Skeletal, Fat, and Vascular Tissues Beth Bragdon, PhD *(Boston University School of Medicine)*
	Improved Fracture Risk Assessment via Bound/Pore Water MRI Jeffry Nyman, PhD *(Vanderbilt University Medical Center)*
	Anabolic PTH Signaling Activates the Canonical Notch Pathway in Osteocytes to Restrain Bone Resorption and Facilitate Bone Gain Jesus Delgado-Calle, PhD *(Indiana University School of Medicine)*
	Characterization of Fibroblast Growth Factor 23 (FGF23) Levels in Patients with Fanconi Syndrome due to Nephropathic Cystinosis Pablo Florenzano, MD *(NIDCR, National Institutes of Health)*
	PPARϒ and PPARα Regulate Osteocyte Activity by Controlling Expression of Sclerostin and DKK1 Proteins Lance Stechschulte, PhD *(University of Toledo)*

8:00 PM - 10:00 PM	**Poster Session with wine and cheese**
	Alice L. Jee Award Winners
	Prx-1 Embryonic Specification Is Retained in a Postnatal Regenerative Stem Cell Population that Gives Rise to Skeletal, Fat, and Vascular Tissues Beth Bragdon, PhD *(Boston University School of Medicine)*
	Anabolic PTH Signaling Activates the Canonical Notch Pathway in Osteocytes to Restrain Bone Resorption and Facilitate Bone Gain Jesus Delgado-Calle, PhD *(Indiana University School of Medicine)*
	Characterization of Fibroblast Growth Factor 23 (FGF23) Levels in Patients with Fanconi Syndrome due to Nephropathic Cystinosis Pablo Florenzano, MD *(NIDCR, National Institutes of Health)*
	RON Kinase: A New Target for Treatment of Cancer-induced Bone Destruction and Osteoporosis Jaime Fornetti, PhD *(Huntsman Cancer Institute)*
	Deletion of CaMKK2 in Osteocytes Elicits Gender-Specific Effects on Bone Mass Mavis Irwin, PhD *(Indiana University / Purdue University)*
	Linking Cortical Bone Mechanics, Structure and Remodeling in the Fibula Mariana Kersh, PhD *(University of Illinois at Urbana-Champaign)*
	Chondro-Protective Function of Statin Is Related to the Inhibition of Small GTPase Activities Mengxi Lv *(University of Delaware)*
	Early Subchondral Bone and Articular Cartilage Compositional Changes in the Medial Compartment after DMM Surgery Quantified by μCT Maleeha Mashiatulla, PhD *(Rush University Medical Center)*
	Inhibition of CaMKK2 Attenuates Subchondral Bone Remodeling in Post-traumatic Osteoarthritis Model Elsa Mevel, PhD *(Indiana University School of Medicine)*
	Promoting Load-induced Bone Formation by Manipulating Primary Cilia Mechanobiology Milos Spasic, MS *(Columbia University)*
	PPARϒ and PPARα Regulate Osteocyte Activity by Controlling Expression of Sclerostin and DKK1 Proteins Lance Stechschulte, PhD *(University of Toledo)*
	Mechanism of Exercise in Preventing Skeletal Muscle Atrophy Nicholas Theilen, MS (*University of Louisville School of Medicine)*

8:00 PM - 10:00 PM	Raman Spectroscopic Parameters Correlates with the Fracture Toughness of Human Cortical Bone Mustafa Unal, PhD *(Vanderbilt University Medical Center)*
	Fatty Acid Binding Protein 4 (FABP4) As A Biomarker for Knee Osteoarthritis Chaofan Zhang, MD, MS *(The University of Hong Kong)*
	Osteoarthritis Award Winner
	Repurposing Glutamate Receptor Antagonists for the Prevention of Post-traumatic Osteoarthritis Cleo Bonnet, PhD *(Cardiff University)*
	Charles H. Turner Young Investigator Bone Research Award Winner
	Impact of High Bone Turnover on Skeletal Muscle Weakness in a Mouse Model of Camurati-Engelmann Disease Trupti Trivedi *(Indiana University)*
	Submitted Poster Presenters
	Positive Adaptations in Cancellous Microarchitecture with Moderate Iron Overload, Even in Hindlimb Unloaded Mice, Are Associated with Elevated Serum Hepcidin Susan Bloomfield, PhD *(Texas A&M University)*
	Point Mutation in Lrp4 Sost Binding Pocket Increases Bone Mass in Mice Whitney Bullock, BS *(Indiana University)*
	Actin Organization and Response to Fluid Flow are Influenced by the Osteocyte Primary Cilium Michael Duffy, MPh (*Columbia University)*
	TGFβ Regulation of Osteocytic Perilacunar Remodeling is Crucial for Maintaining Bone Quality Neha Dole, PhD *(University of California San Francisco)*
	Severe Burn-Induced Inflammation and Remodeling of Achilles Tendon in a Rat Model Paula Hernandez, PhD *(University of Texas Southwestern)*
	The Expansion of Heterotopic Bone in Fibrodysplasia Ossificans Progressiva is Activin A-Dependent Lily Huang, MS *(Regeneron)*
	Trends in the Theory that Inflammation Plays a Causal Role in Tendon Disease: A Systematic Review and Quantitative Analysis of Published Mechanistic Reviews Michael Mosca, MSc *(Columbia University)*
	Mesenchymal Stem Cells Differentiation into Nucleus Pulposus-Like Cells Based On the New Phenotype of Young Healthy Nucleus Pulposus Cells Arjun Sinkemani *(Southeast University School of Medicine)*
	Cell-Free Biomimetic Scaffolds Lead to Non-Unions in Critical Sized Defect Repair as Compared to Identically Structured Stem Cell Infiltrated Scaffolds that Induce Rapid Bone Growth John Szivek, PhD *(University of Arizona)*
	Changes in Intervertebral Disc Structure and Morphology in Back-healthy Humans During Standing Simon Tang, PhD *(Washington University in Saint Louis)*
	Scoliosis in Fibrous Dysplasia/McCune-Albright Syndrome Sri Harsha Tella, MD *(National Institute of Health)*
	The Biphasic Response to Phosphate During Chondrogenic Differentiation Biming Wu, MS *(University of Michigan)*
	LaminA/C Knock Down Enhances Adipogenesis but does not Eliminate Mechanical Response in MSCs Gunes Uzer, PhD *(Boise State University)*

COL11A1 expression is required for normal chondrocyte behavior during skeletal development

Jonathon C. Reeck, PhD,1,2, Julia T. Oxford, PhD1,2
1 Biomolecular Sciences Graduate Program and 2Biomolecular Research Center, Boise State University, Boise, ID.

INTRODUCTION: Chondrogenesis is regulated by multiple factors including transcription factors, soluble and insoluble extracellular biomolecules, cell-cell and cell-matrix interactions. Understanding how these factors interact to regulate cell behavior during skeletal development and growth may lead to the development of novel methods and therapeutic targets for skeletal diseases. Previous studies have established the importance of COL11A1 expression in skeletal development, maintenance and health, but they have not investigated how decreased COL11A1 expression affects the chondroprogenitor cell behavior during chondrogenesis. Cells of the chondrogenic lineage undergo proliferation, condensation and upregulate chondrogenic gene expression to promote cartilage development. Deviation from the normal expression pattern may alter the extracellular matrix environment permanently, causing chondrodysplasia and susceptibility to degenerative cartilage disease. Furthermore, cells interact with and react to the extracellular environment; therefore, dysplastic tissue has the potential to alter downstream cellular behaviors such as differentiation. In addition to nucleation and collagen fibril diameter, we propose the hypothesis that COL11A1 expression is required to promote chondroprogenitor cell maturation and organization during endochondral ossification and chondrogenesis. Based on this hypothesis, we predict that skeletal dysplasia resulting from loss of COL11A1 expression alters chondrocyte phenotype and disrupts cell signaling events during chondrogenesis. To test this hypothesis, we knocked down COL11A1 expression in zebrafish embryos and investigated the effect on skeletal development. Then we utilized the mouse ATDC5 chondrogenic cell line to investigate the mechanisms related to COL11A1 expression during chondrogenesis 1–3.

METHODS:

Zebrafish and antisense morpholino oligionucleotide injection

Vertebrate animal use was approved by the Institutional Animal Care and Use Committee (IACUC). Zebrafish embryos were obtained from ZIRC (Eugene, OR). The *col11a1a* antisense morpholino oligionucleotide targeted the translational start site with the following sequence: 5'GGGACCACCTTGGCCTCTCCATGGT3'. Morpholinos were diluted in water and 0.005% phenol red. The morpholinos were injected at a volume of 2 nL and at a concentration of 3 ng/nL. For vital imaging of calcification, live zebrafish were incubated in 30 mL of the zebrafish housing system water with 200 µL of 0.5% Alizarin Red (final concentration 0.003%) for 3 hours. Fish were subsequently rinsed in zebrafish housing system water prior to imaging. Transgenic Fli1a:EGFP and Sp7:EGFP zebrafish were anesthetized in 0.016% tricaine methanesulfonate (MS-222) in system water prior to mounting in 0.6% (w/v) low melting point agarose containing MS-222. Confocal imaging was performed using a Zeiss LSM 510 Meta inverted laser scanning microscope. Alizarin Red vital stained images were collected by excitation between 530-560 nm and by monitoring emission at 580 nm. GFP transgene-expressing zebrafish images were generated by excitation at 488 and monitoring emission at 509 nm.

ATDC5 cells and Col11a1 siRNA transfection

The mouse chondrogenic ATDC5 cells were cultured in DMEM/F12 containing 5% fetal bovine serum supplemented with Insulin (10 µg/mL), Transferrin (0.5 µg/mL) Selenium (0.0067 µg/mL), 50 µg/mL ascorbic acid 2-phosphate. siRNA targeting *Col11a1* was designed and purchased from Invitrogen. Transfections were performed in triplicate with a siRNA-lipid complex master mix prepared in Opti-MEM media. Control wells were transfected with negative control siRNA and performed in triplicate with each experiment under the same conditions as the experimental siRNA.

Quantitative RT-PCR (qPCR) analysis

RNA was extracted and purified using the RNAeasy minikit following manufacturer's instructions (Qiagen). Isolated RNA was analyzed by spectrophotometry for purity and quantity and used immediately for cDNA synthesis. RNA was reverse transcribed into cDNA using the RT2 first strand kit. The cDNA template was analyzed by qRT-PCR reaction using Sybr Green. Reactions were carried using the Roche Lightcycler 96. The relative amount of PCR product was normalized to the indicated reference genes and the change in threshold cycle (dCt) was compared using Student's t-test. The fold change was calculated using the 2-ΔΔCt method 4.

Luciferase Assays

Cignal 45-pathway reporter array was used to identify changes in transcription factor activity following manufactures instructions. Lipofectamine 2000 was used with Opti-Mem to simultaneously reverse transfect

Col11a1 siRNA and a mixture of transcription factor responsive firefly luciferase reporter and a constitutively expressing Renilla constructs. Dual luciferase reporter assay system and Glomax multi detection system was used to measure the activity of the transcription factors following standard protocol.

Western blot analysis

Cell lysates were extracted using ice-cold radioimmunoprecipitation (RIPA) cell lysis buffer supplemented with protease and phosphatase inhibitor cocktails Western blots were performed using the following rabbit primary antibodies from Cell Signaling Technology at a dilution of 1:1000 unless otherwise stated: phospho-β-catenin (Ser33/37/Thr41), Gsk-3beta, phospho-GSK3-β (Ser9) (5B3) mAb, β-Actin (13E5) mAb.

RESULTS: These results demonstrate that Col11a1 expression is required for normal cell behavior during skeletal development. Col11a1a is required for cells to form columns and regulate mineralization during craniofacial development in the zebrafish. Knockdown of Col11a1a prevented neural crest derived cells from forming stacks of cells (Figure 1A) and establishing a successful cartilage template for bone lining cells expressing Sp7 (Figure 1B). Loss of Col11a1 in ATDC5 cells did not alter the mRNA levels of genes involved in the cell condensation stage of chondrogenesis (Figure 2A). On the other hand, the expression of Col2a1 and Mmp13 were significantly increased during differentiation (Figure 2B). In addition, the several extracellular matrix and adhesion genes were increased (Figure 2C). Investigation of components of cell signaling pathway, including phosphorylation of GSK3B and β-catenin coupled to increased activity of TCF/LEF indicate increased β-catenin signaling activity occurs if Col11a1 expression is inhibited (Figure 2D).

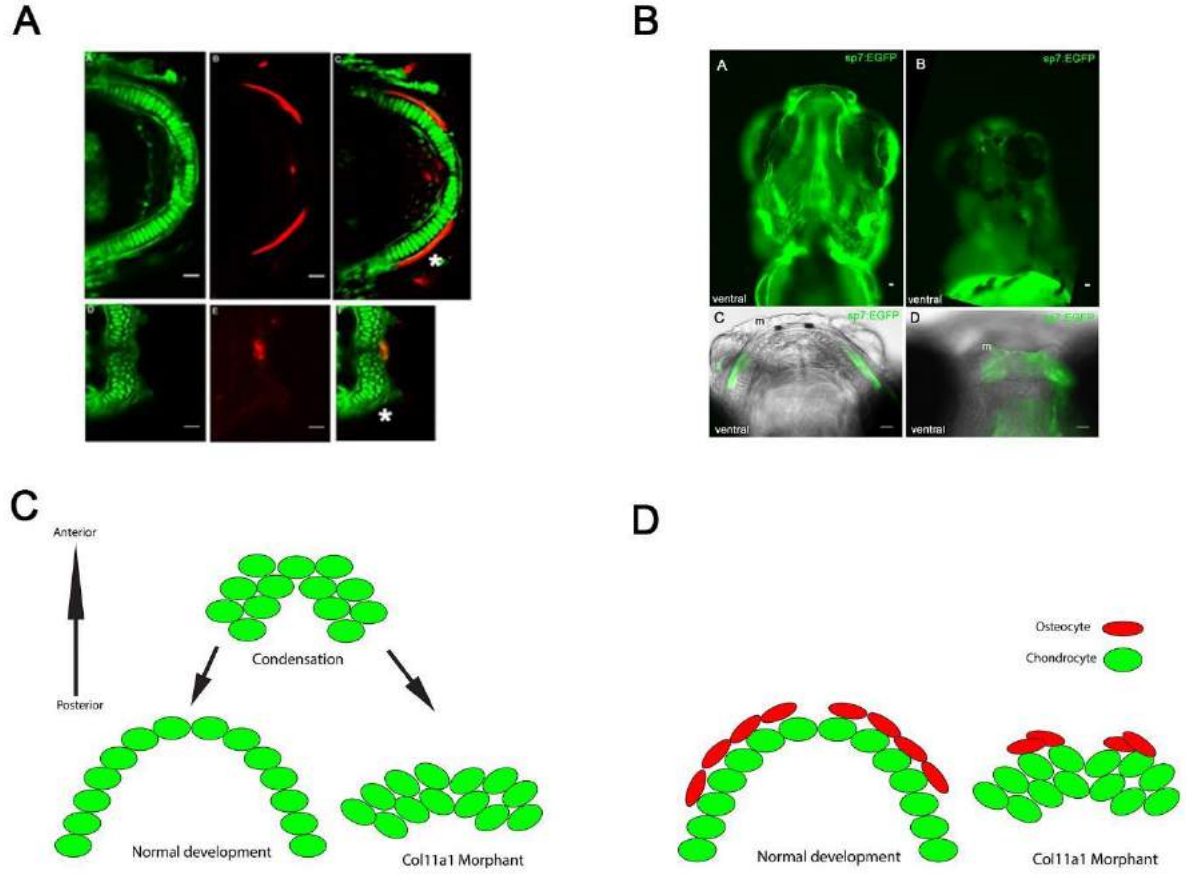

Figure 1. Col11a1a knockdown inhibits jaw morphogenesis in zebrafish. A. The cells contributing to jaw development in the control zebrafish form columns of cells that promote the extension of the jaw cartilage (A). In contrast, the cells in the morphant fail to form a column of cells and the extension of the jaw cartilage fails to occur (C). Mineralization of the morphant cartilage (E and F) is abnormal compared to the control jaw (B and C). B. Bone forming expressing Sp7 line the cartilage template in the control zebrafish (A and C). The bone forming cells are also present in the col11a1a morphant, but, they occupy a smaller area along the cartilage template (B and D). C. The model represents the failure of the cartilage forming cells to organize into columns in the Col11a1 morphant. D. The abnormal cartilage of the developing jaw also affects the bone forming osteocyte organization, leading to mineralization defects.

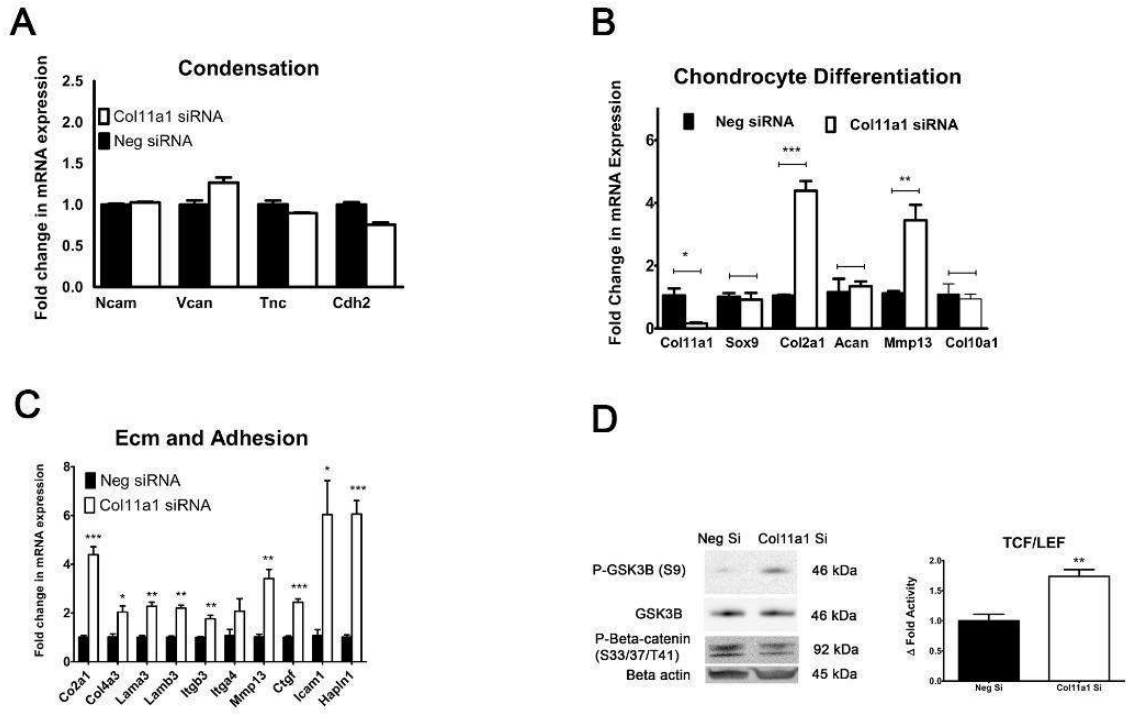

Figure 2. Col11a1 regulates gene expression and TCF/LEF activity during chondrogenesis. Col11a1 siRNA induced significant changes in gene expression during chondrogenesis in ATDC5 cells (A-C). Additionally, the phosphorylation of GSK3B was increased and β-catenin phosphorylation was decreased. The phosphorylation state agreed with increased TCF/LEF activity (D).

CONCLUSIONS: We show that although considered a structural protein, loss of COL11A1 expression impacts cellular behavior and cell signaling pathways. This information may lead to development of cell based therapies and novel tissue regeneration strategies for repairing damaged tissues. Although the morphology of skeletal tissues impacted by COL11A1 mutations have been described radiologically and at the ultrastructural level, the behavior of the cells in the tissue have not been previously characterized 5. Since the cells are ultimately responsible for both generating and maintaining tissues, understanding the consequences of the absence or reduction of COL11A1 expression on cell behavior has important ramifications for skeletal development, disease progression and therapies.

REFERENCES

1. Chen, L., Fink, T., Zhang, X.-Y., Ebbesen, P. & Zachar, V. Quantitative transcriptional profiling of ATDC5 mouse progenitor cells during chondrogenesis. *Differentiation* 73, 350–363 (2005).
2. Altaf, F. M., Hering, T. M., Kazmi, N. H., Yoo, J. U. & Johnstone, B. Ascorbate-enhanced chondrogenesis of ATDC5 cells. *Eur. Cell. Mater.* 12, 64-9-70 (2006).
3. Yao, Y. & Wang, Y. ATDC5: An excellent in vitro model cell line for skeletal development. *J. Cell. Biochem.* 114, 1223–1229 (2013).
4. Schmittgen, T. D. & Livak, K. J. Analyzing real-time PCR data by the comparative C(T) method. *Nat. Protoc.* 3, 1101–8 (2008).
5. Fernandes, R. J., Weis, M., Scott, M. A., Seegmiller, R. E. & Eyre, D. R. Collagen XI chain misassembly in cartilage of the chondrodysplasia (cho) mouse. *Matrix Biol.* 26, 597–603 (2007).

Chondro-Protective Function of Statin Is Related to the Inhibition of Small GTPase Activities

Mengxi Lv, Yilu Zhou, X. Lucas Lu
Department of Mechanical Engineering, University of Delaware, Newark, DE 19716

Introduction

In the early stages of osteoarthritis (OA), catabolic activities are often promoted in chondrocytes by OA-inducing factors; and meanwhile cells undergo a cascade of phenotypic changes, including swelling, proliferation, hypertrophy and apoptosis [1]. The aberrant cellular process is dependent on the activities of small GTPases (Rho, Ras, Rac etc.). The post-translational prenylation of small GTPases requires geranylgeranyl- and farnesyl-pyrophosphates in cells, which are two down-stream products in the mevalonate pathway [2]. Therefore, the inhibition of the mevalonate signaling in chondrocytes might be able to prevent the cells from the aberrant phenotypic shift after joint injuries by disabling the activities of small GTPases. Statins, a class of drugs used for the prevention of cardiovascular diseases, can control cholesterol levels by inhibiting mevalonate signaling. In this study, we hypothesized that inhibition of the mevalonate pathway and its downstream small GTPases in chondrocytes, using statin, can prevent cells from the aberrant phenotypic shift after joint injuries and further suppress the osteoarthritis development.

Chondro-protective Effects of Statin

Cylindrical cartilage explants (diameter = 3 mm and thickness = 2 mm) were harvested from calf knee joints and cultured in a chemically defined medium up to 26 days [3]. A pro-inflammatory cytokine, IL-1β, at 1 ng/mL was introduced into the culture medium of cartilage explants to mimic a moderate inflammation insult to cartilage. Simvastatin was supplemented simultaneously with IL-1β into the medium at day 0. Explants were divided into six groups for in vitro culture: 1) control, 2) IL-1β, 3) IL-1β + 1 μm statin, 4) IL-1β + 3 μm statin, 5) IL-1β + 10 μm statin, and 6) 10 μm statin alone. The loss of GAG and collagen contents from the cartilage explant into the culture medium was measured every other day. As results, statin in medium significantly reduced the IL-1β-induced GAG loss in a dose-dependent manner (Fig. 1A). The collagen loss induced by IL-1β was negligible in the first 10-day culture and became substantial from day 12 to 24. The loss of collagen from explant was almost completely abolished by 10 μm statin treatment (Fig. 1B). Mechanical properties of cartilage explants were measured via indentation test after 8-day culture. Statin treatment (10 μm) prevented the decrease of Young's modulus induced by IL-1β ($P < 0.05$) (Fig. 1C). To track the change of cell volume, *in situ* chondrocytes in the explant were dyed with CellTracker™ (Thermo Fisher). IL-1β in medium increased the volume of chondrocytes by 68.2% after 4 days, while the swelling was fully prevented by statin ($P < 0.001$) (Fig. 1D).

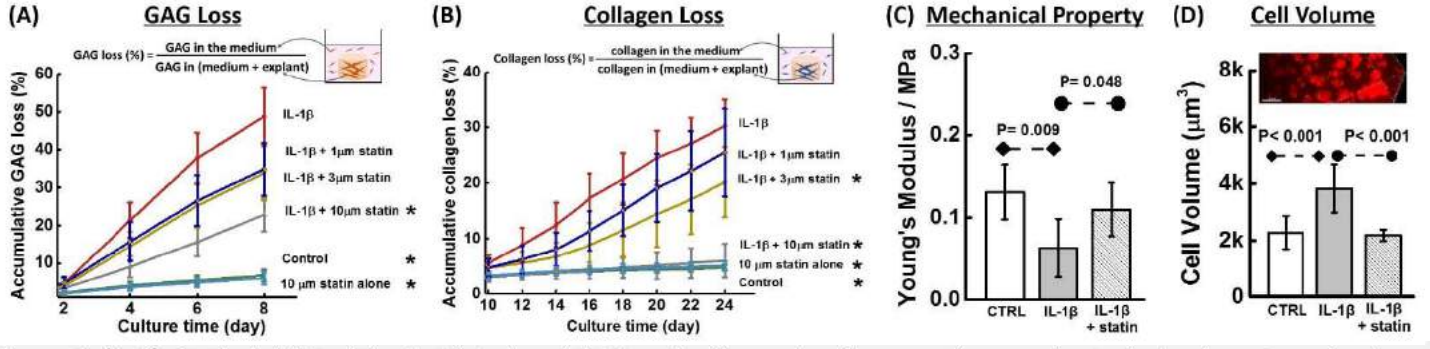

Figure 1: (A-B): Statin inhibited the IL-1β-induced GAG and collagen loss from cartilage explants during long-term *in vitro* culture. Loss of collagen content started 10 days later than GAG content. (N=6 explants from 3 animals. *: vs. IL-1β; $P < 0.01$). **(C)**: Young's modulus of cartilage explants was preserved by 10 μM statin treatment after 8-day culture (N=6 explants from 3 animals). **(D)**: Statin inhibited the cell swelling induced by IL-1β after 4-day culture (N= 32 cells in 2 explants from 2 animals).

Genome-wide Effects of Statin on in situ Chondrocytes

The whole-genomic expression change induced by statin in chondrocytes was assessed by RNA sequencing (RNA-seq). Cartilage explants were cultured in medium supplemented by IL-1β or IL-1β + statin. After 48-hour in vitro culture, the RNA was extracted from explants for sequencing. As results, statin significantly changed the expression of 1,048 genes in chondrocytes, among which 690 genes were up-regulated and 459 genes down-regulated when compared to the IL-1β alone group (absolute fold change > 1.5 and FDR < 0.05) (Fig. 2A). The expression of catabolic genes in ADAMTS- and MMP-family was significantly suppressed by statin (Fig. 2B). RNA-seq also identified that the small GTPases was among the 18 most significantly changed pathways in statin-treated samples (Fig. 2C). The major genes related to mevalonate

pathway were substantially up-regulated in the statin group, which could be a compensatory response to statin regulation (Fig. 2D).

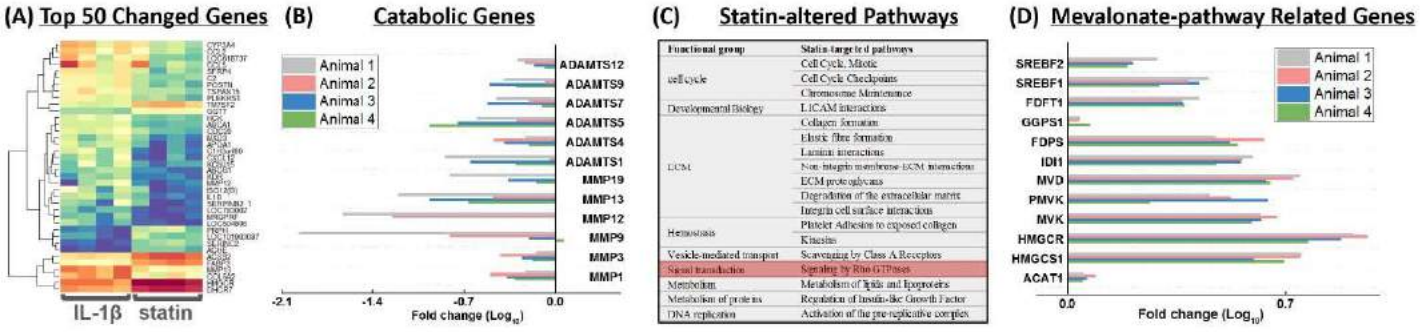

Figure 2: (A): RNA sequencing identified 1,048 genes that are significantly changed by statin treatment. The top 50 changed genes were listed in the heatmap (N=4 explants from 4 animals). **(B):** Catabolic genes (ADAMTS- and MMP-family) were down-regulated by statin treatment. **(C):** Pathway analysis identified 18 pathways in chondrocytes that were significantly changed by statin, including the mevalonate pathway (highlighted in the red box). **(D):** Statin treatment induced compensatory up-regulation of the mevalonate related genes in chondrocytes.

Chondro-protective Effect of Another Mevalonate Inhibitor - Bisphosphonate

In vitro Cartilage Explant Model – To verify the role of mevalonate pathway, we replaced statin with another mevalonate pathway inhibitor, called zoledronate (ZA), in the cartilage explant model. Zoledronate belongs to the bisphosphonate family that is widely used for the treatment of osteoporosis. Bisphosphonates can inhibit the mevalonate pathway in osteoclasts and prevent the formation of ruffled cell membrane [4]. In this study, zoledronate demonstrated protection effects similar to statin, reducing the loss of GAG and type II collagen contents from the IL-1β-treated cartilage explants (Fig. 3A-B). Mechanical integrity of cartilage explant was also preserved by zoledronate, which attenuated the decrease in Young's modulus, dynamic modulus, and the increase of permeability (P = 0.01 for all) (Fig. 3C).

DMM Mouse Model – We further tested the chondro-protective function of zoledronate in a DMM (destabilization of the medial meniscus) mouse model. Significant cartilage degeneration was observed in 12 weeks after the DMM surgery (Fig. 3D Left). Systemic injection of zoledronate (0.15mg/kg, twice per week) significantly suppressed the osteoarthritis development in DMM mice. OARSI score of the drug treated mice is similar to those of the sham groups, and significantly lower than the DMM vehicle group (Fig. 3D Right). Zoledronate inhibited the OA progression in mouse knee joints after the DMM surgery.

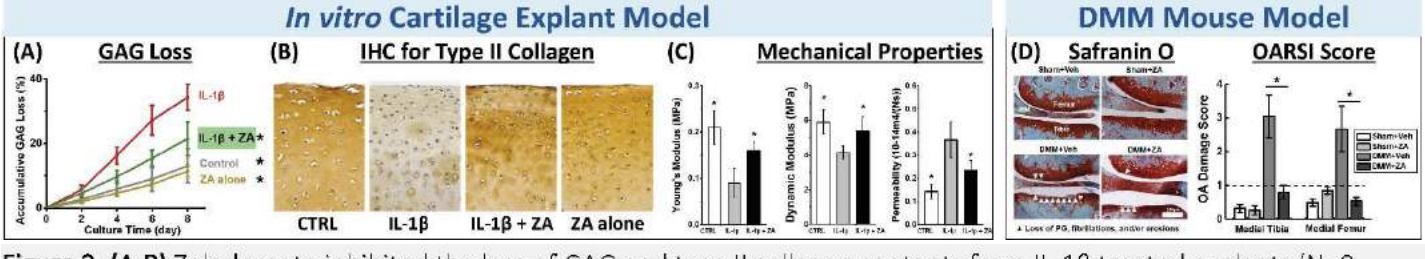

Figure 3: (A-B) Zoledronate inhibited the loss of GAG and type II collagen contents from IL-1β treated explants (N=8 explants from 4 animals, *: vs. IL-1β; P < 0.01). **(C)** Zoledronate protected the mechanical integrity of cartilage from IL-1β attack (N=8 explants from 4 animals, *: vs. IL-1β; P < 0.01). **(D)** Systemic injection of zoledronate inhibited the OA progression in DMM mouse model. L: Histology of knee joints; R: OA damage score (N=10 animals, *: P < 0.01).

Role of Small GTPases in Mevalonate Pathway

Statin inhibits the hydroxyl-methyl-glutaryl Coenzyme A (HMG-CoA) reductase, while bisphosphonates inhibit the FPP synthase of the mevalonate pathway in cells (Fig. 4A). Both HMG-CoA and FPPS play important roles in regulating the prenylation of downstream small GTPases. To test whether the chondro-protective function of mevalonate inhibitors is related to small GTPases, we supplemented the culture medium of explants by statin and GGOH. GGOH is an intermediate derivative of the mevalonate pathway, which can restore the statin-impaired activities of small GTPases. As expected, GGOH substantially abolished the chondro-protective effects of statin. The loss of GAG and collagen contents induced by IL-1β no longer be protected by the statin (Fig. 4B). To confirm this finding, we further tested the effects of two antagonists of small GTPases, GGTI and Rhoi. GGTI can inhibit the function of GGOH, while Rhoi directly interrupts the

activation of Rho protein. In our cartilage explant study, GGTI showed strong chondro-protective effects similar to the statin, by significantly inhibiting the IL-1β-induced loss of GAG and collagen contents (Fig. 4C). Rhoi also reduced the IL-1 β -induced loss of extracellular matrix, although its protective effect is not as potent as that of GGTI or statin. Therefore, the chondro-protective function of statin and bisphosphonate is related to the inhibition of small GTPases in chondrocytes.

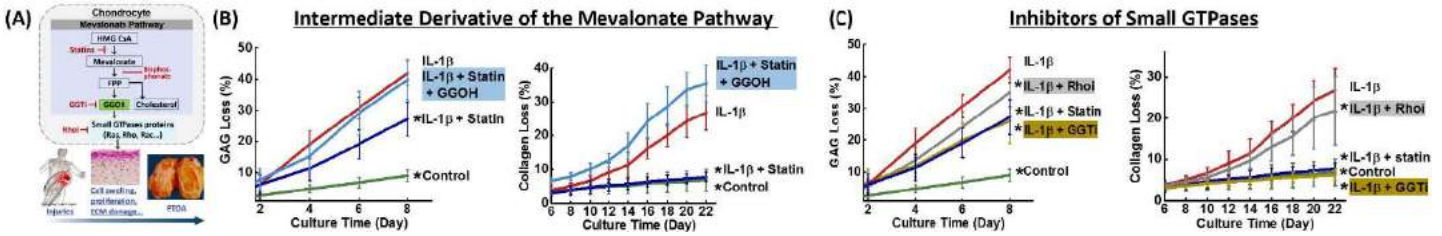

Figure 4: (A) The chondro-protective function of statin and bisphosphonate is related to the inhibition of small GTPases in chondrocytes, which are required for the aberrant phenotypic shift of chondrocytes under inflammatory attack. **(B)** The intermediate derivative of mevalonate pathway (GGOH), which can recover the prenylation of small GTPases, abolished the chondro-protective effects of statin (N=6 explants from 3 animals, *: vs. IL-1β; $P < 0.01$). **(C)** Antagonists of small GTPases, GGTi and Rhoi, also prevented the loss of GAG and collagen contents from IL-1β treated cartilage explants (N=6 explants from 3 animals). (*: vs. IL-1β; $P < 0.05$. $: vs. IL-1β + statin; $P < 0.01$).

Statin and Calcium Signaling of Chondrocytes

In chondrocytes, the intracellular calcium ([Ca2+]i) signaling is one of the earliest cellular responses to mechanical stimulation and regulates a wide range of biological processes. Activities of small GTPases are closely interwoven with [Ca2+]I signaling (Fig. 5A) [5]. To further understand the chondro-protective function of statin, we investigated the [Ca2+]i signaling of *in situ* chondrocytes. Cartilage explants were cultured with 1) IL-1β and 2) IL-1β + 10 μm statin for 2 days, and then dyed with Fluo-8 calcium dye. The spontaneous calcium signaling of *in situ* chondrocytes in cartilage explant was recorded for 16 minutes using a confocal microscope (Fig. 5B). In the IL-1β + statin group, there were more chondrocytes showing [Ca2+]i oscillation than those in the IL-1β alone group ($P < 0.001$). Responsive cells in the statin group also had [Ca2+]i peaks with higher magnitude, and took shorter time to recover from a [Ca2+]i peak (Fig. 5C).

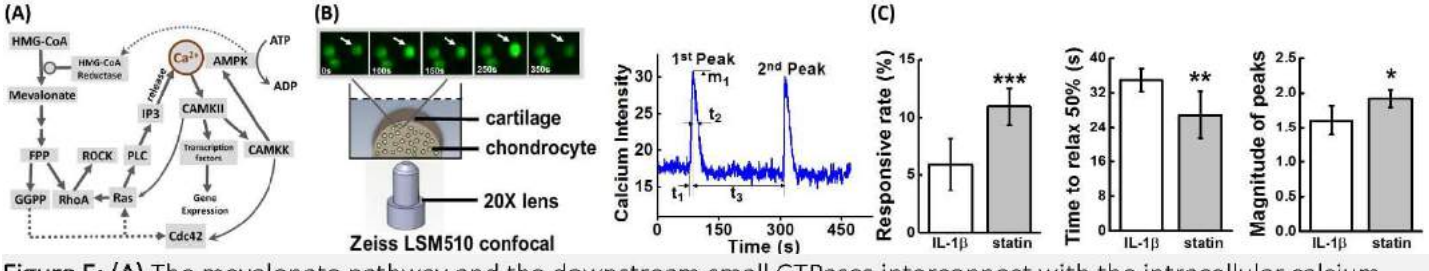

Figure 5: (A) The mevalonate pathway and the downstream small GTPases interconnect with the intracellular calcium signaling. **(B)** The microscopy setup to record the spontaneous $[Ca^{2+}]_i$ signaling of *in situ* chondrocytes in cartilage explant and a typical $[Ca^{2+}]_i$ oscillation curve of chondrocytes. **(C)** Statin promoted the calcium signaling in IL-1β treated cartilage explants in terms of responsive rate, magnitude of $[Ca^{2+}]_i$ peaks, and recovery time of cells after a $[Ca^{2+}]_i$ peak (N=6 from 3 animals). (*: $P < 0.05$; **: $P < 0.01$; ***: $P < 0.001$)

Summary

In this study, we found that two mevalonate inhibitors, statin and bisphosphonate, can protect the integrity of cartilage extracellular matrix in the presence of inflammatory stimulation. The chondro-protective functions of two classes of drugs are related to the inhibition of mevalonate pathway and the subsequent inhibition of the small GTPases in chondrocytes. Loss of small GTPases prevented the chondrocytes from aberrant phenotypic shift and destructing the ECM. Findings in this study provided: 1) critical justifications regarding the application of statins and bisphosphonates for PTOA prevention, 2) guidance for future clinical trials of the mevalonate inhibitors in OA prevention, including the targeted population, design of delivery methods, and timing of drug administration, and 3) a new target pathway in chondrocytes, *i.e.*, small GTPases, for the inhibition of osteoarthritis initiation after joint injuries.

Reference: [1] Pencina, M., et al., NEJM, 2014. [2] Lazzerini, P., et al., Semin in A&R, 2011. [3] Bian, L., et al., J Biomech, 2008. [4] Ken Beauchamp J.Clin. Invest, 2001. [5] Novakofski, K., JOR. 2009.

Fatty Acid Binding Protein 4 (FABP4) As A Biomarker for Knee Osteoarthritis

Chaofan Zhang, MD, MS[1,2], Kwong Yuen Chiu, MBBS[1], Aimin Xu, MD, PhD[3], Chun Hoi Yan, MBBS[1,4] 1. Department of Orthopaedics & Traumatology, The University of Hong Kong, Hong Kong SAR, China; 2. Department of Orthopedics, The First Affiliated Hospital of Fujian Medical University, Fuzhou, China; 3. Department of Medicine, LKS Faculty of Medicine, The University of Hong Kong, Hong Kong SAR, China; 4. Shenzhen Key Laboratory for Innovative Technology in Orthopaedic Trauma, Department of Orthopaedics and Traumatology, The University of Hong Kong-Shenzhen Hospital, Shenzhen, China.

Objectives:
Osteoarthritis (OA) is a common joint disorder that affects millions of people all around the world. The etiology of OA, however, is still poorly understood. Recent studies have suggested that adipokines play important roles in the pathogenesis of OA. Fatty acid binding protein 4 (FABP4) is a novel adipokine that is closely associated with obesity and metabolic diseases. Yet no previous studies have examined FABP4 in OA. The aim of this study is to explore the potential role of FABP4 in the pathogenesis of OA.

Methods:
Both clinical study and animal study were performed. For the clinical study, we included patients with radiologically-confirmed knee OA and non-OA controls. Plasma level of FABP4 was determined by ELISA method. Regression analysis of FABP4 and knee OA severity, which was presented as Kellgren-Lawrence (K-L) grade was performed. For the animal study, we included 36 FABP4 knockout mice (KO) and 36 wild-type littermates (WT) (all male, 6-week-old), and fed the mice with a very high-fat diet (HFD, fat 60% calorie) or standard diet (STD, fat 11.6% calorie), for 3 months, 6 months and 9 months. At each time point, we measured animals' body weight and body fat. We then evaluated knee OA via examination of serum Cartilage Oligomeric Matric Protein (COMP) level, knee histologic assessment, and subchondral bone analyses. In the parallel study, we included 48 WT mice and fed the mice with HFD or STD, and simultaneously treated them with daily oral gavage of FABP4 selective inhibitor BMS309403 (15mg/kg/d) or vehicle (PBS solution), for 4 months and 6 months. At each time point, OA evaluation was performed same as above.

Results:
A total of 226 patients were included. 58 were males and 168 were females. The mean plasma level of non-OA patients, KL-2 patients, KL-3 patients, and KL-4 patients were 12.3±3.0 ng/ml (n=6), 14.6±6.9 ng/ml (n=72), 18.2±11.3 ng/ml (n=65), and 19.3±12.3 ng/ml (n=83), respectively (p=0.023, one-way ANOVA). After stratifying FABP4 into 4 level groups (<10 ng/ml, 10-15 ng/ml, 15-20 ng/ml, >20 ng/ml), FABP4 was positively associated with the severity of knee OA (p=0.031, ordinal regression analysis, age and sex adjusted). (Figure 1) For the animal study, HFD induced significant obesity in mice. However, KO mice were much fatter than WT mice with significantly higher body weight and higher percent body fat. (Figure 2) At 3 months of HFD, KO mice showed less cartilage degradation than WT mice with significantly lower serum COMP ((1.6±0.2)U/L vs (2.3±0.3) U/L, p=0.01) and OARSI score ((0.8±0.4) vs (2.9±0.4), p=0.00). Daily oral gavage of BMS309403 in mice for 4 months protected cartilage from degradation as well, in which the mice with BMS309403 for 4 months showed significantly lower COMP ((1.7±0.2)U/L vs (2.1±0.3) U/L, p=0.04) and OARSI score (5.4±6.0 vs 6.0±0.4, p=0.04) than mice with PBS. (Figure 3) At 9 months of HFD, WT mice underwent serious OA changes with significant osteophyte formation and subchondral bone sclerosis. While in KO mice, the changes were much alleviated. The subchondral bone BMD (p=0.00), bone volume percentage (p=0.00), trabecular thickness (p=0.00), and trabecular number (p=0.01) was significantly lower in KO mice. However, chronic treatment with BMS309403 did not seem to have significant effects on the subchondral bone strcuture. (Figure 4) For lean mice (fed with STD), either genetically knocking out or pharmaceutical inhibition of FABP4 had no significant effects on knee OA.

Conclusions:
Plasma FABP4 level was positively associated with the severity of knee OA. Knocking out or pharmaceutical inhibition of FABP4 alleviated OA induced by a very high-fat diet in mice. FABP4 may be a potential biomarker for knee OA.

Key words:
Osteoarthritis, fatty acid binding protein 4, BMS309403, obesity, subchondral bone sclerosis

Figure 1 Serum FABP4 level in 6 non-OA patients and 220 radiologically-confirmed OA patients. The level was 12.3±3.0 ng/ml, 14.6±6.9 ng/ml, 18.2±11.3 ng/ml, and 19.3±12.3 ng/ml in KL-0, KL-2, KL-3, and KL-4, respectively (p=0.023, one-way ANOVA). Post hoc analyses showed FABP4 of KL-2 patients was significantly lower than KL-4 patients (p=0.028, Tukey HSD). After stratifying FABP4 into 4 level groups (<10 ng/ml, 10-15 ng/ml, 15-20 ng/ml, >20 ng/ml), the ordinal regression analysis showed that FABP-4 was positively associated with the severity of knee OA (p=0.031, age and sex adjusted).

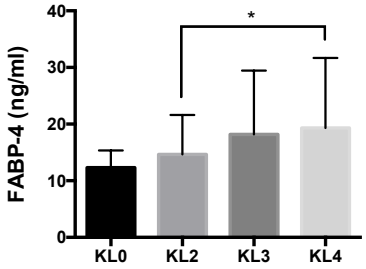

Figure 2 Knocking out or pharmaceutical inhibition of FABP4 significantly increased animals' body weight and body fat percentage. (A) Photos of KO and WT mice after 6-month of HFD and STD showed KO mice were fatter than WT mice, especially under HFD. (B, C) Statistical analyses showed KO mice had significantly higher body weight and body fat. (C) WT mice treated with daily oral gavage of BMS309403 (15mg/kg/d) for 4 months and 6 months had significantly higher body weight and body fat.

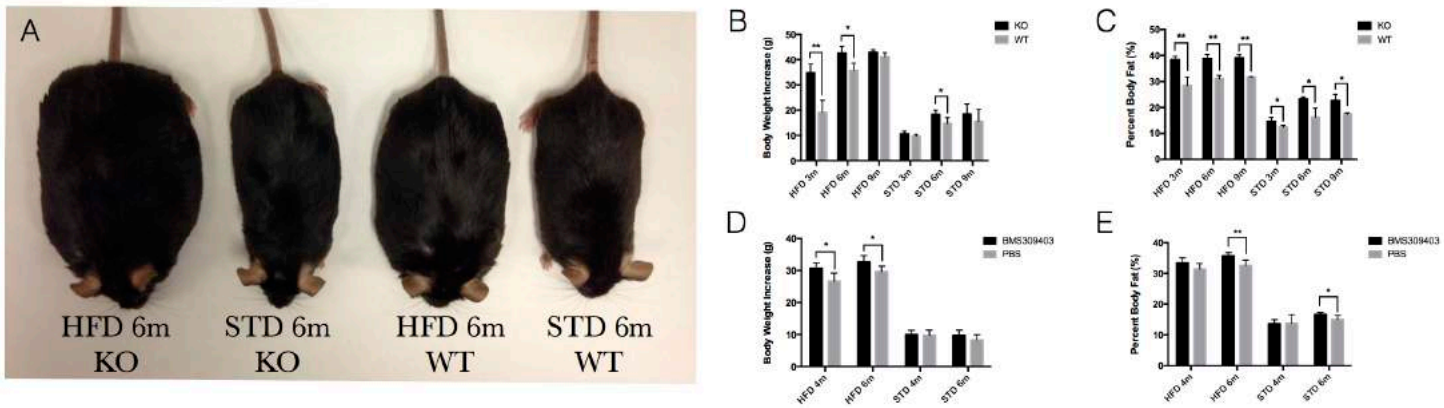

Figure 3 Knocking out or pharmaceutical inhibition of FABP4 significantly alleviated cartilage degradation in mice fed with HFD. The coronal paraffin sections of knees were stained with Safranin O and Fast Green. Loss of Safranin O staining in cartilage indicated a loss of glycosaminoglycan (GAG) content. (A, D, A1, D1) KO and WT mice after 3-month of HFD. Staining loss of cartilage was observed in WT mice but not obviously seen in KO mice. (B, E, B1, E1) KO and WT mice after 6-month of HFD. KO mice started to undergo cartilage degradation, while in WT mice the cartilage were seriously degenerated. In addition, osteophyte formation was seen in WT mice, especially in the medial compartment (arrow). (C, F, C1, F1) KO and WT mice after 9-month of HFD. Both KO and WT mice experienced severe cartilage degradation. In WT mice, serious subchondral bone sclerosis was observed (arrow). (G, I, G1, I1) WT mice treated with BMS309403 or PBS for 4 months. Mice treated with BMS309403 showed less cartilage staining loss than mice treated with PBS. (H, J, H1, J1) WT mice treated with BMS309403 or PBS for 6 months. Mice with PBS showed significant cartilage staining loss. (K) KO mice showed significantly lower level of COMP than WT mice after 3-month of HFD and STD. COMP level at 6-month of HFD in KO mice was significantly higher than WT, which suggested severe cartilage degradation in WT mice. (L) The OARSI score was significantly lower in KO mice than WT mice. (M) Mice treated with BMS309403 for 4 months showed significantly lower serum COMP than mice with PBS. (N) The OARSI score was significantly lower in mice treated with BMS309403 for 4 months. (Data presented as mean±std. Student t-test was performed to compare the means. *: p<0.05.)

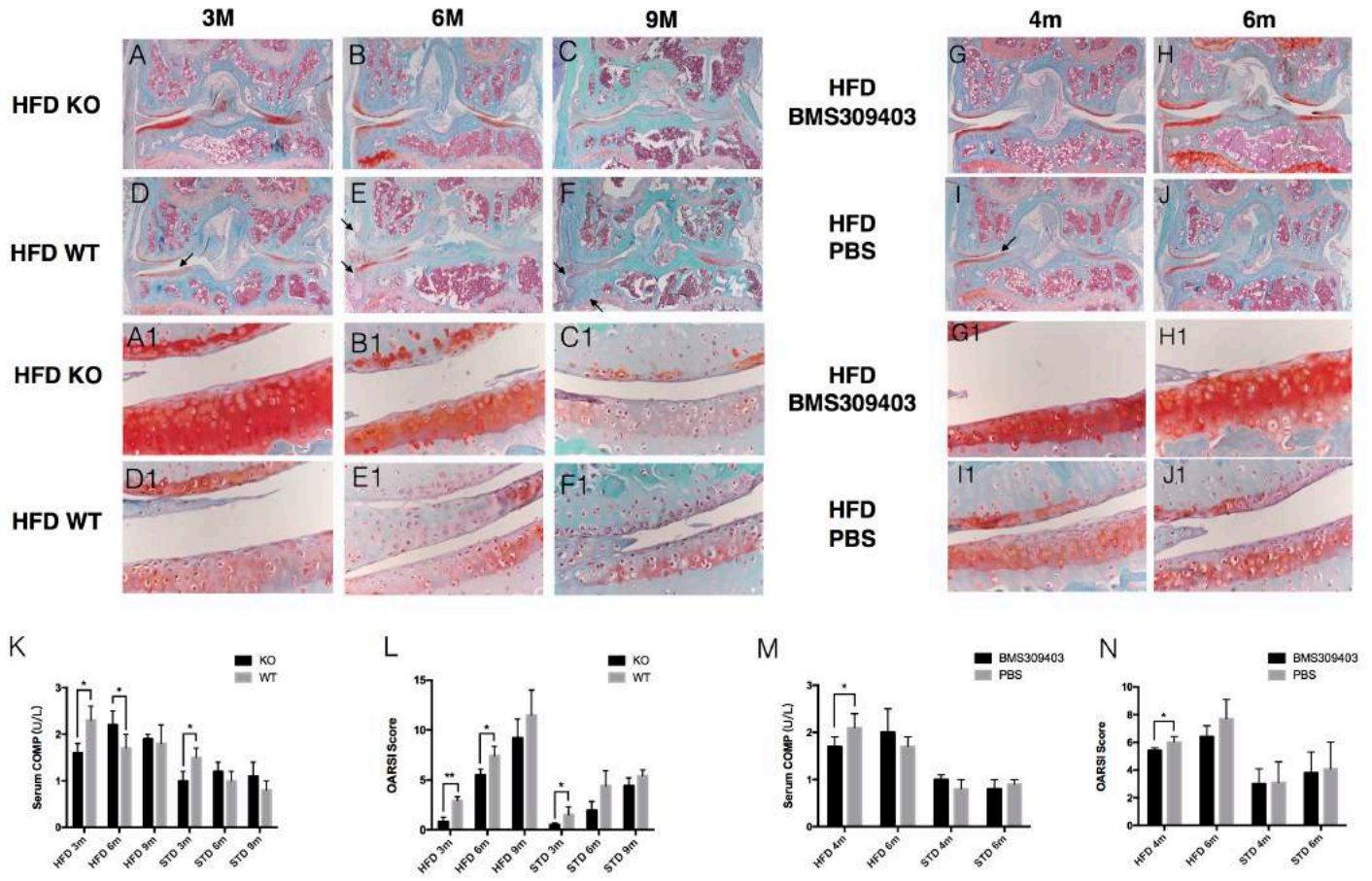

Figure 4. Micro-CT analysis of subchondral bone. Knocking out FABP4 significantly alleviated subchondral bone sclerosis in mice fed with HFD for 6 months and 9 months (A, arrow indicated). The subchondral bone BMD (p=0.00), bone volume percentage (p=0.00), trabecular thickness (p=0.00), and trabecular number (p=0.01) was significantly lower in KO mice after 9-month of HFD. (C, D, E, F) However, chronic treatment of BMS309403 in WT mice for 4 months and 6 months did not seem to have significant effects on the subchondral bone. (B, G, H, I, J) (**:p<0.01)

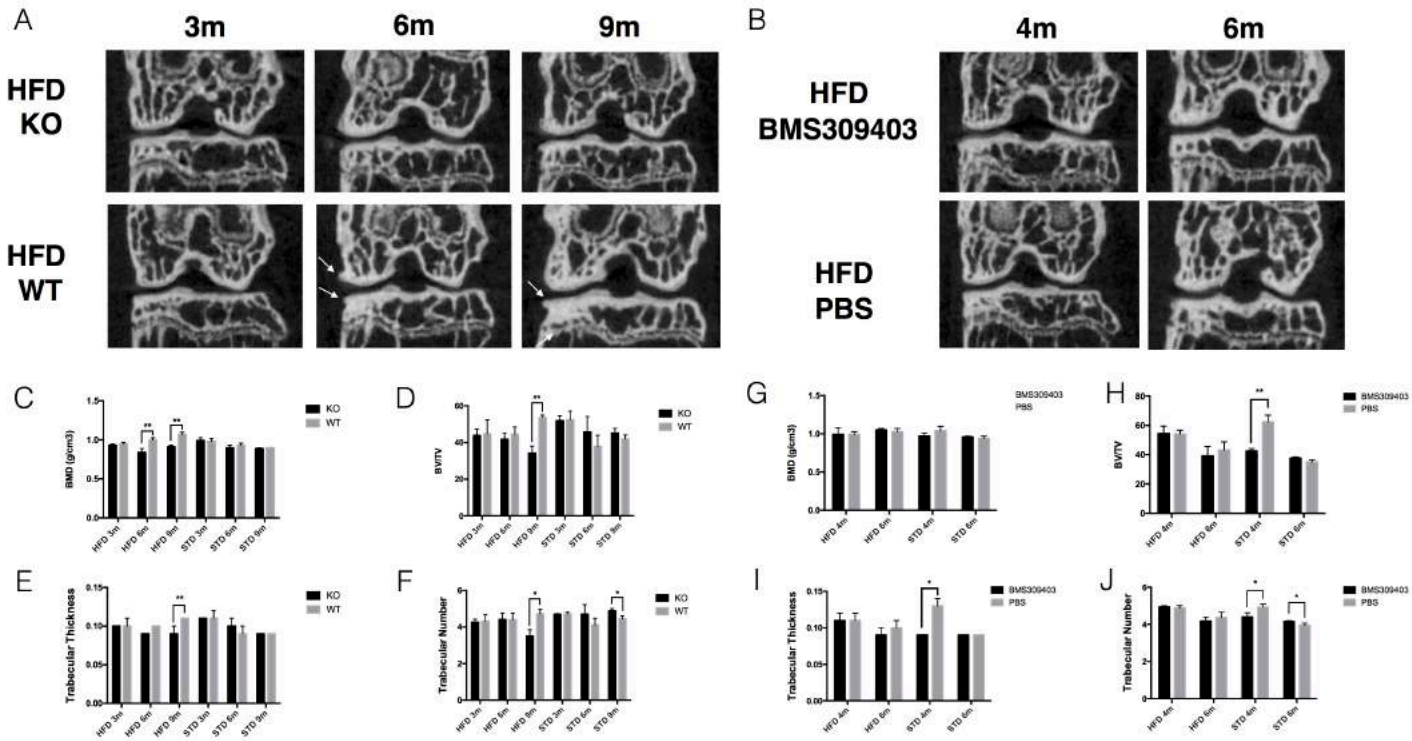

Histopathological Analysis of Healing Responses to a Novel Tendon Transfer Surgery in a Chicken Model

Anthony Le, BS[1], Duncan S. Russell, BVMS(Hons), DACVP[3], Maureen K. Larson, MS[3], Jennifer Warnock, DVM, PhD, DACVS[3], Geoffrey R. Browning, DVM, MS[3], Kay A. Fischer, MS[3], James Sweeney, PhD[1], Ravi Balasubramanian, PhD[2]
[1]School of Chemical, Biological, and Environmental Engineering, College of Engineering, [2]School of Mechanical, Industrial, and Manufacturing Engineering, College of Engineering, [3]College of Veterinary Medicine, Oregon State University, Corvallis, OR, 97331, USA

Introduction: High median-ulnar nerve palsy is a neuromuscular condition where the median and ulnar nerves in the forearm are damaged. As a result, the Flexor Digitorum Profundus (FDP), Flexor Digitorum Superficialis (FDS), and the intrinsic hand muscles are dysfunctional leading to sensory loss and weakness in the index, middle, ring, and little fingers [1][2][3]. Patients with this condition have impaired flexion function in their four fingers, which affects the performance of physical interaction tasks such as grasping a doorknob. The current surgical procedure for restoring finger flexion is a tendon transfer surgery that detaches the four FDP tendons and sutures them directly to the single Extensor Carpi Radialis Long (ECRL) muscle innervated by the radial nerve [4][5]. While this procedure restores finger flexion, it couples the movements of all four fingers and prevents them from individually adapting to an object's shape during grasping tasks. To address this limitation, we are developing a tendon-transfer surgical procedure that incorporates a passive artificial strut-shaped implant in the tendon network to create a differential mechanism between the ECRL muscle and the four FDP tendons. Our previous studies using human and chicken cadavers have shown that this implant-based surgery significantly improves adaptability of the fingers in physical interaction tasks [6][7][8]. As the next step, our group conducted an in vivo pilot study on a chicken model, using histopathology to evaluate the postoperative healing responses to this novel surgery.

Methods: The implant was made of ultra-high-molecular-weight polyethylene and autoclaved. Twenty-nine Cornish Cross chickens were randomly assigned to one of three treatment groups: control (n=7), implant (n=12), and sham (n=10). During surgery, the Extensor Digitorum Longus (EDL) tendon was exposed with a 1.5 cm incision on the dorsal side of the leg at approximately the same level at as the spur. The incision was made in between scales as much as possible, but some scales had to be transected. The EDL tendon was dissected from the surrounding connective tissue at the bifurcation. The implant was placed under and sutured to the EDL tendon branches approximately 10 mm distal to the bifurcation with simple interrupted stitches using 5-0 Prolene (see Fig. 1). The skin was sutured closed with an apposing cruciate pattern using 4-0 Nylon. The sham group underwent the same surgical procedure without implant insertion. Instead, each tendon branch was simply sutured with 5-0 Prolene. The control group did not undergo any surgical procedures. Chickens were euthanized approximately 5 to 10 weeks after surgery, and legs were harvested for routine histopathology. Samples were evaluated for epidermal ulceration, superficial and deep inflammation, hygroma/seroma, fibrosis, periosteal reaction, and cortical resorption. Peritendinous fibrosis levels were graded as absent, mild, moderate and severe.

Results: Both the implant and sham groups had moderate to severe circumferential fibrosis around the tendons, often in close association with fluid-filled cavities (seroma/hygroma) between the tendon and surrounding connective tissue. The control group did not have any peritendinous fibrosis (see Figs. 2 and 3). There was a greater frequency of periosteal reaction in the implant group than in the sham and control groups (6/9 verse 3/8 chickens, respectively). The reaction was more pronounced on the dorsal surface of the metatarsus, frequently accompanied with cortical resorption, in proximity of the implant (see Figs. 2 and 3). Although, the combination of periosteal proliferation and cortical resorption can be an indication of infection, no inflammation or bacteria were identified in histopathology, which suggest that this reaction was sterile. The implant and sham groups had hyperkeratosis of the dorsal skin, but with no indication of epidermal inflammation or ulceration. There was no morphologic evidence of osteomyelitis or deep bacterial infection.

Conclusion: Histopathological responses to injury were similar between the implant and sham groups, with similar peritendinous fibrosis. A marginally greater periosteal reaction in the implant group might warrant implant modifications, including a smoother, thinner profile, a non-fouling coating, with a more minimally invasive attachment mechanism. Overall, the pilot study results were promising as there were no manifestations of infection, no abnormal discharges, and the sutures apposing the skin were not compromised. Nevertheless, we are currently addressing the inherent limitations of the descriptive rank scoring methodology and absence of functional evaluation. We also plan to incorporate both force plate gait analysis and range of motion measurements to supplement the histological data.

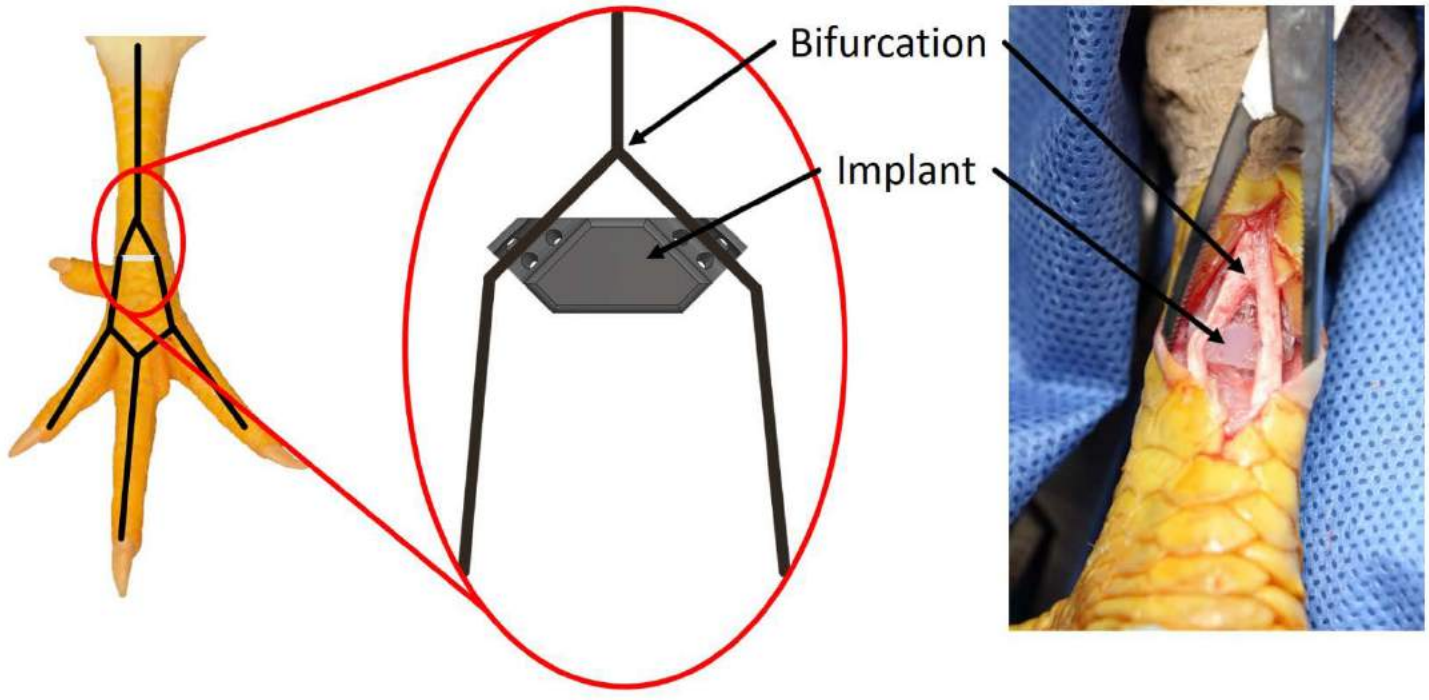

center); implant inserted into the tendon network during surgery (right).

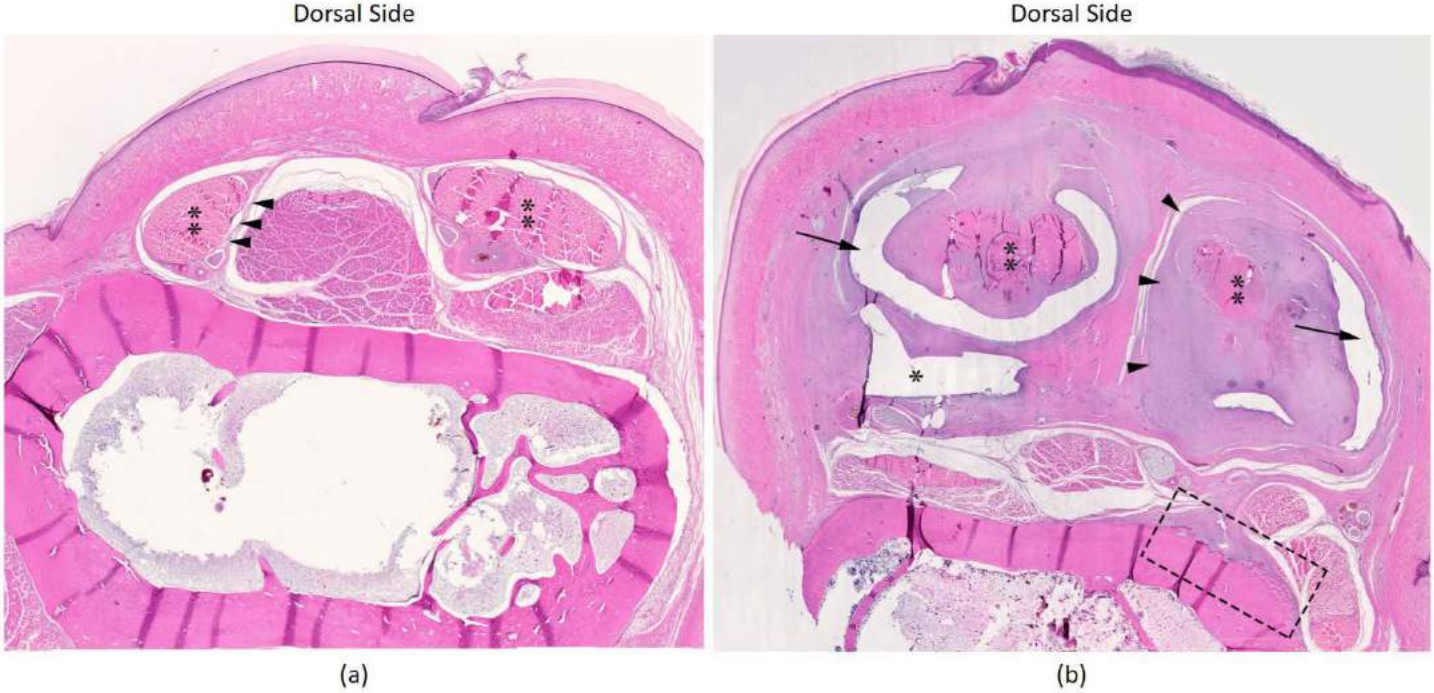

Extensor Digitorum Longus tendons on dorsal surface of the metatarsus; ► indicates morphologically normal epitenon. (b) Histology of an implanted chicken leg stained by Hematoxylin and Eosin, 2x magnification; * indicates artefactual cavity representing implant location; ** indicates the Extensor Digitorum Longus tendons on the dorsal surface of the metatarsus; ► indicates severe circumferential expansion of the epitenon and surrounding connective tissue by fibrosis; ➞ indicates fluid filled cavity(seroma/hygroma); --- rectangle indicates cortical resorption (scalloped surface in upper half) and periosteal proliferation (lower half).

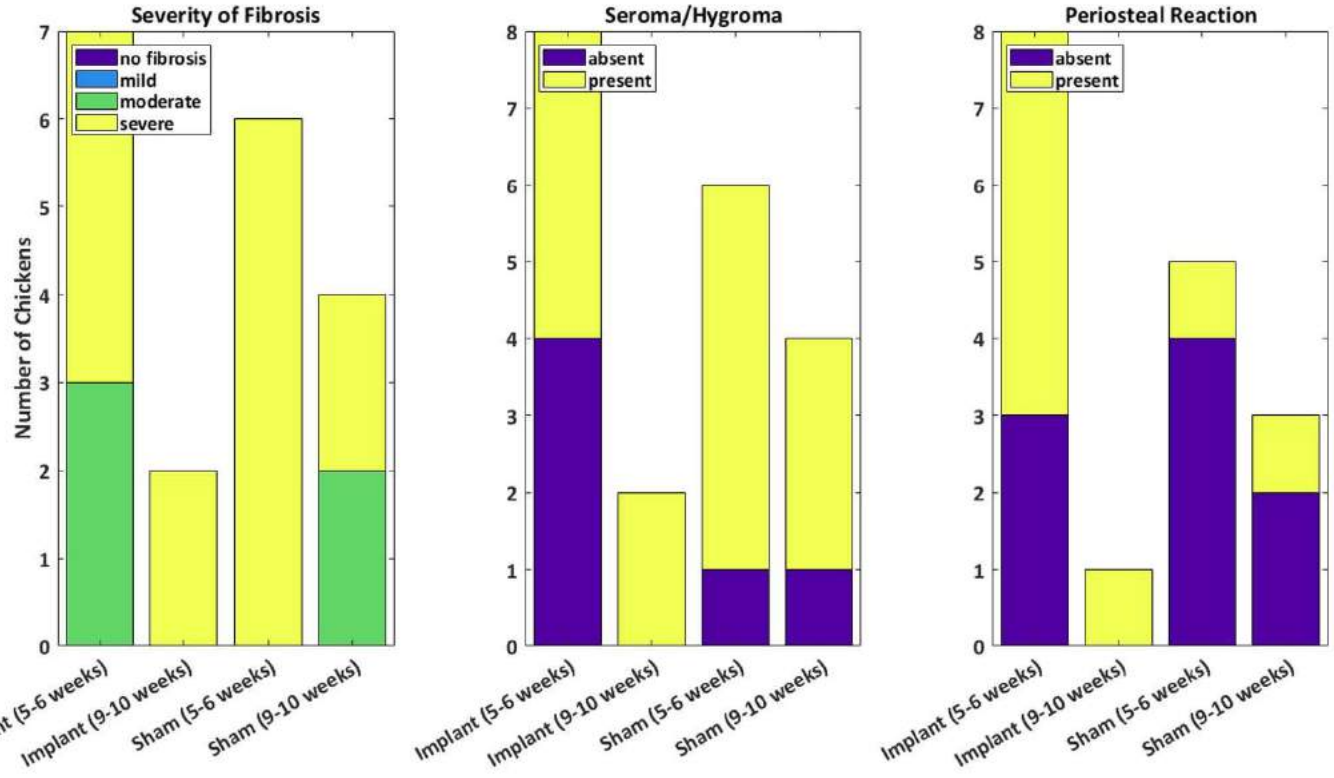

Figure 3: Comparison of fibrosis severity, frequency of hygroma, and frequency of periosteal reactions between the implant and sham groups at 5 to 6 weeks of implantation and at 9 to 10 weeks of implantation. Period of implantation was determined as the time between the surgery and euthanization dates. It is worth noting that these evaluations represent individual chickens, so potential variability can arise within a treatment group. Additionally, it may be concluded that there were more severe cases of fibrosis in the sham group compared to the implant group, but with the inherent limitations of the descriptive rank scoring methodology, the difference between moderate and severe fibrosis may only be marginal. A significance difference in fibrosis severity would be demonstrated if more absent/mild cases of fibrosis were found in one of the groups.

References:

[1] P. W. Brand and A. Hollister, *Clinical Mechanics of the Hand,* 2nd ed. Mosby Year Book Inc., 1993.
[2] D. P. Green, R. N. Hotchkiss, W. C. Pederson, et al., *Green's Operative Hand Surgery,* vol. 1 and 2, 5th ed. Elsevier, 2005.
[3] D. C. Riordan, "Tendon transfers for median, ulnar, or radial nerve palsy," *The Hand,* vol. 1, pp. 42-46, 1969.
[4] J. Hunter, L. Schneider, and E. Mackin, "Tendon Transfers," in *Tendon Surgery in the Hand.* St. Louis: C. V. Mosby Co., 1987, pp. 395-515.
[5] P. W. Brand, "Tendon transfers for median and ulnar nerve paralysis," *Orthop Clin North Am,* vol. 1, no. 2, pp. 447-454, 1970.
[6] T. Homayouni, K. N. Underwood, K. C. Beyer, E. R. Martin, C. H. Allan, and R. Balasubramanian, "Modeling implantable passive mechanisms for modifying the transmission of forces and movements between muscle and tendons," in *IEEE Trans Biomed Eng,* vol. 62, no. 9, pp. 2208-2214, 2015.
[7] K. L. Mardula, R. Balasubramanian, and C. H. Allan, "Implanted passive engineering mechanism improves hand function after tendon transfer surgery: a cadaver-based study," *Hand,* vol. 10, no. 1, pp. 116-122, 2015.
[8] J. Montgomery, R. Balasubramanian, K. L. Mardula, and C. H. Allan, "New tendon-transfer surgery for ulnar-median nerve palsy using embedded adaptive engineering mechanisms," in *Proceedings of 11th Int Sym of Comput Methods Biomech Biomed Engin,* Salt Lake City, UT, 2013.

RON kinase: A new target for treatment of cancer-induced bone destruction and osteoporosis

Jaime Fornetti, PhD[1], Le Zhan, BS[2], Xuli Wang, PhD[2], Alana L. Welm, PhD[1]

[1]Department of Oncological Sciences, Huntsman Cancer Institute, Salt Lake City, UT, [2]Department of Radiology and Imagining Sciences, School of Medicine, University of Utah, Salt Lake City, UT,

Bone-destructive pathological conditions, such as cancer metastasis and osteoporosis, are a significant problem. Over half of Americans age 50 and older are estimated to have osteoporosis or low bone mass[1]. Additionally, over 400,000 people annually in the United States have cancer metastasis to the bone[2]. The severe bone loss associated with osteolytic metastasis causes profound pain, nerve compression, hypercalcemia, and debilitating fractures[3,4]. Despite current therapies, many patients with bone metastasis eventually progress to develop new bone lesions or serious skeletal complications[5], highlighting the need for additional therapies for osteolytic bone disease. Here, we identify the macrophage-stimulating protein (MSP)/RON tyrosine kinase signaling pathway as a potential new therapeutic target for osteolytic metastasis and osteoporosis. Additionally, we use experimental osteolytic bone metastasis models to evaluate novel nanotherapies designed to target osteolytic bone lesions.

Increased expression of the MSP signaling pathway occurs in approximately 40% of breast cancers and is sufficient to drive bone metastasis in a preclinical breast cancer model[6]. In bone metastasis models, MSP expression by tumors leads to increased bone destruction through its receptor, RON tyrosine kinase, on host cells (Figure 1a), via a pathway complementary to RANKL and TGFβ. MSP-induced osteolysis was blocked in mice deficient for RON tyrosine kinase activity or following treatment with the RON inhibitor BMS-777607/ASLAN002 in models of metastasis (Figures 1a and b) and osteoporosis. To determine whether RON inhibitors may also be effective in patients, plasma samples from phase 1 clinical testing of BMS-777607/ASLAN002 were analyzed for the bone resorption marker β-cross-linked C-telopeptide (CTX) and the bone formation marker bone-specific alkaline phosphatase (BSAP). After 15-28 days of treatment, 62% (13 of 21) of subjects experienced a decrease in CTX levels from baseline, with the best responses seen in women (Figure 2a). Notably, 7 of 11 women had a reduction in CTX of ≥25%, meeting the Mayo Clinic guidelines[7] for a positive response to bone antiresorptive therapies. This decrease in CTX following treatment was accompanied by an increase in BSAP (Figure 2b). All patients in the study except for one were greater than 50 years of age; therefore, we speculate that the superior response rate observed in women may be due to the high levels of bone loss associated with menopause. These data indicate that RON inhibitors may be effective in humans with lytic bone diseases.

To further improve bioavailability and effectiveness of RON inhibitors, new bone-targeting, enzyme-activated theranostics are being designed based on novel synthetic multifunctional carriers (MFC). MFC are able to form stable, self-assembling nanoparticles with hydrophobic drugs, such as BMS-777607/ASLAN002, through hydrophobic interactions. Such nanoparticles allow for systemic injection and improved bioavailability. The bone-targeting ligand alendronate (ALN) is attached to MFC, which targets the nanoparticles to skeletal tissue. For optical imaging, Cy5.5 is conjugated into MFC via a MMP-2 cleavable peptide, which under normal conditions diminishes Cy5.5 fluorescence due to FRET, but restores fluorescence in MMP-2 rich microenvironments, such as osteolytic lesions. Our preliminary data show that:

1) Drug-loaded nanoparticles are 102.6 ± 1.6 nm in diameter and aqueous solubility of BMS-777607/ASLAN002 was
   greatly improved.
2) Bone-targeting capacity was achieved; approximately 92 ± 3.3% of ALN-containing nanoparticles could bind to hydroxylapatite within 30 minutes.
3) Cy5.5 fluorescence imaging enhancement was observed in cultured breast cancer cells (MDA-MB-231).
4) The drug release profile showed that 78 ± 2.1% of BMS-777607/ASLAN002 could be released from nanoparticles

Taken together, our preclinical and clinical data indicate that RON inhibitors may be effective against osteolytic bone diseases. Furthermore, our preliminary data show that using synthetic multifunctional carriers to deliver the RON inhibitor BMS-777607/ASLAN002 improves aqueous solubility and drug release in the presence of MMP-2. These data provide rationale for the continued investigation of RON inhibitors for use in patients with osteolytic bone diseases.

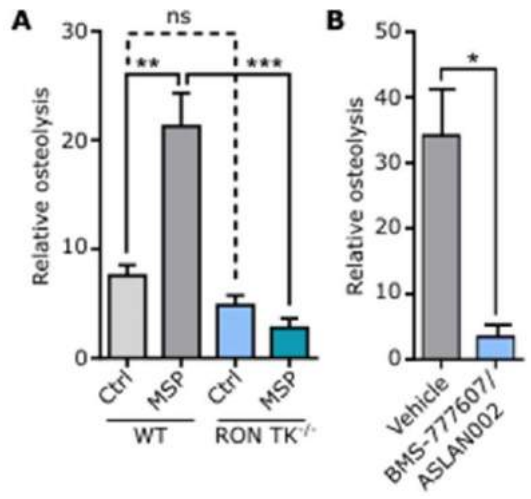

Figure 1. MSP-induced osteolysis requires host RON kinase activity and can be blocked with the RON inhibitor BMS-777607/ASLAN002. Quantification of osteolytic area, determined by high resolution ex vivo x-ray, in tibias of mice 42 days after tumor cell injection in wild-type (WT) or RON tyrosine kinase-deficient hosts (RON $TK^{-/-}$) (A) or in WT hosts treated with BMS777607/ASLAN002 (B). *p=0.021, **p=0.0013, ***p=0.0001, ns=not significant (p<0.05)

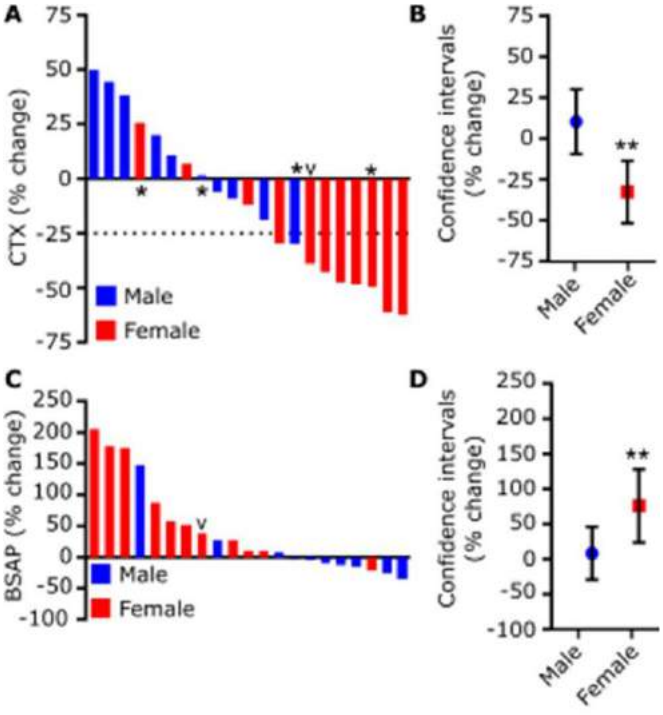

Figure 2. The RON inhibitor BMS-777607/ASLAN002 reduces bone turnover in humans. (A) Quantification of the percent change in plasma CTX levels (compared to baseline prior to drug treatment) in blood plasma of 21 patients that received BMS-777607/ASLAN002 for at least 15 days in a Phase 1 clinical trial. Most patients received BMS-777607/ASLAN002 for 28 days; values reported correspond to the difference between baseline (day 0) and the 28-day time point. Exceptions in duration of treatment and CTX testing are noted (*15 days). Blue bars represent males and red bars represent females. Arrowhead denotes a patient less than 50 years of age (42 years). (B) Ninety-five percent confidence intervals for percent change in CTX for males and females; **p=0.0035, one-sample t tests versus a hypothetical mean of 0 (no change following treatment compared to baseline). (C) Quantification of the percent change in bone-specific alkaline phosphatase (BSAP) levels (compared to baseline) in blood plasma of 22 patients that received BMS-777607/ASLAN002 for 28 days. 18 of the patients are also shown in (A). (D) Ninety-five percent confidence intervals for percent change in BSAP for males and females; **p=0.0090, one-sample t tests versus a hypothetical mean of 0 (no change following treatment compared to baseline). Blue bars represent males and red bars represent females.

References [1]www.nof.org (2011) [2]R. E. Coleman, A. Lipton, G. D. Roodman, T. A. Guise, B. F. Boyce, A. M. Brufsky, P. Clezardin, P. I. Croucher, J. R. Gralow, P. Hadji, I. Holen, G. R. Mundy, M. R. Smith, L. J. Suva, Metastasis and bone loss: advancing treatment and prevention. *Cancer Treat Rev* 36, 615-620 (2010) [3]R. E. Coleman, Future directions in the treatment and prevention of bone metastases. Am J Clin Oncol 25, S32-38 (2002). [4]I. J. Diel, E. F. Solomayer, G. Bastert, Treatment of metastatic bone disease in breast cancer: bisphosphonates. Clin Breast Cancer 1, 43-51 (2000). [5]A. T. Stopeck, A. Lipton, J. J. Body, G. G. Steger, K. Tonkin, R. H. de Boer, M. Lichinitser, Y. Fujiwara, D. A. Yardley, M. Viniegra,

M. Fan, Q. Jiang, R. Dansey, S. Jun, A. Braun, Denosumab compared with zoledronic acid for the treatment of bone metastases in patients with advanced breast cancer: a randomized, double-blind study. J Clin Oncol 28, 5132-5139 (2010). [6]A. L. Welm, Sneddon, J. B., Taylor, C., Nuyten, D.S.A., van de Vijver, M.A., Hasegawa, B. H., and Bishop, J. Michael, The macrophage stimulating protein pathway promotes metastasis in a mouse model for breast cancer and predicts poor prognosis in humans. Proc Natl Acad Sci U S A 104, 7570-7575 (2007). [7]Mayo Clinic Medical Laboratories, Beta-CrossLaps (Beta-CTx), Serum. http://www.mayomedicallaboratories.com/testcatalog/Clinical+and+Interpretive/83175.

The Pros and Cons of FEA

Christopher Jacobs
Columbia University

Computer simulation is one of the most powerful tools available to the applied mechanician to understand the complexities of mechanical behavior. It has revolutionized design of virtually all man-made structures from aircraft and buildings to cell phones and computers. It has also become a relatively important tool in biomechanics and simulation of tissues and implants has become routine. Indeed we appear to be on the verge of patient specific simulation becoming a critical tool in orthopaedic and cardiovascular surgery. However, its use as a tool of basic science is much less clear. In this chapter we explore the potential for mechanical simulation to contribute to improve fundamental understanding of biology. We consider the challenges of creating a model of a mechanobiological system with experimental validation. We propose that the area of cell mechanics is a particular area where simulation can make critically important contributions to understanding basic physiology and pathology and outline potential areas of future advancement.

Cell Mechanics: The Role of Simulation

Christopher Jacobs
Columbia University

Computer simulation is one of the most powerful tools available to the applied mechanician to understand the complexities of mechanical behavior. It has revolutionized design of virtually all man-made structures from aircraft and buildings to cell phones and computers. It has also become a relatively important tool in biomechanics and simulation of tissues and implants has become routine. Indeed we appear to be on the verge of patient specific simulation becoming a critical tool in orthopaedic and cardiovascular surgery. However, its use as a tool of basic science is much less clear. In this chapter we explore the potential for mechanical simulation to contribute to improve fundamental understanding of biology. We consider the challenges of creating a model of a mechanobiological system with experimental validation. We propose that the area of cell mechanics is a particular area where simulation can make critically important contributions to understanding basic physiology and pathology and outline potential areas of future advancement.

Finite Element Analysis for Clinical Assessment of Whole-Bone Strength

David Kopperdahl, PhD[1]
[1]O.N. Diagnostics, Berkeley, CA

Osteoporosis-related fracture remains a devastating clinical problem. Over 300,000 hip fractures occur each year in the U.S. and up to 25% of hip-fracture patients die within a year of their injury.[2] Despite the importance of this clinical problem, only 12–14% of those who need testing receive it, and diagnostic testing rates for osteoporosis are in decline.[4,5] In addition, the current clinical standard for osteoporosis assessment — bone mineral density (BMD) testing by dual energy absorptiometry (DXA) — identifies less than half of the patients who eventually fracture.[6] Thus, there remains a pressing need to improve both testing rates and testing sensitivity so that more patients at high risk of fracture can be correctly identified.

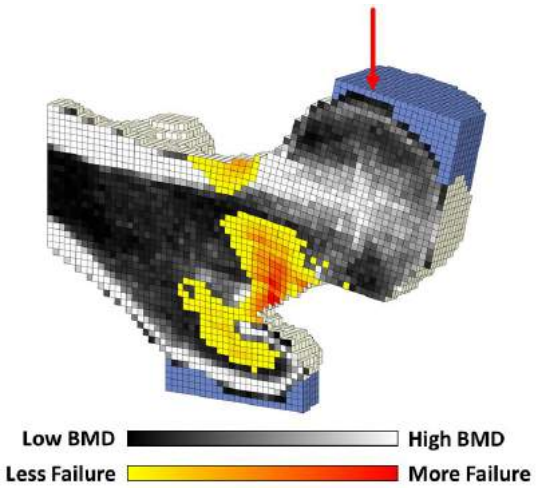

Figure 1: BCT-based virtual stress testing of the proximal femur using a patient's abdominal CT enterography scan, the colored regions showing regions of bone failure under virtual loading for a simulated sideways fall.[1]

Clinical assessment of bone strength using computed tomography (CT) based finite element analysis (FEA) has the potential to improve both the frequency and sensitivity of testing for risk of fragility fracture. In this technique, the three dimensional geometry of the bone of interest, typically a proximal femur or lumbar vertebra, is extracted from a CT image. The bone image is converted to a finite element and each point in the model is assigned material properties based on CT attenuation values. Strength is estimated by virtually loading the bone to failure under conditions typifying a fracture event, such as a sideways fall to the hip or a compressive overload of the spine (**Figure 1**). Cadaver studies used to validate FEA-derived bone strength estimates from clinical resolution CT scans indicate that such estimates better predict experimentally measured bone strength than do BMD-only measurements.[7] FEA-derived strength estimates are highly predictive of incident hip and spine fracture,[3,8,9] and the approach is cleared by the FDA for clinical use.

The ability to apply this technique using CT scans acquired for non-bone related conditions provides the opportunity to substantially expand the number of individuals tested. Each year, over 10 million CT scans with coverage of the hip or lumbar spine are taken in the US for patients meeting the criteria for osteoporosis screening, most of whom have not had a DXA exam.[10] Indeed, many such patients have medical conditions that can compromise bone health, such as inflammatory bowel disease, a history of heavy smoking, diabetes, breast cancer, and chronic kidney disease, but often their bone health is not assessed. Phantomless calibration techniques which do not use a bone mineral calibration phantom, allow the use of standard clinical CT images with the need to retrain radiology personnel or change imaging protocols. With proper calibration, most of these clinical CT scans can be used to assess BMD and bone strength. CT-based measurements of areal BMD are equivalent to those obtained using DXA,[1,11] but there is good reason to look beyond BMD.

Bone strength from FEA may also improve the sensitivity relative to BMD testing for identifying those at high risk of fracture. While average BMD is a key component of bone strength, other factors including bone geometry, the distribution of bone mass, and the direction of applied forces also determine bone strength. Incorporating these other characteristics into the measurement can improve the fidelity of the bone strength estimate, and fracture outcome studies have identified patients without osteoporosis who are nevertheless at high risk of fracture due to fragile bone strength (**Figure 2**).[3,8] Such patients might have, for example, small bones, relatively weak cortical or trabecular compartments, or focally weak sub-regions, features sometimes not detected by measures of BMD.

Despite the success so far of clinical bone strength assessment, important issues remain in order to realize its full potential. First, the field lacks consensus regarding optimal finite element methodologies — including meshing and image processing schemes, constitutive modeling of bone tissue, cortical shell modeling, failure criteria, or loading — for best estimating femoral strength, particularly when utilizing clinical-quality CT scans. Second, current clinical implementations do not account for known biomechanical factors that influence fracture etiology, most importantly the probability of experiencing an overload event such as a fall, and the magnitude and direction of applied forces. CT-based measurements of muscle composition have been associated with hip fracture,[12] as have measurements of soft tissues over the greater trochanter, which can influence applied forces by dissipating the energy of impact.[13] Thus, fracture prediction may be further improved by combining bone strength with the biomechanics of an overload event, informed by additional imaging information and other clinical risk factors. The unique aspect of the finite element modeling approach is that it goes beyond a statistical regression of risk factors and instead provides a framework for incorporating these data mechanistically into a patient-specific, dynamic model of fracture.

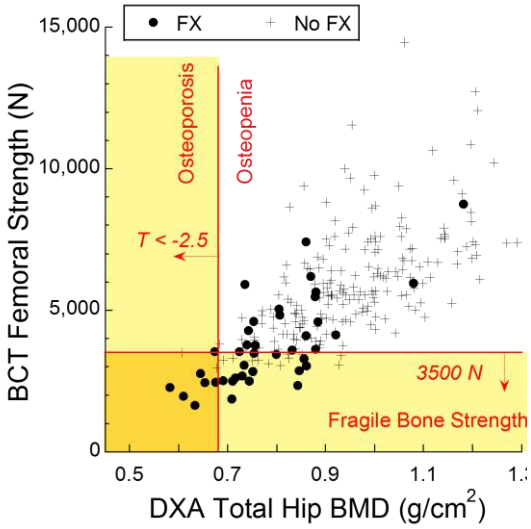

Figure 2: Added clinical value of BCT: Prediction of new hip fractures in elderly men, showing many more men who fractured (solid points) had fragile bone strength (<3,500 N) than had osteoporosis (T<-2.5). "High-Risk" patients (yellow zone) can test positive for either BMD-defined osteoporosis or finite element-derived fragile bone strength.[3]

References

1. Weber, N.K., et al., *Validation of a CT-derived method for osteoporosis screening in IBD patients undergoing contrast-enhanced CT enterography.* Am J Gastroenterol, 2014. **109**(3): p. 401-8.
2. Burge, R., et al., *Incidence and economic burden of osteoporosis-related fractures in the United States, 2005-2025.* J Bone Miner Res, 2007. **22**(3): p. 465-75.
3. Orwoll, E.S., et al., *Finite element analysis of the proximal femur and hip fracture risk in older men.* J Bone Miner Res, 2009. **24**(3): p. 475-83.
4. Curtis, J.R., et al., *Longitudinal trends in use of bone mass measurement among older americans, 1999-2005.* J Bone Miner Res, 2008. **23**(7): p. 1061-7.
5. King, A.B. and Fiorentino, D.M., *Medicare payment cuts for osteoporosis testing reduced use despite tests' benefit in reducing fractures.* Health Aff (Millwood), 2011. **30**(12): p. 2362-70.
6. Schuit, S.C., et al., *Fracture incidence and association with bone mineral density in elderly men and women: the Rotterdam Study.* Bone, 2004. **34**(1): p. 195-202.
7. Zysset, P.K., et al., *Finite element analysis for prediction of bone strength.* Bonekey Rep, 2013. **2**: p. 386.
8. Kopperdahl, D.L., et al., *Assessment of incident spine and hip fractures in women and men using finite element analysis of CT scans.* J Bone Miner Res, 2014. **29**(3): p. 570-80.
9. Wang, X., et al., *Prediction of new clinical vertebral fractures in elderly men using finite element analysis of CT scans.* J Bone Miner Res, 2012. **27**(4): p. 808-16.
10. Berrington de Gonzalez, A., et al., *Projected cancer risks from computed tomographic scans performed in the United States in 2007.* Arch Intern Med, 2009. **169**(22): p. 2071-7.
11. Fidler, J.L., et al., *Comprehensive assessment of osteoporosis and bone fragility with CT colonography.* Radiology, 2016. **278**(1): p. 172-80.
12. Lang, T., et al., *Computed tomographic measurements of thigh muscle cross-sectional area and attenuation coefficient predict hip fracture: the health, aging, and body composition study.* J Bone Miner Res, 2010. **25**(3): p. 513-9.
13. Bouxsein, M.L., et al., *Contribution of trochanteric soft tissues to fall force estimates, the factor of risk and prediction of hip fracture risk.* J Bone Miner Res, 2007. **22**(6): p. 825-31.

Prx-1 Embryonic Specification Is Retained in a Postnatal Regenerative Stem Cell Population that Gives Rise to Skeletal, Fat, and Vascular Tissues

Beth Bragdon, PhD1, Andrew Bennie, MS1, Jenny Lei, BS2, Elise F. Morgan, PhD2, Louis C. Gerstenfeld, PhD1
1Boston University School of Medicine, Boston, MA, 2Boston University, College of Engineering, Boston, MA

Mesenchymal stem cell (MSC) is used to describe a population of adult stem cells that are multipotent and contribute to bone homeostasis and repair. However, this population of cells has not been identified *in vivo* and is recently suggested to be pericytes. A cell population conditionally expressing Prx1 previously shown to identify embryonic appendicular and calvaria tissues and postnatally associated with bone formation and repair was used for *in vivo* lineage tracking studies. Male and female mice aged 8-11 weeks were used in IACUC approved studies. Different models of postnatal bone formation were used: closed stabilized transverse femoral fracture, distraction osteogenesis (limb lengthening), and ectopic bone formation at appendicular and axial sites (limb, sternum, spine). Tamoxifen inducible Prx1 Cre ERT transgenic mice were crossed with B6.Cg-Gt(ROSA)26sor<tm14(CAG-tdTomato)Hze>/J mice to create Prx1/Ai14 reporter. Subsequently Prx1/Ai14 mice were crossed with B6,129S7-Rag1tm1Mom/J to create a transgenic reporter mouse allowing for the implantation of human demineralized bone matrix (DBM) to induce ectopic bone. Tamoxifen was administered and allowed to be washed out for at least 28 days or for only 3 days prior to surgery or ectopic bone induction in order to follow the specified population through postnatal bone formation. Under both homeostatic and short duration labeling conditions cell labeling was observed in differentiated osteoblasts and osteocytes in cortical and trabecular bone and cells on both periosteal and endosteal surfaces of both fore and hind limbs and cranium. Immunofluorescence (IF) confirmed that adipocytes and smooth muscle cells in vessels within the muscle compartment of the appendicular skeleton were also labeled (see figure 1). Prx1 was induced in regenerative tissues after bone injury (fracture, ~61% of cells were derived from Prx1) and distraction osteogenesis within the same lineages as seen under homeostatic labeling. Ectopic bone induced in response to DBM implantation in the limbs showed labelled cells differentiated into chondrocytes, osteoblasts, adipocytes, and vessel associated smooth muscle however ectopic bone induction at axial skeletal sites such as sternum and spine did not show labelled cells. These results suggest that Prx1 expression connotes a multi-potential postnatal MSC that retained its embryonic tissue specification and contributes to both postnatal homeostatic maintenance and tissue repair in response to injury.

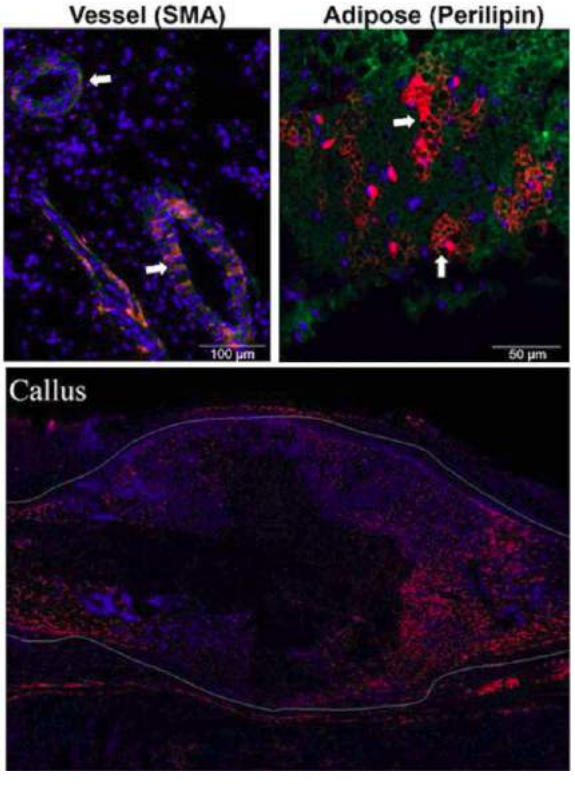

Figure 1. Prx1 driven Ai14 was induced with tamoxifen, labeling cells red. Nuclei were stained with dapi (blue). Top. IF was performed to identify smooth muscle of vessels (SMA shown in green) or perilipin (shown in green) for adipose tissue. Bottom. Fracture callus at day 14. White line outlines callus.

Improved Fracture Risk Assessment via Bound/Pore Water MRI

Jeffry S. Nyman, PhD[1,2], Mary Kate Manhard, PhD[1], S. Bobo Tanner, MD[2], Dong Kyu Kim[1], Kevin D. Harkins, PhD[1], Sasidhar Uppuganti, MS[2], Donald Lee, MD[2], Mark D. Does, PhD[1]

[1]Vanderbilt University, Nashville, TN, USA, [2]Vanderbilt University Medical Center, Nashville, TN, USA

Introduction

The clinical standard imaging tool for evaluating fracture risk, dual-energy X-ray absorptiometry (DXA), is a projection method that does not discern the contributions of macro-structure, trabecular micro-architecture, collagen, or cortical porosity to fracture resistance. Quantitative computed tomography is able to partially circumvent the shortcomings of DXA but remains limited in that it, and other X-ray based methods, are sensitive only to the mineral content of bone. However, the soft-tissue component of bone is critical for conferring toughness and overall fracture resistance to bone. In contrast to X-ray based methods, MRI is sensitive to water, which exists in both the pore spaces of bone mineral (pore water, PW) and bound to the organic matrix (bound water, BW). Thus, MRI has the potential to report on both cortical porosity and the bone matrix, thereby offering unique insight into its health and biomechanical properties.

Previous work on cadaveric cortical bone specimens has demonstrated that BW and PW have unique transverse relaxation characteristics [1] and that their volumetric concentrations (C_{bw} and C_{pw}, respectively) correlate with various biomechanical properties [2-4]. Motivated by these observations, MRI methods to measure BW and PW in a clinically practical manner have been developed using different strategies [5-8], and we have evaluated C_{bw} and C_{pw} in vivo in healthy controls [9]. With these tools in place, BW/PW-MRI studies in two relevant patient populations has begun, and this presentation reports the preliminary findings. With the aim of evaluating the potential for BW/PW-MRI to serve as quantitative biomarkers of osteoporosis, we hypothesize that MRI measures of C_{bw} and C_{pw} are significantly lower and higher, respectively, for women with osteoporosis than compared to age matched controls. Also, for the purpose of evaluating the potential for BW/PW-MRI to better predict fragility fracture risk, we hypothesize that, C_{bw} and C_{pw} will provide more sensitivity and specificity than DXA and age in specific classifications of women with recent history of fragility fracture with respect to controls.

Methods

The Adiabatic Inversion Recovery (AIR) and Double Adiabatic Full Passage (DAFP) sequences [9] were used on a 3T Phillips Achieva scanner with 3D UTE readout to measure C_{bw} and C_{pw}, respectively (Fig 1), in two patient populations and respective controls. In one study, images were collected from the tibia of N=7 untreated osteoporotic patients (mean age: 63.6 yr, range: 58-73 yr) and N=7 age-matched controls (mean: 61.6 yr, range:59-69 yr). These subjects were recruited by a rheumatologist with an osteoporosis clinic. In another study, images were collected from the distal-third radius of 16 female subjects. Seven of these subjects had a recent low-energy fracture of the contralateral distal radius (mean age: 55.5. yr, range: 39-76 yr), and the 9 healthy volunteers (mean age: 44.8 yr, range: 22-63 yr) included 3 who had experienced a high-energy fracture of the contralateral distal radius. Low-energy fractures resulted from a fall from standing height or less, while high-energy fractures resulted from a collision (e.g., motor vehicle accident, fall from a ladder). For this study, DXA scans (Lunar iDXA, GE Healthcare) were acquired within a few days of the MRI measurements.

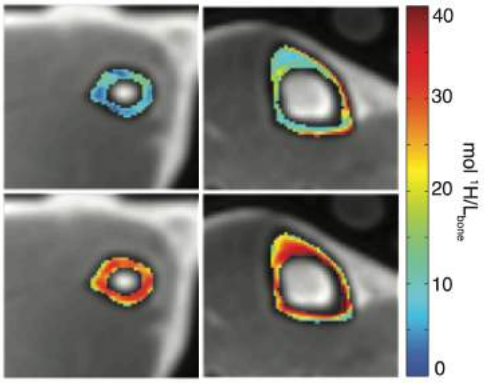

Fig 1 Representative In Vivo C_{pw} (top) and C_{bw} (bottom) maps; radius (left) and tibia (right), extracted from 3D volumes.

Results and Discussion

The results of the study of osteoporosis patients and age-matched controls are shown in Fig 2. Both C_{pw} (left) and C_{bw} (right) show statistically significant differences between these two populations ($p < 0.05$ for C_{pw}; $p < 0.01$ for C_{bw}). Although distinguishing the osteoporosis patients from age-matched controls is not a clinically important measure, these results demonstrate that both C_{bw} and C_{pw} are sensitive to the changes in bone resulting from osteoporosis. Since the osteoporotic women were started on osteoporosis therapy, future studies will involve evaluation of the UTE-MRI measures to determine

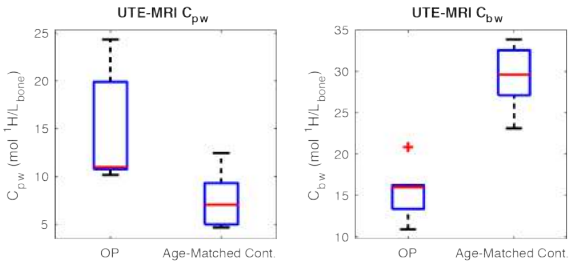

Fig 2 Boxplot comparison of C_{bw} and C_{pw} across 7 osteoporosis (OP) patients and 7 age-matched controls. T-tests show a significant difference between OP and controls for C_{pw} (p=0.03) and C_{bw} (p = 0.001).

how these quantitative biomarkers change in response to treatment.

The results from the study of subjects with and without a recent low-energy radius fracture are shown in Fig 3: age, DXA Hip T-Score, and UTE-MRI measures of C_{pw} and C_{bw} are plotted for every subject. The data from subjects with recent low-energy fracture are plotted in orange, and the data from control subjects are in blue. Also, subjects with T-score in the osteopenia range (-2.5 < T < -1) are further identified with a black dot. It is apparent that each UTE-MRI is a better classifier of fracture vs control than either Age or DXA T-Score since there was less overlap in C_{bw} and C_{pw} between the 2 groups compared to Age and T-scores. Interestingly, C_{bw} separates fragility fracture from control in osteopenic subjects (black dots) perfectly. There was a 40 yr old in the control group with high C_{pw} and and high C_{bw}, and a 22 yr old in the control group with low C_{pw} and and low C_{bw}, suggesting these measurements are not just surrogates of one another. Using logistic regression and ROC analysis, the area-under curve (AUC) for classification of fracture/control by age, DXA, C_{pw}, and C_{bw}, was 0.72, 0.77, 0.79, and 0.89, respectively. Using both C_{pw} and C_{bw} classification resulted in an AUC = 0.92, while using age and DXA resulted in an AUC = 0.81. Given the relatively small sample size of this preliminary study, none of these AUC values are statistically different from any other; however, the results suggest the potential of BW/PW MRI to help identify which osteopenic subjects have an elevated risk of low-energy fracture and, consequently, should be treated.

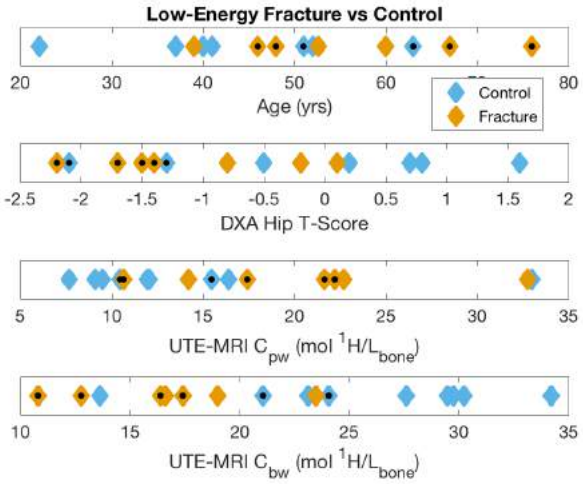

Fig 3 Age, DXA, and UTE-MRI measures of 16 female subjects, 7 with recent low-energy fracture. Subjects with DXA-defined osteopenia identified with a black dot. It is apparent that UTE-MRI is superior to age and DXA at distinguishing fracture from control subjects.

References

1. Horch RA, Nyman JS, Gochberg DF, et al. 2010. Characterization of 1H NMR signal in human cortical bone for magnetic resonance imaging. Magn Reson Med. 64(3):680–687.
2. Horch RA, Gochberg DF, Nyman JS, Does MD. 2011. Non-invasive Predictors of Human Cortical Bone Mechanical Properties: T2-Discriminated 1H NMR Compared with High Resolution X-ray. PLoS ONE. 6(1):e16359.
3. Granke M, Makowski AJ, Uppuganti S, et al. 2015. Identifying novel clinical surrogates to assess human bone fracture toughness. J Bone Miner Res. 30(7):1290–1300.
4. Manhard MK, Uppuganti S, Granke M, et al. 2016. MRI-derived bound and pore water concentrations as predictors of fracture resistance. Bone. 87:1–10.
5. Manhard MK, Horch RA, Harkins KD, et al. 2013. Validation of quantitative bound- and pore-water imaging in cortical bone. Magn Reson Med. 71(6):2166–2171.
6. Chen J, Chang EY, Carl M, et al. 2016. Measurement of bound and pore water T 1relaxation times in cortical bone using three-dimensional ultrashort echo time cones sequences. Magn Reson Med. 77(6):2136–2145.
7. Li C, Magland JF, Zhao X, et al. 2017. Selective in vivo bone imaging with long-T2 suppressed PETRA MRI. Magn Reson Med. 77(3):989–997.
8. Manhard MK, Harkins KD, Gochberg DF, et al. 2017. 30-Second bound and pore water concentration mapping of cortical bone using 2D UTE with optimized half-pulses. Magn Reson Med. 77(3):945–950.
9. Manhard MK, Horch RA, Gochberg DF, et al. 2015. In vivo quantitative MR imaging of bound and pore water in cortical bone. Radiology. 277(1):221–229.

Anabolic PTH Signaling Activates the Canonical Notch Pathway in Osteocytes to Restrain Bone Resorption and Facilitate Bone Gain

Jesus Delgado-Calle[1,2], Jessica Nelson[1], Matthew E. Olson[1], Kevin McAndrews[1,2], Emily G. Atkinson[1], Xiaolin Tu[1], Teresita Bellido[1,2]

[1]Department of Anatomy and Cell Biology, Division of Endocrinology, Department of Medicine, Indiana University School of Medicine, [2]Roudebush Veterans Administration Medical Center, Indianapolis, Indiana.

Intermittent and chronic elevation of parathyroid hormone (PTH) have anabolic and catabolic effects in the skeleton, respectively (1). However, the mechanisms underlying these paradoxical effects remain unknown. PTH regulates the expression of the Notch ligand Jagged1 in bone cells(2). Yet, whether PTH regulates other Notch components and the role of Notch in the skeletal actions of the hormone is unclear. We report that expression of Notch components (receptors, ligands, and target genes) is elevated in bones from transgenic mice with a constitutively active PTH receptor in osteocytes (caPth1r^{Ot})(3) and in WT mice exposed to anabolic regimen of PTH (100ng/g/day; 4wks)(4) (Figure 1).

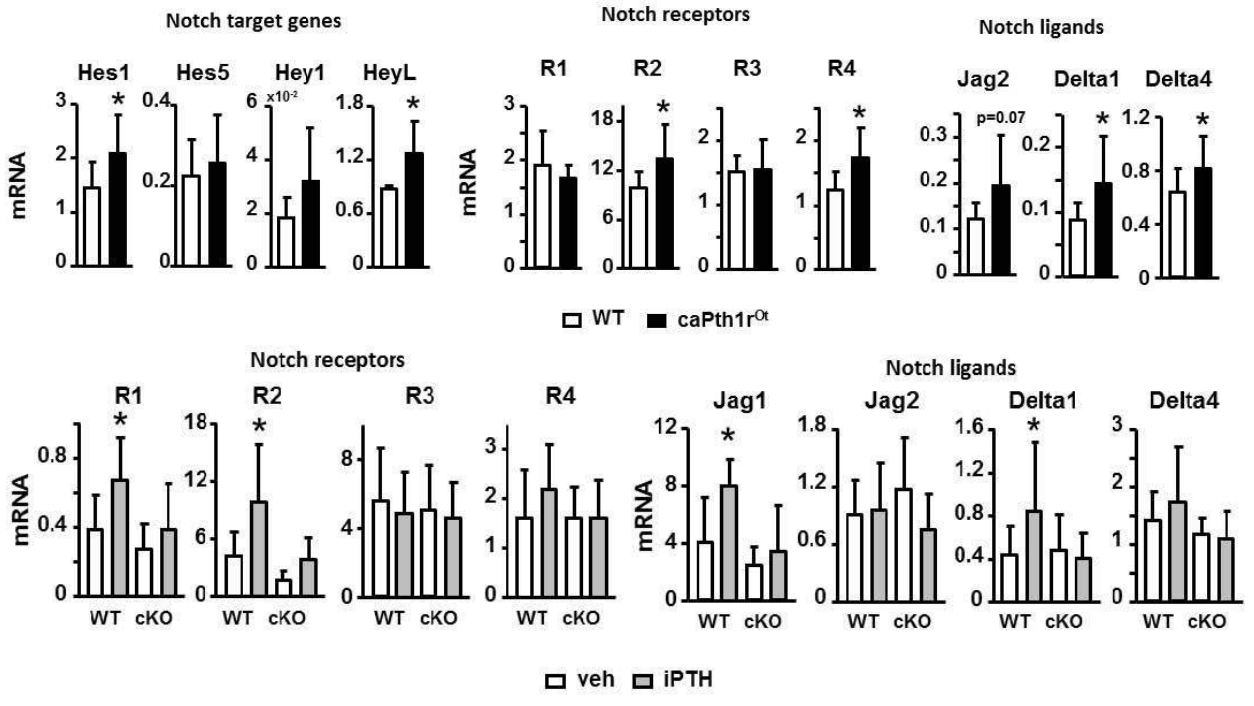

Figure 1. Anabolic PTH signaling activates Notch signaling in bone by direct actions in osetocytes. (A) Four-month old mice with constituve active Pth1r signaling in osteocytes (caPth1r^{Ot}) exhibit increased mRNA expression of Notch target genes, Notch receptors and ligands in bone when compared to wild type (WT) control littermates (n=10/group). (B) Four-month old mice receiving daily injections of PTH for 4 weeks had increased elevated mRNA levels of Notch receptors and ligands in bone compared to mice receiving vehicle injections (n=7-8/group). Genetic deletion of Pth1r in osteocytes blunted the upregulation of Notch receptors and ligands induced by daily PTH. Bars represent mean and SD. *p<0.05 vs WT by t-Test or vs vehicle by Two-Way ANOVA.

In contrast, chronic endogenous elevation of PTH secondary to calcium defiecinecy did not change the expression of Notch-related genes. Notch activation by anabolic PTH was absent in mice lacking Pth1r in osteocytes (cKO) or overexpressing the Wnt antagonist SOST in osteocytes (DMP1-SOST), demonstrating that intermittent, but not chronic, PTH elevation, activates Notch by direct actions in osteocytes and through a mechanism downstream of Sclerostin downregulation (Figure 2).

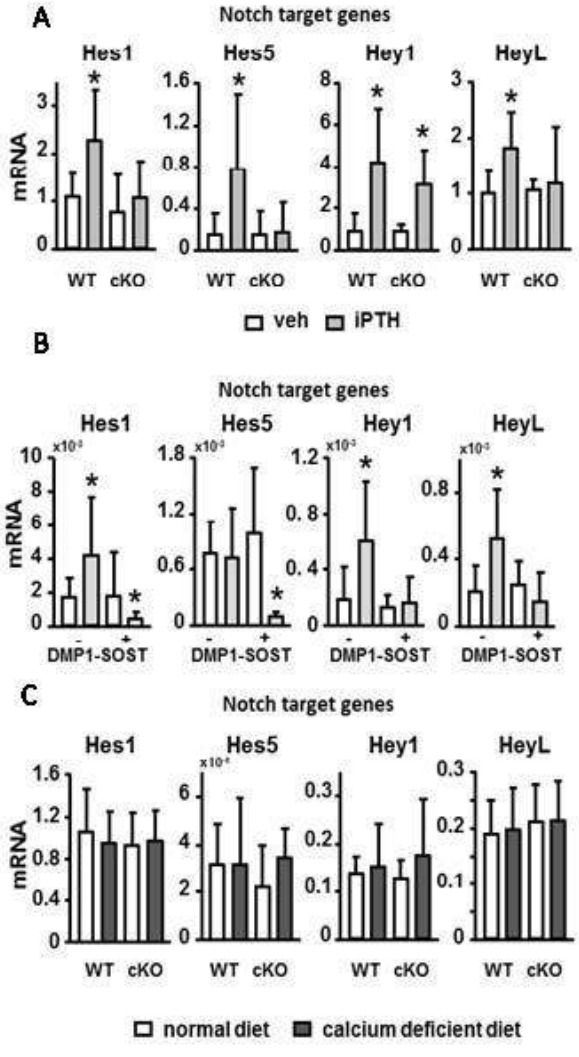

Figure 2. Intermittent, but not chronic, PTH elevation activates Notch signaling through Sclerostin dependent mechanisms. (A) Four-month old mice receiving daily injections of PTH for 4 weeks had increased elevated mRNA levels of Notch target genes (n=7/8/group). Genetic deletion of Pth1r in osteocytes or (B) overexpression of Sclerostin inhibited the increase in Notch target genes induced by daily PTH. (C) Four-month old mice fed a normal or low calcium diet did not exhibit increases in Notch target genes, receptors or ligands (not shown) regardless of the presence/absence of the Pth1r in osteocytes. Bars represent mean and SD. *p<0.05 vehicle by Two-Way ANOVA.

To dissect the contribution of canonical Notch signaling in osteocytes to the bone gain in caPTH1R^{Ot} mice, we genetically deleted the canonical Notch transcription factor RBPjk in osteocytes (with Dmp1-8kb-Cre) in WT and caPth1r^{Ot} and generated WT, caPth1r^{Ot}, RBPjk^{Ot}, and caPth1r^{Ot};RBPjk^{Ot} littermates. Mice lacking RBPjk in osteocytes exhibited a reduction of ~50% in RBPjk mRNA expression in calvarial bone, regardless of whether they express or not the caPTH1R transgene. At 6 months, WT and RBPjk^{Ot} mice exhibited no differences in BMD, cortical or cancellous bone volume, and markers of bone formation and resorption, suggesting that osteocytic canonical Notch signaling is dispensable for bone homeostasis (Figure 3). In contrast, caPth1r^{Ot};RBPjk^{Ot} mice exhibited 5% lower total BMD, decreased femoral cortical bone area (-9%), and reduced L5 cancellous BV/TV/ (-16%) and trabecular thickness (-30%) compared to control caPth1r^{Ot} mice. Moreover, caPth1r^{Ot};RBPjk^{Ot} mice displayed increased serum CTX (40%) and higher Rankl mRNA expression, thus increasing the Rankl/Opg ratio in bone. However, the increase in circulating P1NP and Sost dowregulaltion observed in caPth1r^{Ot} mice remained unchanged in caPth1r^{Ot};RBPjk^{Ot} mice (Figure 3).

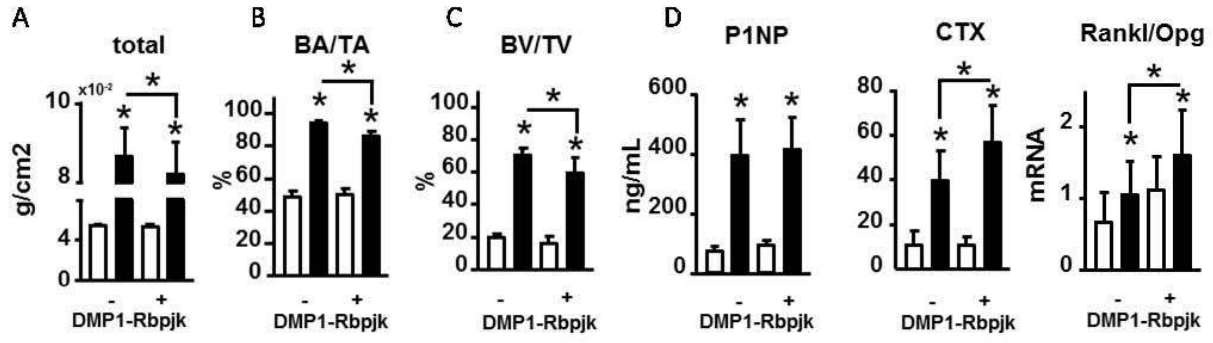

Figure 3. Inhibition of canonical Notch signaling in osteocytes decreases the bone gain induced osteocytic Pth1r signaling. (A) Total bone mineral density, (B) femoral cortical bone area over tissue (BA/TA), and (C) vertebral cancellous bone volume over tissue volume (BV/TV) of six-month old WT and caPTH1R^{Ot} mice with/without genetic deletion of Rbpjk in osteocyets (n=8-9/group). (D) Serum levels of the circulating markers of bone formation (P1NP) and bone resorption (CTX), and Rankl/Opg ratio (mRNA expression in bone) WT and caPTH1R^{Ot} mice with/without genetic deletion of Rbpjk in osteocyets (n=8-9/group) in Bars represent mean and SD. *p<0.05 vehicle by Two-Way ANOVA.

We conclude that anabolic PTH receptor signaling activates the canonical Notch pathway in osteocytes, which in turn, restrains bone resorption and facilitates bone gain.

Reference List

1. Jilka,R.L. 2007. Molecular and cellular mechanisms of the anabolic effect of intermittent PTH. *Bone* 40:1434-1446.

2. Qin,L., Qiu,P., Wang,L., Li,X., Swarthout,J.T., Soteropoulos,P., Tolias,P., and Partridge,N.C. 2003. Gene expression profiles and transcription factors involved in parathyroid hormone signaling in osteoblasts revealed by microarray and bioinformatics. *J. Biol. Chem.* 278:19723-19731.

3. O'Brien,C.A., Plotkin,L.I., Galli,C., Goellner,J., Gortazar,A.R., Allen,M.R., Robling,A.G., Bouxsein,M., Schipani,E., Turner,C.H. et al 2008. Control of bone mass and remodeling by PTH receptor signaling in osteocytes. *PLoS ONE* 3:e2942.

4. Delgado-Calle,J., Tu,X., Pacheco-Costa,R., McAndrews,K., Edwards,R., Pellegrini,G., Kuhlenschmidt,K., Olivos,N., Robling,A., Peacock,M. et al 2017. Control of bone anabolism in response to mechanical loading and PTH by distinct mechanisms downstream of the PTH receptor. *J. Bone Miner. Res.* 32:522-535.

Characterization of Fibroblast Growth Factor 23 (FGF23) levels in patients with Fanconi Syndrome due to Nephropathic Cystinosis

Pablo Florenzano[1-3], Carlos Ferreira[2], Mary Scott Ramnitz[1],Rachel I. Gafni[1],Luis Fernandez de Castro[1],Sri Harsha Tella[1],William A. Gahl[2], Michael T. Collins, MD[1].

[1]Section on Skeletal Disorders and Mineral Homeostasis, National Institutes of Dental and Craniofacial Research. [2]Medical Genetics Branch, National Human Genome Research Institute. National Institutes of Health, Bethesda, MD, United States. [3]School of Medicine, Pontificia Universidad Catolica de Chile.

Background: Cystinosis is a rare autosomal recessive lysosomal storage disorder caused by inactivating mutations of the cystinosin gene, leading to cellular damage from cystine accumulation. Its most frequent form, nephropathic cystinosis (NC), presents in the first year of life and leads to renal failure. Early features include renal Fanconi syndrome and hypophosphatemic rickets. The drug cysteamine depletes lysosomes of cystine and helps preserve glomerular function, but does not prevent tubular dysfunction. Although phosphate wasting is a prominent feature of NC, its association with FGF23 has not been studied.

Objective: Characterize FGF23 levels in patients with hypophosphatemia and chronic kidney disease (CKD) in the context of NC.

Patients and methods: Charts and frozen samples from NC patients with clinically evident Fanconi syndrome before dialysis or renal transplant were analyzed retrospectively. Plasma C-terminal and intact FGF23 levels were determined by ELISA (Immutopics). Spearman`s rank-order correlation for non-parametric variables was used to determine statistical significances.

Results: Twenty-four patients were included, 52% female. The mean age was 13.2 years (2-28). All patients were on cysteamine, 90% on phosphorous supplements and 40% on calcitriol. All patients had low tubular phosphate reabsorption (TRP), however only 71% were frankly hypophosphatemic at the time of the FGF23 measurement. GFR < 90ml/min/1.73m^2 in 79% of subjects. Parathyroid hormone (PTH) and 1,25(OH)$_2$ vitamin D were measured in 19 patients. Median PTH was 36.4 pg/ml (13.4-146) with 26% above the normal range (15-65 pg/ml) due to secondary hyperparathyroidism. Median 1,25(OH)$_2$ vitamin D was 60 pg/ml (24-86); only 15.7% had levels below normal range (24-86pg/ml). eGFR did not correlate significantly with PTH or 1,25(OH)$_2$ vitamin D. All hypophosphatemic patients had low-normal intact and C-terminal FGF23. FGF23 level was not associated with CKD stage (Figure).

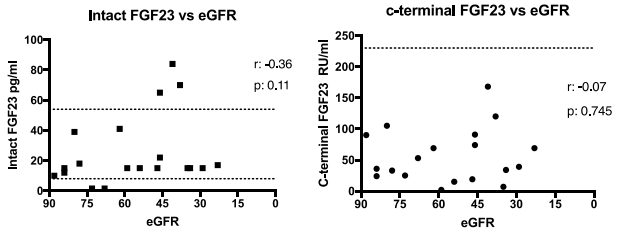

Conclusions: Patients with hypophosphatemia due to NC-induced Fanconi syndrome have low-normal FGF23 levels. In patients with NC-induced CKD, FGF23, PTH or 1,25(OH)$_2$ vitamin D levels generally remain within normal range and do not significantly correlate with GFR, in contrast to patients with more common causes of CKD. While the underlying mechanism for this difference is not clear, it is most likely due to the concomitant tubular phosphate wasting in NC.

PPARγ and PPARα regulate osteocyte activity by controlling expression of Sclerostin and DKK1 proteins

Lance A. Stechschulte1,2, Mathew Mazur1, Dustin Marinelli1, Zach Rotter1, Amit Chougule2,3, Beata Lecka-Czernik1,2,3

1Department of Orthopaedic Surgery; 2Center for Diabetes and Endocrine Research; 3Department of Physiology and Pharmacology, University of Toledo, College of Medicine and Life Sciences, Toledo, OH

Osteocytes orchestrate bone remodeling through regulation of both osteoblast and osteoclast activities. Sclerostin, encoded by *Sost* gene, and DKK1 proteins are released from osteocytes and act as inhibitors of Wnt signaling pathway in osteoblasts. Recently we have showed that PPARγ is a positive regulator of both *Sost* and *Dkk1*, whereas PPARα is a negative regulator of *Sost* expression. Decreased bone formation in mice treated with full PPARγ agonist, rosiglitazone, is associated with increased expression and protein production in osteocytes of both Sclerostin and DKK1. In contrast, mice treated with a new insulin sensitizer SR10171 which acts as PPARγ inverse agonist and PPARα agonist, is associated with decreased expression and production of both Sclerostin and DKK1 resulting in increased bone formation and bone mass. Here we extended our studies by analyzing the mechanism by which PPARγ and PPARα control expression of both genes. Using EpiTect software we have identified two PPRE sequences in *Sost* promoter located -1.8 kb (αPPRE) and -7.0 kb (γPPRE) from the transcription start site. ChIP analysis showed that PPARα binds to αPPRE in basal conditions. Treatment with WY14643 agonist results in augmentation of PPARα binding which correlates with decreased promoter activity measured in luciferase gene reporter assay. In contrast, PPARγ is recruited to the *Sost* promoter only after activation with rosiglitazone, and this correlates with increased promoter activity. Similarly, PPARγ activation, but not PPARα, increases *Dkk1* promoter activity and DKK1 protein production in osteocytes. To demonstrate that PPARγ and PPARα regulate endocrine activities of osteocytes supporting of PBMC differentiation, we tested conditioned media (CM) from primary osteocytes treated with different PPARs selective modulators. CM collected from osteocytes with activated PPARγ increased adipocytic and decreased osteoblastic gene markers expressed in recipient PBMC, whereas CM from osteocytes with activated PPARα decreased adipocytic and increased osteoblastic gene markers. PPARα inhibitory effect on *Sost* expression was confirmed in animals deficient in PPARα protein. Osteocytes derived from PPARα knock-out mice are characterized with high expression of *Sost* and 2-fold increased Sclerostin protein levels. In conclusion, Sclerostin and DKK1 are directly regulated by PPARγ and PPARα and these nuclear receptors can be pharmacological targets to control osteocyte-regulated bone remodeling.

Prx-1 Embryonic Specification Is Retained in a Postnatal Regenerative Stem Cell Population that Gives Rise to Skeletal, Fat, and Vascular Tissues

Beth Bragdon, PhD1, Andrew Bennie, MS1, Jenny Lei, BS2, Elise F. Morgan, PhD2, Louis C. Gerstenfeld, PhD1
1Boston University School of Medicine, Boston, MA, 2Boston University, College of Engineering, Boston, MA

Mesenchymal stem cell (MSC) is used to describe a population of adult stem cells that are multipotent and contribute to bone homeostasis and repair. However, this population of cells has not been identified *in vivo* and is recently suggested to be pericytes. A cell population conditionally expressing Prx1 previously shown to identify embryonic appendicular and calvaria tissues and postnatally associated with bone formation and repair was used for *in vivo* lineage tracking studies. Male and female mice aged 8-11 weeks were used in IACUC approved studies. Different models of postnatal bone formation were used: closed stabilized transverse femoral fracture, distraction osteogenesis (limb lengthening), and ectopic bone formation at appendicular and axial sites (limb, sternum, spine). Tamoxifen inducible Prx1 Cre ERT transgenic mice were crossed with B6.Cg-Gt(ROSA)26sor<tm14(CAG-tdTomato)Hze>/J mice to create Prx1/Ai14 reporter. Subsequently Prx1/Ai14 mice were crossed with B6,129S7-Rag1tm1Mom/J to create a transgenic reporter mouse allowing for the implantation of human demineralized bone matrix (DBM) to induce ectopic bone. Tamoxifen was administered and allowed to be washed out for at least 28 days or for only 3 days prior to surgery or ectopic bone induction in order to follow the specified population through postnatal bone formation. Under both homeostatic and short duration labeling conditions cell labeling was observed in differentiated osteoblasts and osteocytes in cortical and trabecular bone and cells on both periosteal and endosteal surfaces of both fore and hind limbs and cranium. Immunofluorescence (IF) confirmed that adipocytes and smooth muscle cells in vessels within the muscle compartment of the appendicular skeleton were also labeled (see figure 1). Prx1 was induced in regenerative tissues after bone injury (fracture, ~61% of cells were derived from Prx1) and distraction osteogenesis within the same lineages as seen under homeostatic labeling. Ectopic bone induced in response to DBM implantation in the limbs showed labelled cells differentiated into chondrocytes, osteoblasts, adipocytes, and vessel associated smooth muscle however ectopic bone induction at axial skeletal sites such as sternum and spine did not show labelled cells. These results suggest that Prx1 expression connotes a multi-potential postnatal MSC that retained its embryonic tissue specification and contributes to both postnatal homeostatic maintenance and tissue repair in response to injury.

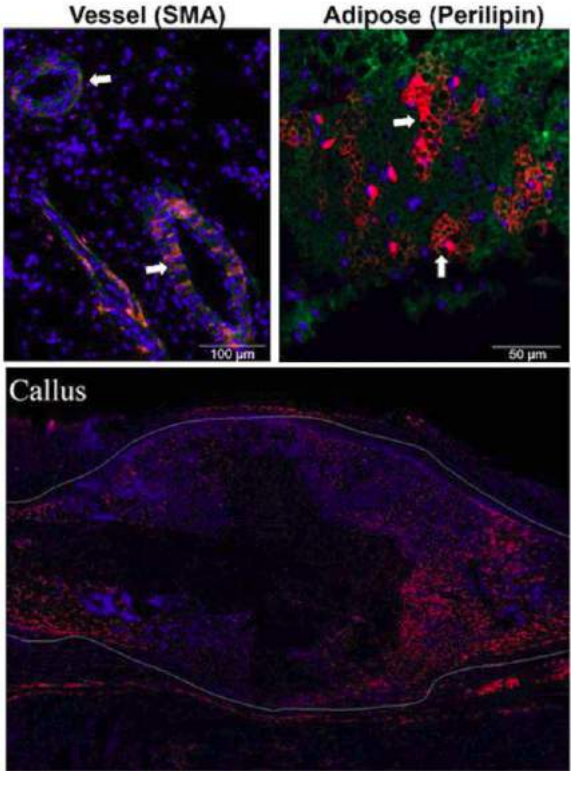

Figure 1. Prx1 driven Ai14 was induced with tamoxifen, labeling cells red. Nuclei were stained with dapi (blue). Top. IF was performed to identify smooth muscle of vessels (SMA shown in green) or perilipin (shown in green) for adipose tissue. Bottom. Fracture callus at day 14. White line outlines callus.

Anabolic PTH Signaling Activates the Canonical Notch Pathway in Osteocytes to Restrain Bone Resorption and Facilitate Bone Gain

Jesus Delgado-Calle[1,2], Jessica Nelson[1], Matthew E. Olson[1], Kevin McAndrews[1,2], Emily G. Atkinson[1], Xiaolin Tu[1], Teresita Bellido[1,2]

[1]Department of Anatomy and Cell Biology, Division of Endocrinology, Department of Medicine, Indiana University School of Medicine, [2]Roudebush Veterans Administration Medical Center, Indianapolis, Indiana.

Intermittent and chronic elevation of parathyroid hormone (PTH) have anabolic and catabolic effects in the skeleton, respectively (1). However, the mechanisms underlying these paradoxical effects remain unknown. PTH regulates the expression of the Notch ligand Jagged1 in bone cells(2). Yet, whether PTH regulates other Notch components and the role of Notch in the skeletal actions of the hormone is unclear. We report that expression of Notch components (receptors, ligands, and target genes) is elevated in bones from transgenic mice with a constitutively active PTH receptor in osteocytes (caPth1r^{Ot})(3) and in WT mice exposed to anabolic regimen of PTH (100ng/g/day; 4wks)(4) (Figure 1).

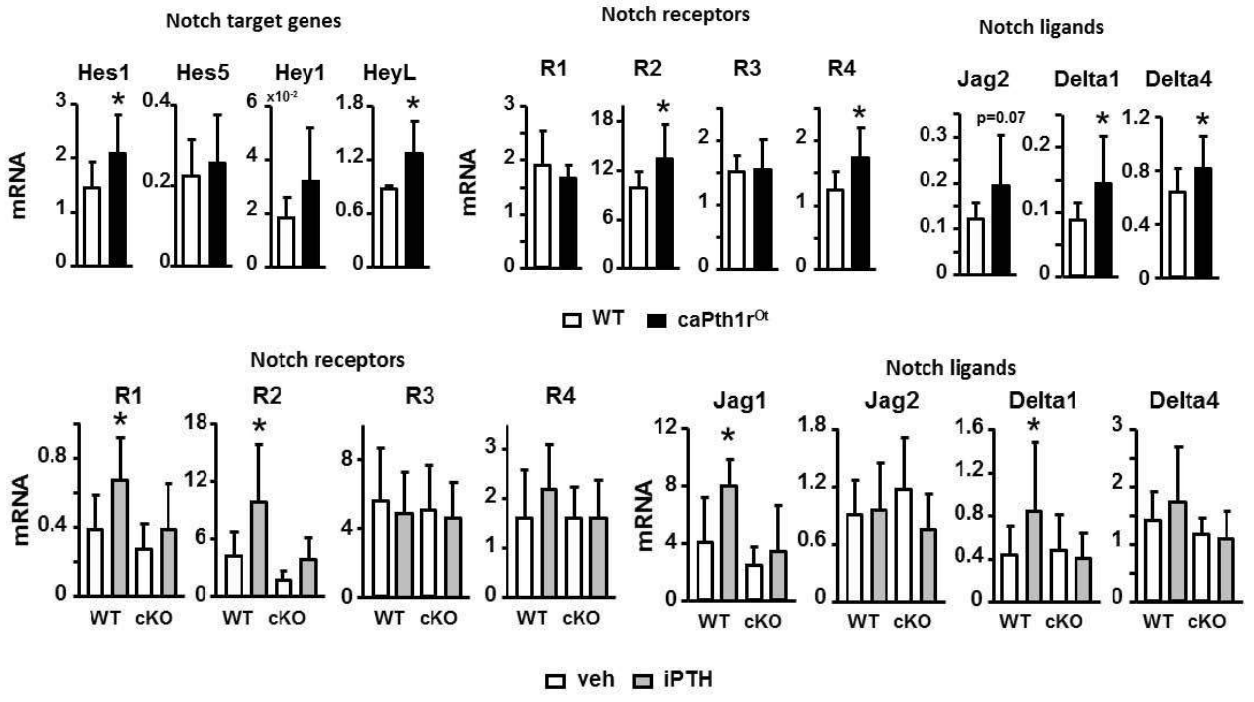

Figure 1. Anabolic PTH signaling activates Notch signaling in bone by direct actions in osetocytes. (A) Four-month old mice with constituve active Pth1r signaling in osteocytes (caPth1r^{Ot}) exhibit increased mRNA expression of Notch target genes, Notch receptors and ligands in bone when compared to wild type (WT) control littermates (n=10/group). (B) Four-month old mice receiving daily injections of PTH for 4 weeks had increased elevated mRNA levels of Notch receptors and ligands in bone compared to mice receiving vehicle injections (n=7-8/group). Genetic deletion of Pth1r in osteocytes blunted the upregulation of Notch receptors and ligands induced by daily PTH. Bars represent mean and SD. *p<0.05 vs WT by t-Test or vs vehicle by Two-Way ANOVA.

In contrast, chronic endogenous elevation of PTH secondary to calcium defiecinecy did not change the expression of Notch-related genes. Notch activation by anabolic PTH was absent in mice lacking Pth1r in osteocytes (cKO) or overexpressing the Wnt antagonist SOST in osteocytes (DMP1-SOST), demonstrating that intermittent, but not chronic, PTH elevation, activates Notch by direct actions in osteocytes and through a mechanism downstream of Sclerostin downregulation (Figure 2).

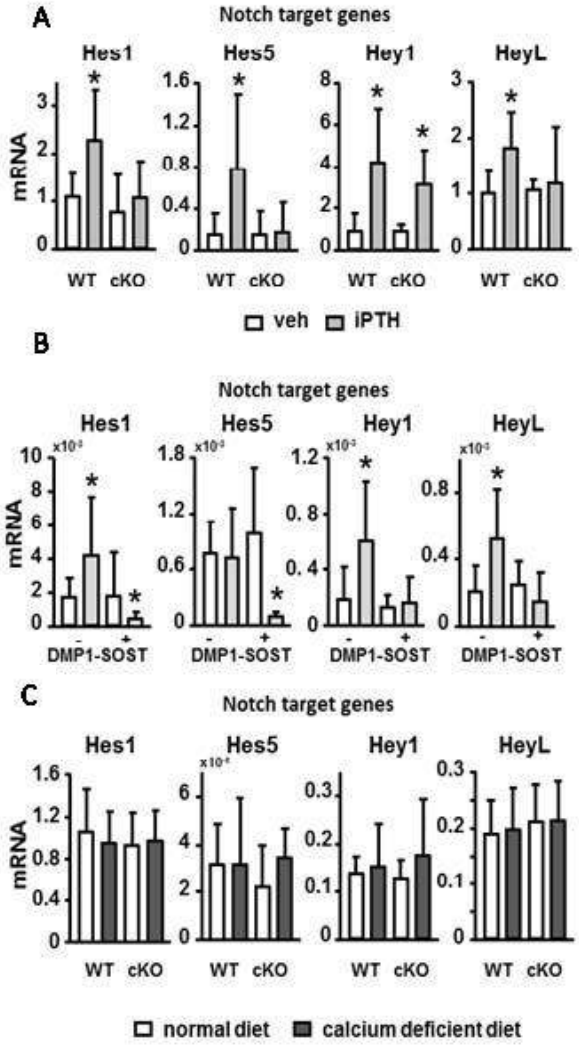

Figure 2. Intermittent, but not chronic, PTH elevation activates Notch signaling through Sclerostin dependent mechanisms. (A) Four-month old mice receiving daily injections of PTH for 4 weeks had increased elevated mRNA levels of Notch target genes (n=7/8/group). Genetic deletion of Pth1r in osteocytes or (B) overexpression of Sclerostin inhibited the increase in Notch target genes induced by daily PTH. (C) Four-month old mice fed a normal or low calcium diet did not exhibit increases in Notch target genes, receptors or ligands (not shown) regardless of the presence/absence of the Pth1r in osteocytes. Bars represent mean and SD. *p<0.05 vehicle by Two-Way ANOVA.

To dissect the contribution of canonical Notch signaling in osteocytes to the bone gain in caPTH1R^{Ot} mice, we genetically deleted the canonical Notch transcription factor RBPjk in osteocytes (with Dmp1-8kb-Cre) in WT and caPth1r^{Ot} and generated WT, caPth1r^{Ot}, RBPjk^{Ot}, and caPth1r^{Ot};RBPjk^{Ot} littermates. Mice lacking RBPjk in osteocytes exhibited a reduction of ~50% in RBPjk mRNA expression in calvarial bone, regardless of whether they express or not the caPTH1R transgene. At 6 months, WT and RBPjk^{Ot} mice exhibited no differences in BMD, cortical or cancellous bone volume, and markers of bone formation and resorption, suggesting that osteocytic canonical Notch signaling is dispensable for bone homeostasis (Figure 3). In contrast, caPth1r^{Ot};RBPjk^{Ot} mice exhibited 5% lower total BMD, decreased femoral cortical bone area (-9%), and reduced L5 cancellous BV/TV/ (-16%) and trabecular thickness (-30%) compared to control caPth1r^{Ot} mice. Moreover, caPth1r^{Ot};RBPjk^{Ot} mice displayed increased serum CTX (40%) and higher Rankl mRNA expression, thus increasing the Rankl/Opg ratio in bone. However, the increase in circulating P1NP and Sost dowregulaltion observed in caPth1r^{Ot} mice remained unchanged in caPth1r^{Ot};RBPjk^{Ot} mice (Figure 3).

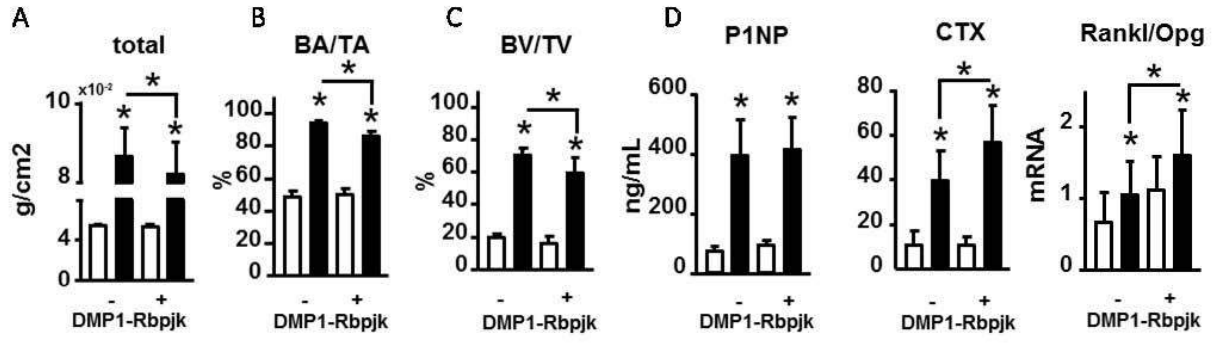

Figure 3. Inhibition of canonical Notch signaling in osteocytes decreases the bone gain induced osteocytic Pth1r signaling. (A) Total bone mineral density, (B) femoral cortical bone area over tissue (BA/TA), and (C) vertebral cancellous bone volume over tissue volume (BV/TV) of six-month old WT and caPTH1R^{Ot} mice with/without genetic deletion of Rbpjk in osteocyets (n=8-9/group). (D) Serum levels of the circulating markers of bone formation (P1NP) and bone resorption (CTX), and Rankl/Opg ratio (mRNA expression in bone) WT and caPTH1R^{Ot} mice with/without genetic deletion of Rbpjk in osteocyets (n=8-9/group) in Bars represent mean and SD. *p<0.05 vehicle by Two-Way ANOVA.

We conclude that anabolic PTH receptor signaling activates the canonical Notch pathway in osteocytes, which in turn, restrains bone resorption and facilitates bone gain.

Reference List

1. Jilka,R.L. 2007. Molecular and cellular mechanisms of the anabolic effect of intermittent PTH. *Bone* 40:1434-1446.

2. Qin,L., Qiu,P., Wang,L., Li,X., Swarthout,J.T., Soteropoulos,P., Tolias,P., and Partridge,N.C. 2003. Gene expression profiles and transcription factors involved in parathyroid hormone signaling in osteoblasts revealed by microarray and bioinformatics. *J. Biol. Chem.* 278:19723-19731.

3. O'Brien,C.A., Plotkin,L.I., Galli,C., Goellner,J., Gortazar,A.R., Allen,M.R., Robling,A.G., Bouxsein,M., Schipani,E., Turner,C.H. et al 2008. Control of bone mass and remodeling by PTH receptor signaling in osteocytes. *PLoS ONE* 3:e2942.

4. Delgado-Calle,J., Tu,X., Pacheco-Costa,R., McAndrews,K., Edwards,R., Pellegrini,G., Kuhlenschmidt,K., Olivos,N., Robling,A., Peacock,M. et al 2017. Control of bone anabolism in response to mechanical loading and PTH by distinct mechanisms downstream of the PTH receptor. *J. Bone Miner. Res.* 32:522-535.

Characterization of Fibroblast Growth Factor 23 (FGF23) levels in patients with Fanconi Syndrome due to Nephropathic Cystinosis

Pablo Florenzano[1-3], Carlos Ferreira[2], Mary Scott Ramnitz[1],Rachel I. Gafni[1],Luis Fernandez de Castro[1],Sri Harsha Tella[1],William A. Gahl[2], Michael T. Collins, MD[1].

[1]Section on Skeletal Disorders and Mineral Homeostasis, National Institutes of Dental and Craniofacial Research. [2]Medical Genetics Branch, National Human Genome Research Institute. National Institutes of Health, Bethesda, MD, United States. [3]School of Medicine, Pontificia Universidad Catolica de Chile.

Background: Cystinosis is a rare autosomal recessive lysosomal storage disorder caused by inactivating mutations of the cystinosin gene, leading to cellular damage from cystine accumulation. Its most frequent form, nephropathic cystinosis (NC), presents in the first year of life and leads to renal failure. Early features include renal Fanconi syndrome and hypophosphatemic rickets. The drug cysteamine depletes lysosomes of cystine and helps preserve glomerular function, but does not prevent tubular dysfunction. Although phosphate wasting is a prominent feature of NC, its association with FGF23 has not been studied.

Objective: Characterize FGF23 levels in patients with hypophosphatemia and chronic kidney disease (CKD) in the context of NC.

Patients and methods: Charts and frozen samples from NC patients with clinically evident Fanconi syndrome before dialysis or renal transplant were analyzed retrospectively. Plasma C-terminal and intact FGF23 levels were determined by ELISA (Immutopics). Spearman`s rank-order correlation for non-parametric variables was used to determine statistical significances.

Results: Twenty-four patients were included, 52% female. The mean age was 13.2 years (2-28). All patients were on cysteamine, 90% on phosphorous supplements and 40% on calcitriol. All patients had low tubular phosphate reabsorption (TRP), however only 71% were frankly hypophosphatemic at the time of the FGF23 measurement. GFR < 90ml/min/1.73m^2 in 79% of subjects. Parathyroid hormone (PTH) and 1,25(OH)$_2$ vitamin D were measured in 19 patients. Median PTH was 36.4 pg/ml (13.4-146) with 26% above the normal range (15-65 pg/ml) due to secondary hyperparathyroidism. Median 1,25(OH)$_2$ vitamin D was 60 pg/ml (24-86); only 15.7% had levels below normal range (24-86pg/ml). eGFR did not correlate significantly with PTH or 1,25(OH)$_2$ vitamin D. All hypophosphatemic patients had low-normal intact and C-terminal FGF23. FGF23 level was not associated with CKD stage (Figure).

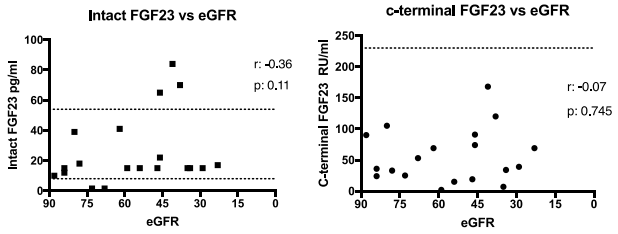

Conclusions: Patients with hypophosphatemia due to NC-induced Fanconi syndrome have low-normal FGF23 levels. In patients with NC-induced CKD, FGF23, PTH or 1,25(OH)$_2$ vitamin D levels generally remain within normal range and do not significantly correlate with GFR, in contrast to patients with more common causes of CKD. While the underlying mechanism for this difference is not clear, it is most likely due to the concomitant tubular phosphate wasting in NC.

RON kinase: A new target for treatment of cancer-induced bone destruction and osteoporosis

Jaime Fornetti, PhD[1], Le Zhan, BS[2], Xuli Wang, PhD[2], Alana L. Welm, PhD[1]

[1]Department of Oncological Sciences, Huntsman Cancer Institute, Salt Lake City, UT, [2]Department of Radiology and Imagining Sciences, School of Medicine, University of Utah, Salt Lake City, UT,

Bone-destructive pathological conditions, such as cancer metastasis and osteoporosis, are a significant problem. Over half of Americans age 50 and older are estimated to have osteoporosis or low bone mass[1]. Additionally, over 400,000 people annually in the United States have cancer metastasis to the bone[2]. The severe bone loss associated with osteolytic metastasis causes profound pain, nerve compression, hypercalcemia, and debilitating fractures[3,4]. Despite current therapies, many patients with bone metastasis eventually progress to develop new bone lesions or serious skeletal complications[5], highlighting the need for additional therapies for osteolytic bone disease. Here, we identify the macrophage-stimulating protein (MSP)/RON tyrosine kinase signaling pathway as a potential new therapeutic target for osteolytic metastasis and osteoporosis. Additionally, we use experimental osteolytic bone metastasis models to evaluate novel nanotherapies designed to target osteolytic bone lesions.

Increased expression of the MSP signaling pathway occurs in approximately 40% of breast cancers and is sufficient to drive bone metastasis in a preclinical breast cancer model[6]. In bone metastasis models, MSP expression by tumors leads to increased bone destruction through its receptor, RON tyrosine kinase, on host cells (Figure 1a), via a pathway complementary to RANKL and TGFβ. MSP-induced osteolysis was blocked in mice deficient for RON tyrosine kinase activity or following treatment with the RON inhibitor BMS-777607/ASLAN002 in models of metastasis (Figures 1a and b) and osteoporosis. To determine whether RON inhibitors may also be effective in patients, plasma samples from phase 1 clinical testing of BMS-777607/ASLAN002 were analyzed for the bone resorption marker β-cross-linked C-telopeptide (CTX) and the bone formation marker bone-specific alkaline phosphatase (BSAP). After 15-28 days of treatment, 62% (13 of 21) of subjects experienced a decrease in CTX levels from baseline, with the best responses seen in women (Figure 2a). Notably, 7 of 11 women had a reduction in CTX of ≥25%, meeting the Mayo Clinic guidelines[7] for a positive response to bone antiresorptive therapies. This decrease in CTX following treatment was accompanied by an increase in BSAP (Figure 2b). All patients in the study except for one were greater than 50 years of age; therefore, we speculate that the superior response rate observed in women may be due to the high levels of bone loss associated with menopause. These data indicate that RON inhibitors may be effective in humans with lytic bone diseases.

To further improve bioavailability and effectiveness of RON inhibitors, new bone-targeting, enzyme-activated theranostics are being designed based on novel synthetic multifunctional carriers (MFC). MFC are able to form stable, self-assembling nanoparticles with hydrophobic drugs, such as BMS-777607/ASLAN002, through hydrophobic interactions. Such nanoparticles allow for systemic injection and improved bioavailability. The bone-targeting ligand alendronate (ALN) is attached to MFC, which targets the nanoparticles to skeletal tissue. For optical imaging, Cy5.5 is conjugated into MFC via a MMP-2 cleavable peptide, which under normal conditions diminishes Cy5.5 fluorescence due to FRET, but restores fluorescence in MMP-2 rich microenvironments, such as osteolytic lesions. Our preliminary data show that:

1) Drug-loaded nanoparticles are 102.6 ± 1.6 nm in diameter and aqueous solubility of BMS-777607/ASLAN002 was
   greatly improved.
2) Bone-targeting capacity was achieved; approximately 92 ± 3.3% of ALN-containing nanoparticles could bind to hydroxylapatite within 30 minutes.
3) Cy5.5 fluorescence imaging enhancement was observed in cultured breast cancer cells (MDA-MB-231).
4) The drug release profile showed that 78 ± 2.1% of BMS-777607/ASLAN002 could be released from nanoparticles

Taken together, our preclinical and clinical data indicate that RON inhibitors may be effective against osteolytic bone diseases. Furthermore, our preliminary data show that using synthetic multifunctional carriers to deliver the RON inhibitor BMS-777607/ASLAN002 improves aqueous solubility and drug release in the presence of MMP-2. These data provide rationale for the continued investigation of RON inhibitors for use in patients with osteolytic bone diseases.

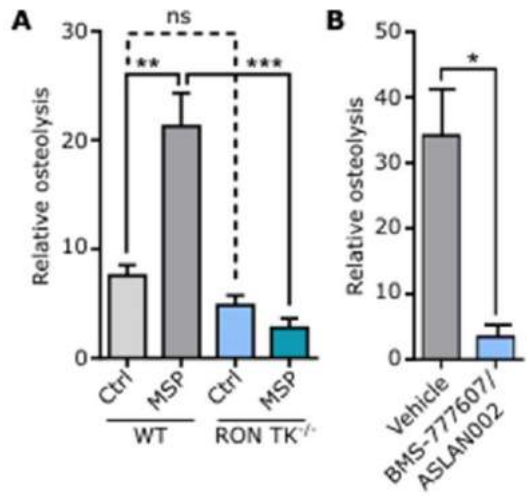

Figure 1. MSP-induced osteolysis requires host RON kinase activity and can be blocked with the RON inhibitor BMS-777607/ASLAN002. Quantification of osteolytic area, determined by high resolution ex vivo x-ray, in tibias of mice 42 days after tumor cell injection in wild-type (WT) or RON tyrosine kinase-deficient hosts (RON $TK^{-/-}$) (A) or in WT hosts treated with BMS777607/ASLAN002 (B). *p=0.021, **p=0.0013, ***p=0.0001, ns=not significant (p<0.05)

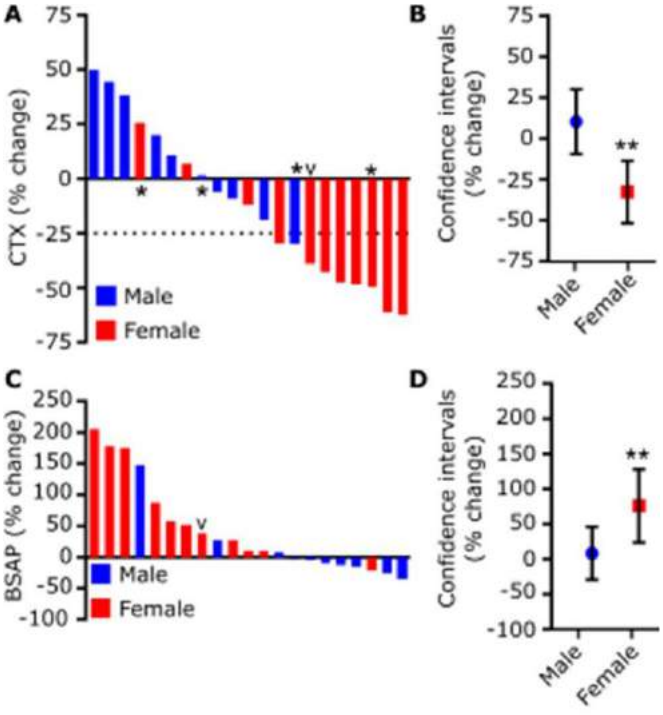

Figure 2. The RON inhibitor BMS-777607/ASLAN002 reduces bone turnover in humans. (A) Quantification of the percent change in plasma CTX levels (compared to baseline prior to drug treatment) in blood plasma of 21 patients that received BMS-777607/ASLAN002 for at least 15 days in a Phase 1 clinical trial. Most patients received BMS-777607/ASLAN002 for 28 days; values reported correspond to the difference between baseline (day 0) and the 28-day time point. Exceptions in duration of treatment and CTX testing are noted (*15 days). Blue bars represent males and red bars represent females. Arrowhead denotes a patient less than 50 years of age (42 years). (B) Ninety-five percent confidence intervals for percent change in CTX for males and females; **p=0.0035, one-sample t tests versus a hypothetical mean of 0 (no change following treatment compared to baseline). (C) Quantification of the percent change in bone-specific alkaline phosphatase (BSAP) levels (compared to baseline) in blood plasma of 22 patients that received BMS-777607/ASLAN002 for 28 days. 18 of the patients are also shown in (A). (D) Ninety-five percent confidence intervals for percent change in BSAP for males and females; **p=0.0090, one-sample t tests versus a hypothetical mean of 0 (no change following treatment compared to baseline). Blue bars represent males and red bars represent females.

References [1]www.nof.org (2011) [2]R. E. Coleman, A. Lipton, G. D. Roodman, T. A. Guise, B. F. Boyce, A. M. Brufsky, P. Clezardin, P. I. Croucher, J. R. Gralow, P. Hadji, I. Holen, G. R. Mundy, M. R. Smith, L. J. Suva, Metastasis and bone loss: advancing treatment and prevention. *Cancer Treat Rev* 36, 615-620 (2010) [3]R. E. Coleman, Future directions in the treatment and prevention of bone metastases. Am J Clin Oncol 25, S32-38 (2002). [4]I. J. Diel, E. F. Solomayer, G. Bastert, Treatment of metastatic bone disease in breast cancer: bisphosphonates. Clin Breast Cancer 1, 43-51 (2000). [5]A. T. Stopeck, A. Lipton, J. J. Body, G. G. Steger, K. Tonkin, R. H. de Boer, M. Lichinitser, Y. Fujiwara, D. A. Yardley, M. Viniegra,

M. Fan, Q. Jiang, R. Dansey, S. Jun, A. Braun, Denosumab compared with zoledronic acid for the treatment of bone metastases in patients with advanced breast cancer: a randomized, double-blind study. J Clin Oncol 28, 5132-5139 (2010). [6]A. L. Welm, Sneddon, J. B., Taylor, C., Nuyten, D.S.A., van de Vijver, M.A., Hasegawa, B. H., and Bishop, J. Michael, The macrophage stimulating protein pathway promotes metastasis in a mouse model for breast cancer and predicts poor prognosis in humans. Proc Natl Acad Sci U S A 104, 7570-7575 (2007). [7]Mayo Clinic Medical Laboratories, Beta-CrossLaps (Beta-CTx), Serum. http://www.mayomedicallaboratories.com/testcatalog/Clinical+and+Interpretive/83175.

Deletion of CaMKK2 in Osteocytes Elicits Gender-Specific Effects on Bone Mass

Mavis Irwin, PhD[1], Uma Sankar, PhD[1]
[1]Indiana University Purdue University of Indianapolis, Indianapolis, IN

Background: Intracellular Ca^{2+}-calmodulin (CaM) complexes bind to and activate a plethora of downstream proteins including the multifunctional serine-threonine protein kinase, Ca2+/CaM dependent protein kinase kinase 2 (CaMKK2) [1]. We previously reported a potent bone anabolic response following either the global deletion (*Camkk2*$^{-/-}$) or selective pharmacological inhibition of CaMKK2 in mice [2]. Mesenchymal stem cells isolated from these mice generate significantly higher numbers of matrix-secreting osteoblasts (OBs) and lower numbers of osteoclasts (OCs), indicating a cell-intrinsic role for CaMKK2 in these cells [3]. Osteocytes (OCYs) are the most abundant cells of the skeleton and have profound roles in bone remodeling [4, 5]. However, we lack a detailed knowledge of the cell-intrinsic role(s) of CaMKK2 in OCYs. We hypothesize that the loss of CaMKK2 in each of the three bone cell types contributes to the overall bone phenotype in *Camkk2*$^{-/-}$mice. In this study, we investigated whether targeted deletion of CaMKK2 from OCYs affects the skeletal phenotype.

Methods: We deleted CaMKK2 expression in OCY by mating *dentin matrix protein 1* (*Dmp1*)-8kb-Cre transgenic mice [6] with *CaMKK2* $^{flox/flox}$ mice to generate the *Camkk2*$^{\Delta OCY}$ mice. We isolated the OB/OC and OCY cell fractions from long bones as previously described [7] to confirm the deletion of CaMKK2 from mature OBs and OCYs, the cell-types targeted by *Dmp1*-8kb-Cre, using real-time reverse transcriptase-polymerase chain reaction (RT-PCR). Further, long bones collected from 3 month-old male and female *Camkk2*$^{\Delta OCY}$ (n=5 male and 6 female), *Camkk2*$^{-/-}$ (n=4 male and 3 female) and wild-type (WT) control (n=4 per gender) mice were analyzed for trabecular and cortical bone parameters using micro-computed tomography (micro-CT; Skyscan 1176 and control software version 1.1 from Bruker in Kontich, Belgium ; setting at 75 kV, 333 µA, 8.41 image pixel size, 0.40 rotation, 656 files per sample). The tibiae were processed for undecalcified dynamic and static histomorphometry using the Bioquant Osteo software version 17.2.60 (Bioquant Image Analysis, Nashville, TN) coupled with a Leica DM2700M (Leica Inc.,Wetzlar, Germany). Serum was collected to evaluate anabolic and catabolic markers as well as RANKL/OPG ratio. RNA was isolated from long bones to perform quantitative real-time RT-PCR analyses of gene expression using CFX Connect (BioRad, Hercules, CA).

Results: Deletion of CaMKK2 in OCYs resulted in significant increases in trabecular bone volume (2.6-fold higher in males and 1.7-fold higher in females) compared to age- and sex-matched control mice. However, gender-specific effects were observed when compared to trabecular bone volume present in age-and sex-matched male *Camkk2*$^{-/-}$ mice. Male *Camkk2*$^{\Delta OCY}$ mice possessed similar trabecular bone volume as male *Camkk2*$^{-/-}$ mice. In contrast, female *Camkk2*$^{\Delta OCY}$ mice possessed a significant 1.6-fold lower bone volume compared to female *Camkk2*$^{-/-}$ mice, although these parameters were significantly higher than those in female control mice. Similar trends were observed in trabecular number, separation and pattern as well as cortical bone thickness. Interestingly, the cortical bone mean polar moment of inertia in *Camkk2*$^{\Delta OCY}$ mice was significantly higher compared to age-matched control and *Camkk2*$^{-/-}$ mice, with higher increases observed in males than females. Altogether, these data suggest a gender-specific effect of CaMKK2 deletion from OCYs.

Discussion: In conclusion, our results indicate that the deletion of CaMKK2 from OCYs potentiates a possible anabolic effect on trabecular and cortical bone that is more pronounced in male mice. This suggests that CaMKK2 regulation of either the OCY activity or the crosstalk between OCYs and the other two types of bone cells is gender-dependent. A pervious study looking at the OCY-specific upregulation of the Wnt-B-catenin signaling pathway also reported a gender-dependent anabolic effect on bone morphology and gene expression [8]. Further analyses are currently underway to identify the cellular and molecular mechanisms underlying the bone phenotype in *Camkk2*$^{\Delta OCY}$ mice and the gender specificity of this effect.

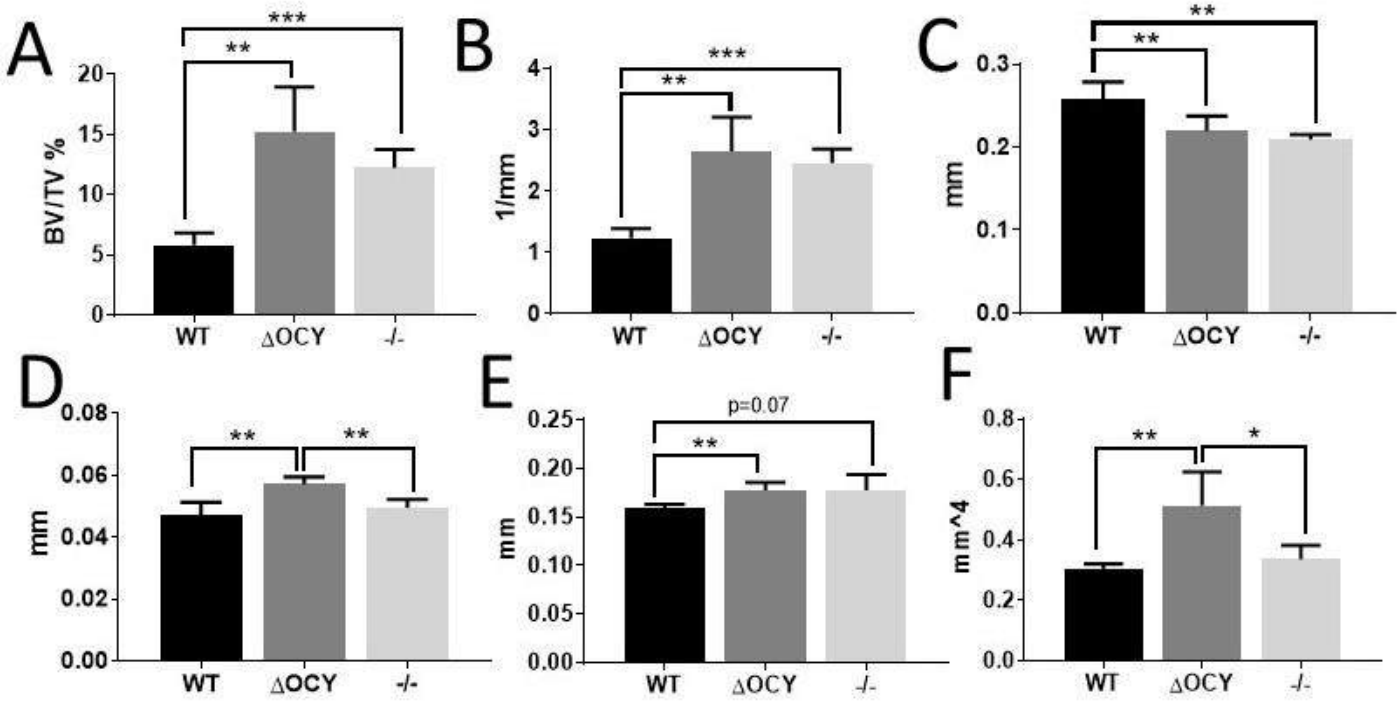

Figure 1: Deletion of CaMKK2 from OCYs in male mice results in enhanced trabecular and cortical bone mass A) Percentage bone volume/tissue volume; B) Trabecular number; C) Trabecular separation; D) Trabecular thickness; E) Cortical thickness; and F) Mean polar moment of inertia (WT n=4; *Camkk2*$^{\Delta OCY}$ n=5; *Camkk2*$^{-/-}$ n=4;*=p<0.05; **=p<0.01; ***=p<0.001; Student's *T*-test).

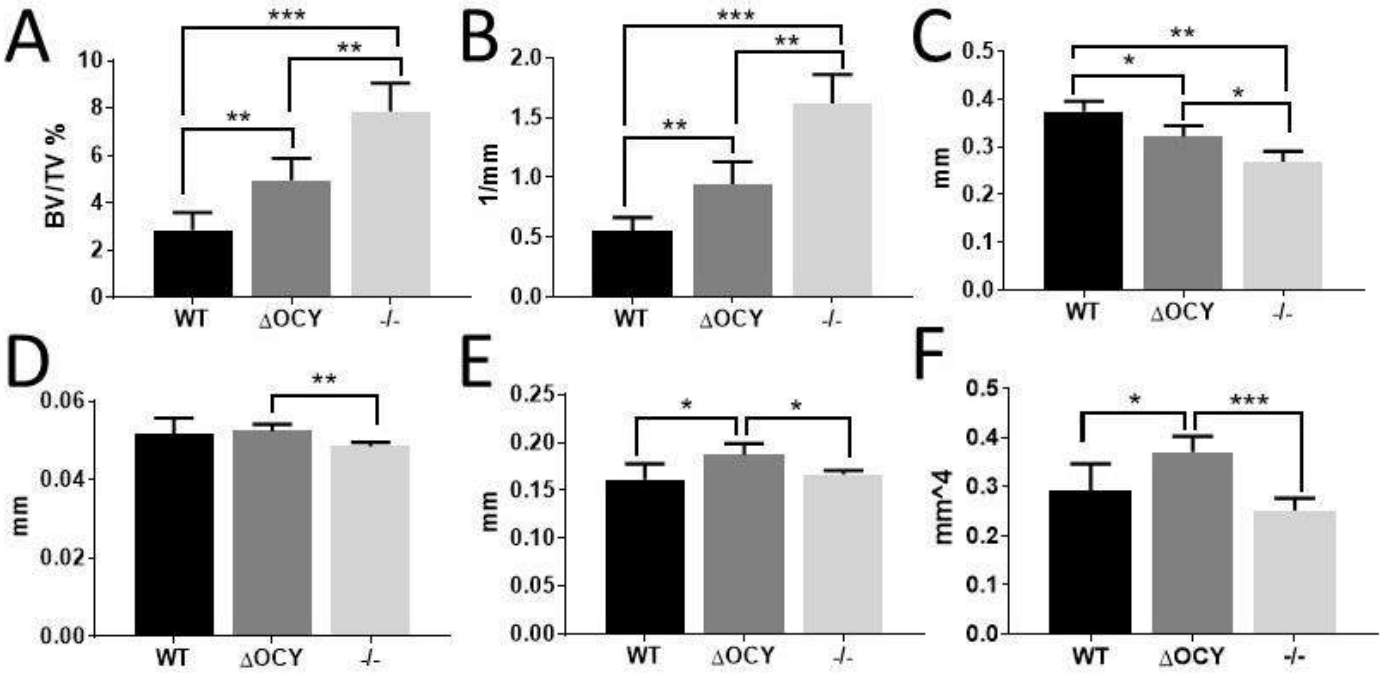

Figure 2: Moderate increases in trabecular and cortical bone mass following the deletion of CaMKK2 from OCYs in female mice. A) Percentage bone volume/tissue volume; B) Trabecular number; C) Trabecular separation; D) Trabecular thickness; E) Cortical thickness; and F) Mean polar moment of inertia (WT n=4; *Camkk2*$^{\Delta OCY}$ n=6; *Camkk2*$^{-/-}$ n=3;*=p<0.05; **=p<0.01; ***=p<0.001; Student's *T*-test).

References:

1. Racioppi, L. and A.R. Means, *Calcium/calmodulin-dependent protein kinase kinase 2: roles in signaling and pathophysiology.* J Biol Chem, 2012. **287**(38): p. 31658-65.
2. Pritchard, Z.J., et al., *Inhibition of CaMKK2 reverses age-associated decline in bone mass.* Bone, 2015. **75**: p. 120-7.
3. Cary, R.L., et al., *Inhibition of Ca(2)(+)/calmodulin-dependent protein kinase kinase 2 stimulates osteoblast formation and inhibits osteoclast differentiation.* J Bone Miner Res, 2013. **28**(7): p. 1599-610.
4. Plotkin, L.I. and T. Bellido, *Osteocytic signalling pathways as therapeutic targets for bone fragility.* Nat Rev Endocrinol, 2016. **12**(10): p. 593-605.
5. Dallas, S.L., M. Prideaux, and L.F. Bonewald, *The Osteocyte: An Endocrine Cell … and More.* Endocrine Reviews, 2013. **34**(5): p. 658-690.
6. Bivi, N., et al., *Cell autonomous requirement of connexin 43 for osteocyte survival: consequences for endocortical resorption and periosteal bone formation.* J Bone Miner Res, 2012. **27**(2): p. 374-89.
7. Stern, A.R., et al., *Isolation and culture of primary osteocytes from the long bones of skeletally mature and aged mice.* Biotechniques, 2012. **52**(6): p. 361-73.
8. Alam, I., et al., *Osteoblast-Specific Overexpression of Human WNT16 Increases Both Cortical and Trabecular Bone Mass and Structure in Mice.* Endocrinology, 2016. **157**(2): p. 722-36.

Linking cortical bone mechanics, structure, and remodeling in the fibula

Lydia P. Bakalova[1], Christina M. Andreasen[2], Jesper S. Thomsen[3], Annemarie Brüel[3], Ellen M. Hauge[4], Birgitte Jul Kiil[5], Jean-Marie Delaisse[6], Thomas Levin Andersen[6], and Mariana E. Kersh[1]

[1]Department of Mechanical Science and Engineering, University of Illinois at Urbana-Champaign Urbana, Illinois, USA

[2]Orthopaedic Research Laboratory, Department of Orthopaedic Surgery and Traumatology, Odense University Hospital, Institute of Clinical Research, University of Southern Denmark, Denmark

[3]Department of Biomedicine Aarhus University Aarhus, Denmark

[4]Department of Rheumatology, Aarhus University Hospital, Aarhus, Denmark

[5]Department of Plastic Surgery, Aarhus University Hospital, Aarhus, Denmark

[6]Dept. of Clinical Cell Biology (KCB), Vejle Hospital – Lillebælt Hospital Institute of Regional Health Research, University of Southern Denmark Vejle, Denmark

Introduction

Osteoporosis is a debilitating bone disease that affects over 200 million people worldwide, and is characterized by an accelerated loss of bone mass and microarchitecture deterioration of both trabecular and cortical bone. This bone loss is the result of a dysfunctional bone remodeling process, in which bone resorption and formation becomes uncoupled and imbalanced, and is suggested to alter its strength and lead to an increased risk of fractures[1,2]. The importance in distinguishing the stages of remodeling is in the resulting morphological map left behind in cortical bone. The aim of this study was to investigate the intracortical compression-induced strain energy distribution, and determine whether the intracortical pores associated with high strain energy density (SED) in the surrounding bone have a different morphology, distribution and remodeling history than pores with low SED.

Methods

The study was conducted on fibula diaphysis specimens from 20 patients undergoing a jaw reconstruction (age range 43-75 years, 14 men and 6 women). Specimens were plastic embedded, µCT-scanned and sectioned for histology. Pore size, circularity, and location with respect to the bone edges was quantified using custom code. Three-dimensional micro-finite element models of each specimen were tested in compression using a linearly elastic analysis, and the SED of the bone immediately surrounding the pores was calculated within a plane of interest corresponding to the histological sections. The statistical distribution of the SED of all pores, per sample, was used to identify high SED pores (SED > 1.5 times the interquartile range from the 75th percentile) and the remaining low SED pores.

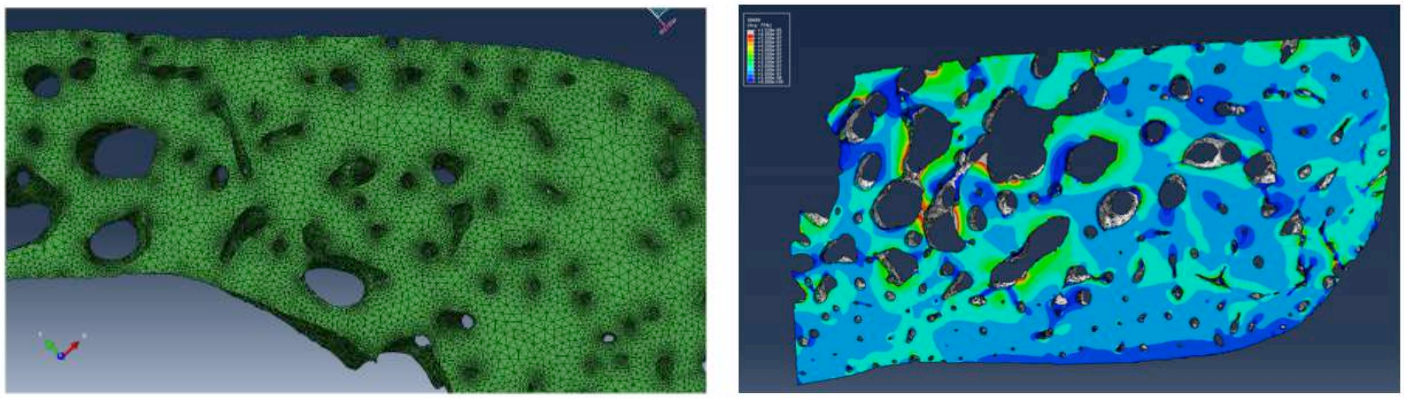

Figure 1: Three-dimensional finite element model of cortical diaphysis (left) and representative strain energy density distribution (right).

Results

Pores with high SED were larger ($p \leq 0.0001$), less circular ($p \leq 0.0001$), and were located closer to the endosteal edge of the cortex ($p \leq 0.0001$) than low SED pores (Figure 2A-C). A detailed histological analysis of the remodeling events generating the pores revealed that the high SED pores compared to low SED pores had 13.3-fold higher odds of being a resorptive (70%) or formative (11%) pore rather than a completely remodeled pore ($p \leq 0.0001$). Compared to the low SED pores, the resorption space associated with the high SED pores had 5.9-fold higher odds of overlapping with the pore of a preexisting osteon (type 2 pore - 91%) than having no overlap (type 1 pore – 9%) ($p \leq 0.0001$).

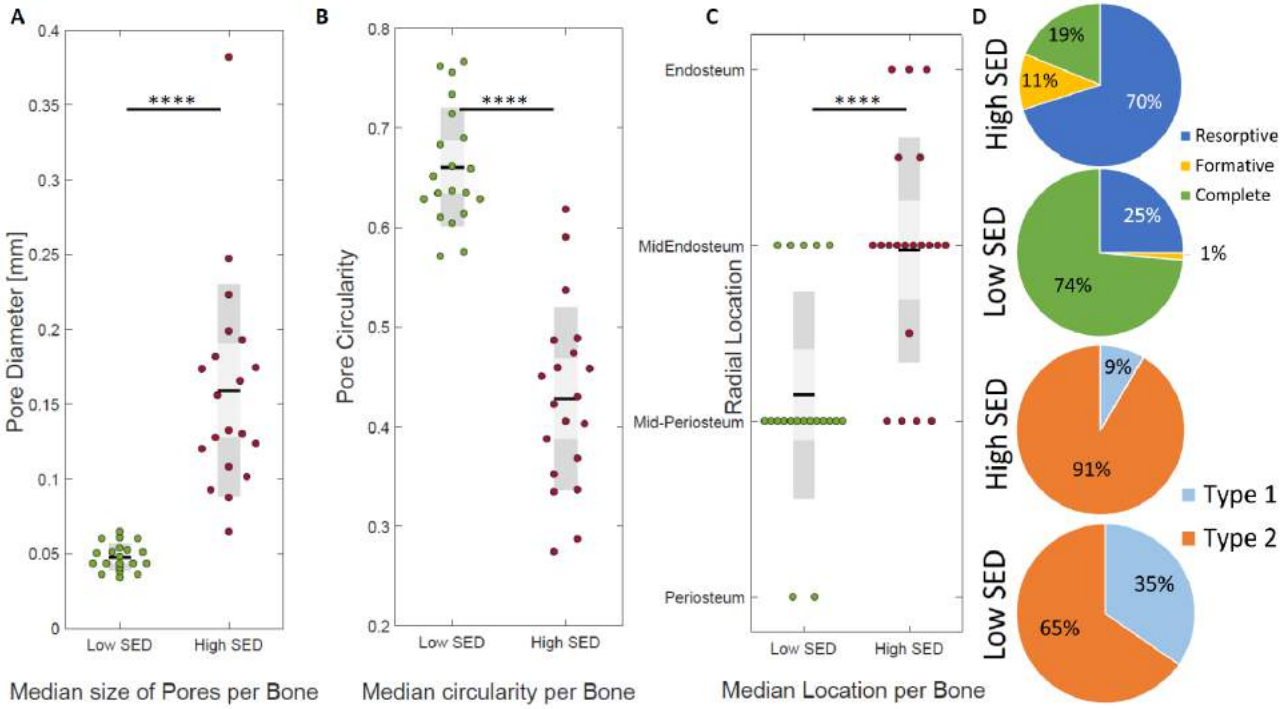

Figure 2: *Structure and cellular events associated with low and high SED pores. Pore size (A), Pore circularity (B), and location (C) per SED category across all samples (n=20); (D) Distribution of type and stage of remodeling with respect to SED. Low SED pores (n = 947 pores), High SED pores (n = 117 pores). (Top) Distribution of remodeling stage. (Bottom) Distribution of type 1 and 2 pores with respect to SED.*

Discussion

Collectively, these data show that the high SED pores are enlarged irregular pores positioned closer to the endosteal surface of the cortex. These pores tend to be resorptive and overlap with the pore of a preexisting parent osteon, suggesting that these pores may originate from resorption within preexisting pores rather than from penetrative resorptions generating new pores. Overall, the study demonstrates a strong relationship between cortical bone mechanics and pore morphology, distribution and remodeling history in the human fibula.

References

1. Andersen, T. L., Abdelgawad, M. E., Kristensen, H. B., Hauge, E. M., Rolighed, L., Bollerslev, J., Kjærsgaard-Andersen, P., and Delaisse, J. M. Understanding coupling between bone resorption and formation: Are reversal cells the missing link? *American Journal of Pathology*, 183(1):235–246, 2013.
2. Hirano, T., Turner, C. H., Forwood, M. R., Johnston, C. C., and Burr, D. B. Does suppression of bone turnover impair mechanical properties by allowing microdamage accumulation? *Bone*, 27(1):13–20, 2000.

United States. **302,** 1573–1579 (2009).
5. Van Der Meulen, M. C. H. & Huiskes, R. Why mechanobiology? A survey article. *J. Biomech.* **35,** 401–414 (2002).
6. Carter, D. R., Beaupré, G. S., Giori, N. J. & Helms, J. A. Mechanobiology of skeletal regeneration. *Clin. Orthop. Relat. Res.* **355,** S41–S55 (1998).
7. Jacobs, C. R. The mechanobiology of cancellous bone structural adaptation. *J. Rehabil. Res. Dev.* **37,** 209–216 (2000).
8. Shefelbine, S. J. & Carter, D. R. Mechanobiological predictions of growth front morphology in developmental hip dysplasia. *J. Orthop. Res.* **22,** 346–352 (2004).
9. Sharma, D. *et al.* Alterations in the Osteocyte Lacunar-Canalicular Microenvironment due to Estrogen Deficiency. *Bone* **51,** 488–497 (2012).
10. Bailey, C. a & Brooke-Wavell, K. Exercise for optimising peak bone mass in women. *Proc. Nutr. Soc.* **67,** 9–18 (2008).
11. Bassey, E. J., Rothwell, M. C., Littlewood, J. J., Pye, D. W. Pre- and postmenopausal women have different bone mineral density responses to the same high-impact exercise. *J. Bone Miner. Res.* **13,** 1805–1813 (1998).
12. Bassey, E. J., Littlewood, J. J. & Taylor, S. J. G. Relations between compressive axial forces in an instrumented massive femoral implant, ground reaction forces, and integrated electromyographs from vastus lateralis during various 'osteogenic' exercises. *J. Biomech.* **30,** 213–223 (1997).
13. Warden, S. J. *et al.* Physical activity when young provides lifelong benefits to cortical bone size and strength in men. *Proc. Natl. Acad. Sci. U. S. A.* **111,** 5337–42 (2014).

Chondro-Protective Function of Statin Is Related to the Inhibition of Small GTPase Activities

Mengxi Lv, Yilu Zhou, X. Lucas Lu
Department of Mechanical Engineering, University of Delaware, Newark, DE 19716

Introduction

In the early stages of osteoarthritis (OA), catabolic activities are often promoted in chondrocytes by OA-inducing factors; and meanwhile cells undergo a cascade of phenotypic changes, including swelling, proliferation, hypertrophy and apoptosis [1]. The aberrant cellular process is dependent on the activities of small GTPases (Rho, Ras, Rac etc.). The post-translational prenylation of small GTPases requires geranylgeranyl- and farnesyl-pyrophosphates in cells, which are two down-stream products in the mevalonate pathway [2]. Therefore, the inhibition of the mevalonate signaling in chondrocytes might be able to prevent the cells from the aberrant phenotypic shift after joint injuries by disabling the activities of small GTPases. Statins, a class of drugs used for the prevention of cardiovascular diseases, can control cholesterol levels by inhibiting mevalonate signaling. In this study, we hypothesized that inhibition of the mevalonate pathway and its downstream small GTPases in chondrocytes, using statin, can prevent cells from the aberrant phenotypic shift after joint injuries and further suppress the osteoarthritis development.

Chondro-protective Effects of Statin

Cylindrical cartilage explants (diameter = 3 mm and thickness = 2 mm) were harvested from calf knee joints and cultured in a chemically defined medium up to 26 days [3]. A pro-inflammatory cytokine, IL-1β, at 1 ng/mL was introduced into the culture medium of cartilage explants to mimic a moderate inflammation insult to cartilage. Simvastatin was supplemented simultaneously with IL-1β into the medium at day 0. Explants were divided into six groups for in vitro culture: 1) control, 2) IL-1β, 3) IL-1β + 1 μm statin, 4) IL-1β + 3 μm statin, 5) IL-1β + 10 μm statin, and 6) 10 μm statin alone. The loss of GAG and collagen contents from the cartilage explant into the culture medium was measured every other day. As results, statin in medium significantly reduced the IL-1β-induced GAG loss in a dose-dependent manner (Fig. 1A). The collagen loss induced by IL-1β was negligible in the first 10-day culture and became substantial from day 12 to 24. The loss of collagen from explant was almost completely abolished by 10 μm statin treatment (Fig. 1B). Mechanical properties of cartilage explants were measured via indentation test after 8-day culture. Statin treatment (10 μm) prevented the decrease of Young's modulus induced by IL-1β ($P < 0.05$) (Fig. 1C). To track the change of cell volume, *in situ* chondrocytes in the explant were dyed with CellTracker™ (Thermo Fisher). IL-1β in medium increased the volume of chondrocytes by 68.2% after 4 days, while the swelling was fully prevented by statin ($P < 0.001$) (Fig. 1D).

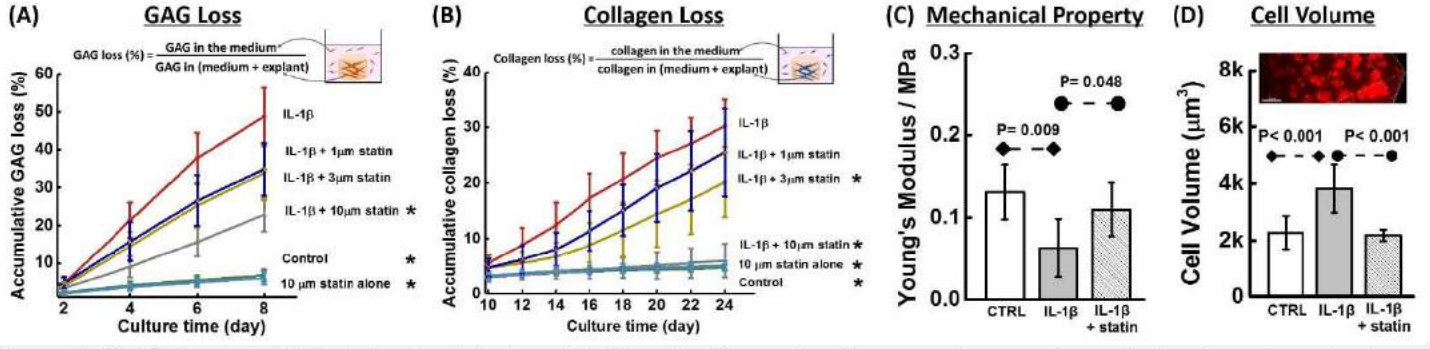

Figure 1: (A-B): Statin inhibited the IL-1β-induced GAG and collagen loss from cartilage explants during long-term *in vitro* culture. Loss of collagen content started 10 days later than GAG content. (N=6 explants from 3 animals. *: vs. IL-1β; $P < 0.01$). **(C)**: Young's modulus of cartilage explants was preserved by 10 μM statin treatment after 8-day culture (N=6 explants from 3 animals). **(D)**: Statin inhibited the cell swelling induced by IL-1β after 4-day culture (N= 32 cells in 2 explants from 2 animals).

Genome-wide Effects of Statin on in situ Chondrocytes

The whole-genomic expression change induced by statin in chondrocytes was assessed by RNA sequencing (RNA-seq). Cartilage explants were cultured in medium supplemented by IL-1β or IL-1β + statin. After 48-hour in vitro culture, the RNA was extracted from explants for sequencing. As results, statin significantly changed the expression of 1,048 genes in chondrocytes, among which 690 genes were up-regulated and 459 genes down-regulated when compared to the IL-1β alone group (absolute fold change > 1.5 and FDR < 0.05) (Fig. 2A). The expression of catabolic genes in ADAMTS- and MMP-family was significantly suppressed by statin (Fig. 2B). RNA-seq also identified that the small GTPases was among the 18 most significantly changed pathways in statin-treated samples (Fig. 2C). The major genes related to mevalonate

pathway were substantially up-regulated in the statin group, which could be a compensatory response to statin regulation (Fig. 2D).

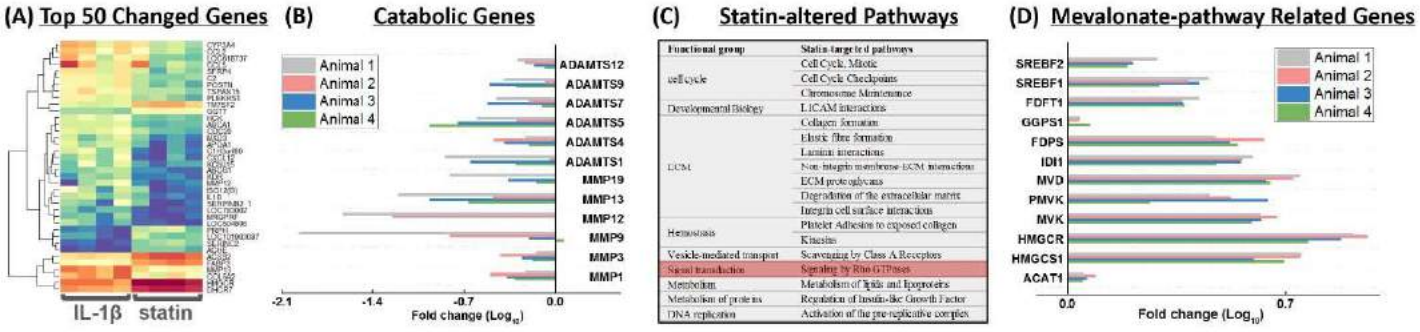

Figure 2: (A): RNA sequencing identified 1,048 genes that are significantly changed by statin treatment. The top 50 changed genes were listed in the heatmap (N=4 explants from 4 animals). **(B):** Catabolic genes (ADAMTS- and MMP-family) were down-regulated by statin treatment. **(C):** Pathway analysis identified 18 pathways in chondrocytes that were significantly changed by statin, including the mevalonate pathway (highlighted in the red box). **(D):** Statin treatment induced compensatory up-regulation of the mevalonate related genes in chondrocytes.

Chondro-protective Effect of Another Mevalonate Inhibitor - Bisphosphonate

In vitro Cartilage Explant Model – To verify the role of mevalonate pathway, we replaced statin with another mevalonate pathway inhibitor, called zoledronate (ZA), in the cartilage explant model. Zoledronate belongs to the bisphosphonate family that is widely used for the treatment of osteoporosis. Bisphosphonates can inhibit the mevalonate pathway in osteoclasts and prevent the formation of ruffled cell membrane [4]. In this study, zoledronate demonstrated protection effects similar to statin, reducing the loss of GAG and type II collagen contents from the IL-1β-treated cartilage explants (Fig. 3A-B). Mechanical integrity of cartilage explant was also preserved by zoledronate, which attenuated the decrease in Young's modulus, dynamic modulus, and the increase of permeability (P = 0.01 for all) (Fig. 3C).

DMM Mouse Model – We further tested the chondro-protective function of zoledronate in a DMM (destabilization of the medial meniscus) mouse model. Significant cartilage degeneration was observed in 12 weeks after the DMM surgery (Fig. 3D Left). Systemic injection of zoledronate (0.15mg/kg, twice per week) significantly suppressed the osteoarthritis development in DMM mice. OARSI score of the drug treated mice is similar to those of the sham groups, and significantly lower than the DMM vehicle group (Fig. 3D Right). Zoledronate inhibited the OA progression in mouse knee joints after the DMM surgery.

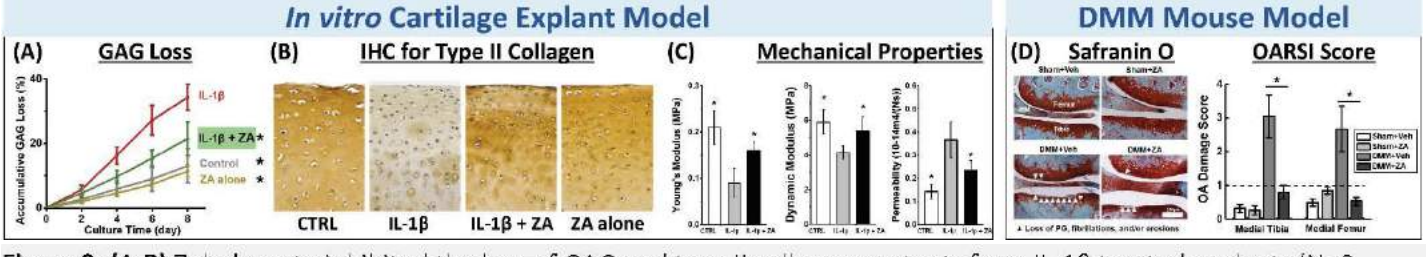

Figure 3: (A-B) Zoledronate inhibited the loss of GAG and type II collagen contents from IL-1β treated explants (N=8 explants from 4 animals, *: vs. IL-1β; P < 0.01). **(C)** Zoledronate protected the mechanical integrity of cartilage from IL-1β attack (N=8 explants from 4 animals, *: vs. IL-1β; P < 0.01). **(D)** Systemic injection of zoledronate inhibited the OA progression in DMM mouse model. L: Histology of knee joints; R: OA damage score (N=10 animals, *: P < 0.01).

Role of Small GTPases in Mevalonate Pathway

Statin inhibits the hydroxyl-methyl-glutaryl Coenzyme A (HMG-CoA) reductase, while bisphosphonates inhibit the FPP synthase of the mevalonate pathway in cells (Fig. 4A). Both HMG-CoA and FPPS play important roles in regulating the prenylation of downstream small GTPases. To test whether the chondro-protective function of mevalonate inhibitors is related to small GTPases, we supplemented the culture medium of explants by statin and GGOH. GGOH is an intermediate derivative of the mevalonate pathway, which can restore the statin-impaired activities of small GTPases. As expected, GGOH substantially abolished the chondro-protective effects of statin. The loss of GAG and collagen contents induced by IL-1β no longer be protected by the statin (Fig. 4B). To confirm this finding, we further tested the effects of two antagonists of small GTPases, GGTI and Rhoi. GGTI can inhibit the function of GGOH, while Rhoi directly interrupts the

activation of Rho protein. In our cartilage explant study, GGTI showed strong chondro-protective effects similar to the statin, by significantly inhibiting the IL-1β-induced loss of GAG and collagen contents (Fig. 4C). Rhoi also reduced the IL-1 β -induced loss of extracellular matrix, although its protective effect is not as potent as that of GGTI or statin. Therefore, the chondro-protective function of statin and bisphosphonate is related to the inhibition of small GTPases in chondrocytes.

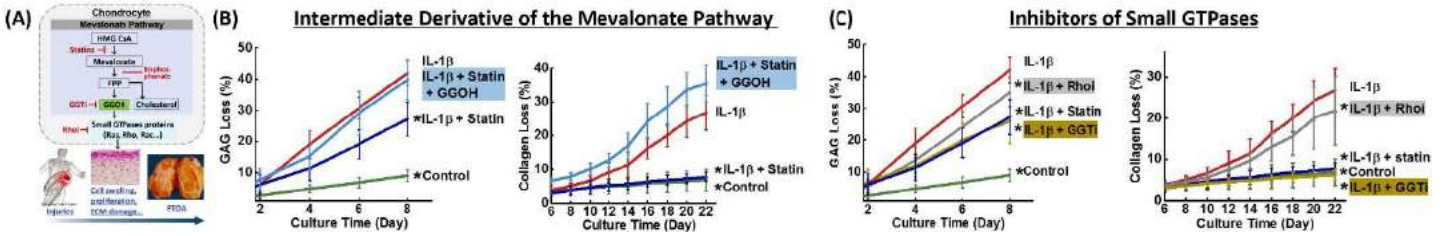

Figure 4: (A) The chondro-protective function of statin and bisphosphonate is related to the inhibition of small GTPases in chondrocytes, which are required for the aberrant phenotypic shift of chondrocytes under inflammatory attack. **(B)** The intermediate derivative of mevalonate pathway (GGOH), which can recover the prenylation of small GTPases, abolished the chondro-protective effects of statin (N=6 explants from 3 animals, *: vs. IL-1β; $P < 0.01$). **(C)** Antagonists of small GTPases, GGTi and Rhoi, also prevented the loss of GAG and collagen contents from IL-1β treated cartilage explants (N=6 explants from 3 animals). (*: vs. IL-1β; $P < 0.05$. $: vs. IL-1β + statin; $P < 0.01$).

Statin and Calcium Signaling of Chondrocytes

In chondrocytes, the intracellular calcium ([Ca2+]i) signaling is one of the earliest cellular responses to mechanical stimulation and regulates a wide range of biological processes. Activities of small GTPases are closely interwoven with [Ca2+]I signaling (Fig. 5A) [5]. To further understand the chondro-protective function of statin, we investigated the [Ca2+]i signaling of *in situ* chondrocytes. Cartilage explants were cultured with 1) IL-1β and 2) IL-1β + 10 μm statin for 2 days, and then dyed with Fluo-8 calcium dye. The spontaneous calcium signaling of *in situ* chondrocytes in cartilage explant was recorded for 16 minutes using a confocal microscope (Fig. 5B). In the IL-1β + statin group, there were more chondrocytes showing [Ca2+]i oscillation than those in the IL-1β alone group ($P < 0.001$). Responsive cells in the statin group also had [Ca2+]i peaks with higher magnitude, and took shorter time to recover from a [Ca2+]i peak (Fig. 5C).

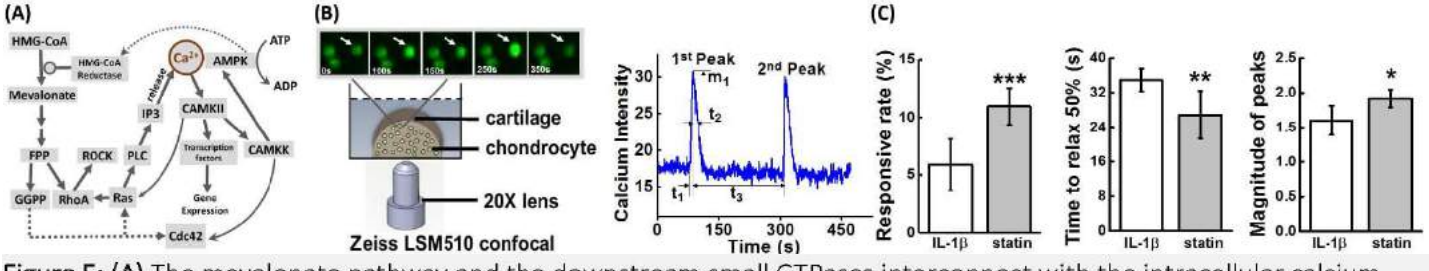

Figure 5: (A) The mevalonate pathway and the downstream small GTPases interconnect with the intracellular calcium signaling. **(B)** The microscopy setup to record the spontaneous $[Ca^{2+}]_i$ signaling of *in situ* chondrocytes in cartilage explant and a typical $[Ca^{2+}]_i$ oscillation curve of chondrocytes. **(C)** Statin promoted the calcium signaling in IL-1β treated cartilage explants in terms of responsive rate, magnitude of $[Ca^{2+}]_i$ peaks, and recovery time of cells after a $[Ca^{2+}]_i$ peak (N=6 from 3 animals). (*: $P < 0.05$; **: $P < 0.01$; ***: $P < 0.001$)

Summary

In this study, we found that two mevalonate inhibitors, statin and bisphosphonate, can protect the integrity of cartilage extracellular matrix in the presence of inflammatory stimulation. The chondro-protective functions of two classes of drugs are related to the inhibition of mevalonate pathway and the subsequent inhibition of the small GTPases in chondrocytes. Loss of small GTPases prevented the chondrocytes from aberrant phenotypic shift and destructing the ECM. Findings in this study provided: 1) critical justifications regarding the application of statins and bisphosphonates for PTOA prevention, 2) guidance for future clinical trials of the mevalonate inhibitors in OA prevention, including the targeted population, design of delivery methods, and timing of drug administration, and 3) a new target pathway in chondrocytes, *i.e.*, small GTPases, for the inhibition of osteoarthritis initiation after joint injuries.

Reference: [1] Pencina, M., et al., NEJM, 2014. [2] Lazzerini, P., et al., Semin in A&R, 2011. [3] Bian, L., et al., J Biomech, 2008. [4] Ken Beauchamp J.Clin. Invest, 2001. [5] Novakofski, K., JOR. 2009.

Early Subchondral Bone and Articular Cartilage Compositional Changes in the Medial Compartment after DMM Surgery Quantified by μCT

Maleeha Mashiatulla[1,2], Jun Li[3], Amit N. Patwa[4], Mark W. Grinstaff[4], Anna Plaas[3], D. Rick Sumner[1,2]

1. Anatomy & Molecular Medicine, Rush University Medical Center, Chicago, IL, USA. 2. Bioengineering, University of Illinois at Chicago, Chicago, IL, USA. 3. Internal Medicine, Rush University Medical Center, Chicago, IL, USA. 4. Biomedical Engineering and Chemistry, Boston University, Boston, MA, USA.

INTRODUCTION: Osteoarthritis (OA) is a degenerative disease characterized by both bone and cartilage damage. Cartilage damage has been widely studied and was thought to be the primary reason for joint degeneration. The hallmarks of cartilage damage are loss of cartilage thickness, fibrillation, and loss in proteoglycan (PG) content[1; 2]. More recently, the role of the subchondral bone has been studied and alterations in bone remodeling, osteocyte density and thickness have been observed[3; 4]. However, it has been difficult to determine whether the initiation or progression of OA is primarily due to alteration in bone or cartilage or both simultaneously. Studies have shown that if a bone remodeling inhibitor is administered post-injury, the damage to both the bone and cartilage can be significantly minimized[5; 6], suggesting that the subchondral bone may play an important role in disease progression. We sought to study early alterations in cartilage and bone to determine which compartment undergoes degeneration first. Specifically, we used the mouse destabilization of the medial meniscus (DMM) model to assess early effects on bone and cartilage composition in 3-dimensions with micro-computed tomography (μCT). For bone, the bone mineral density distribution (BMDD)[7] was characterized and for cartilage the proteoglycan (PG) density was measured using the contrast agent (CA4+)[8]. Previously, in this model we showed simultaneous changes in bone and cartilage when analyzing the entire distal femur[9]. Here, we refine the analysis by focusing on the medial compartment.

METHODS: DMM surgery was performed on the right knee of 50 (n = 8-14/time point) male C57Bl/6 mice. Mice were euthanized ~2 hours after surgery (0), and at 1, 2, 4 and 8 weeks (currently only analyzed n=5/ time point). The right (DMM) and left (contralateral control) femurs were harvested, fixed in 10% formalin for 3 days and stored in 70% EtOH. The distal 1.8 mm of all femurs was imaged for both cartilage and bone. Scans for BMDD analysis were performed at 70 kVp, 57 μA, 1500 ms integration time, 9 mm diameter scanning tube, a voxel size of 2 μm and scanned in storage media (Scanco Medical μCT50, Basserdorf, Switzerland). Hydroxyapatite phantoms (0-1860 mgHA/cm^3) were scanned before and after all bone scans to calibrate linear attenuation coefficients to mineral density values. After completion of bone scans, femurs were incubated in CA4+ for a minimum of 40 minutes at a concentration of 12mg/ml[10] and scanned in air at 45 kVp, 133 μA, 1000 ms, and a voxel size of 2 μm. Contours were drawn to isolate the medial subchondral plate and cartilage for further analysis. The following outputs were quantified: subchondral plate BMDD characteristics (mean mineralization, FWHM, standard deviation, 5% and 95% cutoffs) and cartilage x-ray attenuation (directly proportional to PG density). Repeated measures ANOVAs (side-by-time) were performed and post-hoc paired t-tests were used to identify which specific side differences were significant.

RESULTS: Significant side differences were observed for all bone and cartilage compositional parameters except the heterogeneity measured by the coefficient of variation method (Table 1). Significant side-by-time interactions were observed for only the upper ($p = 0.002$) 5% cutoffs and a significant time effect was observed only for peak mineralization ($p = 0.010$). Specifically, a 24% decrease in peak mineralization was observed between 0 and 4 weeks ($p=0.008$). At 1 week post-surgery, a 21% decrease in lower 5% cutoff was observed in the DMM side compared to the contralateral side ($p = 0.027$). At 2 weeks, decreases of 12% ($p < 0.001$), 7% ($p = 0.008$), 53% ($p = 0.001$), and 6% ($p < 0.001$) were observed for mean mineralization, peak mineralization, lower 5%, upper 5% cutoff, respectively, in the DMM side compared to the contralateral. A 17% increase in heterogeneity in the DMM side compared to the contralateral side was observed at 2 weeks ($p < 0.001$). Further, a 10% ($p = 0.038$) decrease in the upper 5% cutoff was found at 4 weeks between the DMM and contralateral sides. Significant decreases for cartilage attenuation of 3% ($p = 0.019$), 8% ($p = 0.005$) and 8% ($p = 0.026$) were observed in the DMM side compared to the contralateral side at 0, 1 and 2 weeks, respectively, indicating decreases in PG content in the

DMM side. The magnitude of the inferred changes were greater for the subchondral plate compared to the cartilage (Fig. 1).

DISCUSSION: In our previous study using these same specimens, we also reported on alterations in structure (including subchondral plate and articular cartilage thickness and articular surface roughness) for the entire femur. Analysis of these specimens by anatomic compartment (medial condyle, lateral condyle, patellar groove) is ongoing and will present a detailed map of the early responses to DMM surgery in the mouse model. Here we focused on composition of the bone and cartilage in the medial compartment. In this study, we showed that bone mineral and cartilage composition are affected as early as 1 week following surgery in the DMM model of OA. A 3% decrease in cartilage attenuation was observed in the DMM side compared to the contralateral side at the 0-week time point. There are two possible explanations for this; either the cartilage composition changes just hours post-injury or more likely a larger sample size is needed. Currently, we are in the process of analyzing more samples. Side-to-side differences at baseline were not observed for bone. For bone, the emergence of side-to-side differences at 1 week in subchondral plate BMDD is indicative of bone remodeling being initiated early in the disease process. Changes in mineralization have been shown in later stages of OA[4; 11], but had not previously been studied at such early stages of OA development. Further structural analysis of the subchondral plate and cartilage will yield a better understanding of the changes undergone in both compartments due to the initiation of OA.

SIGNIFICANCE: To our knowledge, this is the first study to examine both cartilage and bone compositional changes on the same sample in 3-dimensions in the early stages of OA development. In this study, we found alterations in bone and cartilage composition as early as 1 week post-DMM surgery.

ACKNOWLEDGEMENTS: µCT scanning was performed at the Rush University Medical Center MicroCT/Histology Core. Research reported in this abstract was supported by the National Institutes of Health under award number R01-AR057066 and The Katz-Rubschlager Endowment of OA Research. The content is solely the responsibility of the authors and does not necessarily represent the official views of the National Institutes of Health.

REFERENCES:

(1)Aigner, T. Cell Mol Life Sci., 2002. (2) Plaas A. Osteoarthritis Cartilage. 2011. (3) Burr, DB. Curr Opin Rheumatol. 1998. (4) Bertuglia, A. Osteoarthritis Cartilage. 2016. (5) Hayami, T. Bone. 2012. (6) Hayami, T. Arthritis Rheum. 2004. (7) Roschger, P. Bone. 1998. (8)Bansal, PN. Osteoarthritis Cartilage. 2010. (9) Mashiatulla, M. ORS. 2017. (10)Joshi, N.S. J Am Chem Soc. 2009. (11) Burr, DB. Nat Rev Rheumatol. 2012.

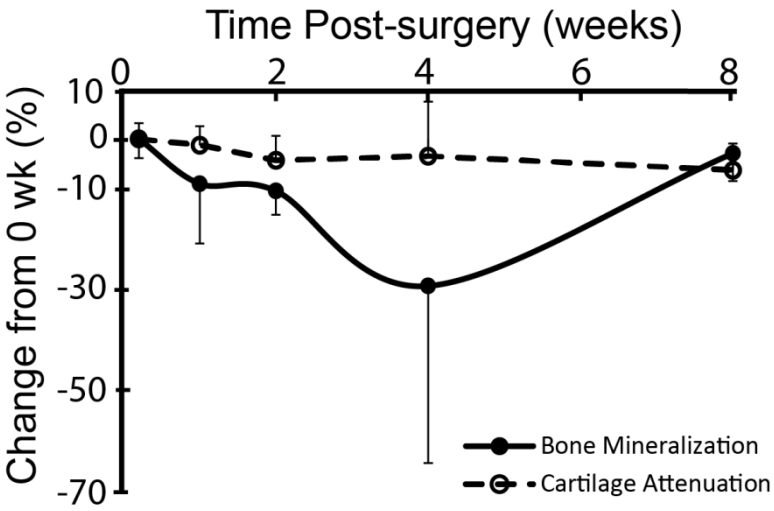

Figure 1: Inferred changes in subchondral plate mean mineralization and articular cartilage PG density post-DMM surgery. These values were calculated by dividing individual values at each time point for the DMM limb by the mean for the DMM limb at time 0.

Table 1: Means and standard deviation for cartilage and subchondral plate compositional parameters, along with results from Repeated Measures ANOVA (α = 0.05).S = side, SxT = Side-by-time, T = time CL = contralateral side and PTT = paired t-test.

Bone Composition																				
	Weeks	**0**			**1**			**2**			**4**			**8**			**S**	**SxT**	**T**
Mean Mineralization ($mgHA/cm^3$)	**CL**	1038	±	38	979	±	89	1060	±	26	982	±	232	1075	±	78	0.008	0.210	0.161
	DMM	1032	±	39	941	±	122	926	±	49	732	±	362	1003	±	57			
	PTT	0.705			0.154			< 0.001			0.198			0.153					
Peak Mineralization ($mgHA/cm^3$)	**CL**	1327	±	52	1398	±	24	1376	±	46	1206	±	373	1432	±	23	0.050	0.129	0.010
	DMM	1344	±	21	1368	±	17	1275	±	90	813	±	558	1399	±	57			
	PTT	0.479			0.080			0.008			0.199			0.207					
Lower 5% Cutoff (mgHA/cm3)	**CL**	170	±	19	167	±	46	180	±	27	174	±	75	187	±	51	< 0.001	0.090	0.341
	DMM	172	±	22	132	±	50	85	±	16	65	±	120	142	±	38			
	PTT	0.921			0.027			0.001			0.142			0.058					
Upper 5% Cutoff (mgHA/cm3)	**CL**	1733	±	49	1743	±	38	1776	±	37	1712	±	144	1802	±	34	< 0.001	0.002	0.073
	DMM	1739	±	28	1719	±	60	1669	±	53	1536	±	202	1764	±	46			
	PTT	0.601			0.283			< 0.001			0.038			0.157					
Heterogeneity (CoV)	**CL**	36.34	±	1.64	40.13	±	4.49	36.40	±	1.50	38.53	±	8.75	36.80	±	4.32	0.093	0.427	0.262
	DMM	36.87	±	1.93	41.77	±	5.57	42.51	±	1.45	59.25	±	38.31	40.17	±	2.75			
	PTT	0.705			0.175			< 0.001			0.318			0.117					
Cartilage Composition																				
	Weeks	**0**			**1**			**2**			**4**			**8**			**S**	**SxT**	**T**
Mean Attenuation (cm^{-1})	**CL**	2.68	±	0.05	2.77	±	0.06	2.71	±	0.06	2.67	±	0.11	2.59	±	0.26	< 0.001	0.821	0.276
	DMM	2.59	±	0.08	2.56	±	0.10	2.48	±	0.12	2.50	±	0.28	2.43	±	0.14			
	PTT	0.019			0.005			0.026			0.208			0.292					

Inhibition of CaMKK2 attenuates subchondral bone remodeling in post-traumatic osteoarthritis model

Elsa Mével1, Anthony Huls1, Yong Li1 and Uma Sankar1
1Department of Anatomy and Cell Biology, Indiana University School of Medicine, Indianapolis, IN 46202, USA

Introduction- OA is a common inflammatory joint disease that disproportionately affects the elderly (1) and associated with a heavy socio-economic burden (2). Clinically, OA is characterized by progressive cartilage loss, subchondral bone sclerosis and remodeling, osteophyte formation and inflammation affecting all joint tissues (3, 4). Changes at subchondral bone play a key role in the disease process. Several studies have demonstrated that the subchondral bone remodeling that occurs in OA involves both bone resorption and formation (5-9). Despite recent advances in the understanding of the cell and molecular processes involved in OA pathogenesis, curative treatments are still lacking. Currently available pharmacological drugs only alleviate inflammation and pain in OA patients but do not alleviate or reverse the progression of cartilage degradation and bone disease (10). Thus, therapeutic strategies that are able to collectively blunt the progressive degradation of joint tissues and subchondral bone while also ameliorating inflammation-associated pain are urgently needed.

Calcium (Ca2+) is a trace element involved in bone mineralization. In skeletal cells, Ca2+ binds to calmodulin (CaM) and activates large numbers of proteins, including CaM-dependent protein kinases (CaMKs) (11, 12). Among these, CaMKK2 plays a crucial role in anabolic and catabolic activities in bone cell biology (13, 14). Pharmacological inhibition or genetic ablation of CaMKK2 protects mice from bone loss (14) by promoting bone formation (increased level of osteoblasts (OBs)), and inhibiting bone resorption (decreased level of osteoclasts (OCs)) (13). Furthermore, CaMKK2 is also implicated in macrophage-mediated inflammation as the global knockout mice are protected from LPS or high-fat diet-induced inflammation, compared to wild type (WT) mice (15). Since CaMKK2 plays a role in bone remodeling and inflammation, two main mechanisms in OA progression, we hypothesized that CaMKK2 could plays a protective role in OA.

Materials and methods- The impact of CaMKK2 deficiency in articular cartilage physiopathology was evaluated in murine articular chondrocytes (MACs) stimulated by interleukin-1 (IL-1β). Real-time PCR was used to monitor the expression of transcripts for inflammatory (iNOS, COX2, IL6) and catabolic (MMP2-9-13 and ADAMTS5) markers. The related inflammation products (nitric oxide (NO), prostaglandin E2 (PGE2), interleukin-6 (IL-6)) were also measured. We also evaluated whether loss or pharmacological inhibition of CaMKK2 would affect subchondral bone remodeling associated with OA using a destabilization of medial meniscus (DMM) model of post-traumatic OA. Ten week-old WT (n=15) or *Camkk2-/-* male mice (n=10) were subjected to unilateral DMM or sham surgery. CaMKK2 pharmacological inhibitor (STO-609) or saline solution were administrated tri-weekly by intra-peritoneal injection for 8 weeks following surgery to the WT mice. Subchondral bone remodeling was evaluated by microcomputed tomography (µCT) 8 weeks after surgery.

Results- Data obtained in MACs reveal that the absence of CaMKK2 (*Camkk2-/-*) did not alter the basal expression of catabolic (MMP2-13 and ADAMTS5; Figure 1 a-c) and inflammatory (iNOS, COX2, IL6; Figure 1 d-f) markers. Stimulation with IL-1β results in a significant elevation of inflammatory (iNOS, COX2, IL6) and catabolic (MMP2-13 and ADAMTS5) markers in WT MACs, but not in *Camkk2-/-* MACs. Consistent with this, the level of related inflammation products (NO, PGE2, IL-6) were significantly elevated in culture supernatants obtained from IL-1β –stimulated WT MACs compared to those from *Camkk2-/-* MACs (Figure 1 g-i). Three dimensional µCT images of coronal view of tibial subchondral bone showed a significant increase by 40% of the tissue volume (TV) and by 18% the bone volume density (BV/TV) in DMM mice relative to sham-operated control mice (Figure 1 j-l). In addition, the thickness of subchondral bone plate (SPB) was 32% higher in DMM mice compared to sham operated cohorts (Figure 1m). Together these results demonstrated an enhanced subchondral bone sclerosis after DMM surgery. Interestingly, such increases in TV and BV/TV following DMM were significantly diminished in CaMKK2 inhibitor-treated WT mice and *Camkk2-/-* mice, indicating protection from subchondral bone sclerosis induced by DMM (Figure 1 j-l). Moreover, SBP thickness was significantly lower in STO-609 treated WT and *Camkk2-/-* mice, compared to saline treated WT cohorts (Figure 1m).

Discussion- Since IL-1β is a major cytokine involved in OA pathogenesis, *in vitro* models of IL-1β-treated chondrocytes have been widely used to screen drugs or natural compounds in the field of OA treatment (16). Interestingly, our data have shown that genetic ablation of CaMKK2 was able to counteract the effects of IL-1β by not only affecting the expression levels of transcripts encoding for catabolic enzymes (MMP2-13 and ADAMTS5) and inflammatory markers (iNOS, COX2 and IL6), but also by reducing their inflammatory related secreted products NO, PGE2 and IL-6 respectively. These data are

consistent with a previous study establishing the anti-inflammatory effect of CaMKK2 in LPS-induced *in vitro* and high fat diet mice models (15). Bone disease is a hallmark of OA (17) as demonstrated by our *in vivo* DMM model which was associated with subchondral bone sclerosis at 8 weeks after surgery. Interestingly, pharmacological inhibition or genetic ablation of CaMKK2 prevents the subchondral bone remodeling induced by the surgical destabilization model of OA, suggesting that the loss of CaMKK2 may have a therapeutic effect on OA. In conclusion, our study indicates a novel role for CaMKK2 in OA pathogenesis and opens new avenues to design innovative therapeutic strategies against OA.

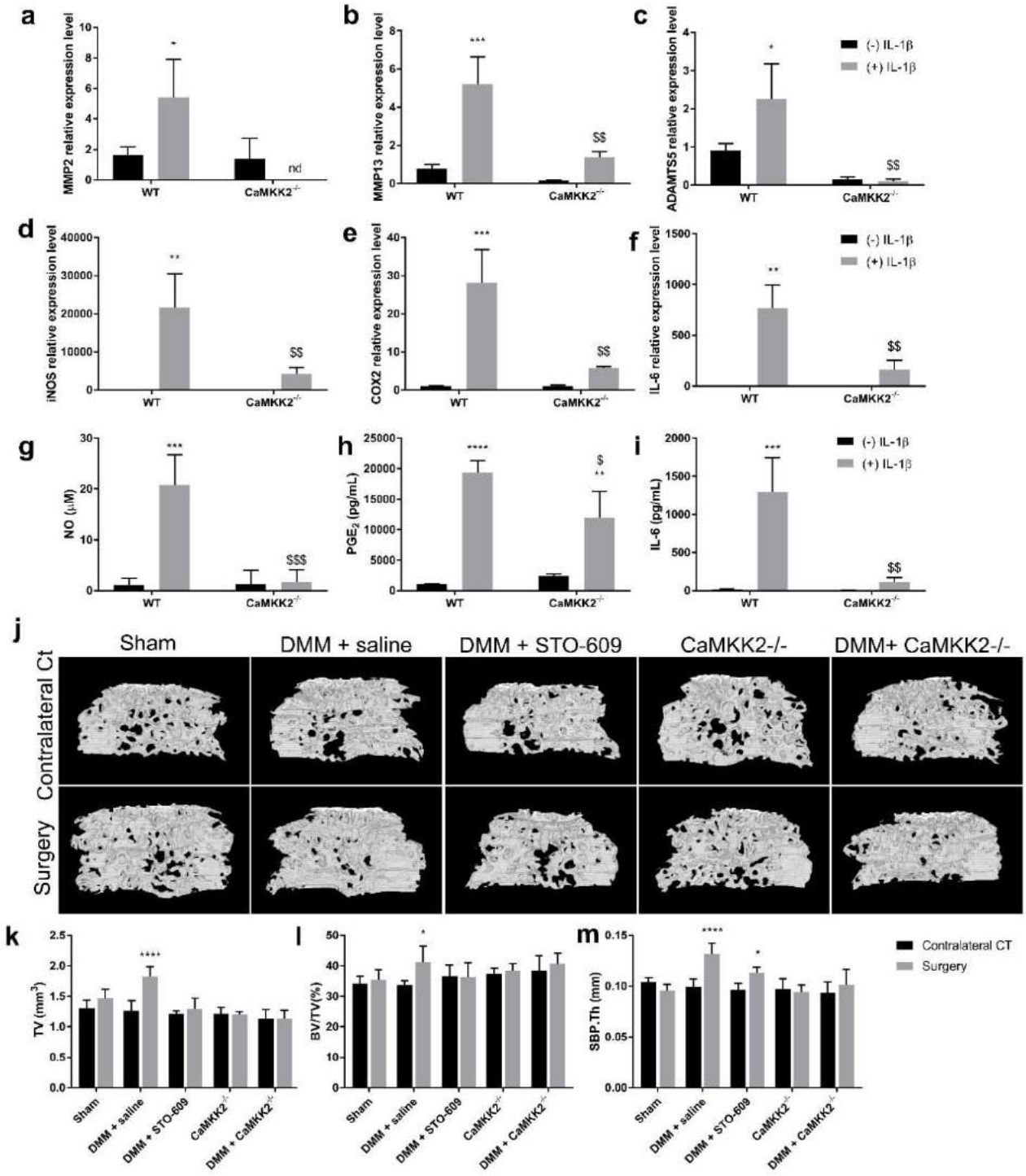

Figure 1: CaMKK2 deficiency induces a decrease of OA phenotype. The expression of catalytic enzymes such as MMP2 (a), MMP13 (b) and ADAMTS5 (c) as well as the expression of inflammatory genes *i.e.* iNOS (d), COX2 (e), and IL6 9 (f) was evaluated in WT and *Camkk2-/-* chondrocytes treated with or without IL-1β for 48h. Secretion of the related inflammatory mediators such as nitric oxide (g), prostaglandin E2 (h), and interleukin-6 (i) was measured in the culture medium of WT and *Camkk2-/-*chondrocytes, treated with or without 10ng/mL IL-1β for 48h. Results are represented with means ± SEM. (*), and ($) indicate significant differences compared to IL-1β untreated group and IL-1β treated WT group, respectively. Two-way ANOVA followed by post-hoc Turkey's test. (j) representative

3D µCT images of the coronal views of the tibial subchondral bone of WT and *Camkk2-/-* mice, 8 weeks after surgical OA induction (DMM) or sham surgery. White arrowhead shows subchondral bone sclerosis. Quantitative analysis of total tissue volume (TV; k), bone volume density (BV/TV; l), and thickness of the SBPs (SBP.Th; m) in subchondral bone determined by µCT analysis. Results are represented with means ± SEM. n=5 per group. (*) indicates significant differences in comparison to the contralateral µCT within the same experimental group. Two-way ANOVA followed by Tukey's test.

References-

1. Nuesch E, Dieppe P, Reichenbach S, Williams S, Iff S, Juni P. All cause and disease specific mortality in patients with knee or hip osteoarthritis: population based cohort study. BMJ. 2011;342:d1165.
2. Leardini G, Salaffi F, Caporali R, Canesi B, Rovati L, Montanelli R. Direct and indirect costs of osteoarthritis of the knee. Clin Exp Rheumatol. 2004;22(6):699-706.
3. Loeser RF, Goldring SR, Scanzello CR, Goldring MB. Osteoarthritis: a disease of the joint as an organ. Arthritis Rheum. 2012;64(6):1697-707.
4. Bijlsma JW, Berenbaum F, Lafeber FP. Osteoarthritis: an update with relevance for clinical practice. Lancet. 2011;377(9783):2115-26.
5. Dedrick DK, Goldstein SA, Brandt KD, O'Connor BL, Goulet RW, Albrecht M. A longitudinal study of subchondral plate and trabecular bone in cruciate-deficient dogs with osteoarthritis followed up for 54 months. Arthritis Rheum. 1993;36(10):1460-7.
6. Bettica P, Cline G, Hart DJ, Meyer J, Spector TD. Evidence for increased bone resorption in patients with progressive knee osteoarthritis: longitudinal results from the Chingford study. Arthritis Rheum. 2002;46(12):3178-84.
7. Brandt KD. Insights into the natural history of osteoarthritis provided by the cruciate-deficient dog. An animal model of osteoarthritis. Ann N Y Acad Sci. 1994;732:199-205.
8. Pastoureau PC, Chomel AC, Bonnet J. Evidence of early subchondral bone changes in the meniscectomized guinea pig. A densitometric study using dual-energy X-ray absorptiometry subregional analysis. Osteoarthritis Cartilage. 1999;7(5):466-73.
9. Pelletier JP, Boileau C, Brunet J, Boily M, Lajeunesse D, Reboul P, et al. The inhibition of subchondral bone resorption in the early phase of experimental dog osteoarthritis by licofelone is associated with a reduction in the synthesis of MMP-13 and cathepsin K. Bone. 2004;34(3):527-38.
10. Clouet J, Vinatier C, Merceron C, Pot-vaucel M, Maugars Y, Weiss P, et al. From osteoarthritis treatments to future regenerative therapies for cartilage. Drug Discov Today. 2009;14(19-20):913-25.
11. Chin D, Means AR. Calmodulin: a prototypical calcium sensor. Trends Cell Biol. 2000;10(8):322-8.
12. Hook SS, Means AR. Ca(2+)/CaM-dependent kinases: from activation to function. Annu Rev Pharmacol Toxicol. 2001;41:471-505.
13. Cary RL, Waddell S, Racioppi L, Long F, Novack DV, Voor MJ, et al. Inhibition of Ca(2)(+)/calmodulin-dependent protein kinase kinase 2 stimulates osteoblast formation and inhibits osteoclast differentiation. J Bone Miner Res. 2013;28(7):1599-610.
14. Pritchard ZJ, Cary RL, Yang C, Novack DV, Voor MJ, Sankar U. Inhibition of CaMKK2 reverses age-associated decline in bone mass. Bone. 2015;75:120-7.
15. Racioppi L, Noeldner PK, Lin F, Arvai S, Means AR. Calcium/calmodulin-dependent protein kinase kinase 2 regulates macrophage-mediated inflammatory responses. J Biol Chem. 2012;287(14):11579-91.
16. Csaki C, Keshishzadeh N, Fischer K, Shakibaei M. Regulation of inflammation signalling by resveratrol in human chondrocytes in vitro. Biochem Pharmacol. 2008;75(3):677-87.
17. Burr DB, Gallant MA. Bone remodelling in osteoarthritis. Nat Rev Rheumatol. 2012;8(11):665-73.

Promoting load-induced bone formation by manipulating primary cilia mechanobiology

Milos Spasic, MS; Michael P. Duffy, MS; Christopher R. Jacobs, PhD
Columbia University, New York, NY

Introduction:

Osteoporosis is a condition marked by low bone mass resulting in heightened risk of fracture, and affects over 50% of the US population over 50 years old [1]. Mechanical stimulation has long been known to be a potent stimulus of bone formation, yet how bone cells actually sense and respond to mechanical cues is incompletely understood, and none of the current treatment strategies to combat bone diseases rely on the inherent mechanosensitivity of bone. The prevailing paradigm is that osteocytes sense mechanical forces and transduce these inputs into molecular signals to direct osteoblastic activity [2]. One potential cellular mechanosensing apparatus is the primary cilium.

Primary cilia are single immotile organelles extending from the surface of nearly every mammalian cell, and have been implicated as mechanosensors in bone [3, 4]. Disruption of cilia formation *in vitro* impairs cell mechanosensitivity, and *in vivo* abrogates load-induced bone formation. Furthermore, when osteocyte cilia formation is disrupted, paracrine signaling between mechanically stimulated osteocytes and mesenchymal progenitors is diminished [5]. It is believed that fluid flow mechanical stimulation causes primary cilia deflection, generating membrane tension to stimulate stretch-activated ion channels such as TRPV4 (transient receptor potential vanilloid 4) and PC2 (polycystin 2) which localize to the primary cilium [6]. Opening of these channels may result in ciliary calcium influx to initiate a signaling cascade mediated by AC6 (adenylyl cyclase 6), a membrane-bound enzyme which catalyzes the conversion of ATP to the second messenger cAMP [7]. These proteins work in concert to dictate primary cilia-mediated mechanosensing, and whole bone adaptation. We have previously demonstrated that primary cilia-mediated mechanotransduction can be pharmacologically manipulated by treatment with small molecules that increase primary cilia length, such as fenoldopam, to enhance mechanosensitivity and osteogenesis [8]. It has also been shown that treatment with histone deacetylase 6 (HDAC6) inhibitors increases primary cilia bending stiffness to impair cell mechanosensitivity [9].

In this work, we study the bone mechanotransduction signaling axis by manipulating primary cilia structure and mechanosensitivity to alter intercellular paracrine signaling and enhance load-induced bone formation.

Methods:

Cell culture: MLO-Y4 osteocytes were cultured on collagen-coated flasks and placed on a rocker platform to apply oscillatory fluid flow as a mechanical stimulus (12 hours at 0.5 Hz and 0.1 Pa shear stress), or left static as a no flow control [5]. Conditioned media was then collected and used to culture MC3T3 osteoblasts for 24 hours. *Drug treatment in vitro:* Osteocytes were treated with 10 μM fenoldopam, 5 μM tubastatin, or DMSO vehicle control for 16 hours prior to initiation of flow. *RNA interference:* Osteocyte primary cilia mechanosensing was impaired by siRNA-mediated knockdown 48 hours prior to experimentation. Cilia formation was disrupted by knockdown of IFT88, and ciliary mechanotransduction was impaired by knockdown of AC6, TRPV4, and PC2 [6, 8]. *Gene expression:* After 24 hours of culture in conditioned media, osteoblasts were lysed for total RNA isolation, and gene expression was assessed by qPCR. Osteopontin expression was assessed as a measure of osteogenic activity, using primer-probes for *Osteopontin* and *GAPDH* endogenous control. *In vivo bone adaptation:* Skeletally mature, 16-week old, C57Bl/6 mice were subcutaneously injected with 20 mg/kg fenoldopam, or vehicle control, on 7 consecutive days. On days 5-7, mice were also subjected to compressive ulnar load (3N, 120 cycles, 2Hz sine wave), with contralateral limbs serving as non-loaded control [10]. Calcein and alizarin were injected 4 days apart and standard dynamic histomorphometric analysis was performed to assess bone adaptation [10]. *Statistics:* All data reported as mean ± SEM, analyzed with one-way ANOVA and Bonferroni post-hoc correction. 2-way ANOVA revealed no difference of *in vivo* drug treatment based on gender. *$p < 0.05$, **$p < 0.01$, ***$p < 0.001$.

Results:

Osteocytes with increased primary cilia length and mechanosensitivity (fenoldopam) displayed enhanced mechanically-induced paracrine signaling to osteoblasts, as measured by osteoblast osteopontin gene expression relative to no flow control (Fig. 1A). When osteocytes were treated with tubastatin to increase cilia stiffness and impair mechanosensing, the osteoblast response is abrogated. Impairing cilia formation (IFT88 knockdown) or diminishing production of key ciliary mechanosensing proteins (AC6/PC2/TRPV4 knockdown) also inhibits pro-osteogenic paracrine signaling from mechanically stimulated osteocytes to osteoblasts (Fig. 1B, C).

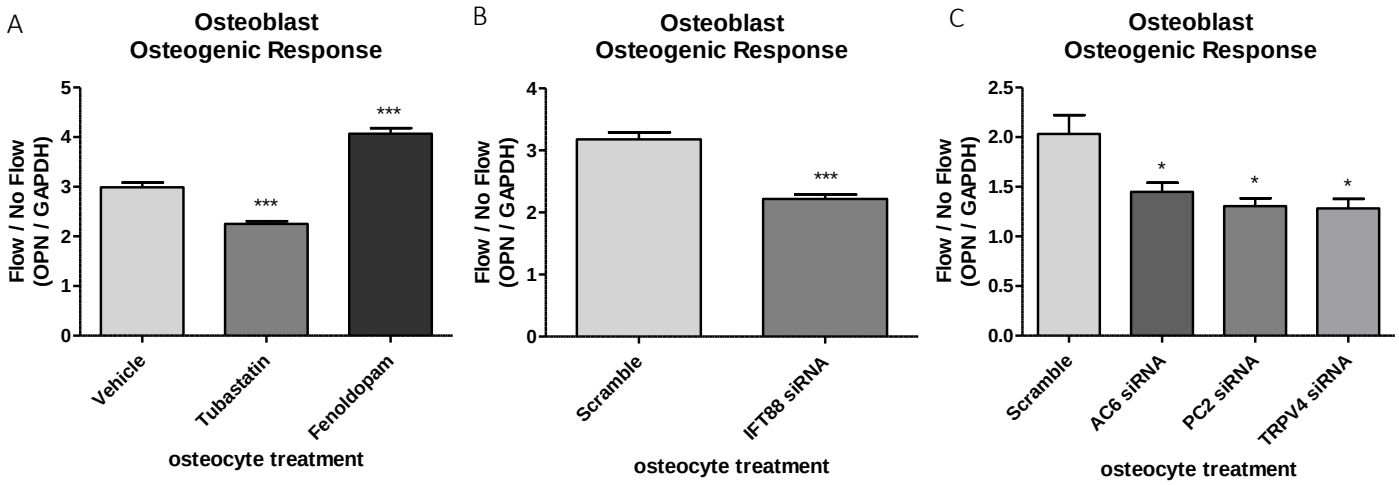

Figure 1: Osteoblast osteogenic activity is diminished with conditioned media from tubastatin treated osteocytes, and enhanced from fenoldopam treated cells (A). Inhibition of osteocyte primary cilia-mediated mechanotransduction also impairs this signaling axis (B, C). n ≥ 4

To translate this work *in vivo*, we utilized compressive ulnar loading as a model of load-induced bone formation [10]. Skeletally mature mice were treated with the cilia lengthening agent, fenoldopam, and mechanically stimulated with bone adaptation assessed by dynamic histomorphometry (Fig. 2A). Mice treated with fenoldopam displayed no change in relative mineralizing surface (rMS/BS), but significant increases in relative mineral apposition (rMAR) and bone formation (rBFR/BS) rates (Fig. 2B, C, D).

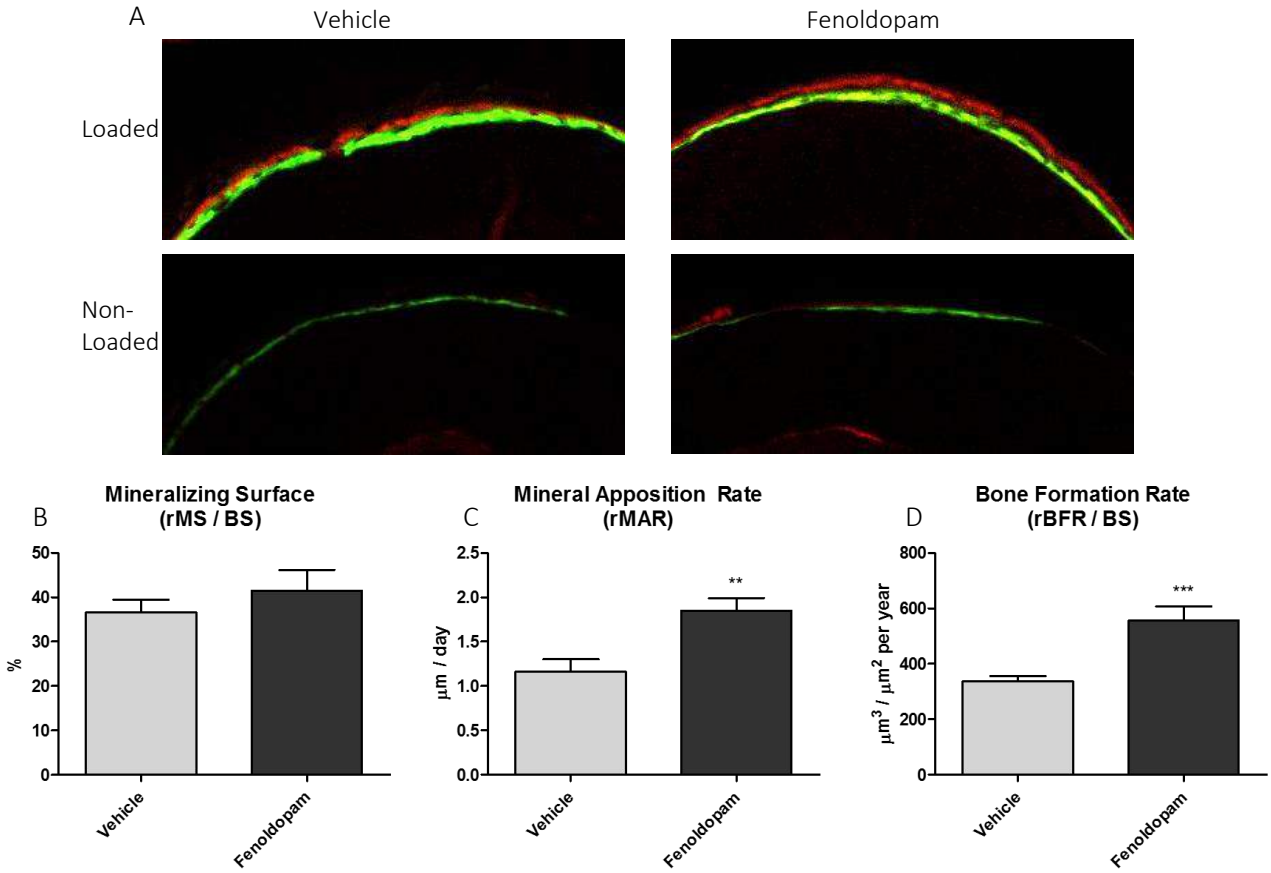

Figure 2: Load induced bone formation assessed by dynamic histomorphometry. Mice were treated with 20 mg/kg fenoldopam or vehicle control on 7 consecutive days, and subjected to compressive ulnar load on days 5-7. Calcein and alizarin were injected 4 days apart to label mineralizing surfaces and quantify bone adaptation (A). All dynamic histomorphometry was assessed as the relative difference between loaded and non-loaded control. No change was examined in the amount of mineralizing surface (B), while significant differences were found in mineral apposition (C) and bone formation rates (D). n ≥ 12

Mice were then assessed for potential of adverse effects of drug treatment. Examination of bone ultrastructure revealed no change in quality of bone formed (Fig. 3A), while µCT analysis demonstrated no change in normal bone microarchitecture in fenoldopam treated mice compared to vehicle control (data not shown due to space limitations). Additionally, kidney morphology (Fig. 3B) and weight (Fig. 3C) were assessed as an initial indicator of drug toxicity, finding no difference with drug treatment.

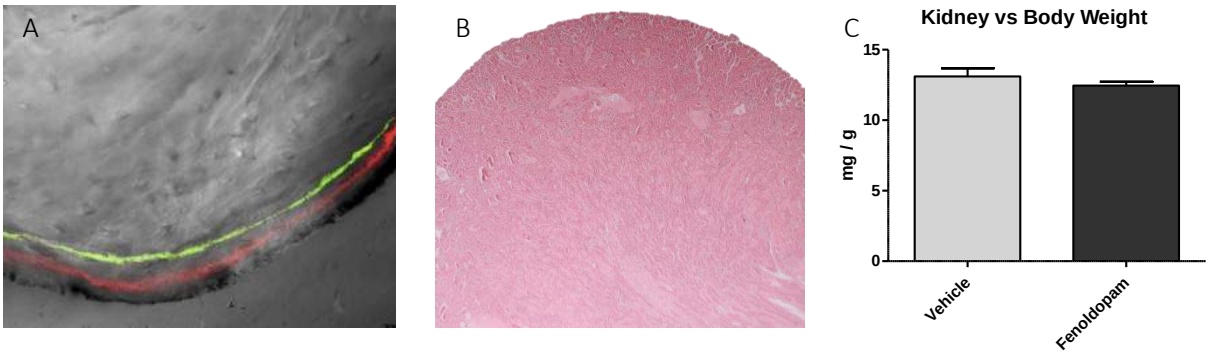

Figure 3: Minimal adverse effects of fenoldopam treatment. Several indicators of adverse effects of drug treatment were examined, including bone ultrastructure (A), kidney morphology (B) and kidney weight (C). n ≥ 12

Discussion:

We demonstrate that the osteocyte primary cilium plays a critical role in regulating the pro-osteogenic paracrine signaling response from mechanically stimulated osteocytes to osteoblasts. These results do not exclude the potential for other mechanisms of intercellular communication, such as direct-cell contact, or any other mechanosensing mechanisms, such as integrin or focal adhesion-mediated mechanosensing, from playing key roles in bone mechanotransduction. Though, these data do suggest that the primary cilia-mediated mechanosensing apparatus can be manipulated to direct the osteocyte-osteoblast signaling axis to augment osteogenesis.

Mice treated with fenoldopam displayed significantly enhanced load-induced bone formation. While mineral apposition and bone formation rates were significantly increased, the amount of mineralizing surface remained unchanged. This suggests that the number of active osteoblasts did not change, but that osteoblasts at existing mineralizing surfaces were further activated with fenoldopam treatment, consistent with our *in vitro* findings. Moreover, fenoldopam treatment displayed no effect on normal bone properties, demonstrating that this cilia-targeted treatment strategy sensitizes bone to mechanical stimulation to bias bone formation. Fenoldopam is a clinically used treatment for hypertension, but its impact on bone biology has never been studied. Furthermore, fenoldopam is not an osteocyte or bone-specific treatment; however, our results suggest minimal adverse effects of drug treatment. Recently, we have established a high-throughput drug screening platform to identify novel compounds which have similar cilia lengthening properties as fenoldopam to enhance cell mechanosensitivity, and may prove more suitable for eventual clinical use.

Significance:

This work demonstrates translation of *in vitro* bone mechanobiology research into an *in vivo* model to demonstrate, for the first time, that primary cilia can be pharmacologically targeted to sensitize bone cells to mechanical stimulation to bias whole bone formation. Furthermore, this work proposes the first bone disease therapeutic strategy that leverages the inherent mechanosensitivity of bone. Finally, fenoldopam is already a clinically approved drug, allowing for significant potential to repurpose this compound for treatment of human bone diseases.

References:

[1] US Department of Health and Human Services, 2004. [2] Tatsumi, G et al. Cell Metab, 5:464-475, 2007.
[3] Malone, A et al. PNAS, 104:13325-30, 2007. [4] Temiyasathit, S et al. PloS ONE, 7, 2012. [5] Hoey, D et al. Biochem Biophys Res Com, 412:182-187, 2011. [6] Lee, KL et al. Cilia, 4:7, 2015. [7] Kwon, R et al. FASEB J, 24:2859-68, 2010. [8] Spasic, M et al. Eur. Cell. Mat., 33:158-168, 2017. [9] Nguyen, A et al. Biology Open, 4:1733-8, 2015 [10] Lee, KL et al. FASEB J, 28:1157-65, 2014.

Acknowledgements:

This work was supported by NIH grant RO1 AR062177.

PPARγ and PPARα regulate osteocyte activity by controlling expression of Sclerostin and DKK1 proteins

Lance A. Stechschulte1,2, Mathew Mazur1, Dustin Marinelli1, Zach Rotter1, Amit Chougule2,3, Beata Lecka-Czernik1,2,3

1Department of Orthopaedic Surgery; 2Center for Diabetes and Endocrine Research; 3Department of Physiology and Pharmacology, University of Toledo, College of Medicine and Life Sciences, Toledo, OH

Osteocytes orchestrate bone remodeling through regulation of both osteoblast and osteoclast activities. Sclerostin, encoded by *Sost* gene, and DKK1 proteins are released from osteocytes and act as inhibitors of Wnt signaling pathway in osteoblasts. Recently we have showed that PPARγ is a positive regulator of both *Sost* and *Dkk1*, whereas PPARα is a negative regulator of *Sost* expression. Decreased bone formation in mice treated with full PPARγ agonist, rosiglitazone, is associated with increased expression and protein production in osteocytes of both Sclerostin and DKK1. In contrast, mice treated with a new insulin sensitizer SR10171 which acts as PPARγ inverse agonist and PPARα agonist, is associated with decreased expression and production of both Sclerostin and DKK1 resulting in increased bone formation and bone mass. Here we extended our studies by analyzing the mechanism by which PPARγ and PPARα control expression of both genes. Using EpiTect software we have identified two PPRE sequences in *Sost* promoter located -1.8 kb (αPPRE) and -7.0 kb (γPPRE) from the transcription start site. ChIP analysis showed that PPARα binds to αPPRE in basal conditions. Treatment with WY14643 agonist results in augmentation of PPARα binding which correlates with decreased promoter activity measured in luciferase gene reporter assay. In contrast, PPARγ is recruited to the *Sost* promoter only after activation with rosiglitazone, and this correlates with increased promoter activity. Similarly, PPARγ activation, but not PPARα, increases *Dkk1* promoter activity and DKK1 protein production in osteocytes. To demonstrate that PPARγ and PPARα regulate endocrine activities of osteocytes supporting of PBMC differentiation, we tested conditioned media (CM) from primary osteocytes treated with different PPARs selective modulators. CM collected from osteocytes with activated PPARγ increased adipocytic and decreased osteoblastic gene markers expressed in recipient PBMC, whereas CM from osteocytes with activated PPARα decreased adipocytic and increased osteoblastic gene markers. PPARα inhibitory effect on *Sost* expression was confirmed in animals deficient in PPARα protein. Osteocytes derived from PPARα knock-out mice are characterized with high expression of *Sost* and 2-fold increased Sclerostin protein levels. In conclusion, Sclerostin and DKK1 are directly regulated by PPARγ and PPARα and these nuclear receptors can be pharmacological targets to control osteocyte-regulated bone remodeling.

Mechanism of Exercise in Preventing Skeletal Muscle Atrophy

Nicholas T. Theilen1, Nevena S. Jeremic, PhD1, Greg Weber, PhD1, Suresh C. Tyagi,, PhD1

[1] *University of Louisville School of Medicine, Louisville, KY, USA*

Skeletal muscle atrophy is the consequence of protein degradation exceeding protein synthesis. This arises for a multitude of reasons including the unloading of muscle during microgravity, post-surgery bedrest, immobilization of a limb after injury, and overall disuse of the musculature. Mitochondrial dysfunction is associated with skeletal muscle atrophy and contributes to the induction of protein degradation and cell apoptosis with the loss of organelle function. The development of therapies to enhance mitochondrial function prior to skeletal muscle atrophy settings to diminish protein degradation is scarce. We are investigating whether an exercise treatment prior to an atrophic setting will diminish the skeletal muscle atrophy incurred during hindlimb suspension (HLS) in mice. Male C57BL/6 (wild-type) mice between 11-14 weeks of age were assigned to control, HLS only (HLS-only), exercise only (Ex-only), and exercise prior to HLS (Ex+HLS), groups. The exercise protocol consisted of 14 progressive exercise sessions over an 18-day period and the HLS protocol lasted 7 consecutive days. At the end of treatments mice were first anesthetized and blood flow imaging of the hindlimb was done using laser Doppler technology. Mice were then sacrificed and the soleus and gastrocnemius muscle were excised and analyzed for muscle weight. Muscle weights were standardized to bodyweight using a muscle/bodyweight ratio (mg/g). Immunofluorescence staining was done to detect fiber cross-sectional area. A dihydroethidium stain was used to detect oxidative stress while markers of mitochondrial biogenesis protein expression were measured by western blot analysis. Soleus muscle weight (mg) to bodyweight (g) ratio decreased 32.2% (.218±.010) in HLS-only while decreasing 7.4% (.298±.003) in Ex+HLS. Immunofluorescence staining for laminin revealed greater cross-sectional area, continuity, and uniformity in Ex+HLS soleus and gastrocnemius muscle fibers compared to HLS-only. Laser Doppler imaging suggests blood flow in the lower hindlimbs is greater in Ex+HLS mice compared to the HLS only group. HLS-only resulted in greater levels of oxidative stress (superoxide anion), while Ex+HLS diminished levels of these ROS. Furthermore, protein expression of mitochondrial biogenesis markers, PGC-1α and TFAM, increased with exercise. Data indicates the time before an atrophic setting, particularly caused by muscle unloading and disuse, is a useful period to intervene progressive exercise training to prevent skeletal muscle atrophy which may be due, in part, to enhanced mitochondrial function.

Raman Spectroscopic Parameters Corelate with the Fracture Toughness of Human Cortical Bone

Mustafa Unal, PhD[1,2], Selin Timur[3], Sasidhar Uppuganti, MSc[1,2,] Ozan Akkus, PhD[3] and Jeffry S. Nyman, PhD[1,2]

1Department of Orthopaedic Surgery & Rehabilitation, Vanderbilt University Medical Center, Nashville, TN, USA; 2VA Tennessee Valley Healthcare System, Nashville, TN, USA; 3Department of Mechanical and Aerospace Engineering, Case Western Reserve University, Cleveland, OH, USA

Introduction

A significant effort continues to be directed towards improvements in current clinical tools to assess bone fracture risk, while in parallel, research into understanding of the fracture resistance is accelerating for assessing factors other than bone mineral density (BMD) because the fracture resistance does not solely depend on BMD, as a matter of fact the overall fracture resistance of cortical bone originates from each level of its organizational hierarchy. At the nano-structural level, changes in the structure and organization of bone matrix (collagen, mineral crystals and water) [1] are among the factors that reduce fracture resistance. Although the crucial contribution of bone matrix to fracture resistance is largely understood, there is currently no clinical tool that assesses the matrix. Raman spectroscopy (RS) is uniquely well suited to address this need in ways that emerging technologies are not. However, to date, only one study showed RS parameters, namely crystallinity, significantly correlate with mechanical properties (tensile) of human cortical bone [2]. Recently, we identified a new RS parameter, 1670/1640, as being sensitive to denatured collagen and significantly correlate with toughness of bovine cortical bone [3]. However, there is currently no consensus on which RS parameters are most important for assessing the fracture resistance of human bone. To establish the potential for RS in assessing the contribution of the matrix to the fracture resistance, we hypothesized that i) the new RS parameter correlates with fracture toughness of human cortical bone and ii) more importantly, RS adds value helping volumetric BMD (vBMD) and age predict fracture toughness properties.

Methods

Cortical bone specimens were obtained from the lateral mid-diaphysis of human femurs (28M/30F, age = 21-101 yrs) and machined into a single-edge notched beam specimen (SENB) (nominal: 20 mm x 2.5 mm x 5.0 mm) with the starter micro-notch oriented such that crack propagation would occur orthogonal to the osteonal direction. Volumetric bone mineral density (vBMD) ahead of the crack tip was assessed by µCT (µCT50, Scanco Medical) at an isotropic voxel size of 5 µm, and corresponding vBMD was calculated. A non-linear fracture mechanics approach (R-curve testing) was used to determine crack initiation (Kinit), crack growth toughness (Kgrow) and overall J integral (J-int). Thirty-two Raman spectra per sample were each acquired by 12 accumulations (5 s), and distributed throughout the entire surface of bone specimens neighboring each SENB (785 nm Horiba confocal RS, 20x obj). From the average spectrum per donor, we calculated traditional RS parameters (mineral to matrix ratios (MMRs), carbonate substitution, and crystallinity) as well as matrix maturity ratio (1670/1690) and the new 1670/1640 and 1610/1670 ratios. Of note, the intensities of Amide I shoulders were identified by the local maxima, not by band-fitting as guided by second derivative spectra (Fig 1).Correlations between Raman parameters and fracture toughness properties or age were tested for significance using linear correlation coefficient (R2) at a significance level of 0.05 in which the data was bootstrapped because the normality assumption in parametric testing did not hold for most properties. Age, vBMD, and Raman outcomes were considered as independent predictors in linear regressions with the fracture toughness properties as dependent variables to determine which combination of

Results and Discussions

As for the effect of matrix properties on fracture toughness, matrix maturity (1670/1690) and v1PO4/Proline (MMR parameter) did not correlate with any of the fracture toughness properties, and only correlated with age quite weakly (Table 1). Other traditional RS parameters and 1610/1670 only explained up to 18% of the variance for the fracture toughness properties (Table 1). Although Type-B carbonate substitution (CO3/v1PO4) and 1610/1670 (a new parameter that may be

related to conformation change of collagen) correlated with age, they correlated with fracture toughness properties quite weakly (Table 1). On the other hand, the new parameter, 1670/1640, was negatively associated with all fracture toughness properties and it explained 20% of variance in age, 48% of the variance in J-int and 35% of the variance for Kinit (reported as R2). Correlations between 1670/1640 and fracture toughness properties were modest (Table 1), but greater than those between fracture toughness and avBMD (max. R2=0.23, see Table 1), suggesting that information about bone matrix could be more valuable than measure of BMD to assess bone fracture resistance. Inverse correlations between 1670/1640 and fracture toughness properties indicate that an increase in amount of denatured collagen, or increase in impairment of collagen integrity likely decrease the stress required to initiate crack growth and decrease in the energy dissipated during fracture. Overall, finding very strong correlations between fracture toughness and RS parameters are rather difficult because of the fact that multiple factors across the length scales of bone's hierarchical organization contribute to fracture toughness properties. Therefore, a multifactorial diagnostic approach is likely necessary to ultimately predict an individual's true risk of fracture. For this purpose, we included age and vBMD in multilinear regressions as covariates and 1670/1640 significantly improved the prediction of J-int (from adj-R2= 12.35 to 46.55) and the prediction of Kinit (from adj-R2= 40.73 to 50.49). Adding v1PO4/Amide I as another covariate in the multilinear regression further improved the prediction of J-int from adj-R2= 46.55 to 54.84. In summary, the present research is the first to demonstrate that RS parameters predict fracture toughness of human cortical bone, and suggest that RS assessment has a great potential to assist existing clinical tools in assessing an individual's fracture risk with the unique advantage of probing disease and age-related changes in bone tissue at the nano-structural level of organization.

References

[1] Zimmermann et al. J Bone Miner Res 2015, 30(2):264-73
[2] Yerramshetty JS et al. Bone. 2008; 42(3):476–82.
[3] Unal et al. J Bone Miner Res 2016, 31(5):1015–25

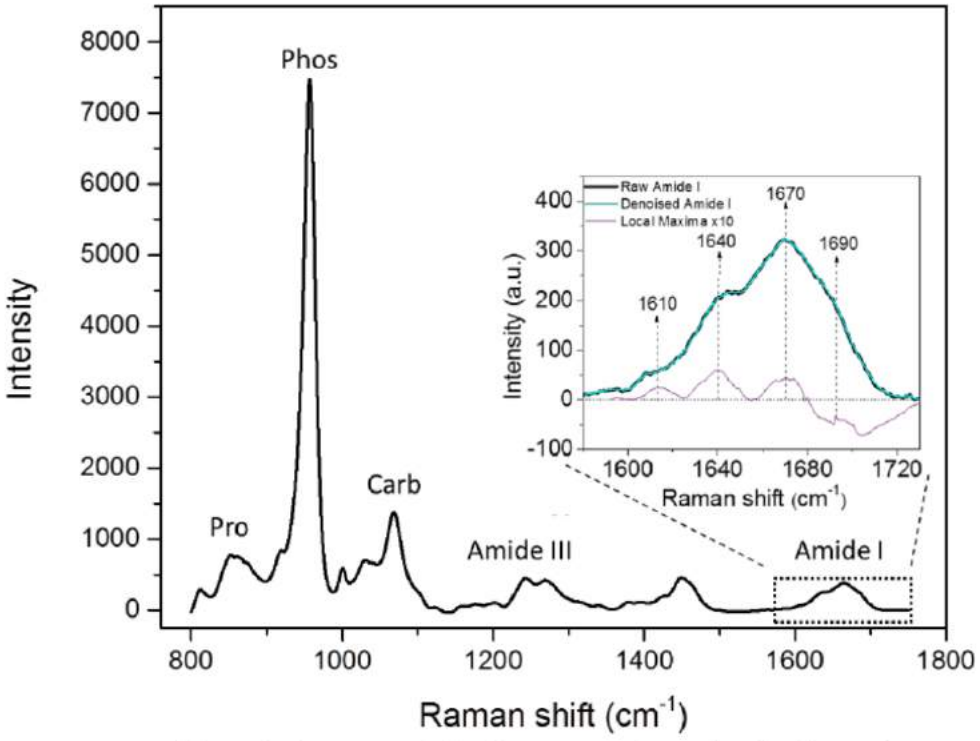

Figure 1. A representative Raman spectrum showing the major peaks in bone spectrum. The intensities of Amide I shoulders were identified by the local maxima, not by band-fitting as guided by second derivative spectra.

Table 1. Significant linear correlation coefficients (R^2) in bold and corresponding p-values below (in italics) as calculated from bootstrapped data.

Characteristic Property		*Age*	*Fracture Toughness*		
			K_{init}	K_{grow}	*J-int*
Age		1	**0.21** *(0.0001)*	**0.17** *(0.003)*	**0.13** *(0.004)*
Bone mineral density	vBMD	NS	**0.23** *(<0.001)*	NS	**0.05** *(0.046)*
Mineral-to-matrix (MMR)	ν_1PO_4/AmideI	NS	**0.16** *(0.002)*	**0.11** *(0.020)*	**0.38** *(<0.001)*
	ν_1PO_4/AmideIII	**0.10** *(0.016)*	**0.15** *(0.003)*	**0.08** *(0.045)*	**0.11** *(0.009)*
	ν_1PO_4/Proline	**0.15** *(0.002)*	NS	NS	NS
Carbonate substitution	CO_3/ν_1PO_4	**0.35** *(<0.001)*	**0.16** *(0.002)*	**0.09** *(0.036)*	**0.08** *(0.035)*
Crystallinity	1/FWHM(ν_1PO_4)	**0.17** *(0.001)*	NS	**0.13** *(0.011)*	NS
Matrix Maturity	1670/1690	**0.14** *(0.003)*	NS	NS	NS
Collagen Denaturation	1670/1640	**0.20** *(<0.001)*	**0.32** *(<0.001)*	**0.18** *(0.003)*	**0.48** *(<0.001)*
Conformation Change of Collagen	1610/1670	**0.40** *(<0.001)*	**0.15** *(0.003)*	**0.10** *(0.026)*	**0.18** *(<0.001)*

Fatty Acid Binding Protein 4 (FABP4) As A Biomarker for Knee Osteoarthritis

Chaofan Zhang, MD, MS1,2, Kwong Yuen Chiu, MBBS1, Aimin Xu, MD, PhD3, Chun Hoi Yan, MBBS1,4 1. Department of Orthopaedics & Traumatology, The University of Hong Kong, Hong Kong SAR, China; 2. Department of Orthopedics, The First Affiliated Hospital of Fujian Medical University, Fuzhou, China; 3. Department of Medicine, LKS Faculty of Medicine, The University of Hong Kong, Hong Kong SAR, China; 4. Shenzhen Key Laboratory for Innovative Technology in Orthopaedic Trauma, Department of Orthopaedics and Traumatology, The University of Hong Kong-Shenzhen Hospital, Shenzhen, China.

Objectives:
Osteoarthritis (OA) is a common joint disorder that affects millions of people all around the world. The etiology of OA, however, is still poorly understood. Recent studies have suggested that adipokines play important roles in the pathogenesis of OA. Fatty acid binding protein 4 (FABP4) is a novel adipokine that is closely associated with obesity and metabolic diseases. Yet no previous studies have examined FABP4 in OA. The aim of this study is to explore the potential role of FABP4 in the pathogenesis of OA.

Methods:
Both clinical study and animal study were performed. For the clinical study, we included patients with radiologically-confirmed knee OA and non-OA controls. Plasma level of FABP4 was determined by ELISA method. Regression analysis of FABP4 and knee OA severity, which was presented as Kellgren-Lawrence (K-L) grade was performed. For the animal study, we included 36 FABP4 knockout mice (KO) and 36 wild-type littermates (WT) (all male, 6-week-old), and fed the mice with a very high-fat diet (HFD, fat 60% calorie) or standard diet (STD, fat 11.6% calorie), for 3 months, 6 months and 9 months. At each time point, we measured animals' body weight and body fat. We then evaluated knee OA via examination of serum Cartilage Oligomeric Matric Protein (COMP) level, knee histologic assessment, and subchondral bone analyses. In the parallel study, we included 48 WT mice and fed the mice with HFD or STD, and simultaneously treated them with daily oral gavage of FABP4 selective inhibitor BMS309403 (15mg/kg/d) or vehicle (PBS solution), for 4 months and 6 months. At each time point, OA evaluation was performed same as above.

Results:
A total of 226 patients were included. 58 were males and 168 were females. The mean plasma level of non-OA patients, KL-2 patients, KL-3 patients, and KL-4 patients were 12.3□3.0 ng/ml (n=6), 14.6□6.9 ng/ml (n=72), 18.2□11.3 ng/ml (n=65), and 19.3□12.3 ng/ml (n=83), respectively (p=0.023, one-way ANOVA). After stratifying FABP4 into 4 level groups (<10 ng/ml, 10-15 ng/ml, 15-20 ng/ml, >20 ng/ml), FABP4 was positively associated with the severity of knee OA (p=0.031, ordinal regression analysis, age and sex adjusted). (Figure 1) For the animal study, HFD induced significant obesity in mice. However, KO mice were much fatter than WT mice with significantly higher body weight and higher percent body fat. (Figure 2) At 3 months of HFD, KO mice showed less cartilage degradation than WT mice with significantly lower serum COMP ((1.6±0.2)U/L vs (2.3±0.3) U/L, p=0.01) and OARSI score ((0.8□0.4) vs (2.9□0.4), p=0.00). Daily oral gavage of BMS309403 in mice for 4 months protected cartilage from degradation as well, in which the mice with BMS309403 for 4 months showed significantly lower COMP ((1.7±0.2)U/L vs (2.1±0.3) U/L, p=0.04) and OARSI score (5.4□6.0 vs 6.0□0.4, p=0.04) than mice with PBS. (Figure 3) At 9 months of HFD, WT mice underwent serious OA changes with significant osteophyte formation and subchondral bone sclerosis. While in KO mice, the changes were much alleviated. The subchondral bone BMD (p=0.00), bone volume percentage (p=0.00), trabecular thickness (p=0.00), and trabecular number (p=0.01) was significantly lower in KO mice. However, chronic treatment with BMS309403 did not seem to have significant effects on the subchondral bone strcuture. (Figure 4) For lean mice (fed with STD), either genetically knocking out or pharmaceutical inhibition of FABP4 had no significant effects on knee OA.

Conclusions:
Plasma FABP4 level was positively associated with the severity of knee OA. Knocking out or pharmaceutical inhibition of FABP4 alleviated OA induced by a very high-fat diet in mice. FABP4 may be a potential biomarker for knee OA.

Key words:
Osteoarthritis, fatty acid binding protein 4, BMS309403, obesity, subchondral bone sclerosis

Figure 1 Serum FABP4 level in 6 non-OA patients and 220 radiologically-confirmed OA patients. The level was 12.3±3.0 ng/ml, 14.6±6.9 ng/ml, 18.2±11.3 ng/ml, and 19.3±12.3 ng/ml in KL-0, KL-2, KL-3, and KL-4, respectively (p=0.023, oneway ANOVA). Post hoc analyses showed FABP4 of KL-2 patients was significantly lower than KL-4 patients (p=0.028, Tukey HSD). After stratifying FABP4 into 4 level groups (<10 ng/ml, 10-15 ng/ml, 15-20 ng/ml, >20 ng/ml), the ordinal regression analysis showed that FABP-4 was positively associated with the severity of knee OA (p=0.031, age and sex adjusted).

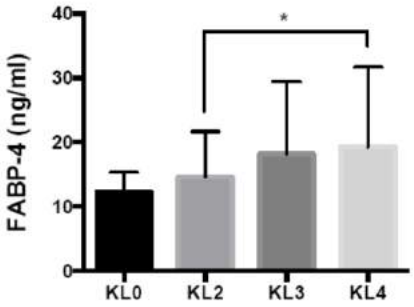

Figure 2 Knocking out or pharmaceutical inhibition of FABP4 significantly increased animals' body weight and body fat percentage. (A) Photos of KO and WT mice after 6-month of HFD and STD showed KO mice were fatter than WT mice, especially under HFD. (B, C) Statistical analyses showed KO mice had significantly higher body weight and body fat. (C) WT mice treated with daily oral gavage of BMS309403 (15mg/kg/d) for 4 months and 6 months had significantly higher body weight and body fat.

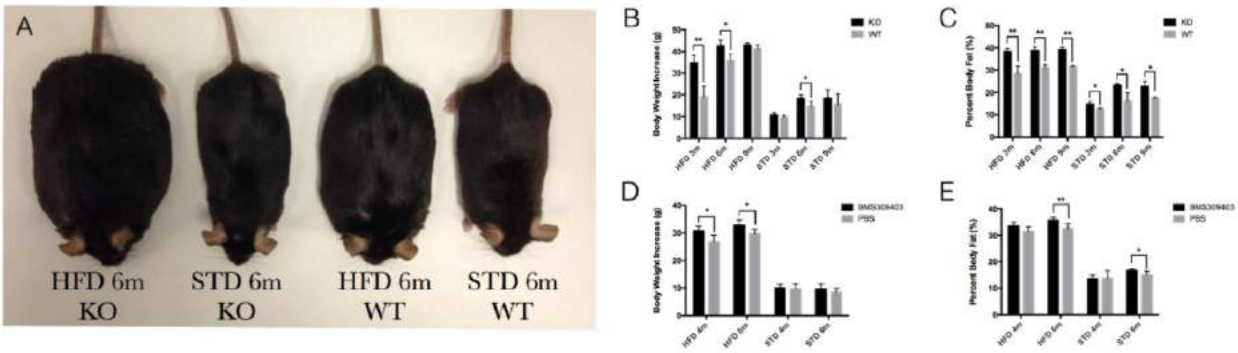

Figure 3 Knocking out or pharmaceutical inhibition of FABP4 significantly alleviated cartilage degradation in mice fed with HFD. The coronal paraffin sections of knees were stained with Safranin O and Fast Green. Loss of Safranin O staining in cartilage indicated a loss of glycosaminoglycan (GAG) content. (A, D, A1, D1) KO and WT mice after 3-month of HFD. Staining loss of cartilage was observed in WT mice but not obviously seen in KO mice. (B, E, B1, E1) KO and WT mice after 6-month of HFD. KO mice started to undergo cartilage degradation, while in WT mice the cartilage were seriously degenerated. In addition, osteophyte formation was seen in WT mice, especially in the medial compartment (arrow). (C, F, C1, F1) KO and WT mice after 9-month of HFD. Both KO and WT mice experienced severe cartilage degradation. In WT mice, serious subchondral bone sclerosis was observed (arrow). (G, I, G1, I1) WT mice treated with BMS309403 or PBS for 4 months. Mice treated with BMS309403 showed less cartilage staining loss than mice treated with PBS. (H, J, H1, J1) WT mice treated with BMS309403 or PBS for 6 months. Mice with PBS showed significant cartilage staining loss. (K) KO mice showed significantly lower level of COMP than WT mice after 3-month of HFD and STD. COMP level at 6-month of HFD in KO mice was significantly higher than WT, which suggested severe cartilage degradation in WT mice. (L) The OARSI score was significantly lower in KO mice than WT mice. (M) Mice treated with BMS309403 for 4 months showed significantly lower serum COMP than mice with PBS. (N) The OARSI score was significantly lower in mice treated with BMS309403 for 4 months. (Data presented as mean±std. Student t-test was performed to compare the means. *: p<0.05.

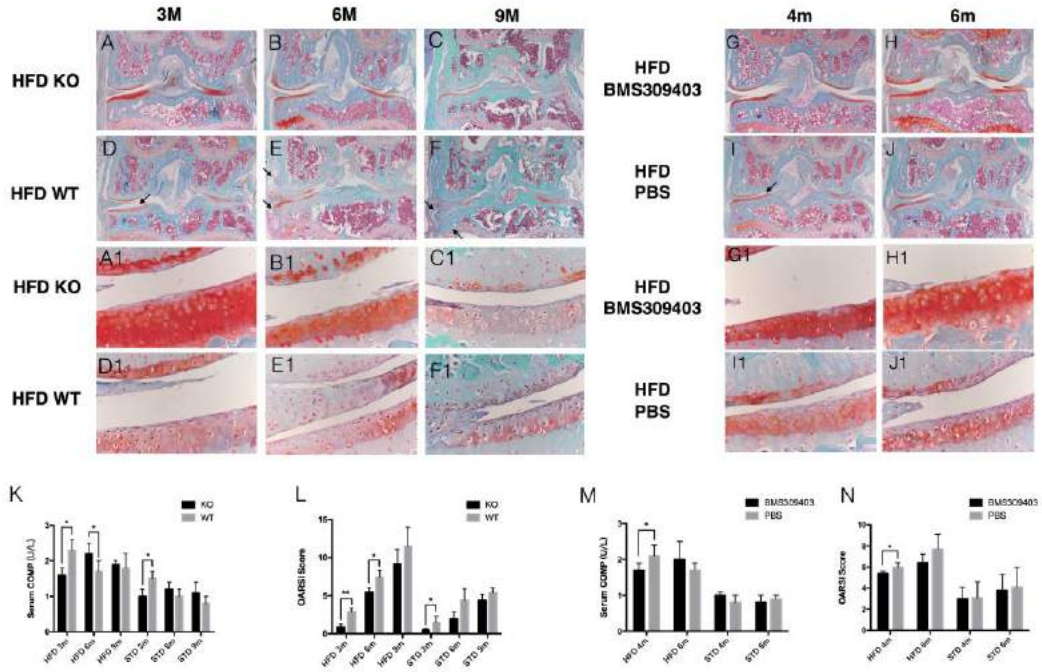

Figure 4. Micro-CT analysis of subchondral bone. Knocking out FABP4 significantly alleviated subchondral bone sclerosis in mice fed with HFD for 6 months and 9 months (A, arrow indicated). The subchondral bone BMD (p=0.00), bone volume percentage (p=0.00), trabecular thickness (p=0.00), and trabecular number (p=0.01) was significantly lower in KO mice after 9-month of HFD. (C, D, E, F) However, chronic treatment of BMS309403 in WT mice for 4 months and 6 months did not seem to have significant effects on the subchondral bone. (B, G, H, I, J) (**:p<0.01)

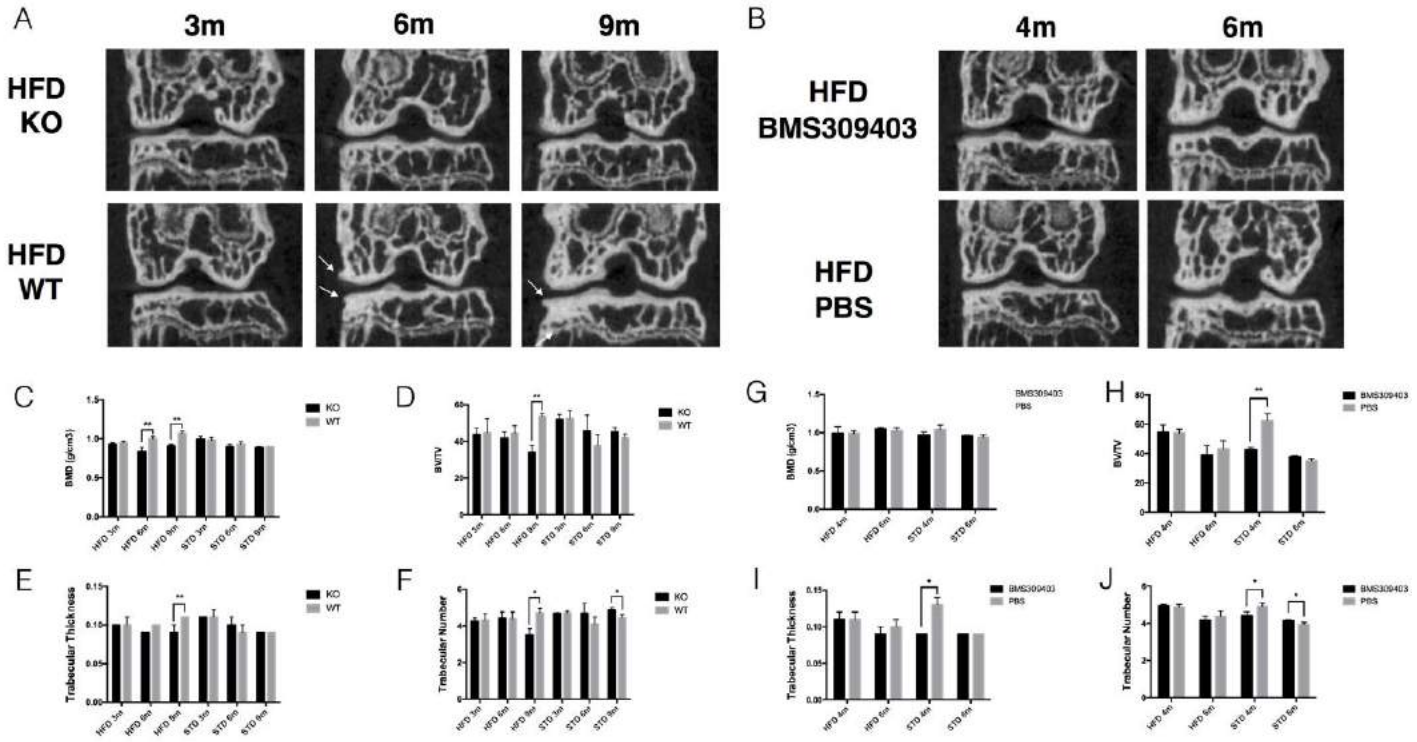
A
3m
6m
9m
HFD KO
HFD WT
B
4m
6m
HFD BMS309403
HFD PBS
C
BMD (g/cm3)
KO
WT
D
BV/TV
KO
WT
G
BMD (g/cm3)
BMS309403
PBS
H
BV/TV
BMS309403
PBS
E
Trabecular Thickness
KO
WT
F
Trabecular Number
KO
WT
I
Trabecular Thickness
BMS309403
PBS
J
Trabecular Number
BMS309403
PBS

Repurposing glutamate receptor antagonists for the prevention of post-traumatic osteoarthritis

Cleo S. Bonnet PhD, Sophie J. Gilbert PhD, Christopher Wilson MD, Deborah J Mason PhD.
Arthritis Research UK Biomechanics & Bioengineering Centre, Cardiff University, Pathophysiology and Repair Division, School of Biosciences, Cardiff, CF10 3AX, UK

Objectives: Synovial fluid glutamate concentrations increase in arthritis. Activation of kainate (KA) and AMPA glutamate receptors (GluRs) increase interleukin-6 release and cause pain. We previously found that AMPA and KA GluRs localise to osteoarthritic bone, cartilage and synovium and that NBQX (AMPA/KA antagonist) reduced knee swelling, gait abnormalities and joint destruction in a rat inflammatory arthritis model and two models of post-traumatic osteoarthritis: rat medial meniscal transection (MNX), mouse non-invasive anterior-cruciate ligament rupture. NBQX is not approved for use in humans, therefore we have sought to repurpose AMPA/KA GluR antagonists which have passed Phase 1 clinical trials. We hypothesise that these drugs will have similar therapeutic effects to NBQX in the mouse ACL rupture post-traumatic osteoarthritis model, and could represent a new treatment.

Methods: Synovial fluid was obtained from patients following ACL rupture or meniscal tear injuries. Due to confidentiality purposes, drugs have been anonymised to A, B, C and D. For ACL rupture, custom built cups were used to hold the knee in flexion and a 12N load (ElectroForce® 3200, BOSE) was applied to the right knees of anaesthetised 12-week-old C57Bl6 mice. Ligament rupture occurred on load application, revealed by a continued increase in displacement following release of the applied compressive force during the loading cycle. A single intra-articular injection of drug A, B, C or D was administered to 5 mice each immediately following ACL rupture, whilst another 5 received an intra-articular injection of vehicle immediately following ACL rupture. Contralateral knees (intact ACL) were used as controls. Over 21 days, lameness was scored and knee swelling measured (days 0, 1, 2, 3, 7, 14, 21). On day 21, all animals were culled and knees taken for histology.

Results: Synovial fluid glutamate concentrations were increased in ACL rupture and meniscal tear patients (Figure 1). By day 2, drug A had reduced knee swelling by ~50% to levels no longer significantly different to day 0 pre-ACL rupture measurements (Figure 2A). Vehicle control knee swelling remained significantly higher until day 7 ($p<0.01$, general linear model (GLM)) (Figure 2A). Drug C also reduced knee swelling to day 0 levels by day 2, whereas drug D ($p<0.05$, GLM) and vehicle control ($p<0.001$, GLM) remained significantly increased until day 7, and drug B ($p<0.05$, GLM) until day 14 (Figure 2B). Lameness scores were reduced by all drugs, with significant reductions compared to vehicle control on day 3 by drug B ($p<0.001$, GLM), drug C ($P<0.05$, GLM) and drug D ($p<0.05$, GLM) (Figure 3). At day 21, drug A reduced histological knee degradation score by ~40% compared to vehicle control. Drugs B, C and D had no effect.

Conclusions: This study provides evidence that AMPA/KA GluR antagonists, approved for use in humans, are effective at relieving inflammation, lameness and joint degradation in post-traumatic OA. The repurposing of these drugs offers a rapid route to treatment of human post-traumatic OA, since it can occur within 4 years of discovery.

Figure 1. Synovial fluid glutamate concentrations are increased after ACL and meniscal injury compared with those reported for non-arthritic (cadaveric) joints (red). Values on Y-axis are removed for confidentiality purposes.

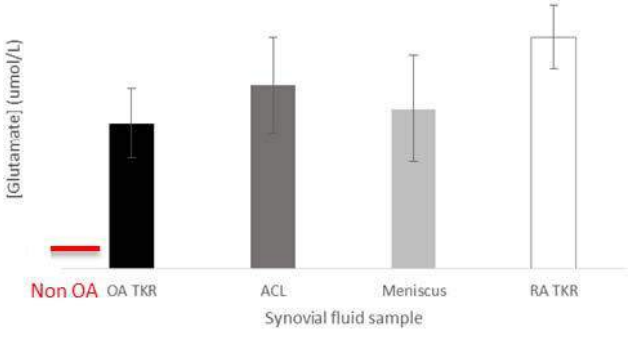

Figure 2. Reduction of knee swelling following a single intra-articular injection of glutamate receptor antagonists (drugs A, B, C and D). (A) Drug A significantly reduced swelling (GLM ANOVA, time p<0.001, treatment p<0.027) in the ACL-rupture mouse model. Tukey post-hoc tests revealed that by day 2 swelling was no longer different to day 0 measurements following drug A treatment, whereas vehicle control remained significantly higher until day 7 (++p<0.01, +++p<0.001, GLM). (B) Drugs B, C and D significantly reduced swelling in the ACL-rupture model (GLM ANOVA, time p<0.001, treatment p=0.001). ACL rupture (with vehicle) significantly increased swelling on Days 1, 2 and 3 (ΔΔΔp<0.001), time-points where the reduced swelling induced by D (□□p<0.01, □p<0.05) and B (**p<0.01, *p<0.05) were still greater than baseline. However, C restored swelling to baseline (day 0 before injury) after day 1 (•••p<0.001).

A B

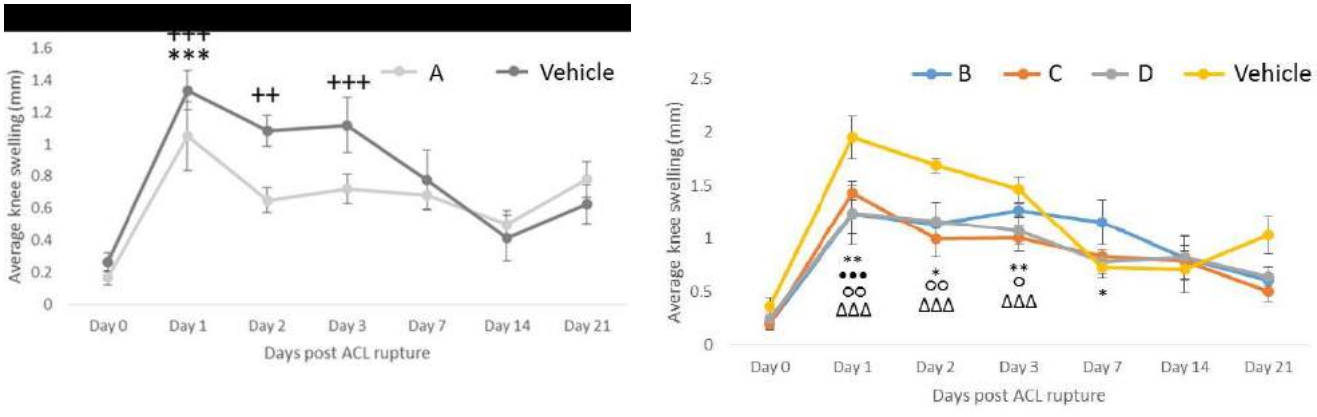

Figure 3. Reduction of lameness score following a single intra-articular injection of glutamate receptor antagonists (drugs A, B, C and D). (A) Drug A significantly reduced lameness score (GLM ANOVA, time p<0.001, treatment p<0.001) in the ACL-rupture mouse model. Tukey post-hoc tests on individual days revealed no significant differences. (B) Drugs B, C and D significantly reduced lameness in the ACL-rupture model over time (GLM ANOVA, time p<0.001, treatment p<0.001). Tukey post-hoc tests reveal largest effects on day 3, where B (***p<0.001), C (•p<0.05) and D (□p<0.05) treatments significantly reduced lameness compared with vehicle controls.

A B

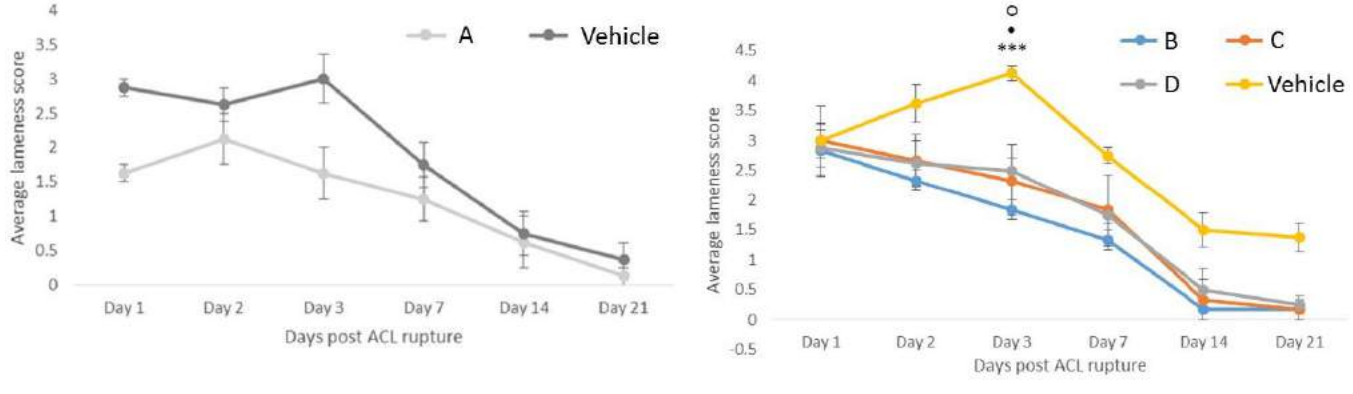

Impact of high bone turnover on skeletal muscle weakness in a mouse model of Camurati-Engelmann Disease

Trupti Trivedi1, Jenna N. Regan1, David L. Waning2, Sutha John1, Yun She1, Sreemala Murthy1, Khalid S. Mohammad1 and Theresa A. Guise1

1Indiana University School of Medicine, Indianapolis, IN 46202, USA
2The Pennsylvania State University College of Medicine, Hershey, PA 17033, USA

Camurati-Engelmann Disease (CED) is a rare sclerosing bone dysplasia associated with skeletal muscle weakness. Most CED patients carry mutations in the latent peptide region of TGF-β that impair the ability of the latent peptide to keep TGF-β in an inactive state. The systemic release of unrestrained active TGF-β causes accelerated bone turnover and leads to bone pain and deformities. Large amounts of activated TGF-β are also released in pathophysiological settings characterized by high bone resorption, such as osteolytic tumors. We and others have shown that TGF-β released from the bone matrix has effects both within the immediate bone microenvironment as well as systemically, where it leads to skeletal muscle weakness. Therefore, we are now expanding on the role of bone-to-muscle signaling in bone diseases other than cancer using a mouse model of CED. The CED mouse model was generated by osteoblast-specific expression of CED mutant TGF-β1 exclusively in bone. The elevated rate of bone turnover in CED mice led to increased fracture rate, callous formation at diaphysis, and haphazard bone formation. To examine whether the increased bone turnover in CED is associated with skeletal muscle weakness, we measured *ex-vivo* whole muscle contractility of the extensor digitorum longus (EDL) muscle. Compared to wild type (WT) littermates, mice with CED had significantly reduced EDL specific force production ($p<0.001$). The weights of the tibialis anterior, gastrocnemius and soleus muscles were significantly reduced in CED mice compared to their WT littermates. Next we tested whether the prevention of bone loss using zoledronic acid (ZA), a bisphosphonate commonly used in the clinic to preserve bone, can improve the muscle weakness in CED. We treated CED and WT mice with either vehicle or ZA (5 µg/kg, 3 days a week) for four weeks. ZA treatment significantly increased bone mineral density in CED mice compared to vehicle. Importantly, ZA treatment increased muscle specific force production in CED mice compared to vehicle treatment. We further looked into the effects of ZA treatment on skeletal muscle
phenotype using microCT, histology, and immunohistochemistry. Tibialis anterior muscle fiber diameter was significantly reduced by 2-fold in CED mice compared to WT mice treated with vehicle. However, fiber diameter was significantly increased following ZA treatment ($p<0.05$). Consistent with the increase in muscle fiber diameter, mid-calf cross sectional area (as evaluated *in-vivo* by microCT) was significantly increased in CED mice following ZA treatment compared to vehicle treated mice. Finally, mice with CED showed significantly elevated TGF-β signaling, as evaluated by phosphorylation of SMAD2/3 proteins in muscle fibers obtained from CED mice ($p<0.001$). This effect was reversed following ZA treatment, indicating that blocking bone resorption attenuates the excess TGF-β available to signal to skeletal muscle. Overall, our data supports the link between increased bone turnover and skeletal muscle weakness, which we have now demonstrated in a non-cancerous mouse model of high bone turnover. Future studies will be directed at understanding the mechanisms of bone-muscle crosstalk that may represent therapeutic targets in other conditions of bone loss such as osteoporosis, vitamin D deficiency, and anti-estrogen treatment.

Positive Adaptations in Cancellous Microarchitecture with Moderate Iron Overload, Even in Hindlimb Unloaded Mice, Are Associated with Elevated Serum Hepcidin

[1]Susan A. Bloomfield PhD, [1]Corinne E. Metzger MS, [1]Rihana S. Bokhari BS, [1]Heather C. Allaway PhD, [2]Nancy D. Turner PhD, [3]Matthew R. Allen PhD, [4]Sara R. Zwart PhD
[1]Departments of Health and Kinesiology and [2]Nutrition and Food Science, Texas A&M University, College Station, TX; [3]Dept. of Anatomy & Cell Biology, Indiana University School of Medicine, Indianapolis, IN; [4]Nutritional Biochemistry Laboratory, NASA JSC, Houston, TX

Moderate elevations in iron stores accelerate loss of BMD in middle-aged men and women over 3 years, but are associated with elevated vertebral fracture incidence in women only (Kim et al. JBMR 2012). One potential mechanism for this observation might be oxidative damage incurred as a result of accumulating free iron (Fe^{+2}, Fe^{+3}), contributing to the generation of reactive oxygen species. Oxidative damage is increasingly recognized as an underlying mechanism for bone loss with aging and estrogen deficiency (Almeida et al., 2010). International Space Station crew members demonstrate 20% elevations in serum ferritin (Zwart et al., 2013), hence oxidative damage secondary to this change in iron status may exacerbate bone loss incurred with prolonged microgravity exposure. We earlier determined that in adult rats combined dietary iron overload and radiation exposure resulted in decrements in cancellous BV/TV that correlated well with % osteocytes positive for 8-OHdG, a DNA adduct marker for oxidative damage (Yuen et al., ASBMR 2012). To test our hypothesis that dietary iron overload would exacerbate disuse-induced bone loss and to explore sex differences in this response, we exposed both male and female C57BL/6 mice to moderately elevated dietary iron and/or hindlimb unloading (HU). Early results indicated a *positive* impact of moderate elevations in iron stores on cancellous BV/TV and microarchitecture (Bokhari et al., NASA Human Research Program Investigator Workshop, 2016). To explore potential mechanisms, we then assayed for anti-oxidant enzyme activities, iron status markers and hepcidin, the key regulatory molecule of iron homeostasis. Iron overload conditions upregulate hepcidin release from the liver, resulting in declines in circulating iron.

Study Design and Methods: Male and female C57BL/6 mice (n=40 male and n=40 female; age 16 wks) were allowed to acclimate to an AIN93-G purified diet with normal (45 mg FE/kg, LoFE) or high (650 mg FE/kg, HiFE) iron content for four weeks before being randomized to (within sex and diet groups) to either weightbearing cage controls (CC) or hindlimb unloading (HU) for a subsequent four weeks of treatment, while continuing on their assigned LoFE or HiFE diets. HU mice were suspended via a surgically implanted steel suture tail ring at ~30° angle, with 2 HU mice per cage. Serum was collected after completion of the experiment by cardiac puncture and stored in multiple aliquots at -80°. Excised distal femurs were scanned with uCT (SkyScan) for cancellous microarchitecture. Liver anti-oxidant enzyme activity assays were performed using commercially available kits and serum ferritin and hepcidin assayed with ELISA's. A first statistical analysis used 3-way ANOVA to detect any main effects for sex, weightbearing status and iron status (Lo or Hi); subsequently, to detect intra-sex group differences, a 2-way ANOVA and post-hoc tests were run for all paired comparisons. Linear regression analyses tested the relationships between serum ferritin and hepcidin to distal femur %BV/TV and trabecular microarchitecture parameters.

Results: Four weeks of HU induced the expected reductions in distal femur cancellous bone volume/tissue volume (%BV/TV; 26-28% lower in both sexes) and corresponding deficits in trabecular thickness, number and spacing; relative changes in these variables were similar for both sexes. The HiFE-fed mice of both sexes had 32-37% higher %BV/TV than control fed mice, even in matched HU groups.

There were no main effects for sex, weightbearing, or iron status on liver catalase activity. Liver GPx was higher in female mice and in those on the HiFE diet, but there was no impact of HU. Similarly, serum ferritin was higher in female mice and in those on the HiFE diet, with a significant sex by weightbearing status interaction; HU males tended to have higher serum ferritin than CC mice, whereas female HU mice values were slightly lower than those for CC mice. Serum hepcidin was increased in all mice on the HiFE diet (38% higher in males, 43% higher in females), but there was no main effect of sex nor of HU. Pooling all data within each sex for serum hepcidin and cancellous microarchitecture outcomes, we found in male mice a small but significant R^2 of 0.217 (p=0.004) for hepcidin predicting %BV/TV, R^2=0.238 for hepcidin predicting Tb.N (p=0.003), and R^2=0.218 for hepcidin predicting Tb.Sp (p=0.004). For female mice, we found a significant R^2 only for hepcidin to Tb.Th (R^2=0.145, p=0.031). No significant regressions were found for serum ferritin to these microarchitecture parameters.

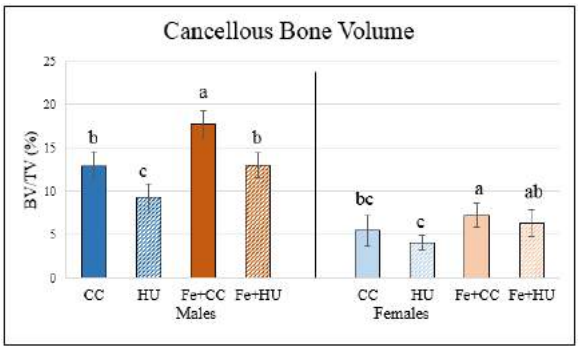

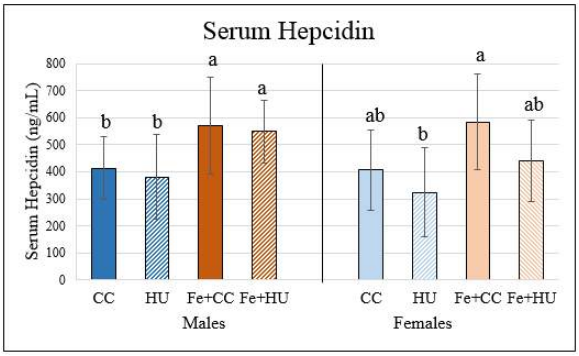

Conclusion: Although individuals and mice with pathologically high iron stores (as in hemochromatosis) incur significant bone loss (Tsay et al., *Blood*, 2010), our data provide evidence for a positive impact of physiological elevations in iron stores on cancellous BV/TV and microarchitecture. The modest but significant regressions between serum hepcidin and cancellous microarchitecture parameters suggest an osteogenic effect of hepcidin. There are published data supporting the impact of hepcidin on both osteoblast and osteoclast activity. *In vitro* hepcidin promotes differentiation of osteoblasts and mineralization (Li GF et al., *Mol Cell Biochem*, 2012) and facilitates osteoclast differentiation by increasing intracellular iron levels (Zhao GY et al., *Inflammation*, 2015). Mice null for hepcidin display defects in bone microarchitecture and altered bone formation markers (Shen GS et al, *Calcif Tissue Int*, 2014). HU-induced bone loss is exacerbated in mice treated with siRNA for hepcidin (Xu Z et al., *Bone*, 2017). These interesting links between iron metabolism and bone cell activity merit more investigation.

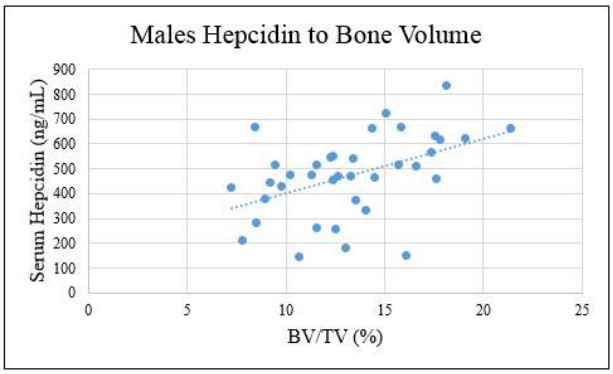

R^2=.217, p=0.004

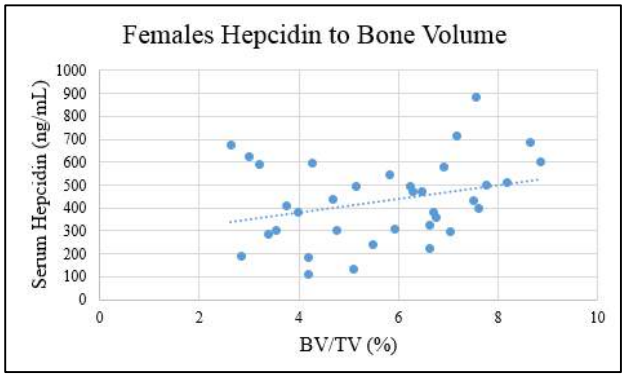

R^2=.110, p=0.063

Support from NASA via Space Biology Grant NNX13AL25G is gratefully acknowledged.

Point Mutation in Lrp4 Sost Binding Pocket Increases Bone Mass in Mice

Whitney Bullock1, Alexander Robling, PhD1
1Indiana University, Indianapolis, IN

The low-density lipoprotein receptor related protein 4 (Lrp4) is a membrane-bound receptor for Agrin and is involved in neuromuscular junction (NMJ) assembly in skeletal muscle cells. Recently, Lrp4 has also been identified as a protein important for the action of Wnt pathway inhibitors, and in particular, for their binding to Wnt co-receptor targets (e.g., Lrp5/Lrp6). In bone cells, Lrp4 functions to bind the soluble Wnt inhibitor, Sost, and potentially mediates the interaction between Sost and Lrp5/6. Lrp4 is ubiquitously expressed, and global deletion of Lrp4 results in perinatal lethality due to Lrp4's role in NMJ formation. Deletion or disruption of Lrp4 in osteoblasts increases bone mass and bone formation both *in vitro* and *in vivo*1,2. Previously, a patient with unusually high bone mass (HBM) was found to harbor a missense mutation in the third β-propeller of Lrp4. This mutation—R1170W—was hypothesized to reduce Sost-mediated inhibition of Wnt signaling, resulting in increased bone mass. To explore this possibility, we generated a mutant mouse model using the Crisper/Cas9 system to knock in the Lrp4 R1170W point mutation. Our aim was to generate an orthologous mouse model of the human patient. The mice were assessed for phenotypic changes in bone mass during growth and into adulthood. To measure changes in bone mass, serial DEXA was performed bi-weekly until 18 weeks of age, and in vivo pQCT scans of the tibia were collected at 8 weeks of age. At 18 weeks of age, femurs were collected and analyzed by µCT. While mice with a single knock-in allele (KI/+) did not have increased bone mass, mice in which both alleles were altered (KI/KI) displayed dramatic increases in bone mass relative to wild type (WT). pQCT at 8 weeks of age show trabecular content at the proximal tibia was increased 15% in females (0.088 ± 0.008 in WT versus 0.102 ± 0.008 in KI/KI) while total density at the midshaft increased 12.7% and 11.9% in males and females respectively (Fig 1). Serial DEXA showed significant increases in whole body BMD, beginning at 8 weeks of age in KI/KI mice (+39% in males and +34% in females at 18 weeks) (Fig 2). µCT of the distal femur also showed increased bone mineral content (BMC) in KI/KI mice, but not KI/+ mice (Fig 3). Additionally, KI/KI mice show severe malocclusion, excessive incisor growth and skull thickening. This high bone mass phenotype is consistent with that seen in the HBM patients with Lrp4 point mutations. Our data implicate the third β-propeller binding pocket in Lrp4 as a key element in the regulation of bone mass, and highlight this domain as a high priority candidate for potential novel pharmacologic bone therapies. Generation of this mouse model will help address the role of Lrp4 in mechanotransduction and the mechanistic role of Lrp4 in facilitating sclerostin-mediated inhibition of the Wnt/Lrp5/Lrp6 pathway.

References

1. Chang, M.K., et al., Disruption of Lrp4 function by genetic deletion or pharmacological blockade increases bone mass and serum sclerostin levels. Proceedings of the National Academy of Sciences of the United States of America, 2014. 111(48): p. E5187-E5195.
2. Xiong, L., et al., Lrp4 in osteoblasts suppresses bone formation and promotes osteoclastogenesis and bone resorption. Proc Natl Acad Sci USA, 2015.
3. Leupin, O., et al., Bone Overgrowth-associated Mutations in the LRP4 Gene Impair Sclerostin Facilitator Function. Journal of Biological Chemistry, 2011. 286(22): p. 19489-19500.

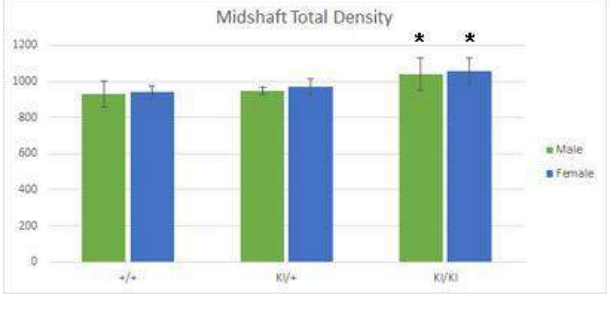

Figure 1. Midshaft Density was increased in both male and female KI/KI mice at 8 weeks of age
*p< 0.05 relative to +/+, n=9-10

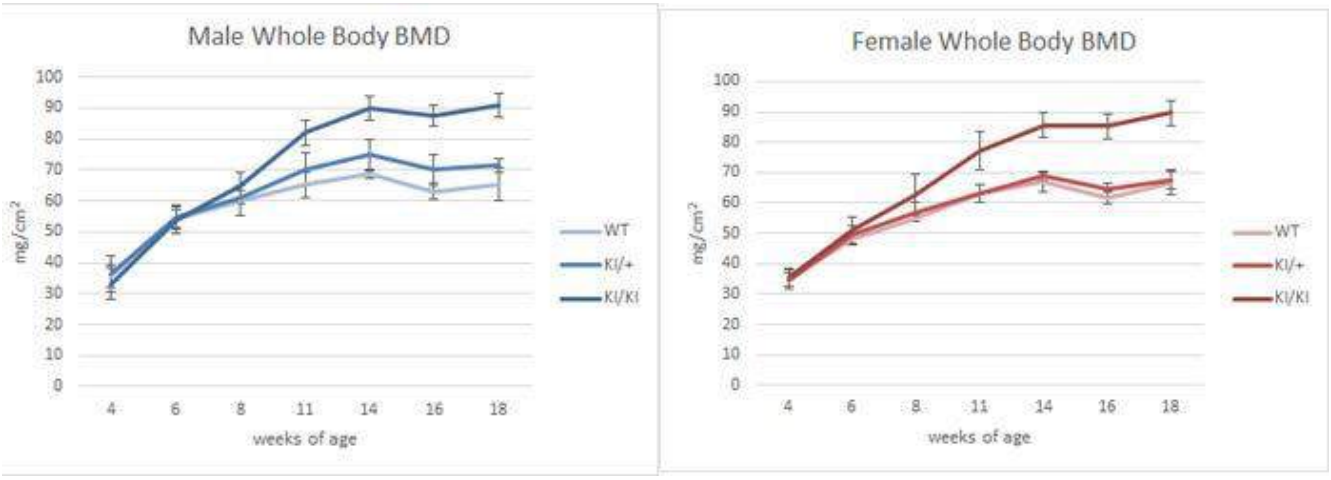

Figure 2. Whole body BMD was increased in KI/KI mice from 11 weeks, n=5

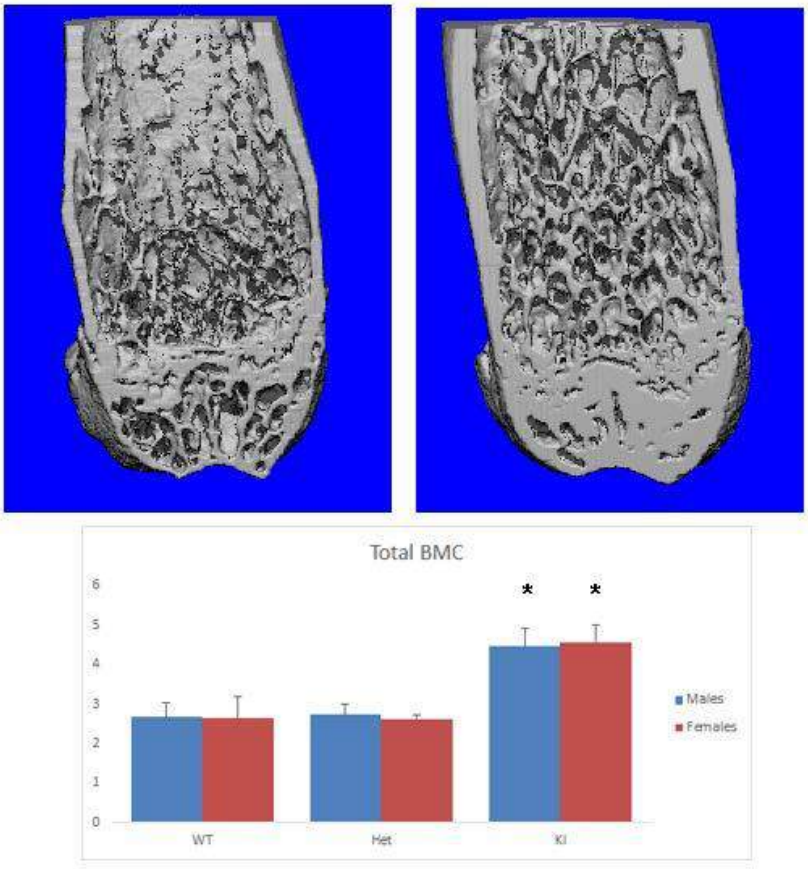

Figure 3. Total BMC was increased in KI/KI mice at 18 weeks of age. Distal femur was analyzed by microCT. *p<0.05, n=9-10

Actin organization and response to fluid flow are influenced by the osteocyte primary cilium

Michael P. Duffy, MPh[1], McKenzie E. Sup [1], Christopher R. Jacobs, PhD[1]
[1]Columbia University in the City of New York, New York City, NY

Introduction: Due to the continued financial and quality-of-life burden of low bone mass and osteoporosis, it is critical to further elucidate the mechanism of bone cell mechanotransduction in order to identify improved therapeutic targets. The osteocyte actin cytoskeleton has been shown to be important for nitric oxide and prostaglandin E_2 release in response to fluid flow [1,2]. Separately, the primary cilium, a solitary antenna-like organelle, has also been implicated as a signaling nexus in bone cell mechanotransduction [3,4]. Whether these two apparently distinct systems function cooperatively is unknown, though a link has been implicated between actin dynamics and small ciliary motions [5]. We hypothesize that the cilium influences actin organization and response to fluid-flow stimulation. We implemented a model of cilia impairment using an IFT88 siRNA mediated knock-down. IFT88 contributes to anterograde transport along the ciliary axoneme and impairing translation results in a decreased ciliary length and incidence. We applied fluid flow to cells with a ciliary impairment (KD) and a control group to assess the role of the primary cilium in regulating actin cytoskeletal organization.

Methods

Cell Culture: MLO-Y4 cells were cultured on collagen-coated dishes and maintained in MEM α supplemented with 5% fetal bovine serum, 5% calf serum and 1% Penicillin-Streptomycin.

Fluid Flow Experiments: MLO-Y4 cells (2500 cells/cm_2) were plated on collagen-coated glass slides three days before flow. Twenty-four hours after cell seeding, we performed a siRNA-mediated knockdown of IFT88 with Lipofectamine 2000 to disrupt cilia formation. A medium GC scramble siRNA was used for control samples. After 6 hours of incubation, we applied fresh media with 2.5% fetal bone serum, 2.5% calf serum and 1% Penicillin-Streptomycin. Similar to Spasic et al. [8], glass slides were loaded into fluid flow chambers and allowed to equilibrate for 30 mins before 60 mins of 1 Hz oscillatory fluid flow was applied at a peak fluid-shear stress of 1 Pa. Samples were washed twice in cold PBS and fixed in neutral buffered formalin. During the 1.5 hour experiment, flow (F) and no-flow (NF) samples were kept in a 37^o incubator at 5% CO_2.

Immunocytochemistry: Samples were permeabilized in 0.1% Triton X-100 and blocked in 1% BSA and 10% goat serum. Phalloidin conjugated to Alexa Fluor 488 was applied with an anti-acetylated alpha-tubulin primary antibody (C3B9 hybridoma cell line, Sigma) to stain for the primary cilium. Alexa Fluor 568 secondary was applied followed by NucBlue (Molecular Probes) as a nuclear stain. Slides were mounted with Prolong Gold Antifade mountant (Molecular Probes).

Microscopy and Image Analysis: Images were acquired on an Olympus IX71 inverted epifluorescence microscope with a 1.30 NA 40x oil objective and a xenon lamp. Images were analyzed using ImageJ. Cilia incidence was calculated manually along with cell morphology. Cell morphology was categorized as rounded/cuboidal, elongated, triangular or dendritic as has been previously used to describe changes in osteocyte actin networks [9]. An average cell area for each micrograph was determined for by thresholding the image to calculate total cell area and separately to count the number of nuclei.

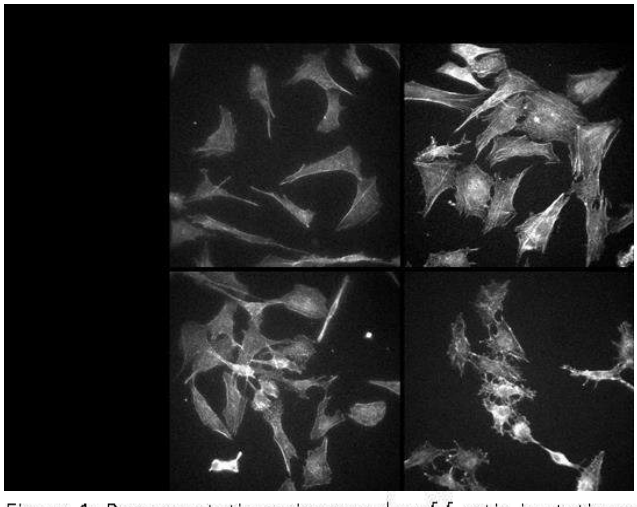

Figure 1: Representative micrographs of f-actin in static and mechanically stimulated cells. Control cells had increased stress fiber formation and similar morphology to static controls. Cells lacking a primary cilium did not have a comparable stress fiber formation and actin cortical localization was lost in many.

Results

The cilia incidence was significantly ($p < 0.001$, two-proportion z-test) reduced in the IFT88 siRNA group (45%, n = 716 cells) compared to the control group (63%, n = 686 cells). Control cells responded to fluid flow with increased stress fiber formation and area while cells lacking a primary cilium were not able to form similar stress fibers. Cilia impairment resulted in a more rounded, spindly morphology with reduced cortical actin (Figure 1). Cell area (Figure 2A) was significantly greater in the control flow group than all other groups, while there was no significant differences between the KD no-flow, KD flow or control NF (1-way ANOVA followed by a Bonferonni's Multiple

Comparison Test). Control cells had about a 1.5-fold increase in area compared to no change in cell area in the KD group (Figure 2B), despite observable changes in morphology (Figure 2C). In the control group, the majority of cells had greater cell spreading, either triangular or dendritic, compared to rounded or elongated. In response to flow, there number of rounded cells increased by 12% and the number of dendritic cells decreased by 12%. A ciliary knockdown resulted in more

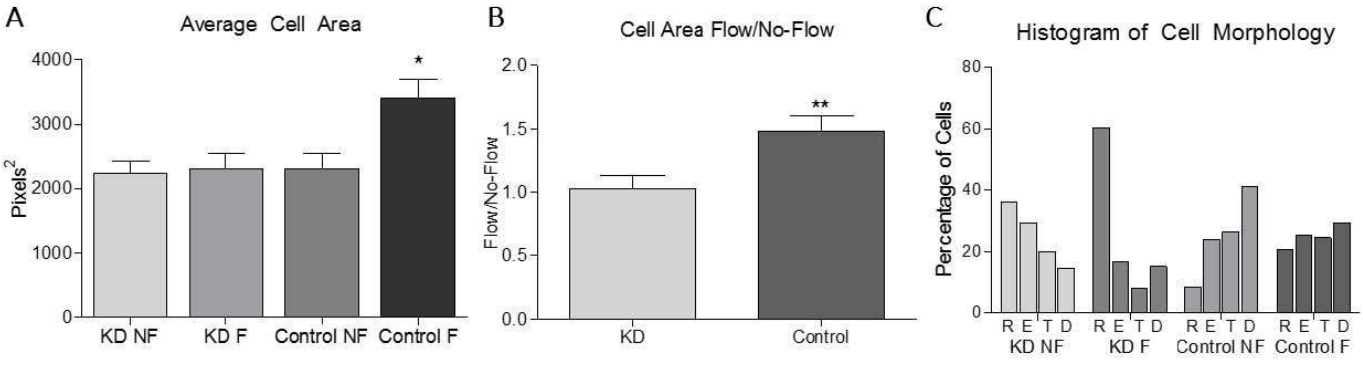

Figure 2: Cells lacking a primary cilium did not increase in cell area in response to fluid flow and had a more elongated and rounded morphology compared to control. (A) Average cell area calculated per micrograph ($n \geq 16$ from minimum 6 flow/no-flow slides per group, $p < 0.05$). (B) Cell area fold change for knock-down (KD) and control ($p < 0.01$). (C) Cell morphology categorized into round (R), elongated (E), triangular (T), or dendritic (D). There is a minimum of 75 cells per group.

Discussion

With a modest 18% reduction in primary cilia incidence, changes in the osteocyte actin cytoskeleton could be observed along with an abrogated actin-remodeling in response to fluid flow. It is unclear if the primary cilium interacts directly with the actin cytoskeleton or through an intermediary, such as the microtubule cytosolic network. Recent proteomic studies have found actin-binding proteins in the cilium [10]. Due to the importance of the actin cytoskeleton to osteocyte mechanotransduction [1,2], and the recently demonstrated ability to target osteocyte mechanosensing through the primary cilium [8], the increased understanding of the interplay between the actin cytoskeleton and the primary cilium could lead to novel therapeutics to improve mechanotransduction in diseases such as osteoporosis.

Citations

1. Ajubi NE, Klein-Nulend J, Nijweide PJ, Vrijheid-Lammers T, Alblas MJ, Burger EH. Pulsating Fluid Flow Increases Prostaglandin Production by Cultured Chicken Osteocytes—A Cytoskeleton-Dependent Process. Biochem Biophys Res Commun. 1996 Aug 5;225(1):62–8.
2. McGarry JG, Klein-Nulend J, Prendergast PJ. The effect of cytoskeletal disruption on pulsatile fluid flow-induced nitric oxide and prostaglandin E2 release in osteocytes and osteoblasts. Biochem Biophys Res Commun. 2005 Apr 29;330(1):341–8.
3. Malone AM, Anderson CT, Tummala P, Kwon RY, Johnston TR, Stearns T, et al. Primary cilia mediate mechanosensing in bone cells by a calcium-independent mechanism. Proc Natl Acad Sci. 2007;104(33):13325–30.
4. Lee KL, Hoey DA, Spasic M, Tang T, Hammond HK, Jacobs CR. Adenylyl cyclase 6 mediates loading-induced bone adaptation in vivo. FASEB J. 2014 Mar 1;28(3):1157–65.
5. Battle C, Ott CM, Burnette DT, Lippincott-Schwartz J, Schmidt CF. Intracellular and extracellular forces drive primary cilia movement. Proc Natl Acad Sci. 2015 Feb 3;112(5):1410–5.
6. Espinha LC, Hoey DA, Fernandes PR, Rodrigues HC, Jacobs CR. Oscillatory fluid flow influences primary cilia and microtubule mechanics. Cytoskeleton. 2014 Jul 1;71(7):435–45.
7. Baik AD, Lu XL, Qiu J, Huo B, Hillman EMC, Dong C, et al. Quasi-3D Cytoskeletal Dynamics of Osteocytes under Fluid Flow. Biophys J. 2010 Nov 3;99(9):2812–20.
8. Spasic M, Jacobs CR. Lengthening primary cilia enhances cellular mechanosensitivity. Eur Cell Mater. 2017 Feb 20;33:158–68.
9. Ponik SM, Triplett JW, Pavalko FM. Osteoblasts and osteocytes respond differently to oscillatory and unidirectional fluid flow profiles. J Cell Biochem. 2007 Feb 15;100(3):794–807.
10. Mick DU, Rodrigues RB, Leib RD, Adams CM, Chien AS, Gygi SP, et al. Proteomics of Primary Cilia by Proximity Labeling. Dev Cell. 2015 Nov 23;35(4):497–512.

TGFβ regulation of osteocytic perilacunar remodeling is crucial for maintaining bone quality

Neha S. Dole, PhD[1], Courtney M. Mazur, BS[1], Claire Acevedo, PhD[1,2], Justin Lopez, BS[1], David A. Monteiro, MS[1], Tristan W. Fowler, PhD[1], Bernd Gludovatz, PhD[2,3], Flynn Walsh, BS[2,3], Robert O. Ritchie, PhD[2,3], Khalid S. Mohammad, MD, PhD[4], Tamara Alliston, PhD[1]

[1]Department of Orthopaedic Surgery, University of California San Francisco, CA; [2]Materials Science Division, Lawrence Berkeley National Laboratory Berkeley, CA; [3]Department of Materials Science and Engineering, University of California Berkeley, CA; [4]Department of Medicine, Indiana University School of Medicine, Indianapolis, IN

Half of atraumatic fractures are bone mass independent, and result from impaired bone quality. However, an incomplete understanding of the cellular and molecular mechanisms controlling bone quality has limited the ability to target it therapeutically. TGFβ signaling is one of the few molecular pathways known to affect bone quality, but its cellular target is unknown. Since osteocyte perilacunar remodeling (PLR) has been associated with changes in bone quality, we tested the hypothesis that TGFβ regulates bone quality via osteocyte PLR.

We systemically inhibited TGFβ signaling *in vivo* using TGFβ receptor type I inhibitor (TβRI-I) and found a coordinated repression of key PLR enzymes, including MMP13, MMP14, and Cathepsin K. Inhibition of TGFβ also caused a severe deterioration of osteocyte lacuno-canalicular network (LCN) connectivity and these impaired PLR hallmarks strongly suggested of TGFβ's regulatory role in PLR. Additionally, we found that TGFβ induced PLR gene expression in MLO-Y4 osteocyte-like cells, and reduced their intracellular pH, which is a functional measure of PLR. This indicated that TGFβ modulated PLR in an osteocyte-intrinsic manner. We tested this hypothesis in vivo using a novel osteocyte specific TGFβ receptor type II-deficient ($T\beta RII^{ocy-/-}$) mouse model. Similar to the TβRI-I administered mice, $T\beta RII^{ocy-/-}$ also exhibited a stark reduction in expression of PLR enzymes and osteocyte LCN connectivity compared to wild-type (WT) littermates. Thus, our data show that TGFβ regulates osteocyte mediated PLR.

Using flexural strength tests and nanoindentation, we tested whether osteocyte-intrinsic TGFβ signaling is sufficient to regulate bone quality. Despite high trabecular bone mass and normal cortical bone mass and thickness, $T\beta RII^{ocy-/-}$ bones showed reduction in yield strength, bending modulus and tissue elastic modulus, suggesting a defect in bone quality. During in situ fracture toughness testing, $T\beta RII^{ocy-/-}$ bones showed a 65% reduction in fracture toughness due to unchecked crack propagation. SEM analysis revealed that $T\beta RII^{ocy-/-}$ bone has inferior extrinsic toughening mechanisms with significantly linear, shorter crack paths, and less branching and uncracked ligament bridging relative to WT. These data implicate osteocytes as an essential target of TGFβ in the control of bone quality.

Overall, this study reveals the novel role of osteocyte-intrinsic TGFβ in the control of PLR and the importance of PLR in the regulation of bone quality.

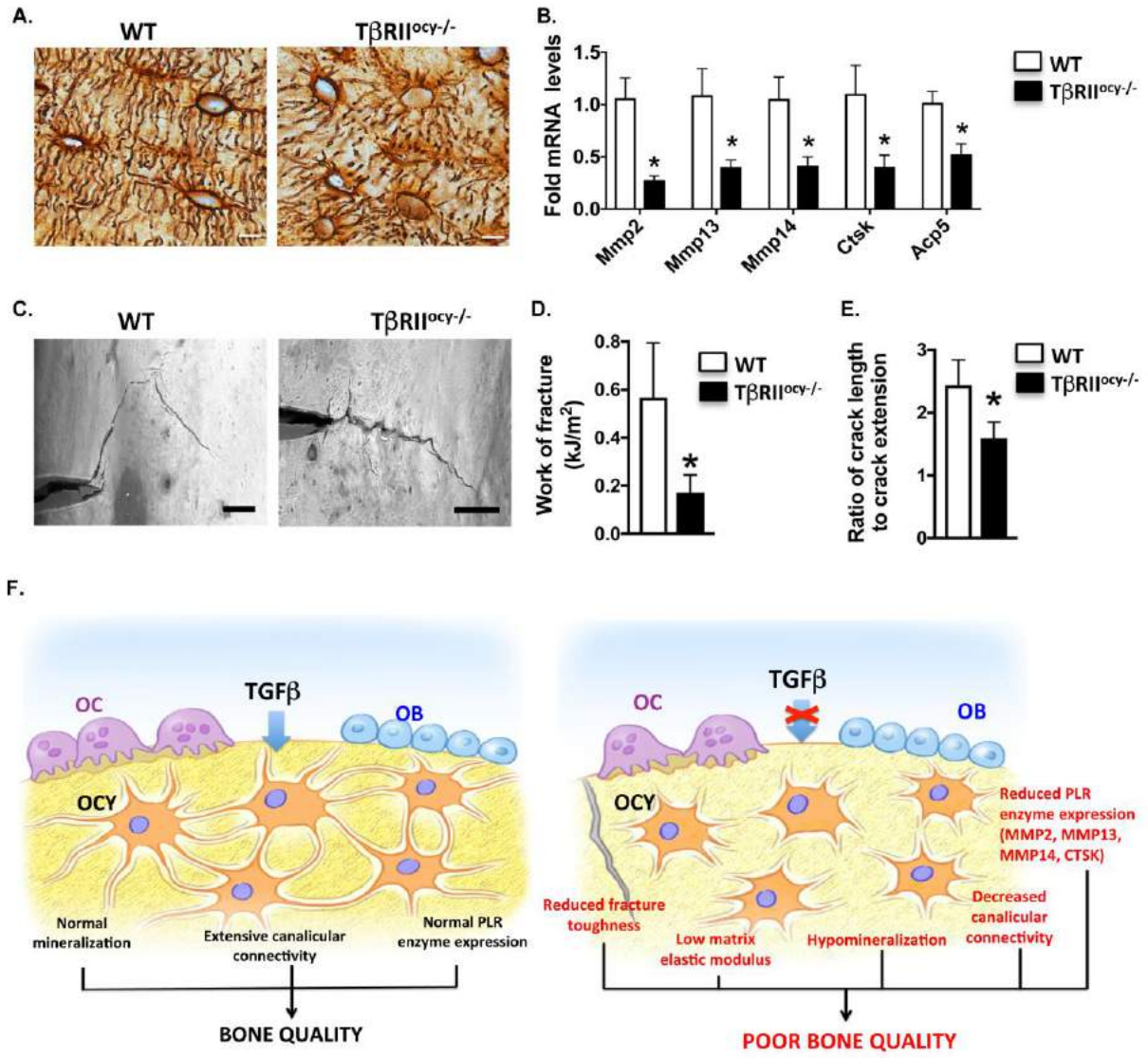

Figure 1: Osteocyte lacuno-canalicular network in the femoral cortical bone of WT and T□RII$^{ocy-/-}$ mice was detected by silver nitrate staining (N=5 mice/group and 4 images/mouse) and representative images of the lacuno-canalicular network is shown (A) (scale bar = 20 µm). Gene expression of Mmp2, Mmp13, Mmp14, Ctsk and Acp5 from the bones of WT and T□RII$^{ocy-/-}$ mice was quantified and normalized to 18s mRNA (B) (N=8-10 mice/group). In situ fracture toughness testing was used to evaluate differences in extrinsic toughening mechanisms of WT and T□RII$^{ocy-/-}$ bones by observing crack propagation. At the end of stable crack growth, differences in the extrinsic toughening mechanism crack deflection are readily seen in two representative samples (C) (scale bar = 100 µm), total work of fracture (WoF) (D) and crack deflection quantified as the ratio of total crack length to crack extension (E) (N=5 mice/group). Schematic figure illustrates the mechanistic role of TGF□ signaling in osteocyte perilacunar remodeling and in maintenance of bone quality (F).

Severe Burn-Induced Inflammation and Remodeling of Achilles Tendon in a Rat Model

Paula Hernandez, PhD[1]; Dustin Buller, BS[1];Thomas Mitchell , BS[1]; Jamie Wright, PhD[2]; Haixiang Liang, MD[4]; Kshitij Manchanda, MD[1]; Tre Welch, PhD[2]; Ryan M. Huebinger, PhD[3]; Deborah L. Carlson, PhD[3]; Steven E. Wolf, MD[3]; Juquan Song, MD[3]*

[1]Department of Orthopaedic Surgery, [2]Department of Cardiovascular and Thoracic Surgery, [3]Department of Surgery, University of Texas Southwestern Medical Center, Dallas, TX; [4]Orthopedic Research Laboratory, Feinstein Institute for Medical Research, Northwell Health, Manhasset, NY. *paula.hernandez2@utsouthwestern.edu

Introduction: Severe burn is defined as a full-thickness burn of greater than 30% of total body surface area (TBSA). It occurs at a rate of approximately 5/100,000 persons per year globally and may affect multiple organs, even those distantly located from the burn site (*1*). In the musculoskeletal system, severe burn induces hypercatabolism in muscle and bone due to the activation of systemic inflammation, and disuse from long immobilization periods (*2, 3*). Muscle loss and atrophy post burn have been associated with increased levels of TNF-α (*4*), while bone mass loss has been associated with circulating IL-1β and IL-6, which are increased from 24 hours post burn (*5*). Despite the findings of mass loss in both skeletal muscle and bone, there are limited studies on the molecular and structural effects of burn injury on tendon.

We hypothesize that the systemic inflammation caused by severe burn will induce molecular and structural changes in Achilles tendon that ultimately debilitate this tissue.

Methods: *Severe burn injury:* 40 adult male Sprague-Dawley rats, 270-300 g, were used. The animal protocol was approved by the Institutional Animal Care and Use Committee at the University of Texas Southwestern Medical Center at Dallas. Animals were randomly divided into 5 groups: Control (n = 11), 1 day (n = 6), 3 days (n = 6), 7 days (n = 6), and 14 days (n = 11) post burn. Under anesthesia, animal hair was removed from the dorsal and lateral surfaces. Dorsal skin amounting to 40% of TBSA was immersed in 95°C-100°C water for 10 seconds. Control animals received sham treatment. *Gene and protein expression*: Tendon RNA was extracted and analyzed for expression of IL-6, TNF, IL-1β, col1a1, col3a1, MMP9 and MMP13 by qPCR. 10 µg of total protein was used for Western blot. Antibodies included anti-collagen I (Abcam), anti-collagen III (Abcam). *Histology*: Tendons were fixed in 10% neutralized buffer formalin and decalcified with 10% formic acid. Paraffin sections were processed for H&E and Picrosirius red staining. Samples were visualized in a Nikon Eclipse Ti microscope or in an Olympus BH2-RFCA using polarized light. *Image analysis*: for Picrosirius red was performed with ImageJ (NIH). 320 x 320 pixels regions were selected from the central area of each tendon in an 8-bit and 256 color image. For each piece, the (green + blue)/red color intensities were calculated and grouped as control versus 14 days post burn, where green + blue represent more organized fibers compared to red. *Biomechanics:* Testing was done in an Instron 5565 universal testing system equipped with a 5 kN load cell. Samples were pulled until failure at a cross-head speed of 6 mm/min collecting force and deformation data throughout the test. *Statistics*: Data are presented as mean ± error propagation for gene expression and mean ± standard deviation elsewhere. Data were analyzed in GraphPad Prism 7 with one-way ANOVA and Fisher's LSD posthoc test, or by unpaired Student's t test when comparing two variables, ($p < 0.05$ being significant).

Results: Gene expression of IL-6 and IL-1β as well as MMP9 and MMP13 increased in rat tendon 3 days after burn, $p < 0.05$. TNF did not reached significant difference. The levels of col1a1 and col3a1 gene expression did not change significantly on all the time points analyzed (control, 7 and 14 days post burn). However, the protein ratio for collagens I/III decreased at day 14, $p < 0.05$, indicating signs of tendon remodeling. Histological analysis with H&E and Picrosirius red staining further indicated remodeling, by revealing a decrease in organized collagen fibers 14 days after burn. Biomechanical analysis showed a decrease in stiffness and ultimate force of tendons in burn rats after 14 days of injury.

Discussion: The upregulation of both IL-1β and IL-6 indicates the initiation of acute inflammation in the tendon. Previous reports have shown the involvement of IL-1β in the upregulation of MMPs and tissue remodeling in tendon (*6, 7*). When tendon experiences remodeling or injury, collagen III content increases, resulting in a decrease in tensile strength (*8*). On the other hand, metalloproteinases such as the collagenase MMP13 can cleave the collagen triple helix, creating fragments that are further degraded by gelatinases such as MMP9 (*9*). Our results revealed a significant decrease in the collagen I protein level at 7 days post burn, with a subsequent increase akin to the control level by day 14. We propose that the initial decrease in collagen I can be explained by the upregulation of MMP13 and MMP9, generated by IL-1β. Along with this, collagen III protein was elevated by day 14 post burn. The synthesis of collagen III protein and the decrease in the collagen I/III protein ratio suggests an induction of scar tissue or remodeling (*8*). Histological observations of collagen alignment and tenocyte distributions showed less tissue organization 14 days post burn compared to control. H&E staining showed less fiber alignment, cell aggregations and even round nuclear morphology on some cells. To address whether molecular changes in tissue structure will also affect its functional mechanics, the tensile force and deformation were measured. Overall, our findings showed that ultimate force and stiffness were reduced at 14 days post burn compared to controls.

These biomechanical results correlate with histological findings of less organized fibers. It is possible that the initial loss in collagen I followed by an induction of synthesis of both collagens I and III results in fiber disorganization (*8*). Although previous reports have shown that Achilles tendon could react to an inflammatory event produced in surrounding tissue (*10*), this study is the first to report that remote systemic inflammation is capable of inducing a local inflammatory response and remodeling in the tendon.

Significance: Tendinopathy was observed in Achilles tendon 14 days after severe burn, via the induction of inflammation and remodeling. The current study provides a model of tendinopathy that may be used for the development of therapeutic approaches following burn. Future investigation regarding the modulation of the inflammatory cascade and MMP inhibition accompanied by physical therapy may be promising for the improvement of recovery after severe burn and other traumatic injuries.

References:

1. L. H. Evers et al., *Exp Dermatol* **19**, 777-783 (2010).
2. D. W. Hart *et al.*, *Ann Surg* **232**, 455-465 (2000).
3. G. L. Klein et al., *J Burns Wounds* **5**, e5 (2006).
4. J. Song et al., *Shock* **44**, 479-486 (2015).
5. S. Tamgadge *et al.*, *J Orofac Sci* **7**, 119 (2015).
6. J. Archambault et al., *J Orthop Res* **20**, 36-39 (2002).
7. M. Tsuzaki *et al.*, *J Orthop Res* **21**, 256-264 (2003).
8. H. A. Eriksen et al., *J Orthop Res* **20**, 1352-1357 (2002).
9. G. P. Riley *et al.*, *Matrix Biol* **21**, 185-195 (2002).
10. C. P. Vieira et al., *Acta Ortop Bras* **20**, 266-269 (2012).

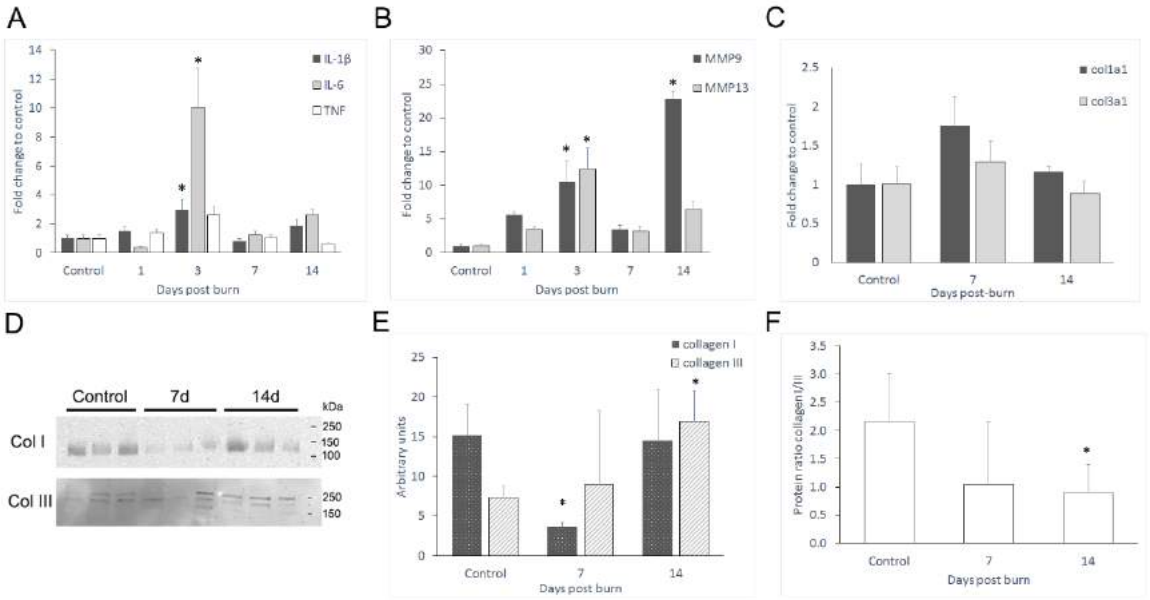

Figure 1. *Changes in expression of pro-inflammatory cytokines, metalloproteases, and collagens in Achilles tendon after severe burn.* (A) Gene expression of cytokines IL-1β, IL-6, and TNF (B) metalloproteinases MMP9 and MMP13 and (C) collagens col1a1 and col3a1 were examined with qPCR; (D) Representative Western blot showing 1 band for Collagen I and 3 bands for Collagen III on Control, 7 and 14 days post-burn. (E) Protein levels of collagen I and collagen III were calculated from Western blot and (F) the collagen I/III protein ratio was analyzed. Data are shown as mean with error propagation in A and B. Data are shown as mean ± SD in C and D. **p* < 0.05 versus control.

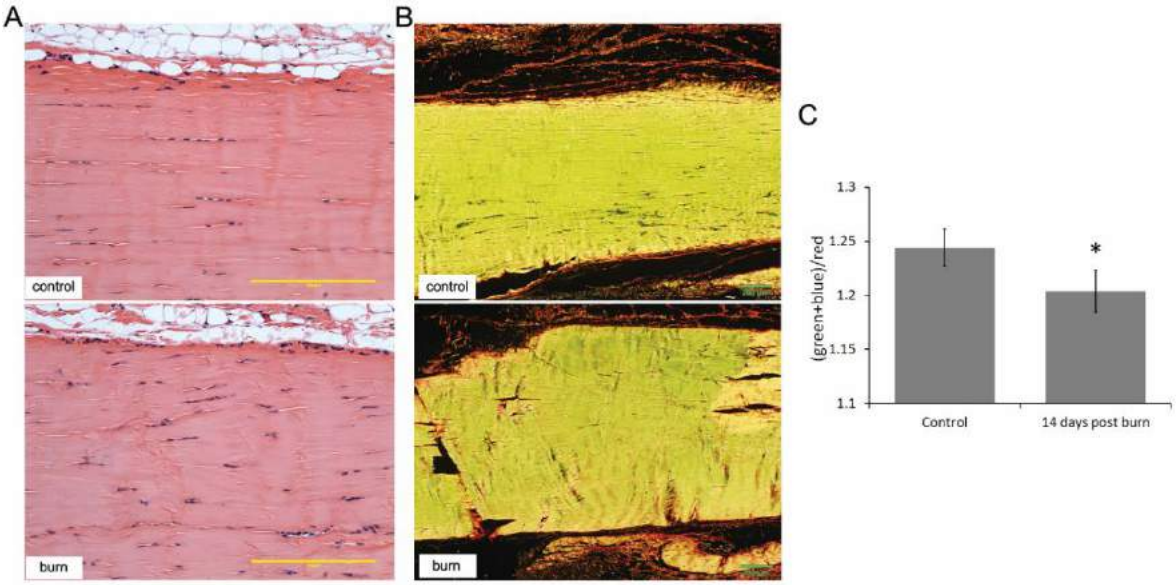

Figure 2. *Histological evidence of changes in Achilles tendon after severe burn*. (A) Tendons from control rats (upper panel) and 14-day post burn rats (lower panel) were stained with hematoxylin and eosin to show cell morphology and gross fiber organization. (B) Slides from the same tendons were used for Picrosirius red staining and analyzed with polarized light to show fiber organization of control (upper panel) versus 14-day post burn rats (lower panel). (C) Quantification of (green + blue)/red of the Picrosirius red images under polarized light was used to determine organization of fibers. Scale bars = 200 µm. *$p < 0.05$ versus control.

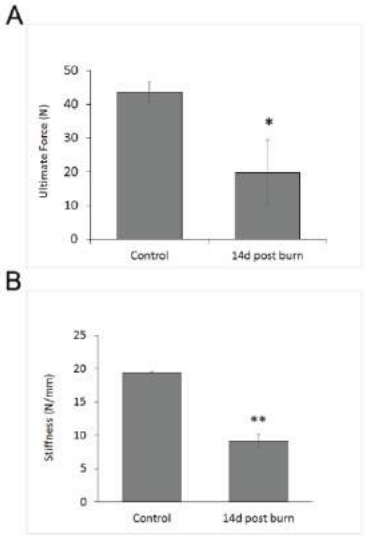

Figure 3. *Biomechanical changes in Achilles tendon after severe burn.* (A) Force-deformation curves of representative tendons obtained from 3 control rats and 5 burn rats (14 days post burn). (B) Maximum load values obtained from the force-deformation curve of control rats versus 14-day post burn rats. (C) Stiffness values calculated from force-deformation curves comparing no-burn versus 14-day post burn tendons. *$p < 0.05$, **$p < 0.001$ versus control.

The Expansion of Heterotopic Bone in Fibrodysplasia Ossificans Progressiva is Activin A-Dependent

Lily Huang[1], Sarah J Hatsell[1], Jaymin Upadhyay[1],, LiQin Xie[1],*, Nanditha Das[1], Rachel Stewart[2], Morgan C. Lyon[2], Keryn Palmer[2], Saathyaki Rajamani[1], Chris Graul[2], Merryl Lobo[2], Tyler J Wellman[2], Edward J Soares[3], Matt Silva[2], Jacob Hesterman[2], Kalyan Nannuru[1], Vincent Idone[1], Andrew J Murphy[1], and Aris N Economides[1,4]*

[1]Regeneron Pharmaceuticals, 777 Old Saw Mill River Road, Tarrytown, NY 10591
[2]InviCRO, LLC, 27 Drydock Avenue, Boston, MA 02210
[3]College of Holy Cross, 1 College Street, Worcester, MA 01610
[4]Regeneron Genetics Center, 777 Old Saw Mill River Road, Tarrytown, NY 10591
**Indicates equal contribution.*

Fibrodysplasia Ossificans Progressiva (FOP) is a rare autosomal dominant disorder that is characterized by episodic, progressive, and cumulative heterotopic ossification (HO) in tendons, ligaments, and a subset of skeletal muscles over a patient's lifetime. FOP is caused by missense mutations in the type I Bone Morphogenetic Protein (BMP) receptor-encoding gene, ACVR1. We have shown that HO in FOP requires activation of mutant ACVR1 by Activin A. Activin A – a BMP/TGFß family member which is not osteogenic – induces formation of HO in FOP mice, whereas its inhibition blocks the formation of HO. Here we extend our previous studies by piecing together a 'natural history' of developing HO lesions, and determining where in the continuum of HO Activin A is required, using imaging (T2-MRI, µCT, 18F-NaF PET/CT) coupled with pharmacologic inhibition of Activin A at different times during the progression of HO in FOP mice (MGI:5763014). As disease progresses, expansion of HO lesions comes about through growth and fusion of independent HO events that tend to arise within a neighborhood of existing lesions, indicating that already formed heterotopic bone lesions likely trigger the formation of new lesions. The process appears to be depended on Activin A, as inhibition of this ligand not only suppresses the growth (and can even cause partial regression) of nascent HO lesions but also stops the emergence of new HO events. These results provide evidence for a model where HO is triggered by inflammation, and where existing or developing HO lesions become 'self-propagating' by a process that may involve re-initiation of inflammation (by already formed heterotopic bone lesions) and that also requires Activin A. This new data extends the potential utility of prophylactic treatment with inhibitors of Activin A as a therapy for FOP that might not only stop the emergence of new lesions but also limit the growth and expansion of the heterotopic bone field in subjects with ongoing disease activity.

Trends in the Theory that Inflammation Plays a Causal Role in Tendon Disease: A Systematic Review and Quantitative Analysis of Published Mechanistic Reviews

Michael J. Mosca, MSc1, Mustafa S. Rashid, MSc1, Stephanie G. Dakin, DPhil BVetMeD1, Sarah J. Snelling, DPhil1, Shona Kirtley, MSc1, Professor Andrew J. Carr1
1 Botnar Research Centre, Nuffield Department of Orthopaedics, Rheumatology and Musculoskeletal Sciences, Windmill Road, Headington, Oxford, OX3 7LD, United Kingdom

Background: The relationship between inflammation and tendinopathy has been debated in the scientific literature. Several factors contribute to the lack of clarity in this field, including in consistent definitions of inflammation, and variable quality of published reviews. We hypothesized that the adoption and/or rejection of a causal link varied as a function of the characterization of the "inflammatory component" (e.g. immune cell types and molecular mediators) included in reviews.

Objective: To conduct a systematic literature search and quantitative analysis of 'mechanistic' reviews published prior to 2016 to evaluate potential predictors of the conclusion that inflammation is a contributing mechanism in tendinopathy.

Data sources: We searched the following databases from inception to 15 December 2015: Medline (OVID); Embase (OVID), Cochrane Database of Systematic Reviews (Wiley); CINAHL (EbscoHost); SPORTDiscus (EbscoHost). Search terms included a combination of both controlled vocabulary terms and free-text terms (searched in the title or abstract fields) such as tendinopathy, tendinitis, tendinosis, and terms relating to tendon injuries, rupture, disease or tears. Validated systematic review search filters were applied for each database.

Eligibility for selecting reviews: A review was deemed 'mechanistic' if its primary purpose was to discuss the pathogenesis of tendinopathy, potential causes or risk factors for tendinopathy, pathways associated with the development of tendinopathy, histological characteristics of diseased tendon tissue, or reasons for the failure of healing in diseased tendons. Figure 1 shows the search identified 2261 unique publications: 137 fulfilled inclusion criteria after abstract and full text screenings by two independent reviewers and adjudication if needed (kappa range 0.62-1.0).

Design: Twenty data items were collected for each review to assess conclusions about the role of inflammation in tendinopathy, quality of the review using a modified version of Assessing the Methodological Quality of Systematic Reviews (AMSTAR), specific definitions of the 'inflammatory component,' and other potential correlates. We used binomial logistic regression to identify factors relating to a review's conclusions relating inflammation to tendinopathy.

Results: Trends in mechanistic paradigms revealed little support for an inflammatory contribution to tendinopathy until recently (2012-2015); Figure 2 illustrates this with the majority of reviews concluding that immune cells and/or mediators play key roles in tendinopathy (59%, 24 out of 41 reviews). Prior to 2012, most of published mechanistic reviews did not discuss monocytes, macrophages, or lymphocytes in tendinopathy, rather they focused on the lack of neutrophils, often referred to as 'the inflammatory infiltrate,' or immune cells were not discussed (Figure 3). Prior to 2012, less than half of published mechanistic reviews included discussions of signaling molecules, growth factors, activation pathways, and/or molecular effectors in tendon disease; in contrast to 73% included in the discussion section post-2012. Figure 4 shows the correlation between types of immune cells discussed and the reviews' conclusions about the role of inflammation in tendinopathy. Reviews including monocytes and lymphocytes in their discussions were 5.23 times more likely to conclude inflammation was important than reviews that did not, $p < 0.001$. Reviews that concluded inflammation contributes to tendinopathy had significantly higher mean quality scores compared to reviews that refuted a link ($p = 0.015$, binomial linear regression).

Conclusions: These data show there has been growing support for an inflammatory component to tendinopathy, particularly among reviews of high quality and those that utilized more robust definitions of the 'inflammatory component.' This finding may have implications for explaining dissonance in the literature regarding a causal role for inflammation in the pathogenesis of tendinopathy.

Figure 1: PRISMA flowchart for identification and screening of reviews

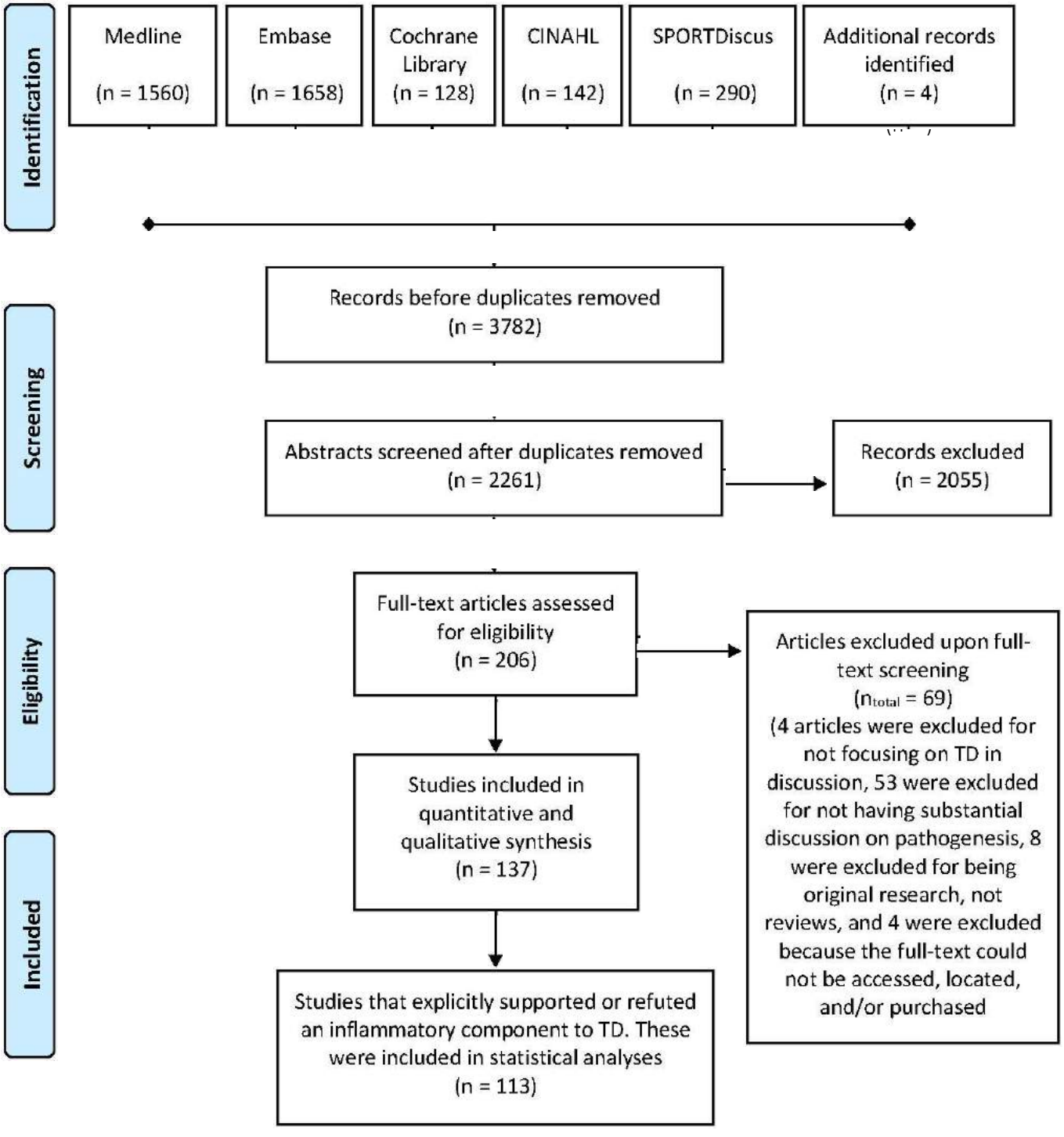

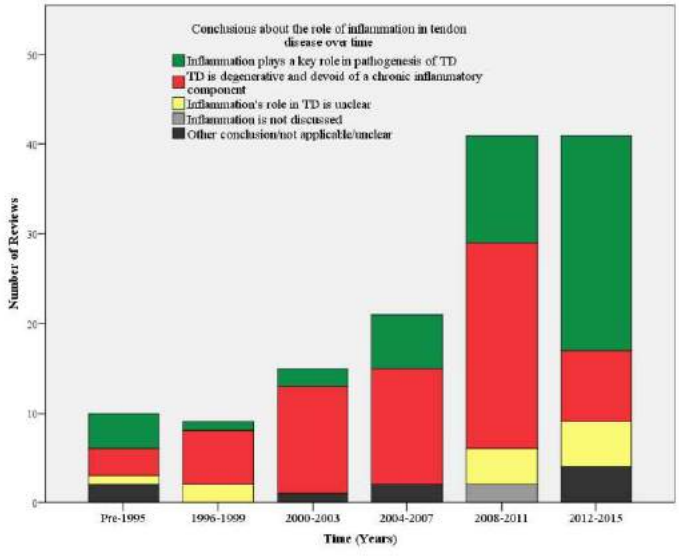

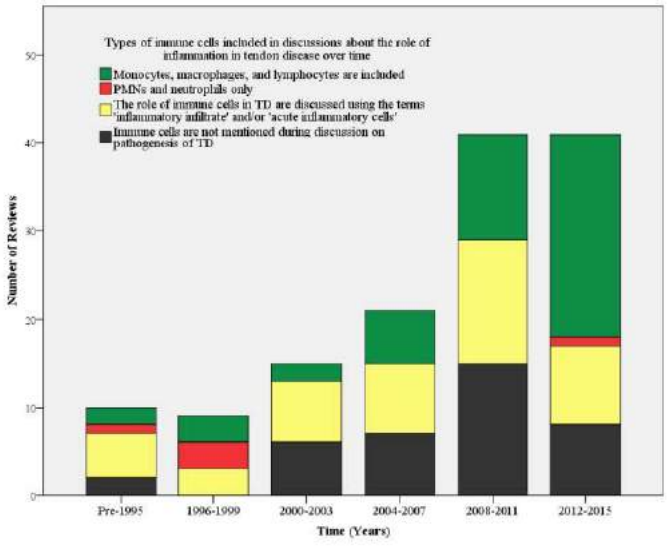

Figure 2 (Left): Conclusions about the role of inflammation in tendon disease over time (intervals of 3 years). Reviews were categorized based on their overall conclusion about the role of inflammation in TD, if discussed.

Figure 3 (Right): Types of immune cells included in discussions about the role of inflammation in TD over time (intervals of 3 years). Reviews were categorized based on the specific immune cells mentioned, referred to, or discussed when conclusions about the role of inflammation in TD were made.

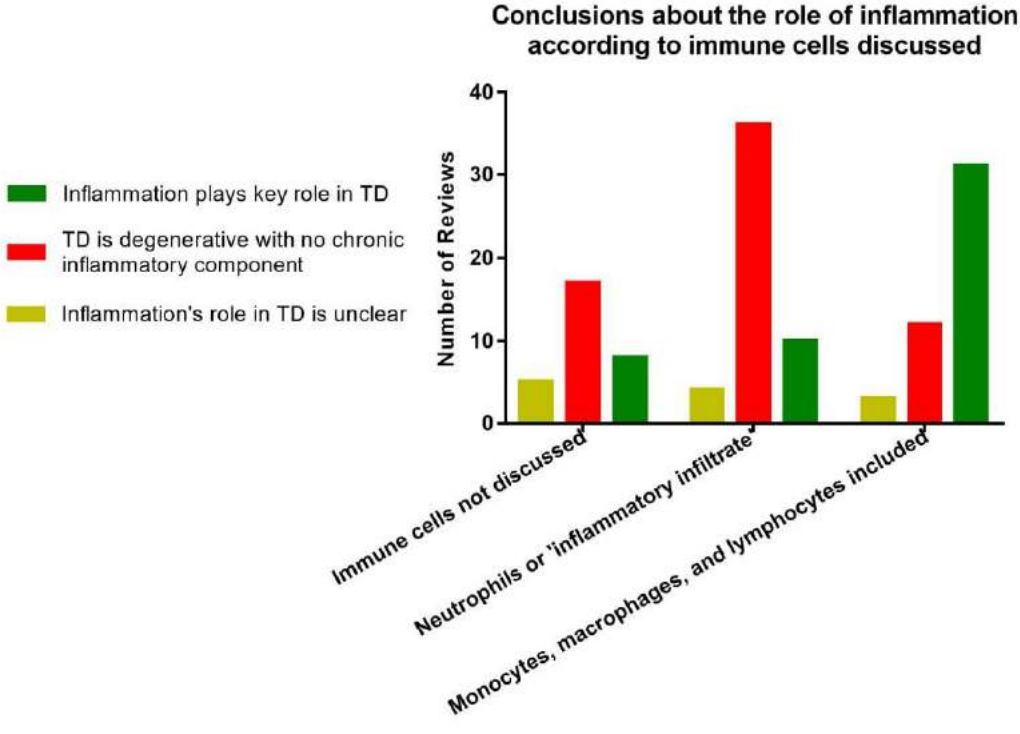

Figure 4: Conclusions about the role of inflammation according to immune cells discussed. A clear association is present between the inclusion of monocytes, macrophages, and/or lymphocytes in the discussion and concluding that inflammation plays a role in TD. Reviews that did not include monocytes/ lymphocytes were more likely to refute an inflammatory component, regardless of inclusion or exclusion of other leukocytes.

Mesenchymal Stem Cells Differentiation into Nucleus Pulposus-Like Cells Based On the New Phenotype of Young Healthy Nucleus Pulposus Cells

Arjun Sinkemani, PhD1, Feng Wang, PhD1, Zhi-Yang Xie, PhD1, Lu Chen, PhD1, Cong Zhang, PhD1, Xiao-Tao Wu*, MD, PhD1
1Department of Spine Surgery, Zhongda Hospital, Southeast University School of Medicine
187# Dingjiaqiao Road, 210009 Nanjing, China
First Author E-mail address: sinkemani@hotmail.com
**Corresponding Author E-mail address: wuxiaotao@medmail.com.cn*

Abstract
INTRODUCTION:
Low back pain (LBP) is the major cause of disability worldwide [1], with more than 84% population experiencing pain in their life time [2]. Studies claimed that intervertebral disc (IVD) degeneration is very complicated and is usually due to some various biomechanical changes within the IVD and the causes of IVD degeneration is still debated with various environmental and genetic factors influencing in its pathogenesis [3]. Biological and cell based therapies are on progress as an optional treatment for IVD degeneration. Mesenchymal stem cells (MSCs), which can be easily obtained from bone marrow or adipose tissue, can be rapidly divided and are also able to differentiate into mesenchymal lineage [4]. Many studies have also revealed that MSCs can also be differentiated into NP-like cells phenotype [5-7]. This study aimed to determine the newly defined nucleus pulposus (NP) cells markers of rat[8], whether these markers can be expressed in MSCs under co-culture condition and could be identified the differentiation of MSCs into NP-like cells.

METHODS:
NP cells and bone marrow derived MSCs from Sprague-Dawley rats were cultured under normal oxygen and MSCs were co-cultured with NP cells supernatant with the concentration of 50% and 100% for 7 days. Differentiation of MSCs and expression of recommended newly defined young healthy NP cells phenotypes8 were evaluated by quantitative real-time PCR (qPCR), western blot, immunofluorescence and flow cytometry assays.

RESULTS:
qPCR and immunofluorescence demonstrated that newly defined healthy phenotypes (aggrecan, brachyury, carbonic anhydrase 3, carbonic anhydrase 12, CD24, collagen II, HIF1/2α, Cytokeratins 8/18/19) were expressed in MSCs after the coculture with NP cells supernatant with the concentration of 50% and 100%. While the MSCs treated with the concentration of 50% and 100% NP cells supernatant, collagen II and Cytokeratin 18 showed significant increased expression compared with the MSC control group. Whereas, aggrecan, carbonic anhydrase 3, HIF1/2α, Cytokeratins 8/19 showed significant differences compared with the MSC control group, which suggested that MSCs differentiated to NP-like cells.

CONCLUSIONS:
This study showed that NP cells can stimulate MSCs differentiation to NP-like cells with cellular interaction between MSCs and NP cells under co-culture condition. However, MSCs differentiation to NP-like cells have no gold standard phenotypic markers but from our study, we can recommend these markers as an identification of MSCs differentiated to NP-like cells.

Keywords: Co-culture, Mesenchymal Stem Cell, Intervertebral Disc Degeneration, Cell Phenotype, Nucleus Pulposus Cell

REFERENCES:

1. Stewart WF, Ricci JA, Chee E, et al. 2003. Lost productive time and cost due to common pain conditions in the US workforce. Jama 290:2443-2454.

2. Walker BF. 2000. The prevalence of low back pain: a systematic review of the literature from 1966 to 1998. Journal of spinal disorders 13:205-217.
3. Mayer JE, Iatridis JC, Chan D, et al. 2013. Genetic polymorphisms associated with intervertebral disc degeneration. The spine journal : official journal of the North American Spine Society 13:299-317.
4. Gilbert HT, Hoyland JA, Richardson SM. 2013. Stem cell regeneration of degenerated intervertebral discs: current status (update). Current pain and headache reports 17:377.
5. Risbud MV, Albert TJ, Guttapalli A, et al. 2004. Differentiation of mesenchymal stem cells towards a nucleus pulposus-like phenotype in vitro: implications for cell-based transplantation therapy. Spine 29:2627-2632.
6. Strassburg S, Richardson SM, Freemont AJ, et al. 2010. Co-culture induces mesenchymal stem cell differentiation and modulation of the degenerate human nucleus pulposus cell phenotype. Regenerative medicine 5:701-711.
7. Thorpe AA, Binch AL, Creemers LB, et al. 2016. Nucleus pulposus phenotypic markers to determine stem cell differentiation: fact or fiction? Oncotarget 7:2189-2200.
8. Risbud MV, Schoepflin ZR, Mwale F, et al. 2015. Defining the phenotype of young healthy nucleus pulposus cells: recommendations of the Spine Research Interest Group at the 2014 annual ORS meeting. Journal of orthopaedic research : official publication of the Orthopaedic Research Society 33:283-293.

IMAGES:

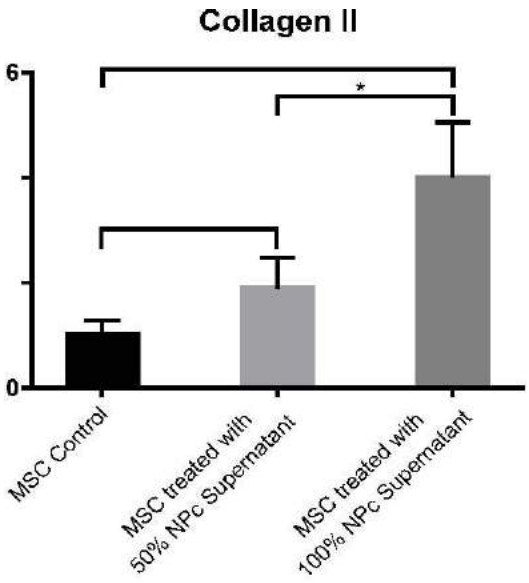

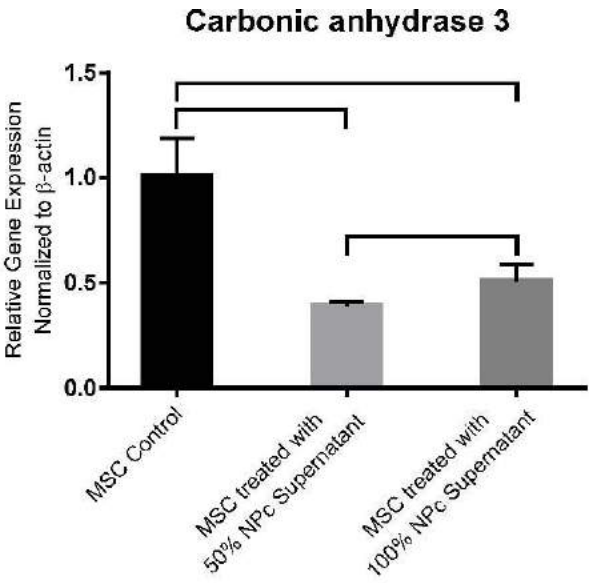

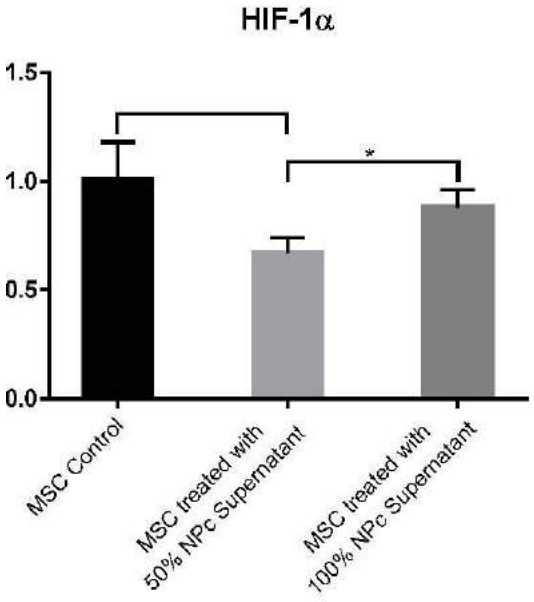
HIF-1α
1.5
1.0
0.5
0.0
*
MSC Control
MSC treated with 50% NPc Supernatant
MSC treated with 100% NPc Supernatant

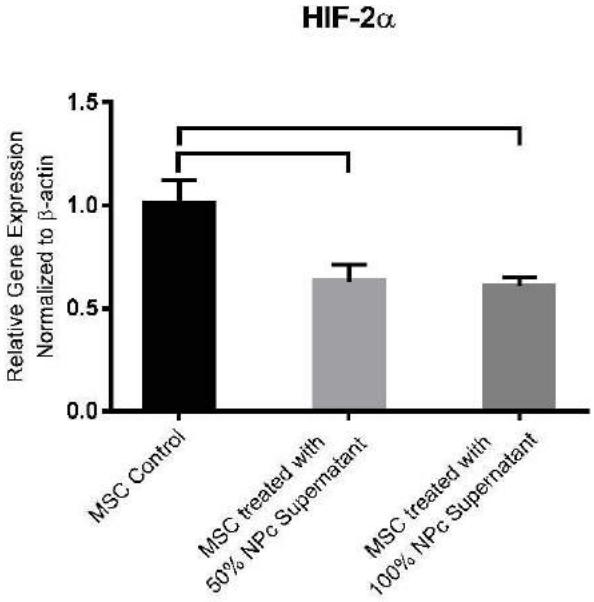
HIF-2α
Relative Gene Expression Normalized to β-actin
1.5
1.0
0.5
0.0
MSC Control
MSC treated with 50% NPc Supernatant
MSC treated with 100% NPc Supernatant

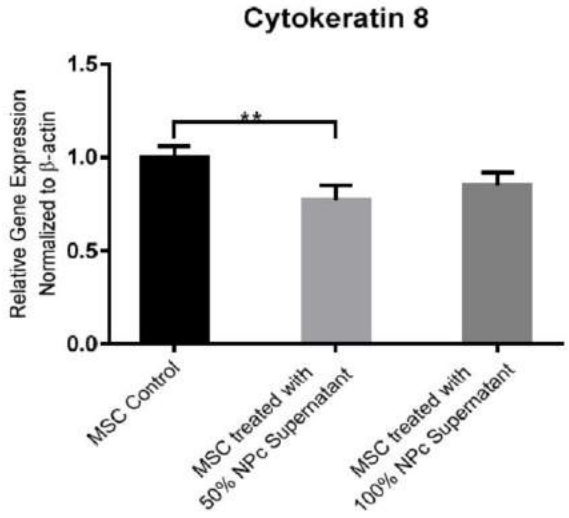
Cytokeratin 8
Relative Gene Expression Normalized to β-actin
1.5
1.0
0.5
0.0
**
MSC Control
MSC treated with 50% NPc Supernatant
MSC treated with 100% NPc Supernatant

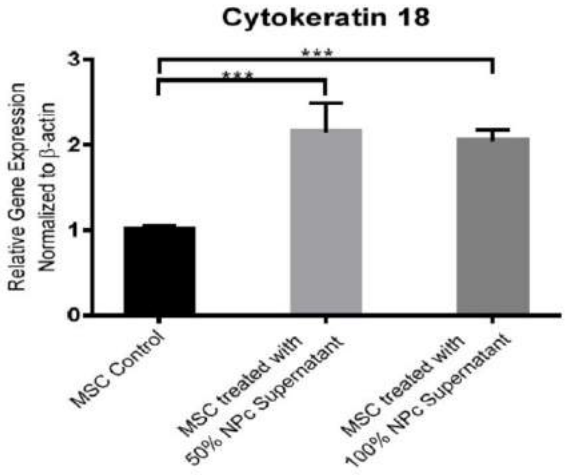
Cytokeratin 18
Relative Gene Expression Normalized to β-actin
3
2
1
0
***
***
MSC Control
MSC treated with 50% NPc Supernatant
MSC treated with 100% NPc Supernatant

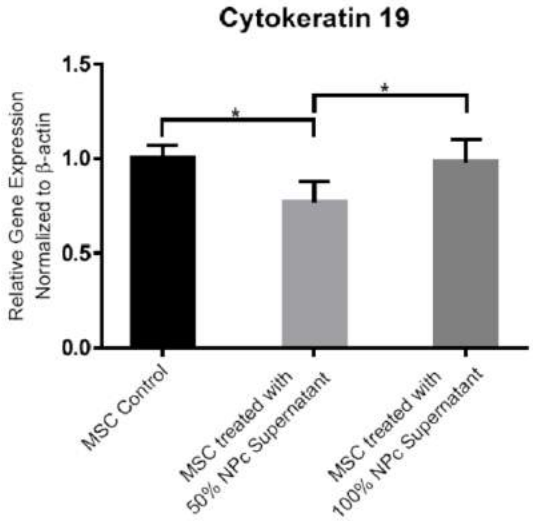
Cytokeratin 19
Relative Gene Expression Normalized to β-actin
1.5
1.0
0.5
0.0
*
*
MSC Control
MSC treated with 50% NPc Supernatant
MSC treated with 100% NPc Supernatant

Fig. 1: Markers recommended for use in defining the young healthy phenotype. Relative gene expression by qPCR in mesenchymal stem cells after co-culture with NP cells supernatant (50% and 100% concentration) for 7 days. Gene expression for each samples were normalized with housekeeping gene β-actin.
*p<0.05, **p<0.01, ***p<0.001 MSC: Mesenchymal stem cell, NPc: Nucleus pulposus cell

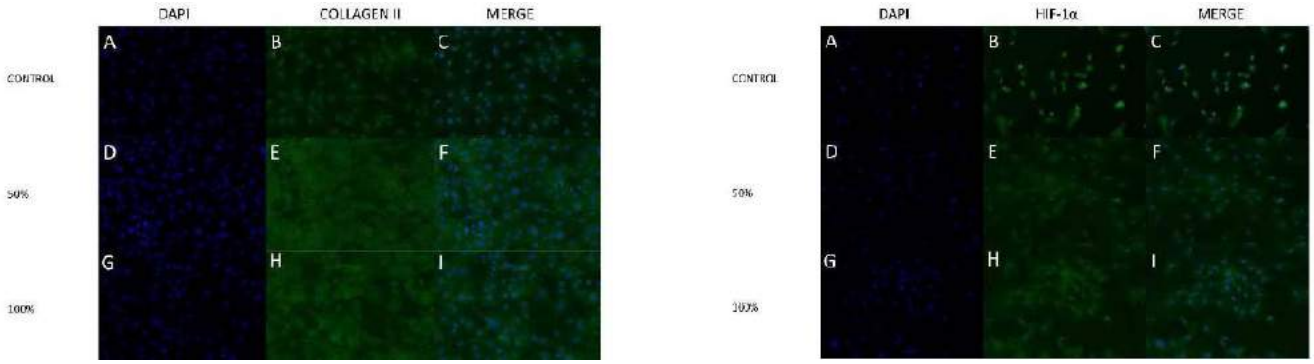

Fig.2: Immunofluorescence analysis showing the expression of the respective antibodies in mesenchymal stem cells after coculture with NP cells supernatant (50% and 100% concentration) for 7 days.

Cell-Free Biomimetic Scaffolds Lead to Non-Unions in Critical Sized Defect Repair as Compared to Identically Structured Stem Cell Infiltrated Scaffolds that Induce Rapid Bone Growth

John A. Szivek, PhD, David A. Gonzales, BS, Robert D. Kay, BS, David S. Margolis, MD/PhD, Jordan L. Smith, MD
Orthopedic Research Laboratory, College of Medicine, The University of Arizona, Tucson, Arizona

Introduction: Rapid bone formation that bridges critical sized bone defects is essential to completely regenerating large bone defects. Biomimetic scaffolds (Figure 1) induced more rapid bone formation compared to scaffolds with similar sized pores with geometric patterns after 6 months in our large animal model (1, 2, 3). Cell-infiltrated scaffolds induced rapid and complete critical sized defect bridging in a sheep model after 3 months (4, 5). In this study, the same sheep model was used to investigate bone bridging and growth in control animals with either the scaffold and no cells, or no scaffold and no cells. This was done to determine the relative contribution of scaffolds alone or scaffolds with cells to achieving complete bone bridging. As such, the goal of this study was to determine whether cell-free scaffolds or defects without scaffolds, induce sufficiently rapid bone formation to fill a critical sized defect within 6 months.

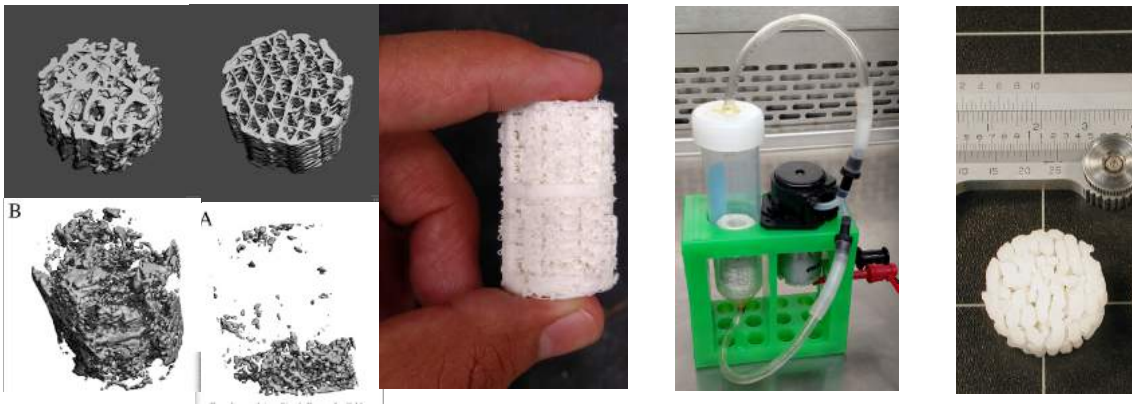

Figure 1: (Left most) B. A biomimetic porous scaffold design and below it a µCT scan of bone ingrowth into the biomimetic pattern at 6 months in a dog. A. 3D printed pattern of a simple geometric porous scaffold design and below it a µCT scan of bone ingrowth into the geometric patterned scaffold at 6 months in a dog. (Second from Left) This picture shows a critical sized defect length 3D printed scaffold. (Second from Right) Cell and tricalcium phosphate infiltration bioreactor. (Right most) Inverse biomimetic polybutylene terephthalate scaffolds printed using free form fabrication utilizing µCT data sets collected from trabecular bone and modified to the size of the femoral mid-diaphysis of a sheep. Scaffold is identical to the inverse trabecular pattern of the sheep bone, to induce ingrowth that has the form of a trabecular pattern (6).

Methods: First, a 3D printed biomimetic scaffold was placed without cells, and held in place using our standard approach in which a rod with locking screws stabilize the scaffold. Next, only a locked rod was used to stabilize a sheep critical sized defect in which no scaffold was placed.

As in our previous studies, cylinders of trabecular bone from the femoral head and critical defect sized cortical bone samples collected from adult male sheep were imaged in a SCANCO µCT 20 at a 12µm resolution. STL files created from the images were exported to build polybutylene terephthalate (PBT) scaffolds using a Stratasys 1650 FDM (3, 6). Structural accuracy of the scaffolds was verified by scanning the scaffolds in the µCT and comparing scans to the scans of the bones.

Rosette strain gauges on scaffolds were used to assess stiffness while scaffolds were compressed to 294 N at up to 294 N/s in an MTS. Data was collected with LabView and exported to Excel. Stress vs. principal strain curves were used to assess strength and stiffness.

Male sheep underwent one IACUC approved procedure. In both sheep, a 42-mm femoral segment was removed. In one sheep, a modified lockable IM rod was used in combination with the scaffold (Figure 2). In the second sheep, no scaffold was placed and only the lockable IM rod was placed. Sheep were held for 26 weeks. Activity was monitored with 24 hr. video. Monthly radiography, post sacrifice µCT scanning and histomorphometry were used to determine the extent of tissue ingrowth and rate of bone formation. ANOVA's were used to determine difference between these animals and previously reported test animals with cell-infiltrated scaffolds placed using the same procedures.

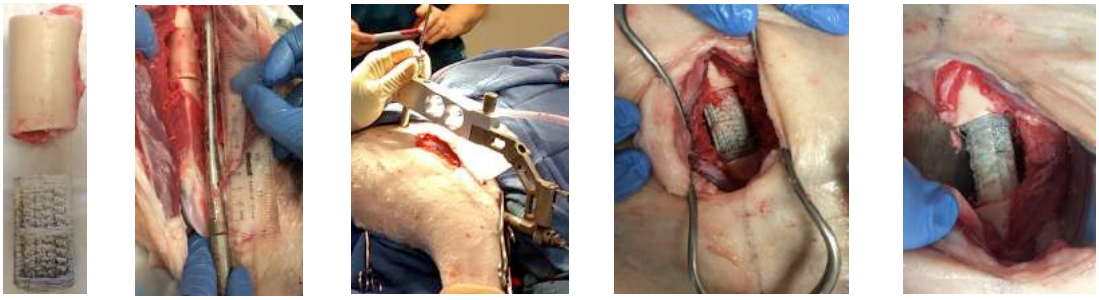

Figure 2: (Left most) Picture of scaffold and bone segment it replaced below it. (Second from left) This picture shows the surgical exposure with the cut segment and intramedullary rod in the image. The rod provided temporary stability while healing occurred. (Middle image) Picture of surgical instrumentation used to lock rod following segment placement. (Second from right image) Scaffold in place prior to removing retraction. (Right most) Scaffold in place prior to closure.

Results: Scaffolds were 71.6 ± 0.2% porous. Mechanical testing of scaffolds indicated a linear elastic response with a stiffness of 2.8 GPa and a compressive strength of 9.44 ± 0.94 MPa, which was sufficient to support physiological loading.

Surgery was uneventful and sheep were load bearing within hours. Activity monitoring indicated the sheep spent approximately one quarter of their time standing or walking and the remainder resting. After 14 weeks, radiographs showed very little bone formation in the defect sites (Figure 3). Post sacrifice radiographs showed non-unions in the surgically treated limbs of both control sheep.

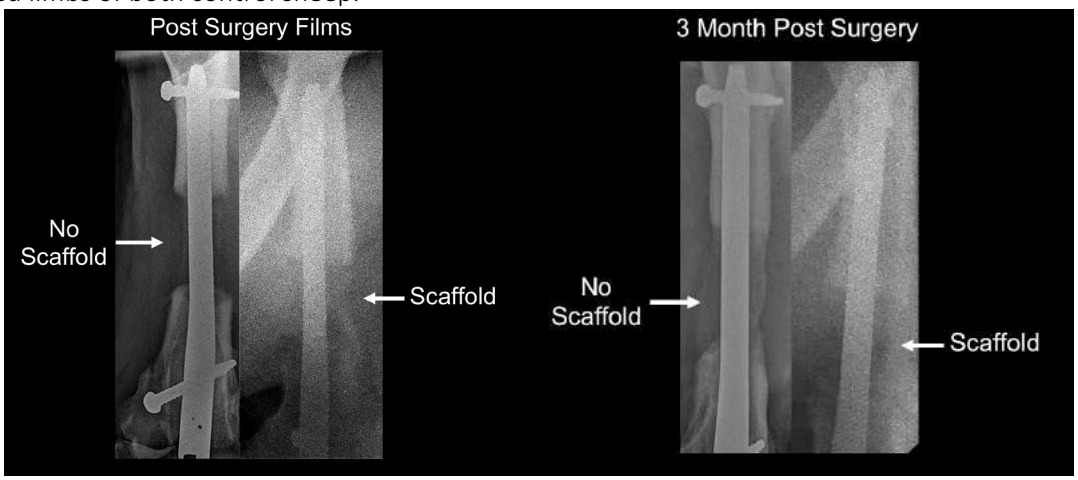

Figure 3: (left) Post-operative films showing location of long segment defect. (right) Three-month post-operative films showing virtually no bone formation at this time point.

MicroCT scans after 3 or 6 months in vivo collected in earlier studies (5) using scaffolds and stem cells demonstrated complete bone bridging of the long segment defect along the surfaces of the scaffolds (Left image Figure 4). In the current study, microCT scans of control animals (the animal with a scaffold but no cells and the animal with no scaffold and no cells) showed non-unions at the center of the defect site (Figure 4). There was some tissue formation proximal to and distal to the non-union sites in both the control animals. Preliminary results of histology indicate that most tissue in these animals was soft tissue, particularly in the control with no scaffold and no cells.

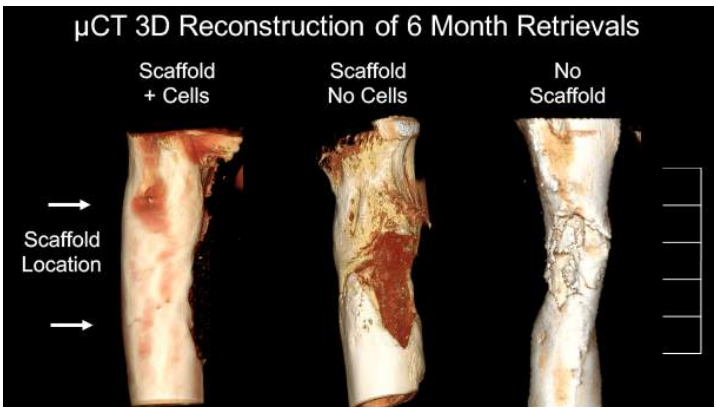

Figure 4: Micro CT's of 6-month explanted femora showing: (left) extensive bone formation along the length of a cell-infiltrated scaffold (4), (middle) a non-union and incomplete tissue coverage in the middle of the scaffold, (right) a non-union and some fragmented calcified tissue along the length of the scaffold with a region devoid of tissue in the middle.

Area measurements collected from each experimental and intact femur within the same animal expressed as a percentage of experimental cross sectional area divided by intact cross sectional area showed that more bone was present in the experimental femora in the area of the original defect when scaffolds were used with and without cells (Table 1). Cell-free scaffolds demonstrated some bone formation after 6-months, however they did not induce as much remodeling as the cell-containing scaffolds. As a result, more bone was present in the control bones in comparison to the contra-lateral intact femora in the animals with cell-free scaffolds. Substantially less bone was present in the area of the original defect in the experimental limb relative to the intact limb of the animal that received no scaffold with no TCP and no cells (Table 1). In fact, bone formation was clearly absent in the mid region of the femur in this animal and was instead filled with soft tissue.

Table 1: Percent Bone Area in Eperimental/Intact Limb

20 slices sampled from each site

Implant Configuration test duration	Location	% Bone ± STD Experimental/Intact
Scaffold + TCP + cells	Proximal	24 ± 0.7%
3 month	Middle	23 ± 1.8%
	Distal	45 ± 4.9%
Scaffold + TCP + cells	Proximal	8 ± 0.3%
6 month	Middle	10 ± 0.3%
	Distal	23 ± 2.1%
Scaffold + no TCP + no cells	Proximal	31 ± 1.2%
6 month	Middle	15 ± 0.6%
	Distal	48 ± 5.3%
No scaffold + no TCP + no cells	Proximal	-33 ± 5.9%
6 month	Middle	-48 ± 2.9%
	Distal	-46 ± 7.4%

Discussion and Conclusions: A long segment regeneration biomimetic scaffold infiltrated with endogenous adult sheep stem cells facilitated rapid bone growth throughout the length of a critical sized defect in a sheep femur despite the fact that sheep were relatively inactive (4, 5). Preliminary results indicate that this design induces sufficient bone growth to be able to support physiological loads as early as 4 weeks. After 3 months, the entire length of the scaffold was covered with bone on the anterior and medial surfaces. After 6 months, better bone infiltration into the scaffold was noted and bone remodeling was apparent. Little bone formation was noted on the posterior lateral surface in the region coinciding with the location of the linea aspera. Although more extensive amounts of bone were noted in the femur with a scaffold but no cells at the 6-month time point, the scaffolds with cells had demonstrated earlier bone formation and evidence of remodeling by the 6-month time point to reshape the femoral cortical bone to its original cross section in the defect site.

In the next stage of this study, scaffolds instrumented with sensors (strain gauges) will be used to measure loading of the femur during healing using published procedures (3, 8).

References:

1. Novel Biomimetic Polymer Scaffold Design enhances Bone Ingrowth, CP Geffre, JA Szivek, JT Ruth, DW DeYoung, B Tellis, DS Margolis, Online Dec 2, DOI: 10.1002/jbm.a.32251 JBMR-A, 2008.
2. Comparison of Bone Ingrowth into Scaffolds with Simple and Novel Biomimetic Porous Architectures, CP Geffre, JA Szivek, DS Margolis, J Invest Med, 56 (1) 242 Suppl., Jan 2008
3. In Vivo Telemetric Determination of Shear and Axial Loads on a Regenerative Cartilage Scaffold following Ligament Disruption, Szivek JA, et al. J Biomed Mater Res–B, DOI: 10.1002/jbm.b.33120, 2014.
4. A Biomimetic Inverse Trabecular-Pattered Scaffold to Accelerate Bone Ingrowth for Long Segment Repair, John A. Szivek, David A. Gonzales, Michael A Martinez, Andrew J. Sikorsky, Jordan L. Smith, Orthopaedic Research Society - Sun Valley Workshop, Sun Valley ID, August 2015
5. Stem Cell Infiltrated Trabecular-Pattered Scaffolds Induce Extensive Bone Growth during Critical Sized Defect Repair, Andrew M Wotanowski, David A Gonzales, Jordan L. Smith, John A Szivek, Orthopaedic Research Society - Sun Valley Workshop, Sun Valley ID, August 2016
6. Trabecular Scaffolds Created Using Micro CT Guided Fused Deposition Modeling, BC Tellis, JA Szivek, CL Bliss, DS Margolis, RK Vaidyanathan, P Calvert, J Mat Science & Engineering-C, Vol. 28/1 pp. 171-178, 2008.
7. TGF-ß1-enhanced TCP-coated Sensate Scaffolds can detect bone bonding, JA Szivek, D Margolis, BK Garrison, E Nelson, RK Vaidyanathan, DW DeYoung, J Biomed Mate Res-B, Vol.: 73B-1, 43-53, 2005.
8. An Instrumented Scaffold can Monitor Loading in the Knee Joint, JA Szivek, et al., J Biomed Mater Res - B, 79B, 218-228, 2006

Acknowledgements: Preliminary research was supported in part by NSF grant # CMMI 0855493 and through an NSF sponsored student support program (W.A.E.S.O.).

Changes in Intervertebral Disc Structure and Morphology in Back-healthy Humans During Standing

Christian I. Weber[1], Ching-Ting Hwang[2], Linda R. Van Dillen[2,3,4], Simon Y. Tang[1,4]
[1]Biomedical Engineering; [2]Movement Science; [3]Physical Therapy; [4]Orthopaedic Surgery
Washington University in St. Louis, St. Louis, MO

DISCLOSURES: None

INTRODUCTION: Low back pain (LBP) is a function-limiting condition that affects up to 80% of the population at least once in their lifetime. The estimated healthcare costs exceed $100 billion a year [1]. The intervertebral disc (IVD) is a suspected pain generator due to its load-bearing nature and susceptibility to degeneration [2]. Currently, Magnetic Resonance Imaging (MRI) is the most commonly utilized clinical technique to visualize and assess the IVD [3]. The Open Upright® MRI systems allow an individual to stand during imaging thus allowing the examination of the spine in a loaded state. The objective of this study was to examine the changes in the spine between supine and standing by measuring changes in the intervertebral (IV) angles.

METHODS: Twelve back-healthy people were recruited (age 18-35, 3 female, BMI <30). Images of the lumbar spine (L1-S1) were obtained in supine (unloaded) and standing (loaded) using a 0.6 T Open Upright® MRI system. A 3-plane localizer was used to acquire sagittal T2 weighted images (repetition time = 610 ms, echo time = 17 ms, field of view = 24 cm, acquisition matrix = 210 x 210, slice thickness = 3 mm, gap = 0 mm, scan duration = 2 min) [4]. Initially, the participant stepped into the scanner and a pillow was placed behind the head. The MRI table then was moved to a horizontal position. The participant remained in supine and scans were acquired after 10 minutes. The MRI table then was moved back into vertical (standing) and the pillow was removed. The participant then was imaged in standing. From the acquired images in both positions, the IV angles were measured for the L1/L2 through L5/S1 vertebral levels. The IV angle was calculated as the angle created by a vector formed between the anterior and posterior edge of the inferior endplate and a vector formed between the anterior and posterior edge of the superior endplate at a given vertebral level that intersects at the posterior midpoint of the disc. For each participant, the change in IV angle from supine to standing was calculated for each vertebral level (L1-S1). The mean and standard deviation of percent change in lumbar IV angle across levels then was calculated. For each participant, the percent change in IV angle for each vertebral level also was calculated and plotted. This study was conducted with the approval from the Human Research Protection Office at Washington University School of Medicine.

RESULTS: Figure 1 provides data for 12 back-healthy (denoted as S1…S12) participants. Individual participant data are displayed. The change in IV angle from supine to standing is expressed as a percentage, with positive values indicating an increase in IV angle (increased posterior loading), and negative values indicating a decrease in IV angle (decreased posterior loading). For each participant, the mean and standard deviation for the percent change of all of the lumbar IV angles, as well as the percent change for each individual vertebral level (L1/L2-L5/S1) are presented. The plots show the variability in the percent change in IV angles within and across participants. Within a participant some IV angles display much larger changes relative to the other levels. Across participants some (S1 - S5) display low variability in the percent change in IV angle across levels, while others (S6 -S12) display high variability in percent change in IV angle across levels.

DISCUSSION: Compared to supine, standing imposes increased loads on the spine, and these loads are transmitted through the IVD. As a result of the change in loading, the IVDs adapt and distribute these loads through changes in their morphology. We use the IV angle here to quantify the morphological changes of the IVDs at each vertebral level. Positive increases in the IV angle indicate increased loading on the posterior elements of the vertebral unit. Thus, the distribution of each participant's percent change in IV angles provides insight as to how loads are shared and distributed across the participant's lumbar spine between supine and standing. A small standard deviation of the percent change in the IV angles suggests that each of the lumbar IVDs under go similar changes, while a large standard deviation suggests an uneven distribution in the loading on individual IVDs. The variability in IV angles both within and across participants may be particularly revealing for back-healthy participants. Those IVDs with large percent changes in IV angle that lie outside of the participant's standard deviation may be susceptible to fatigue damage given the large changes in loading. Since there is data to suggest that back-healthy individuals can develop low back symptoms in prolonged standing [5], these 'at-risk' IVDs that are sustaining elevated posterior loading could be potential pain generators in these individuals. Further analyses are required to examine whether these IV angle changes are associated with the stresses and strains within the IVDs.

SIGNIFICANCE: This work illustrates the potential importance of studying the differences exhibited in IVDs within an individual between supine and standing. The assessment of the IVD when loaded may provide important insights into the mechanisms for the development and treatment of low back pain.

REFERENCES:[1] Balagué F et al 2012 [2] Risbud MV et al 2014 [3] Jarvik JG et al 2002 [4] Rodriquez-Soto AE et al 2013 [5] Sorensen CJ et al 2015.

ACKNOWLEDGEMENTS: This work was supported by the Washington University Musculoskeletal Research Center (NIH P30 AR057235) NIH 5T32EB018266, and NIH K01AR069116.

FIGURE 1: The percent change of the IV angle from supine to standing for each vertebral level and the mean IV angle percent change with standard deviation bars are plotted for each participant (S1-S12). A positive change represents a decrease in angle (increase in posterior loading), while a negative change represents an increase in angle (decrease in posterior loading). Using this approach, the distribution of loads across vertebral levels can be identified in individuals.

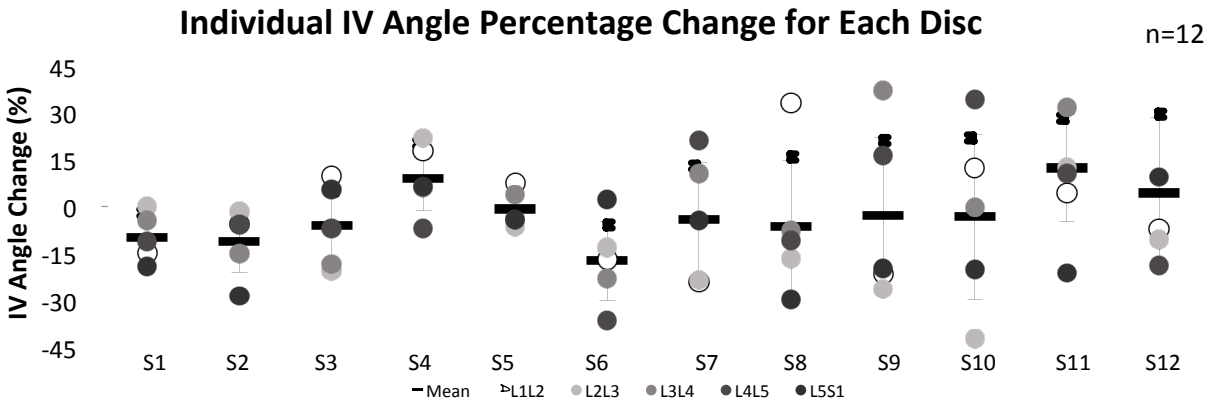

Scoliosis in Fibrous Dysplasia/McCune-Albright Syndrome

Sri Harsha Tella, MD1, Jason A Berglund BS1, Lauren Kim MD2, Lori C. Guthrie, RN-C, BSN1, Robert Stanton MD3, Michael T Collins MD1, Alison M Boyce MD1

1Section on Skeletal Disorders and Mineral Homeostasis, National Institute of Dental and Craniofacial Research, National Institutes of Health, Bethesda, MD. 2Radiology and Imaging Sciences, National Institutes of Health Clinical Center, National Institutes of Health, Bethesda, MD. 3Department of Orthopedics, Nemours Children's Health System, Orlando, FL

Objectives: Fibrous dysplasia (FD) is a rare disorder in which proliferation of undifferentiated stromal cells results in skeletal lesions prone to fracture, deformity, and pain. Lesions may affect one bone or many, and may occur in isolation or in association with endocrinopathies, termed McCune-Albright syndrome (MAS). Scoliosis is a potentially serious, even lethal complication; however, the spectrum and optimal management have not been established. The purpose of this study was to characterize scoliosis in a large cohort of FD/MAS patients, and to identify features associated with progressive disease.

Methods: Clinical, biochemical, and radiographic data from 138 subjects in a natural history study were reviewed.

Results: Scoliosis was present in 84/138 subjects (61%), categorized as mild (Cobb angle $>10^{o}$-$\leq 30^{o}$) in 65% (n=55), moderate (>30-$\leq 45^{o}$) in 13% (n=11), and severe ($>45^{o}$) in 21% (n=18). There was no difference in age between severity groups. Severity of scoliosis was highly correlated with leg length discrepancy ($p=0.002$), impaired mobility ($p<0.0001$), skeletal burden score ($p<0.0001$), and bone turnover [osteocalcin ($p>0.0027$), NTX telopeptides ($p>0.008$)](Fig 1). MAS endocrinopathies associated with scoliosis included FGF-23 mediated hypophosphatemia ($p>0.0004$) and hyperthyroidism ($p>0.0001$).

Serial imaging was available for 69 subjects over 4.9 years (range 0.9–14.7)(Fig 2). Of these, 59 were managed non-operatively, and 10 had spinal fusion. The median change in Cobb angle for non-operative subjects was 1.5^{o} (IQR 0-12.8, range -20.6-66.9), with 18/59 progressing $\geq 10^{o}$. For subjects who underwent spinal fusion, the median change in Cobb angle was -1.9^{o} (IQR -10.0-4.7, range -13.1-10.5), with only 1 subject progressing $\geq 10^{o}$. Spinal fusion was associated with significantly decreased progression in Cobb angle ($p=0.02$).

One operative subject had instrumentation failure after 3 months. Two non-operative subjects (age 19 and 41) died from respiratory complications of progressive scoliosis. No fatalities occurred in operative subjects.

Conclusions: Scoliosis is common in FD and frequently progresses into adulthood. Leg length discrepancy and MAS endocrinopathies are risk factors for the development and progression of scoliosis. Long-term outcomes from spinal fusion are favorable in most patients. We report the first scoliosis-related fatalities in FD, demonstrating the critical importance of monitoring and treatment for spinal disease in this population.

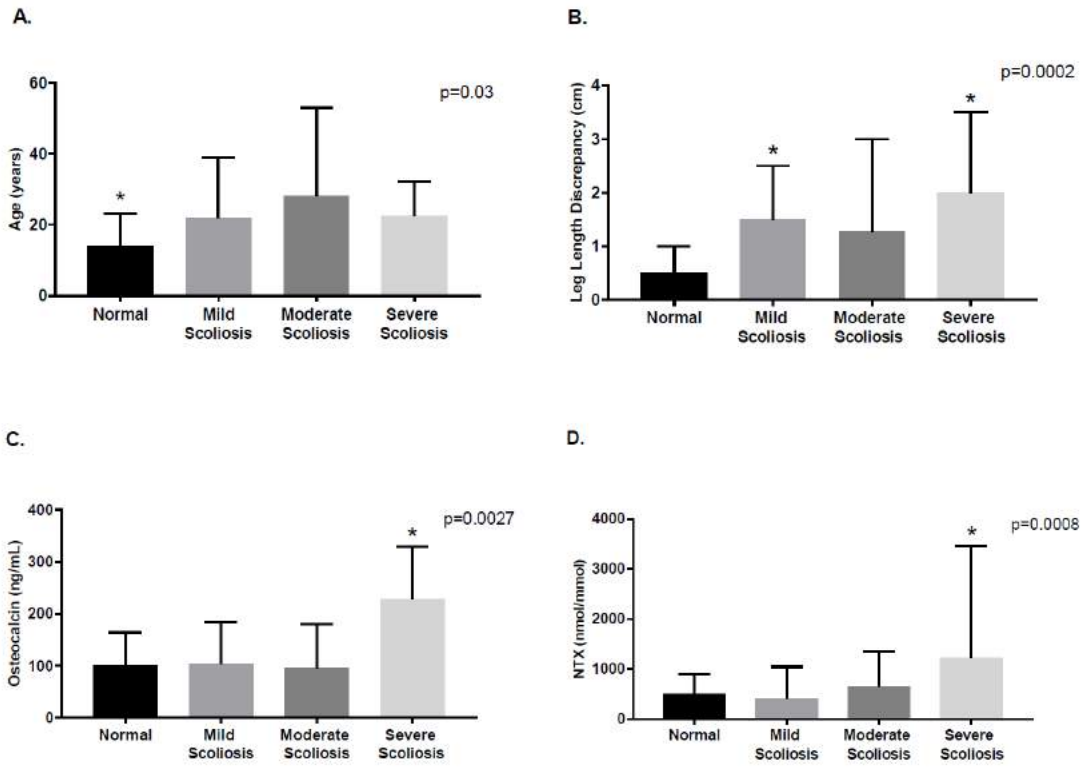

Figure 1. Clinical and biochemical features associated with scoliosis. Features were correlated with scoliosis severity, including normal subjects (n=54), those with mild (Cobb angle >10^{o} and ≤30^{o}, n=55), moderate (>30-≤45^{o}, n=11), and severe scoliosis (>45^{o}, n=18). Panels A-D indicate the association with age at most recent evaluation (A), amount of discrepancy between leg lengths (B), and markers of bone turnover (C and D).

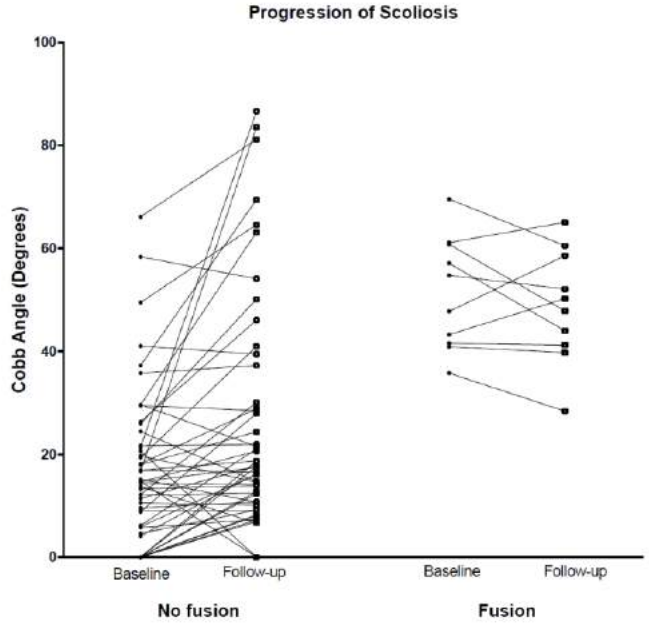

Figure 2. Progression of scoliosis with and without spinal fusion. Longitudinal analyses over a median of 4.3 years (non-fusion) and 9.6 years (fusion) demonstrated decreased progression of scoliosis in subjects who underwent spinal fusion.

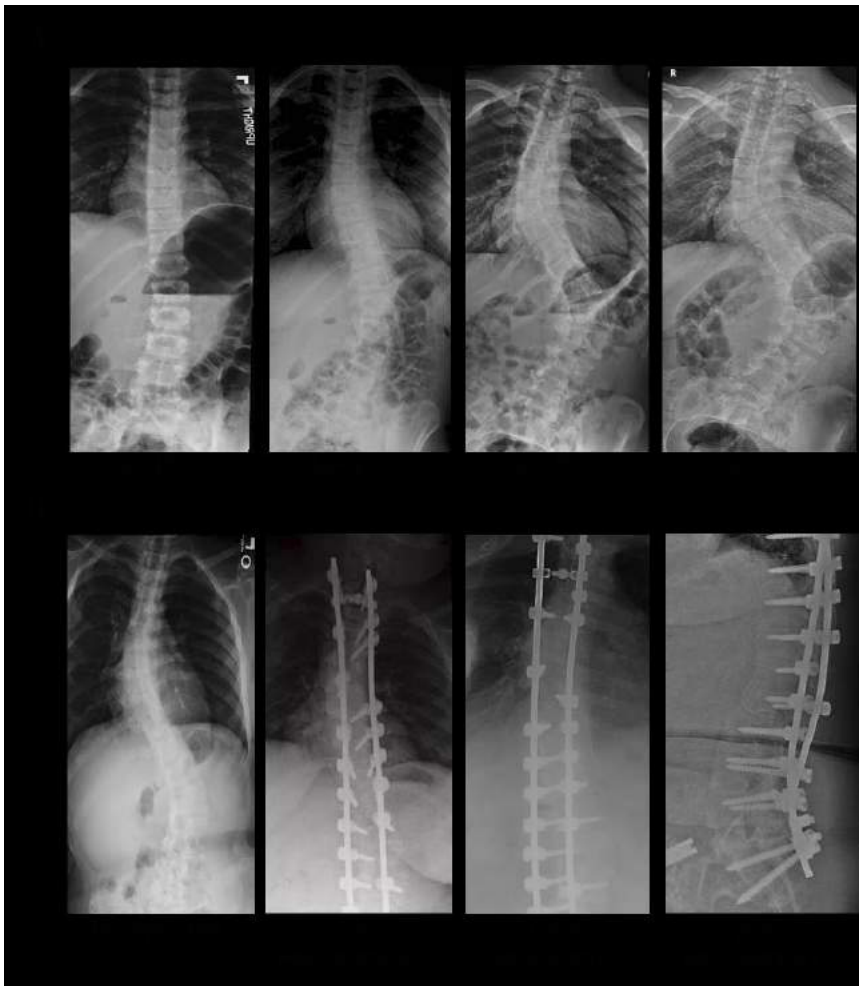

Figure 3. Radiographic images of scoliosis. Panel A shows progressive scoliosis over a 12-year period from a Cobb angle at baseline of 21.3^{o} (age 10, far left) to 86.7^{o} (age 22, far right).

The Biphasic Response to Phosphate During Chondrogenic Differentiation

Biming Wu[1], Emily K. Durisin[2], Rhima M. Coleman[1,3]

[1]Department of Biomedical Engineering, University of Michigan; Ann Arbor, MI 48109

[2]Department of Material Science and Engineering, University of Michigan; Ann Arbor, MI 48109

[3]Department of Mechanical Engineering, University of Michigan; Ann Arbor, MI 48109

Inorganic phosphate (Pi) has been recognized as an important signaling molecule that modulates chondrocyte maturation and cartilage mineralization. However, conclusive experimental evidence for its involvement in early chondrogenesis is still lacking. Here, using high-density monolayer (2D) and pellet (3D) ATDC5 chondrogenic models treated with ITS+, β-glycerophosphate (βGP), or ITS+/βGP, we evaluated the individual and synergistic effects of Pi on ITS+ induced chondrogenesis. Both 2D and 3D cultures exhibited a similar trend of chondrogenic gene expression (*Acan* & *Col2a1*) and matrix accumulation when they were treated with ITS+ or βGP individually. The response to combined ITS+/βGP treatment, however, was dissimilar in the two systems. In monolayer culture, cells differentiated with ITS+/βGP showed significantly higher mRNA levels of *Acan* and *Col2a1* (Fig 1a) as well as a 1.6-fold increase in accumulation of an sGAG-rich matrix (Fig 1b & 1d) compared the ITS+ alone group. Conversely, the addition of βGP to ITS+ treated pellet cultures suppressed expression of *Acan* and *Col2a1* genes and matrix accumulation and stimulated mineralization. Further measurement of the Pi concentration in the culture medium shows that the cell response to Pi does not correlate with the Pi concentration in the culture medium but is better predicted by the availability of Pi on a per cell basis (Pi abundance). Three levels of abundance were found: basal (Pi/DNA < 10 ng/μg), moderate (Pi/DNA=25.3 – 32.3 ng/μg), and high abundance (Pi/DNA > 60 ng/μg). Moderate Pi abundance enhanced early chondrogenesis and production of aggrecan and type II collagen whereas high Pi abundance inhibited chondrogenic differentiation and induced rapid mineralization. Together, our results suggest that it is important to evaluate the signaling effect of Pi on chondrogenesis by examining its availability on a per cell level.

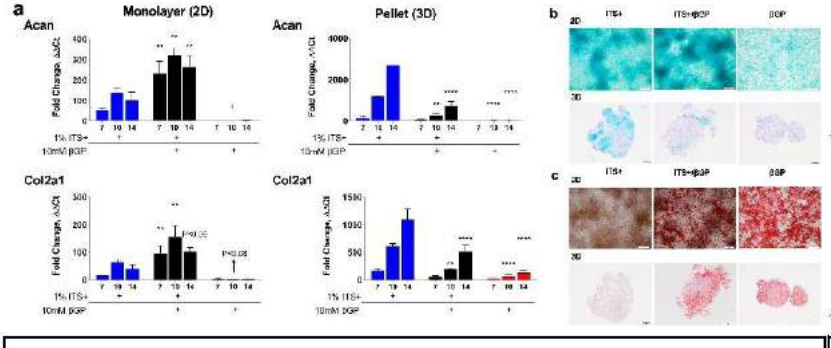

Fig 1. (a) Quantification of mRNA expression (relative to day 0 and the housekeeping genes Hprt and Ppia) of early chondrogenic markers (Acan and Col2a1) in monolayer (2D) and pellet (3D) cultures over 14 days of differentiation. Alcian blue (b) and Alizarin Red (c) staining of 2D and 3D cultures at day 14 to show accumulation of sGAG-rich matrix and calcium, respectively.

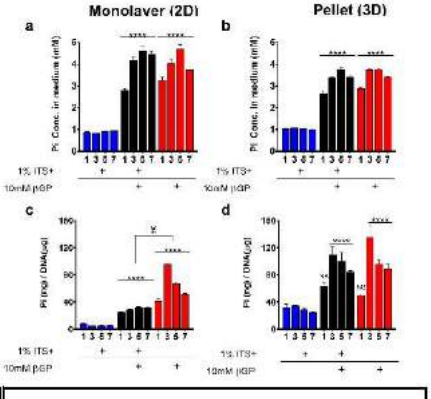

Fig 2. (a & b) Pi concentration (mM) present in the medium, and (c & d) Pi availability on a per cell basis during the first seven days of differentiation in 2D and 3D cultures treated with ITS+, ITS+/βGP, or βGP (n=3).

LaminA/C knock down enhances adipogenesis but does not eliminate mechanical response in MSCs.

Melis Olcum[3], Guniz Bas[1], Engin Ozcivici[3], Janet Rubin[2], Gunes Uzer[1]
[1]Boise State University, [2]University of North Carolina Chapel Hill, [3]Izmir Institute of Technology, Turkey

Mesenchymal stem cells (MSC) provide regenerative capacity to bone. Regulation of MSC fate depend on their ability to sense and respond to mechanical signals. Mechanical signals, when applied in the form of low intensity vibration (LIV) – a well-recognized exercise mimetic – increases MSC osteogenesis and decreases adipogenesis. Our team shown that LIV-induced MSC mechanotransduction that activates Focal Adhesion Kinase (FAK) and RhoA signaling relies on LINC (Linker of Nucleoskeleton and Cytoskeleton) complexes connecting the cytoskeleton to the nuclear lamina. Inside the nucleus, nuclear lamina element LaminA/C is a major constituent providing mechanical stiffness and intra-nuclear structuring to nucleus. LaminA/C provides a scaffold by which transcription factors can access to chromatin to regulate MSC differentiation program. While, deletion of LaminA/C in MSCs results in increased adipogenesis and decreased osteogenesis, it is not clear if LaminA/C deficiency compromises the MSC response to mechanical challenges to cause such a phenotype.

Here, we asked if loss of LaminA/C would decrease mechanically induced signaling in MSCs. We eliminated LaminA/C expression using an Lmna specific siRNA (siL). LaminA/C deletion resulted in decreased nuclear height (-50%, p<.05) suggesting a softer nuclei. Consistent with the reduced nuclear stiffness, LaminA/C deficient (siL) nuclei showed blebbing and reduced circularity (-11%, p<.001). Shown in **Fig.1a**, siL accelerated adipogenic differentiation when compared to control siRNA (siC) as measured by adipogenic differentiation marker Adiponectin (APN, 430%, p<.01). We next probed cell mechanoresponse to low intensity vibration (LIV, 20min, 0.7g acceleration, 90Hz) as well as high magnitude strain (HMS, 20min, 2% strain, 0.2Hz) via measuring FAK phosphorylation (pFAK, Tyr397). pFAK was increased in both siL+LIV (42%, p<.05) and siL+HMS (40%, p<.05) groups compared to non-mechanically-stimulated controls (**Fig1b-c**). Further, the magnitude of pFAK response in siL groups were not significantly different than siC groups, suggesting an intact mechanoresponse. Application of LIV further reduced the APN levels in siL+LIV groups when compared to siL controls (-32%, p<.05).

In sum, LaminA/C deletion increases MSC adipogenesis but does not compromise mechanotransduction. Partial reversal of siL-induced adipogenesis under application of LIV indicates that mechanical-regulation of MSC fate does not entirely depend on LaminA/C. This suggests that transcriptional or mechanical adaptations of other adaptor proteins such as LINC complexes may modulate chromatin organization and transcriptional activity in MSCs.

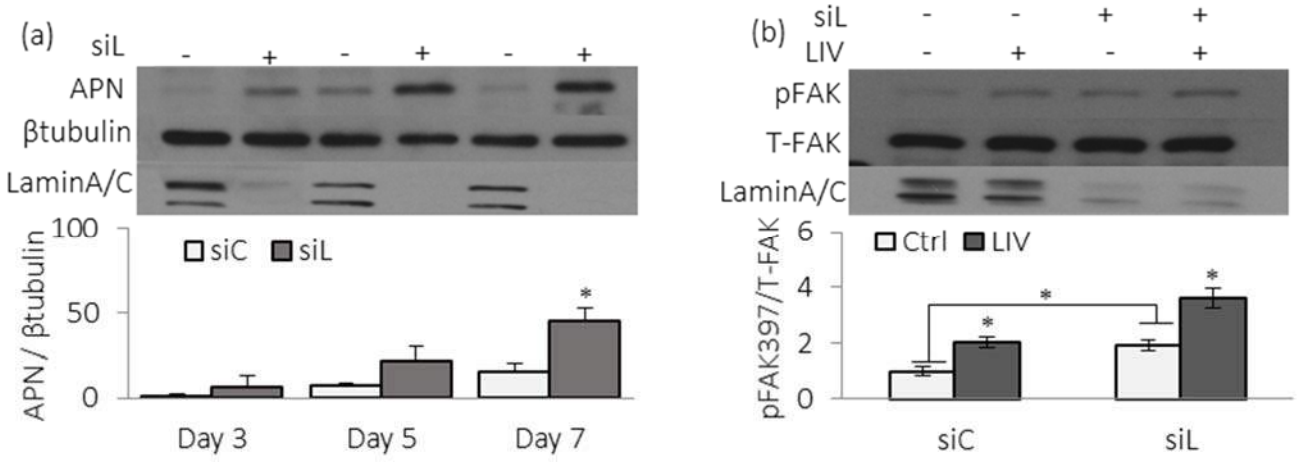

Fig.1. (a) Deletion of Lamin A/C via siRNA against Lmna (siL) suppressed LaminA/C levels during a 7-day experiment, resulting in increased adipogenesis (p<0.05). **(b)** siL treated MSCs are equally responsive to LIV in terms of FAK activation when compare to control siRNA (siC).

7:00 AM – 8:00 AM	Breakfast & Registration

8:00 AM – 9:00 AM	ASBMR/Harold M. Frost Young Investigator Award Presentations Chair: Teresita Bellido, PhD *(Indiana University)*
	Increased Ca2+ Signaling Through Altered CaV1.2 L-type Ca2+ Channel Activity Promotes Bone Formation and Prevents Estrogen Deficiency-induced Bone Loss Chike Cao, PhD *(Duke University Medical Center)*
	A Human Induced Pluripotent Stem Cell Model for Elucidating Cell Fate Defects in McCune-Albright Syndrome Kelly Wentworth, MD *(University of California San Francisco)*
	Identification of Osteoclast-Derived Factors And Target Pathways that Couple Bone Resorption to Bone Formation Megan Weivoda, PhD *(Mayo Clinic)*

9:15 AM - 12:00 PM	Problems in Endocrinology: Rare Bone Diseases - Fibrous Dysplasia Chair: Michael Collins, MD *(NIDCR, NIH)*
	Overview of Fibrous Dysplasia. A Complex Mosaic of Dease of Activated Gαs Michael Collins, MD *(NIDCR, NIH)*
	Clinical Perspectives of Fibrous Dysplasia/McCune-Albright Syndrome Alison Boyce, MD *(NIDCR, NIH)*
	Challenges and Approcahes for Fibrous Dysplasia Research Ed Hsiao, MD, PhD *(University of California San Francisco)*

1:30 PM - 4:00 PM	Career Development Workshop: Research Funding Chair: Marjolein van der Meulen, PhD *(Cornell University)* *Sponsored by* SCANCO MEDICAL

7:30 PM - 9:30 PM	New Progress in Imaging Musculoskeletal Tissues Chair: Felix Wehrli, PHD *(University of Pennsylvania)*
	Quantitative MRI of Cortical and Trabecular Bone Felix Wehrli, PhD *(University of Pennsylvania)*
	Using MRI to Detect Cartilage Damage Corey Neu, PhD *(University of Colorado)*
	In Vivo MRI Hollis Potter, MD *(Hospital for Special Surgery)*

Increased Ca^{2+} signaling through altered CaV1.2 L-type Ca^{2+} channel activity promotes bone formation and prevents estrogen deficiency-induced bone loss

Chike Cao[1], Yinshi Ren[2], Anthony J. Mirando[2], Adam Barnett[1], Douglas Rouse[3], Se Hwan Mun[4], Kyung-Hyun Park-Min[4], Amy L. McNulty[2], Farshid Guilak[5], Courtney M. Karner[2], Matthew J. Hilton[2], Geoffrey S. Pitt[1,6]

[1]Ion channelResearch Unit and [2]Department of OrthopaedicSurgery and [3]Department of Lab Animal Resources & Rodent Surgical and Genetic Services, Duke University Medical Center, Durham, NC 27710; [4]Arthritis and Tissue Degeneration Program, Hospital for Special Surgery, New York, NY 10021; [5]Department of Orthopaedic Surgery, Washington University Medical Center, St. Louis MO 63110; [6]Cardiovascular Research Institute, Weill Cornell Medicine, New York, NY 10021

A G406R gain-of-function mutation in the CACNA1*C* gene, encoding the cardiac CaV1.2 L-type calcium channel, causes the multi-organ disorder Timothy syndrome (TS), characterized by cardiac arrhythmias and developmental abnormalities. G406R reduces channel inactivation and increases Ca^{2+} flux into the cell. Here, we exploit the mutant channel in bone formation and bone remodeling.

Using a CaV1.2 *lacZ* reporter mouse we observed that CaV1.2 was highly expressed in the perichondrium/periosteum during skeletogenesis and in proliferating chondrocytes and BMSCs postnatally, suggesting important roles for endogenous CaV1.2 channels during skeletal development and homeostasis. Expression of the TS-mutant CaV1.2 channel (*Rosa26*-$CaV1.2^{TS}$) driven by *Prx1-Cre*, *Col2a1-Cre* or *2.3Col1a1-Cre* dramatically enhances bone mass, whereas expression of the wild type channel (*Rosa26*-$CaV1.2^{WT}$) has no effect. This indicates that abnormal channel behavior—and not just overexpression—is necessary to increase bone mass. Using dynamic histomorphometry and TRAP staining, we observed an increase in osteoblast activity and fewer osteoclasts from $CaV1.2^{TS}$ mutant long bones. Furthermore, in primary bone marrow stromal cell (BMSC) cultures, qPCR analyses revealed that $CaV1.2^{TS}$ enhances *Runx2*, *Sp7*, *Alpl*, *Ibsp* and *Bglap* gene expression. Von Kossa staining confirmed the enhanced osteogenic differentiation and mineralization of $CaV1.2^{TS}$-expressing BMSCs. In contrast, inhibition of CaV1.2 activity by nifedipine (10 μM) or diltiazem (10 μM) decreased BMSCs mineralization. Gene expression analyses also demonstrated that $CaV1.2^{TS}$ decreased the *Rankl/Opg* ratio, whereas the CaV1.2 blockers nifedipine or diltiazem increased the *Rankl/Opg* ratio. These data indicate that Ca^{2+} signaling through the CaV1.2 channel interfered with osteoblast-mediated osteoclastogenenesis via the OPG/RANKL pathway. Moreover, postnatal induction of $CaV1.2^{TS}$ in *Sp7*-lineage cells markedly increased bone formation and *Sp7*-$CaV1.2^{TS}$ mice were protected from bone loss induced by ovariectomy (OVX). Dynamic histomorphometry and TRAP staining revealed enhanced bone formation and reduced bone resorption in *Sp7*-$CaV1.2^{TS}$ OVX mice compared to WT OVX mice. Taken together, these studies demonstrate that increased Ca^{2+} signaling through $CaV1.2^{TS}$ promotes osteoblast differentiation and inhibits osteoclast formation. Our results suggest that enhancing CaV1.2 signaling may be a novel and effective therapeutic strategy for treating osteoporosis.

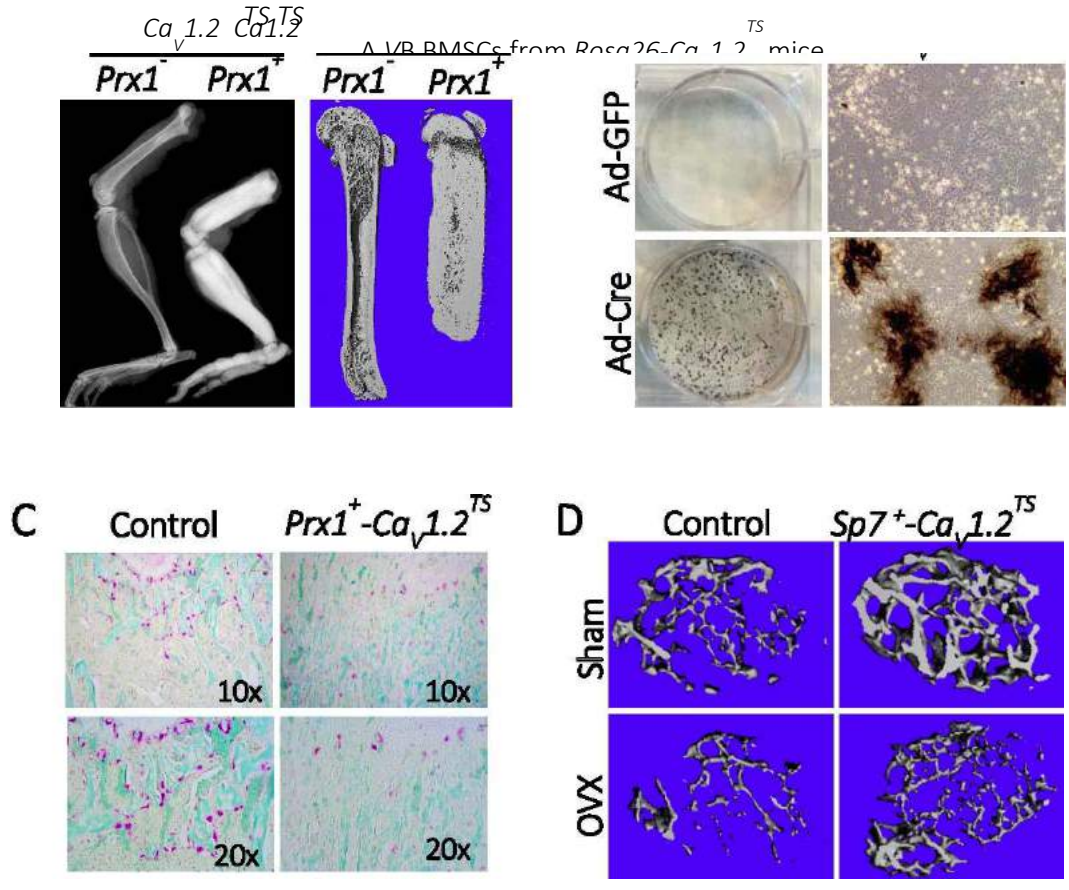

Figure 1. X-ray image of hindlimbs and μCT reconstruction image of femurs of 6-week-old control littermate (Prx1^{-}-CaV1.2^{TS}) and mutant (Prx1^{+}-CaV1.2^{TS}) littermate mice show CaV1.2^{TS} channel promotes bone formation in vivo (A); Von Kossa staining of normal (Ad-GFP) versus CaV1.2^{TS} – expressing (Ad-Cre) BMSCs after 10 days of differentiation shows CaV1.2^{TS} channel enhances osteoblast differentiation (B). Representative images of TRAP staining in femur sections from 6week-old control (*Prx1*$^{-}$*-CaV1.2*^{TS}) and *CaV1.2*^{TS} *(Prx1*$^{+}$*-CaV1.2*^{TS}) littermate mice show CaV1.2^{TS} channel decreases osteoclast differentiation (C). μCT reconstruction images of metaphyses of distal femurs show postnatal induction of CaV1.2^{TS} in *Sp7*-lineage cells increases bone formation and prevents bone loss induced by ovariectomy (OVX).

A Human Induced Pluripotent Stem Cell Model for Elucidating Cell Fate Defects in McCune-Albright Syndrome

Kelly L. Wentworth[1], Edward C. Hsiao[1]

[1] University of California, San Francisco- Department of Endocrinology and Metabolism, Institute for Human Genetics

G-protein coupled receptor (GPCR) signaling pathways mediate a wide spectrum of biological activities in humans. McCune-Albright Syndrome (MAS) is a rare, mosaic disease caused by a somatic activating mutation in the GNAS gene (c.602G>A, p.R201H). The GNAS locus encodes the stimulatory alpha subunit of the guanine nucleotide binding protein ($G_s\alpha$) and regulates cAMP production. MAS is characterized by polyostotic fibrous dysplasia, café-au-lait skin lesions, and precocious puberty, in addition to other endocrinopathies and solid organ malignancies. The R201H mutation is thought to occur post-zygotically as germline mutations are thought to be embryonically lethal. However, the precise mechanism leading to lethality is not understood.

Evidence suggests that G_s-signaling may help maintain stem cell pluripotency and differentiation capacity. We hypothesize that constitutive G_s-signaling regulates cell fate in early development and may inhibit the formation of a critical cell lineage. Since there are no currently available models containing the GNAS R201H mutation in the endogenous locus, we are addressing this hypothesis using a two-pronged approach with human induced pluripotent stem cells (iPSCs). First, we treated 3 control human iPSC lines (1323, WTC11, and BJ2) with increasing concentrations of forskolin (0mM, 0.01mM, 0.05mM, 0.1mM), a potent activator of cAMP production. We assessed if the iPSCs maintained their pluripotency by measuring expression levels of pluripotency markers (Oct4 and Nanog) at 24 hours using quantitative PCR. Control iPSCs treated with forskolin at all concentrations retained expression of these markers at 24 hours compared to untreated iPSCs, suggesting that human iPSCs can survive in the presence of elevated cAMP levels. Second, we are creating an engineered human iPSC model of MAS using CRISPR/Cas9 technology to insert the R201H mutation into the endogenous GNAS locus. We designed single-stranded guide RNAs co-expressed with the Cas9n protein that target exon 8 of the endogenous human GNAS locus. We were able to identify targeted iPSCs using a sib-selection protocol without the use of reporters or selection markers. These modified iPSCs will be a valuable tool for understanding if cAMP elevation alone or other genetic factors related to GNAS expression contribute to embryonic lethality or changes cell fate.

Identification of osteoclast-derived factors and target pathways that couple bone resorption to bone formation

Megan M. Weivoda, PhD1, Ming Ruan, MS1, Christine M. Hachfeld1, Glenda Evans1, Stephanie Youssef1, Rachel Davey, PhD2, Jeffrey D. Zajac, PhD, MBBS2, Brendan Lee, MD, PhD3, Jennifer J. Westendorf, PhD4, Sundeep Khosla, MD1, Merry Jo Oursler, PhD1

1Division of Endocrinology, Mayo Clinic, Rochester, MN, USA; 2Austin Health, University of Melbourne, Melbourne, Australia; 3Baylor College of Medicine, Houston, TX, USA; 4Orthopedic Surgery, Mayo Clinic, Rochester, MN, USA

Matrix-embedded TGFβ is released and activated by osteoclasts and contributes to the coupling of bone resorption to bone formation. These processes are uncoupled in mice with impaired osteoclast TGFβ signaling (Tgfbr2OclKO) suggesting that TGFβ promotes coupling in part through the induction of osteoclast derived "coupling factors". To identify TGFβ-induced coupling factors we performed RNA-Seq of mature osteoclasts treated with vehicle or 1ng/mL TGFβ; we then evaluated candidate coupling factor target gene expression in freshly isolated bone marrow mesenchymal progenitors (MPs) from WT or Tgfbr2OclKO mice. RNA-Seq revealed that *Wnt1* and *Wnt7b* were the most highly upregulated secreted factors in response to TGFβ (51 and 125 fold, respectively). Other significantly upregulated factors included *Wnt10b*, *Osm*, *Ephb2, Notch4*, *Ngf*, *Il10*, and *Bmp1*. Evaluation of Tgfbr2OclKO MP gene expression showed a significant increase in osteoblast genes *Bsp, Col1a1, Col1a2, Osx*, and *Ocn*. Together with published data showing decreased osteoblast number in Tgfbr2OclKO mice, this suggests that impaired osteoclast TGFβ signaling prevents osteoblast differentiation, leading to increased bone marrow osteoblast progenitors. Consistent with TGFβ inducing osteoclast Wnt expression, Tgfbr2OclKO MPs exhibited reduced canonical Wnt target gene expression (*Lef1, Postn, Fra1*, *Opg)*. In addition, Notch (*Lfng, Hey1*) and Ngf (*Ier3, Cxcr4, Egr2*) target genes were significantly reduced. Because mutations to Wnt1 cause low bone mass in humans and Wnt1 is the second most highly upregulated TGFβ-induced secreted factor, we investigated the effect of osteoclast-specific Wnt1 deletion on bone (*CtskCre;Wnt1ff*). 22 week female Wnt1OclKO femurs exhibited significantly reduced BV/TV with reduced Conn.D and increased SMI, and histomorphometry revealed significantly reduced BFR/TV and a trend for reduced osteoblast number (n=6). Similar to Tgfbr2OclKO MPs, MPs isolated from the Wnt1OclKO showed increased expression of osteoblast genes (*Osx, Ocn)*, along with reduced canonical Wnt target gene expression (*Ccn1, Lef1, Postn, Fra1*). In contrast, Wnt1OclKO MPs exhibited increased TGFβ and Notch target gene expression. These data are consistent with a paradigm in which TGFβ induces Wnt expression by osteoclasts in order to couple bone resorption to bone formation. Furthermore, additional factors secreted by osteoclasts are disrupted in Tgfbr2OclKO and may contribute to the more severe uncoupling in these mice.

Background and Overview of the Biology and Pathophysiology of Fibrous Dysplasia

Michael T. Collins, MD

Genetic/Molecular: Fibrous dysplasia (FD) is an uncommon skeletal disorder that presents with bone pain, deformity, and fractures. It is a mosaic disease that can affect a single focus of one bone (monostotic), in which case it is usually clinically insignificant and often discovered incidentally. It can affect multiple bones (polyostotic), or rarely the entire skeleton (panostotic), and result in significant functional impairment. Not infrequently, it is associated with hyperfunctioning endocrinopathies (McCune-Albright syndrome, MAS, see Figure 1).(1) The underlying genetic/molecular pathophysiology of FD/MAS is somatic, activating mutations in Gαs (2) one of the transcripts of the complex, imprinted gene locus, *GNAS*. Gαs is ubiquitously expressed and central in G-protein coupled receptor (GPCR) signaling. Upon ligand binding, GDP-bound Gαs dissociates from the trimeric α/β/γ complex, exchanges GDP for GTP and couples with membrane-associated adenylyl cyclase (AC) to generate the key second messenger, cAMP. The intrinsic GTPase activity of Gαs hydrolyzes GTP to GDP, Gαs dissociates from AC and terminates AC-mediated cAMP production. All of the mutations that cause FD/MAS identified thus far are in the GTPase domain of Gαs, specifically >90% at the R201 position (roughly equally divided between R201C and R201H). The result of these mutations is increased cAMP production, the primary signal for FD/MAS-associated cellular dysfunction. Regulation of intracellular cAMP levels is also controlled by metabolism of cAMP to 5'AMP by phosphodiesterase(s) (PDE). The balance between AC and PDE activity determines intracellular cAMP levels. The complexity of this system is amplified by the fact there are 10 human AC genes and 16 PDE genes, with different cells expressing a different array of each of these key regulatory enzymes in a tissue-specific fashion.

Development: Consistent with this assertion that FD/MAS is a mosaic disease is the observation that there are no documented cases of vertical transmission, there are many reported cases of discordance between monozygotic twins, and that ectodermally-derived café-au-lait macules of the skin in MAS follow the developmental lines of Blaschko. Since in MAS, tissues derived from all three germ layers can be affected in a mosaic pattern, it is postulated that the sporadic mutations arise early in embryogenesis, prior to gastrulation. By such reasoning, the "map" of affected tissue is established in utero. This is consistent with the clinical findings in which, with careful phenotyping, virtually all affected tissues are can be identified early in life. Inconsistent with this hypothesis though is a mouse model of FD in which FD-like lesions arise in an animal bearing a germline, transmissible R201C mutation in which the mice survive, and are fertile.(3) The endocrine-related features of MAS in this mouse model have not been described.

Cell Biology: Clinically, FD lesions arise in the intramedullary space, increase in size, thin the cortex, and lead to expansion of the bone. Lesions are composed of a fibroosseous tissue that is an admixture of highly cellular fibrotic tissue composed of fibroblast-like cells with varying amounts of mineralized bone tissue (see Figure 2).(4) The osseous component of FD lesions is not the remnant of partially resorbed, normal lamellar bone that persists as lesions expand, but is woven bone that has arisen de novo within the FD lesions. Intralesional bone is generally poorly mineralized with significant osteoid. The histological appearance is often described as "Chinese writing" and is composed of disconnected pseudo trabeculae that provide little or no mechanical support. Active bone formation by atypical osteoblastic cells and resorption by osteoclastic cells is often seen, especially in younger children with active disease. The source of the cells that cause FD was predicted by the eminent bone pathologists Lichtenstein and Jaffe in 1938, who were the first to use the term "fibrous dysplasia" to describe the disease.(5) They made the assertion that lesion-forming cells are derived from the "perverted activity of the bone-forming mesenchyme", a.k.a. skeletal stem cells. The skeletal stem cell nature of FD-forming cells was eventually proven by Bianco and Robey in 1998 when they elegantly demonstrated that FD derives bone skeletal stem cell-derived

marrow stromal cells (BMSCs).(6) An extremely important observation that Bianco and Robey made is that FD is a mosaic disease, even at the tissue level. FD lesions are composed of mixture of both mutation-positive and mutation-negative cells. In fact, as they demonstrated experimentally, FD can only form when both mutant and non-mutant cells are present, suggesting a sort of symbiotic relationship between the two. Clinically, FD lesions tend to become more quiescent with age, and there is evidence that there is an age-dependent loss of mutation-bearing cells, such that in older patients there are relatively more wild type than mutant cells, which can even lead to microscopic areas of histologically normal bone within areas that are radiographically, grossly FD.(7) This point not only helps to explain the observed natural history of the disease, but may also have important implications for therapy.

Additional important pathophysiologic features of FD is that lesional cells overproduce the important phosphate- and vitamin D-regulating hormone, fibroblast growth factor 23 (FGF23)(8), and that osteoclast-like giant cells that highly express RANK and RANKL, key regulators of osteoclastogenesis, are common in FD lesions.(9) The discovery of FGF23 production by FD cells not only explained the observed hypophosphatemia, osteomalacia and rickets in the subset of FD patients with extensive disease, it also led to the identification of bone cells as the normal physiologic source of FD – a major finding in the bone field that emphasizes the importance and contribution of studying rare diseases to our understanding of normal biology. Abundant numbers of multinucleated giant cells, and robust expression of RANKL and RANK by lesional cells, especially in areas of lesions with high cellularity and robust proliferation, and not in association with bone resorption, suggest that activation of the RANKL/RANK pathway, which is primarily regulated by the PTH/cAMP pathway, may play an important etiologic role in the development and expansion of FD lesions, and have implications for treatment.(10)

FD's derivation from mutations in an essential signaling protein in skeletal stem cell-derived cells, the mosaic nature of the disease, and the clinical complexity created by concomitant endocrine dysfunction all come to bear upon creating a fascinating and challenging skeletal disease. Progress has been steady; improved definition of the spectrum and natural history of the disease, advances in understanding the molecular and cell biology, together with creation of important new animal models suggest that rational, targeted therapies can be developed and tested, giving hope to the patients and families who suffer as a result of this disease.

References

1. Boyce AM, Collins MT. Fibrous Dysplasia/McCune-Albright Syndrome. In: Pagon RA, Adam MP, Ardinger HH, Wallace SE, Amemiya A, Bean LJH, et al., editors. GeneReviews(R). Seattle (WA)2015.
2. Weinstein LS, Shenker A, Gejman PV, Merino MJ, Friedman E, Spiegel AM. Activating mutations of the stimulatory G protein in the McCune-Albright syndrome. N Engl J Med. Dec 12 1991;325(24):1688-95.
3. Saggio I, Remoli C, Spica E, Cersosimo S, Sacchetti B, Robey PG, et al. Constitutive expression of Gsalpha(R201C) in mice produces a heritable, direct replica of human fibrous dysplasia bone pathology and demonstrates its natural history. J Bone Miner Res. Nov 2014;29(11):2357-68.
4. Riminucci M, Fisher LW, Shenker A, Spiegel AM, Bianco P, Gehron Robey P. Fibrous dysplasia of bone in the McCune-Albright syndrome: abnormalities in bone formation. The American journal of pathology. Dec 1997;151(6):1587-600.
5. Lichtenstein L. Poloyostotic fibrous dysplasia. Arch Surg. 1938;36:874-98.
6. Bianco P, Kuznetsov SA, Riminucci M, Fisher LW, Spiegel AM, Robey PG. Reproduction of human fibrous dysplasia of bone in immunocompromised mice by transplanted mosaics of normal and Gsalpha-mutated skeletal progenitor cells. J Clin Invest. Apr 15 1998;101(8):1737-44.

7. Kuznetsov SA, Cherman N, Riminucci M, Collins MT, Robey PG, Bianco P. Age-dependent demise of GNAS-mutated skeletal stem cells and "normalization" of fibrous dysplasia of bone. J Bone Miner Res. Nov 2008;23(11):1731-40.
8. Riminucci M, Collins MT, Fedarko NS, Cherman N, Corsi A, White KE, et al. FGF-23 in fibrous dysplasia of bone and its relationship to renal phosphate wasting. J Clin Invest. Sep 2003;112(5):683-92.
9. Piersanti S, Remoli C, Saggio I, Funari A, Michienzi S, Sacchetti B, et al. Transfer, analysis, and reversion of the fibrous dysplasia cellular phenotype in human skeletal progenitors. J Bone Miner Res. May 2010;25(5):1103-16.

10. Boyce AM, Chong WH, Yao J, Gafni RI, Kelly MH, Chamberlain CE, et al. Denosumab treatment for fibrous dysplasia. J Bone Miner Res. Jul 2012;27(7):1462-70.

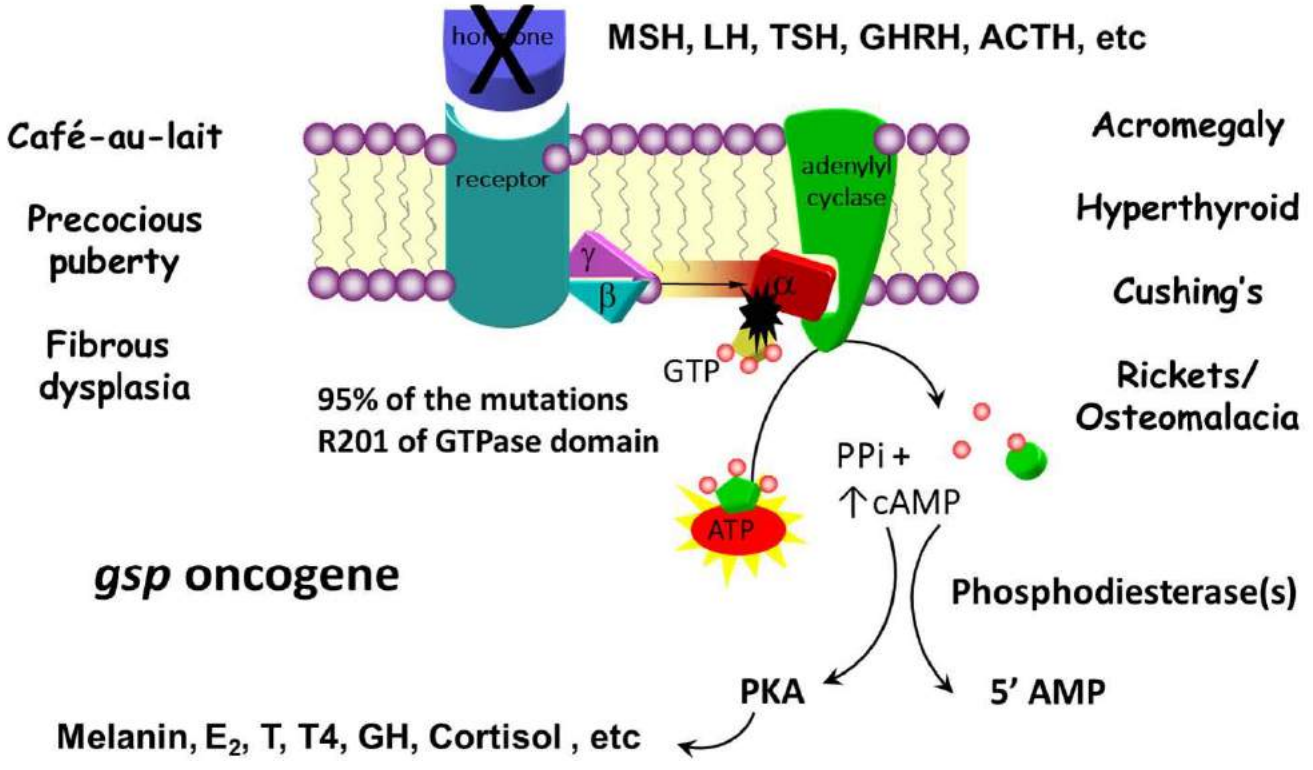

Figure 1. Genetic and molecular etiology of FD/MAS. Fibrous dysplasia (FD)/McCune-Albright syndrome (MAS) is caused by somatic, activating, mutations in the GTPase domain of Gαs that impair the intrinsic GTPase activity (the so-called *gsp* oncogene). GTP-bound Gαs dissociates from the α/β/γ complex, interacts with adenylyl cyclase (AC) and leads to dysregulated generation of cAMP. Ligand-independent signaling in G-protein coupled (GPCR) /Gαs/AC/cAMP/protein kinase A (PKA)-dependent cells ensues with, depending on which cell bears the mutation, downstream effects. For example, cells expressing the melanocyte stimulating hormone (MSH) receptor will overproduce melanin leading to café-au-lait macules. Similarl pathophysiology holds true for luteinizing hormone (LH) receptor-expressing gonadal cells, thyrocyte-stimulating hormone (TSH) thyrocytes, etc. The ubiquitous expression of Gαs underlies the broad spectrum of phenotypic features possible in FD/MAS that include the original triad of café-au-lait macules, precocious puberty, shown on the left, as well as many other features, some of which are shown on the right, inincluding acromegaly (pituitary growth hormone overproduction), hyperthyroidism, etc. cAMP is inactivated by phosphodiesterase (PDE) to 5' AMP. PDE expression and activity may be increased in mutation-bearing cells, but is apparently not sufficient to compensate for increased cAMP production.

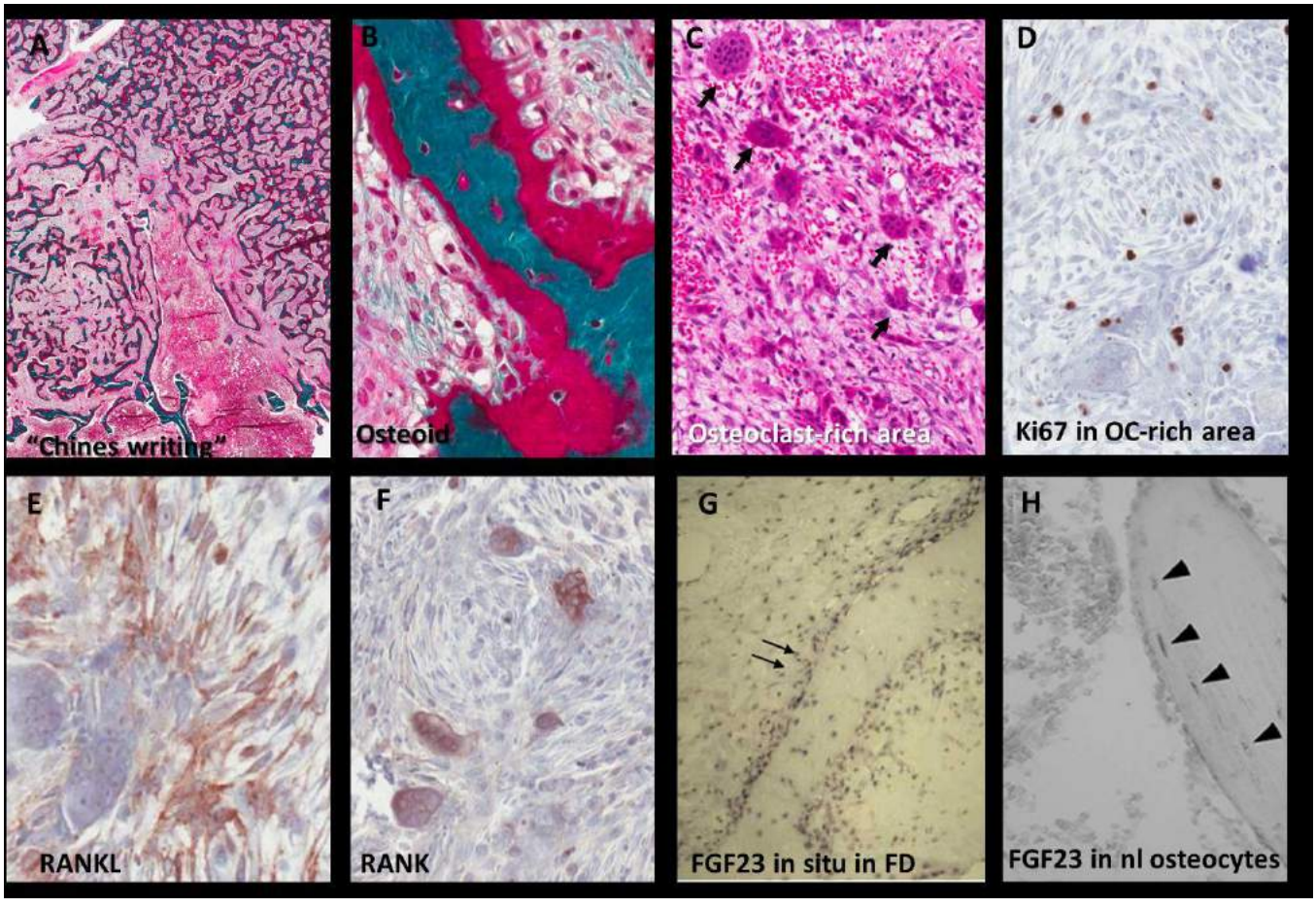

Figure 2. Histological findings that represent the underlying pathophysiology of fibrous dysplasia (FD). (A) demonstrates the so-called "Chinese character" appearance of FD seen on histological sections, which is created by de novo formation of disconnected, mechanically irrelevant pseudo trabeculae of woven bone, features of which are better visualized in (B), including significant osteoid (red) commonly seen in FD. (C) Multinucleated giant cells (osteoclasts) are common in FD, and often appear independent of associated bone. (D) Giant cell-rich areas are often the most proliferative in FD lesions, as shown by Ki67 staining. (E) The giant cell-associated stromal cells show high levels of RANKL staining, and (F) the associated giant cells high levels of RANK staining. (G) As shown by in situ hybridization, FD cells are the source of the high levels of FGF23 seen in patients with extensive disease. (H) The discovery of FGF23 in the stromal cells of FD led to the identification of normal bone cells, osteocytes shown here, as the physiologic source of FGF23.

Clinical Perspectives in Fibrous Dysplasia/McCune-Albright Syndrome

Alison M Boyce, MD

Clinical presentation in fibrous dysplasia/McCune-Albright syndrome (FD/MAS) reflects age-related changes in skeletal development. Somatic *GNAS* mutations acquired during embryogenesis determine areas of future disease involvement. Bone formation *in utero* appears to be relatively unaffected by Gαs activation, with grossly normal skeletal development in the fetal period. Over the first several years of life, bone lesions become clinically evident, and expand gradually during skeletal growth. By age 5 years, 50% of future disease burden can be detected on radioisotope scans, with final disease burden present by age 15 years [1]. The result is a relatively predictable sequence of progressive disease throughout infancy, early childhood, and adolescence, which typically remains static in adulthood. Understanding this pattern of disease development has important implications for the development of therapeutic strategies, which would optimally target young patients to prevent primary establishment of bone lesions.

The mosaic nature of FD/MAS results in a broad clinical spectrum, with extensive phenotypic variability between patients. Clinical problems arise according to the region of the skeleton affected. Appendicular disease results in fractures and progressive deformities, particularly in weight-bearing bones. Lesions in the proximal femora result in characteristic varus deformities ("shepherd's crook")(Fig 1b); lesions in this area are a primary cause of impaired ambulation in severely affected patients. Craniofacial lesions present with focal areas of expansion, resulting in facial asymmetry, and less commonly functional deficits. Axial FD may lead to scoliosis, which is further exacerbated by lower limb deformities and functional deficits (Fig 1a). Bone pain is common, typically increases with age, and does not appear to correlate with disease burden. MAS-associated endocrinopathies may exacerbate skeletal disease. Overproduction of the phosphaturic hormone fibroblast growth factor-23 by mutation-bearing mesenchymal cells leads to rachitic changes, pain, worsening deformity, and fractures [2]. Growth hormone excess fuels expansion of craniofacial FD, resulting in macrocephaly and increased risk of vision and hearing deficits [3].

The current mainstay of treatment for FD is surgical, however optimal techniques have not been established, and commonly used strategies have proven ineffective. In the appendicular skeleton, bone grafting with allograft or autograft is associated with high rates of resorption and is not useful for long-term management, particularly in children with active disease [4]. Complete resection of craniofacial lesions is not feasible in most patients, and debulking procedures frequently result in post-operative regrowth, with recurrence or even worsening of deformities [5]. Outcomes from spinal fusion are generally favorable in patients with progressive scoliosis. Physiatry is an underutilized modality which may augment surgical care by targeting hip strength and range of motion, correcting leg length discrepancies, and helping to preserve ambulation ability [6]. Optimizing surgical care, including defining indications, timing, and developing novel techniques and devices, is an area of high priority for clinical research in FD.

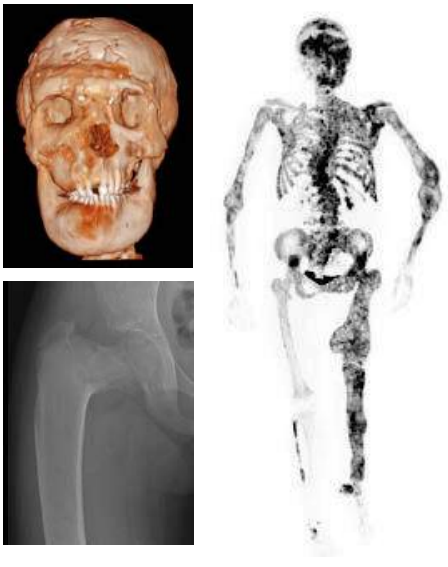

Figure 1. Representative images in patients with FD. A. Computed Tomography scan shows severe facial deformity and mandibular overgrowth. B. Radiograph demonstrating proximal femoral FD with characteristic genu valgus ("shepherd's crook") deformity. C. 18F-NaF PET/CT scan in a patient with severe FD shows patchy, asymmetric radiotracer uptake, consistent with a mosaic distribution.

No medical therapies have been shown to alter the disease course in FD. Bisphosphonates have been advocated due to prominent osteoclastogenesis in FD tissue, and initial case series reported beneficial effects on pain, bone turnover, and radiographic appearance of FD lesions; however, larger series found inconsistent results [7, 8]. A placebo-controlled trial of alendronate demonstrated decreased resorption markers and increased density on DXA scans, but no effects on pain or radiographic appearance of FD lesions [9]. Recent evidence suggests RANKL may play a role in FD pathogenesis, serving as a potential therapeutic target. Case reports of treatment with denosumab, a monoclonal antibody to RANKL, report preliminarily positive effects on FD pain, lesion expansion, and bone turnover [10, 11]. Post-discontinuation rebound effects include increased bone turnover, which has resulted in life-threatening

Identification of clinically-relevant, surrogate markers for FD activity is a key area of unmet need. Clinical sequalae in FD are challenging endpoints for research, because they develop over extended periods of time (deformity, disability), and/or occur at infrequent intervals (fractures). Surrogate markers are needed to serve as validated endpoints for clinical trials. They are also important for early identification of patients who are likely to suffer a severe disease course, thus defining the optimal target population for intervention. An optimal surrogate marker would allow for quantification of lesion-specific skeletal activity, and correlate with clinically meaningful outcomes. Current methods for evaluating FD activity are inadequate because they are either qualitative (including technetium-99 scintigraphy and radiographs), or non-specific (serum bone turnover markers). 18F-NaF PET/CT imaging is a promising nuclear imaging technique in which quantification of lesion activity has been correlated with clinical outcomes, including fractures, surgeries, and ambulation status (Fig 1c). Additional research is needed to validate and extend these findings, and to identify other novel endpoints that will facilitate interventional studies.

References

1. Hart, E.S., et al., *Onset, progression, and plateau of skeletal lesions in fibrous dysplasia and the relationship to functional outcome.* J Bone Miner Res, 2007. **22**(9): p. 1468-74.
2. Leet, A.I., et al., *Fracture incidence in polyostotic fibrous dysplasia and the McCune-Albright syndrome.* J Bone Miner Res, 2004. **19**(4): p. 571-7.
3. Boyce, A.M., et al., *Optic neuropathy in McCune-Albright syndrome: effects of early diagnosis and treatment of growth hormone excess.* J Clin Endocrinol Metab, 2013. **98**(1): p. E126-34.
4. Leet, A.I., et al., *Bone-Grafting in Polyostotic Fibrous Dysplasia.* J Bone Joint Surg Am, 2016. **98**(3): p. 211-9.

5. Boyce, A.M., et al., *Surgical Management of Polyostotic Craniofacial Fibrous Dysplasia: Long-Term Outcomes and Predictors for Postoperative Regrowth.* Plast Reconstr Surg, 2016. **137**(6): p. 1833-9.
6. Paul, S.M., et al., *Disease severity and functional factors associated with walking performance in polyostotic fibrous dysplasia.* Bone, 2014. **60**: p. 41-7.
7. Plotkin, H., et al., *Effect of pamidronate treatment in children with polyostotic fibrous dysplasia of bone.* J Clin Endocrinol Metab, 2003. **88**(10): p. 4569-75.
8. Liens, D., P.D. Delmas, and P.J. Meunier, *Long-term effects of intravenous pamidronate in fibrous dysplasia of bone.* Lancet, 1994. **343**(8903): p. 953-4.
9. Boyce, A.M., et al., *A randomized, double blind, placebo-controlled trial of alendronate treatment for fibrous dysplasia of bone.* J Clin Endocrinol Metab, 2014: p. jc20141371.
10. Boyce, A.M., et al., *Denosumab treatment for fibrous dysplasia.* J Bone Miner Res, 2012. **27**(7): p. 1462-70.

11. Benhamou, J., D. Gensburger, and R. Chapurlat, *Transient improvement of severe pain from fibrous dysplasia of bone with denosumab treatment.* Joint Bone Spine, 2014. **81**(6): p. 549-50.

"Challenges and Approaches for Fibrous Dysplasia Research"

Edward Hsiao, MD, PhD

Fibrous dysplasia accounts for 2.5% of all bone lesions and 7% of benign skeletal dysplasias (4), with craniofacial FD being the most common site. However, few options are available for treating this disfiguring disorder (3; 5). FD can occur as part of McCune-Albright Syndrome (MAS), a mosaic genetic condition characterized by polyostotic FD (both within and outside of the craniofacial region), café-au-lait skin hyperpigmentation, precocious puberty, and other endocrinopathies including Cushing's disease, hyperthyroidism, acromegaly, and solid organ malignancies (6-8).

Although MAS affects numerous tissues, FD is arguably the most significant manifestation because there are no effective pharmacologic treatments for the bone complications. In addition, craniofacial FD leads to severe deformities that are cosmetically disfiguring and affect critical functions such as hearing, vision, and eating. The mainstay of craniofacial FD treatment remains watchful waiting and judicious surgical resection, which is often complex due to the size and location of the affected bones.

MAS/FD is commonly caused by a somatic activating mutation in the GNAS gene (c.602G>A, p.R201H), which encodes the α subunit of the stimulatory guanine nucleotide binding protein (Gsα) and regulates production of intracellular cyclic AMP (cAMP). The R201H mutation causes constitutive activation of Gsα and over-activation of downstream pathways in affected cells by inhibiting the GTP hydrolase activity of Gsα, leading to constitutive activation and persistently elevated intracellular cAMP. The R201H mutation is likely acquired during early embryogenesis since tissues derived from all three germ layers can be affected (7).

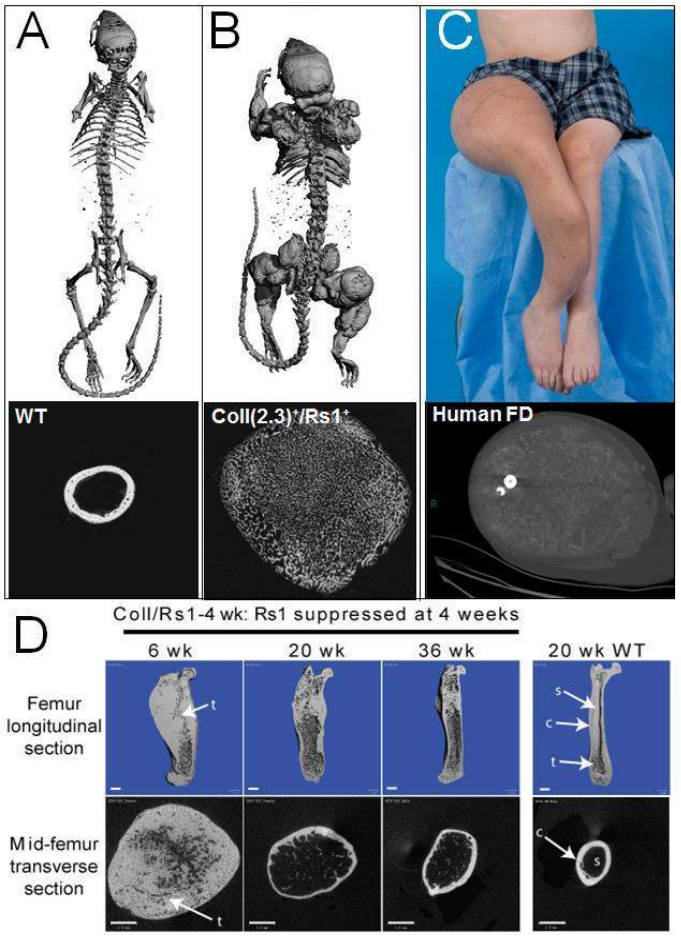

Figure 1: Rs1-mediated G_s activation in osteoblastic cells causes fibrous dysplasia. (A) 9-week old normal mouse. Mid-femur microCT cross sections are shown below. **(B)** 9-week-old Coll(2.3)$^+$/Rs1$^+$ mouse with increased trabecular bone resembling FD. **(C)** Patient with severe FD showing similar trabecularization in the femur. Clinical image from M. Collins. **(D)** Suppressing G_s-GPCR activity in osteoblasts can reverse the FD bone lesions. s, bone marrow space; c, cortical bone, t, trabecular bone. Scale bar, 1 mm. (1-3)

Our ability to understand the effects of cAMP elevation vs. other effects of the GNAS locus (i.e., other transcripts) on early cell fate in FD is limited by our lack of suitable disease models. The complexity of the GNAS locus has made it difficult to create *in vivo* models with the R201H mutation in its endogenous locus. Several strategies have been implemented to circumvent this issue, including mouse models with tissue-specific activation of the Gs-signaling pathways using engineered receptors to activate Gs-signaling in bone, as developed by our group (9) (**Figure 1**). These Coll(2.3)+/Rs1+ mice showed many characteristics found in human FD, including massive expansion of trabecular bone, infiltration by fibroblastic-like cells, loss of hearing, and low bone quality (1). Activation of Gs signaling in osteoblastic cells led to more immature osteoblasts and bone stromal cells, suggesting that a non-cell autonomous pathway may drive expansion of cell lineages not expressing Rs1. Stopping the abnormal Gs-GPCR signaling dramatically reversed the FD bone lesions (2), suggesting that therapies aimed at reversing the pathway's activity have a high likelihood of being effective.

Other approaches have also been taken. A transgenic mouse model that expresses the less common GNAS R201C mutation (10) can also develop features of FD. Although these tools have allowed us to explore key

aspects of MAS biology, models containing the R201H mutation in its endogenous locus remain elusive. Thus, the precise mechanisms through which cAMP signaling or GNAS ultimately drive FD disease pathogenesis remain major challenges that need to be explored to develop targeted pharmacologic treatment strategies for FD/MAS and related structural birth defects.

Although many of the GNAS mutations that cause FD and MAS are known, we still face significant limitations in our understanding of FD disease pathogenesis that hamper our ability to identify potential treatment targets. This session will focus on three key challenges that need to be addressed:

1- The development of robust stem cell and mouse models that carry the endogenous GNAS mutation, or an inducible form, to facilitate identification of mechanisms and thus potential therapies;

2- Understanding what factors lead to the dramatic variability in disease presentation (i.e., are there genetic, hormonal, or environmental factors that potentiate disease progression?); and

3- Understanding how the GNAS mutation affects different cell types to lead to disease pathogenesis, both in the bone and in other tissues typically affected in MAS.

References:

1. Hsiao, E.C., Boudignon, B.M., Chang, W.C., Bencsik, M., Peng, J., Nguyen, T.D., Manalac, C., Halloran, B.P., Conklin, B.R., and Nissenson, R.A. (2008). Osteoblast expression of an engineered Gs-coupled receptor dramatically increases bone mass. Proc Natl Acad Sci U S A *105*(4), 1209-1214.
2. Hsiao, E.C., Boudignon, B.M., Halloran, B.P., Nissenson, R.A., and Conklin, B.R. (2010). Gs G protein-coupled receptor signaling in osteoblasts elicits age-dependent effects on bone formation. J Bone Miner Res *25*(3), 584-593.
3. Hsiao, E.C., Millard, S.M., and Nissenson, R.A. (2016). Gs/Gi Regulation of Bone Cell Differentiation: Review and Insights from Engineered Receptors. Horm Metab Res *48*(11), 689-699.
4. Ricalde, P., and Horswell, B.B. (2001). Craniofacial fibrous dysplasia of the fronto-orbital region: a case series and literature review. J Oral Maxillofac Surg *59*(2), 157-167; discussion 167-158.
5. Chapurlat, R.D., and Orcel, P. (2008). Fibrous dysplasia of bone and McCune-Albright syndrome. Best practice & research Clinical rheumatology *22*(1), 55-69.
6. Turan, S., and Bastepe, M. (2015). GNAS Spectrum of Disorders. Curr Osteoporos Rep *13*(3), 146-158.
7. Collins, M.T., Singer, F.R., and Eugster, E. (2012). McCune-Albright syndrome and the extraskeletal manifestations of fibrous dysplasia. Orphanet J Rare Dis *7 Suppl 1*, S4.
8. Dumitrescu, C.E., and Collins, M.T. (2008). McCune-Albright syndrome. Orphanet journal of rare diseases *3*, 12.
9. Hsiao, E.C., Nguyen, T.D., Ng, J.K., Scott, M.J., Chang, W.C., Zahed, H., and Conklin, B.R. (2011). Constitutive Gs activation using a single-construct tetracycline-inducible expression system in embryonic stem cells and mice. Stem Cell Res Ther *2*(2), 11.
10. Saggio, I., Remoli, C., Spica, E., Cersosimo, S., Sacchetti, B., Robey, P.G., Holmbeck, K., Cumano, A., Boyde, A., Bianco, P., and Riminucci, M. (2014). Constitutive expression of Gsalpha(R201C) in mice produces a heritable, direct replica of human fibrous dysplasia bone pathology and demonstrates its natural history. J Bone Miner Res *29*(11), 2357-2368.

Quantitative MRI of Cortical and Trabecular Bone

Felix W Wehrli
Department of Radiology
Perelman School of Medicine
University of Pennsylvania

Magnetic Resonance Imaging (MRI) is the modality of choice for clinical evaluation of musculoskeletal soft tissues (muscle, cartilage, tendon, ligaments, bone marrow). However, so far, it has played a lesser role for the study of calcified tissues, which have largely been the domain of X-ray CT and DXA. Nevertheless, MRI has more recently made significant inroads as a potential tool for assessment of degenerative and metabolic bone disease. Unlike CT, MRI is truly noninvasive as it does not use ionizing radiation and is therefore particularly suited for follow-up studies in patients undergoing treatment, as well as in children. Lastly, MRI is widely available with an estimated population of over 25,000 MRI systems worldwide.

This brief talk reviews the major advances made during the past decade. Key among these is technology enabling visualization and quantification of the trabecular bone network by high-resolution MRI, similar to pQCT, albeit by means of general-purpose clinical MRI systems requiring only minimal customization in terms of radiofrequency coils, imaging pulse sequences, processing and analysis software. More recently, 3D voxel models of the MRI data have been used as input into a custom-built finite-element solvers yielding as output measures representative of the bone's mechanical competence (e.g. stiffness, elastic modulus or failure strength). Applications include assessment of treatment response in terms of the structural and mechanical parameters measured. While much of prior work has focused on the wrist or distal tibia (the latter serving as a surrogate site, recent advances have demonstrated structural MRI's potential to generate image-based models of the femur, the site of the most traumatic fractures, as a means for assessing osteoporotic fracture risk.

Lastly, MRI has shown promise for quantifying structural remodeling changes involving cortical bone, including quantification of periosteal expansion and thinning of the cortex, as well as assessment of changes in porosity. The latter has become possible owing to emergence of solid-state MRI techniques that can detect and quantify the tightly bound water associated with collagen and residing in pore spaces.

Using MRI to Detect Cartilage Damage

Corey P. Neu
Department of Mechanical Engineering
College of Engineering & Applied Sciences
University of Colorado Boulder

Recent advances in magnetic resonance imaging (MRI) have been introduced with exciting potential to identify and track changes in damage and disease of articular cartilage. In particular, MRI techniques have sought to discover early changes in osteoarthritis (OA), when emerging disease-modifying interventions may be most effective. Moreover, the breakdown and structural loss of major macromolecules such as aggrecan and type II collagen leads to altered strains and material properties (e.g. moduli) within the tissue, suggesting MRI of cartilage biomechanics may be sensitive to degeneration. Unfortunately, noninvasive diagnosis of OA remains poor, especially in early disease stages, and several challenges remain, including the need for sensitive and specific imaging biomarkers that predict damage outcomes, and the need to relate imaging biomarkers to tissue function and biomechanics.

This talk will focus on the use of MRI to detect cartilage damage, with an emphasis on functional imaging, or the visualization of organ or tissue physiology using medical image modalities. Changes in strain, stress, and material properties occur in cartilage damage, providing an opportunity to probe the evolution of tissue function. Primary discussion points will include: 1) biomechanical measures in cartilage and related joint tissues as imaging biomarkers in the evaluation of damage, and 2) relative utility of kinematic, structural, morphological, and biomechanical measures as functional imaging biomarkers. Numerous study systems will briefly be covered, including tissue explant models and *in vivo* studies in sheep and humans. Finally, the relative value of MRI techniques like T2 and T1rho will be discussed for probing early OA, and the potential for improved diagnostic specificity through the combination of multiple imaging biomarkers with unique contrasts, including elastography.

Clinical MRI Applications

Hollis G. Potter, MD
Hospital for Special Surgery, New York City, NY

MR imaging of articular cartilage is well established as a standard by to which to assess cartilage morphology. Clinical applications include accurate assessment of the magnitude of osteoarthritis, which is important when determining treatment options such as arthroscopic surgery versus arthroplasty. The advent of 3D techniques allows for modeling to enable accurate tissue transfer in the setting of prior trauma or ischemic bone loss. In addition to imaging of tissue morphology, imaging of cartilage ultrastructure is now possible using relaxometry techniques. Techniques which have been established to evaluate proteoglycan include sodium MRI, gagCEST, dGEMRIC, and T1rho, while assessment of collagen is largely confined to T2 and T2* mapping. Each of these techniques has advantages and disadvantages, all of which will be discussed, and the application of these techniques to clinically relevant cohorts will be demonstrated, including use of parametric mapping in a comparative effectiveness of surgical versus non-surgical treatment of femoroacetabular impingement. More robust analysis can sometimes be assessed with texture analysis, in which there is a detection of the spatial variation of individual pixel values, rather than just measuring the mean within a chosen tissue voxel. More recently, voxel based relaxometry has been efficacious in assessing longitudinal change in large cohorts of patients at risk for early osteoarthritis such as ACL disruption. Application to cartilage repair, obviating the need for arthroscopic tissue biopsy, will also be demonstrated. Finally, the use of relaxometry to tissue structures other than articular cartilage will be demonstrated, including meniscus and ligament, as well as the ability to use relaxometry to assess tissue material properties.

<u>*References –*</u>

Barber L, Koff MF, Virtue P, Lipman JP, Hotchkiss RJ, Potter HG. Cartilage. 2012;3(2):188-93.
Singh A, Haris M, Cai K, Kassey VB, Kogan F, Reddy D, Hariharan H, Reddy R. Magn Reson Med. 2012;68(2):588-94.
Xia Y1, Moody JB, Burton-Wurster N, Lust G. Osteoarthritis Cartilage. 2001;9(5):393-406.
Cunningham T, Jessel R, Zurakowski D, Millis MB, Kim YJ. J Bone Joint Surg Am. 2006 Jul;88(7):1540-8.
Hingsammer AM, Kalish LA, Stelzeneder D, Bixby S, Mamisch TC, Connell P, Millis MB, Kim YJ. JBJS 2015;97(7):544-50.
Chandrasekaran S, Gui C, Hutchinson MR, Lodhia P, Suarez-Ahedo C, Domb BG. J BJS Am 2015;97(16):1340-7.
Rakhra KS, Lattanzio PJ, Cárdenas-Blanco A, Cameron IG, Beaulé PE. JBJS Br 2012;94(9):1187-92.
Gallo MC, Wyatt C, Pedoia V, Kumar D, Lee S, Nardo L, Link TM, Souza RB, Majumdar S. OA & C 2016;24(8):1399-407.
Potter HG, Jain SK, Ma Y, Black BR, Fung S, Lyman S. Am J Sports Med 2012; 40:276-285.
Pedoia V, Li X, Su F, Calixto N, Majumdar S. J Magn Reson Imaging. 2016;43(4):970-80.
Russel C, Pedoia V, Amano K, Potter HG, Majumdar S. J Orthop Res 2017; 35(3): 688-696.
Pedoia V, Neumann J, Heilmeier U, Haefeli J, Ferguson AR, Link T, Majumdar S. Predicting osteoarthritis radiographic incidence by coupling quantitative compositional MRI and deep learning. ISMRM 2017. Honolulu, HI.
Prasad AP, Nardo L, Schooler J, Joseph GB, Link TM. OA&C 2013;21:69-76.
Maier CF, Tan SG, Hariharan H, Potter HG. JMRI 2003;17:358-64
Anderson K, Seneviratne AM, Izawa K, Atkinson BL, Potter HG, Rodeo SA. AJSM 2001;29(6):689-98.
Verdonk PC, Verstraete KL, Almqvist KF, De Cuyper K, Veys EM, Verbruggen G, Verdonk R. Knee Surg Sports Traumatol Arthrosc. 2006;14(8):694-706.
Vundelinckx B, Bellemans J, Vanlauwe J. AJSM 2010;38(11):2240-7.
Robson MD, Gatehouse PD, Bydder M, Bydder GM. J Comput Assist Tomogr. 2003;27(6):825-46.
Pownder et al, ISMRM 2013. Salt Lake City, UT.
Koff MF, Pownder SL, Shah PH, Yang LW, Potter HG. J Biomech. 2014;47(13):3428-32.

7:00 AM – 8:00 AM	Breakfast & Registration
7:00 AM – 7:30 AM	Industry Breakfast Session presented by: REGENERON SCIENCE TO MEDICINE
	Lessons from Rare Genetic Diseases: From Novel Biology to Drug Discovery *Presenter: Aris N. Economides, PhD*

8:00 AM – 9:00 AM	ASBMR/Harold M. Frost Young Investigator Award Presentations Chair: Alexander Robling, PhD *(Indiana University)*
	TGFβ Regulation of Osteocytic Perilacunar Remodeling is Crucial Neha Dole, PhD *(University of California San Francisco)*
	Role of Panx1-P2X7R Signaling in Anabolic Bone Response of Type 1 Diabetic Mice Zeynep Seref-Ferlengez, PhD *(Albert Einstein College of Medicine)*
	Overexpression of MitoNEET in Osteoblasts Leads to Impaired Bone Mass and Energy Metabolism in Mice Anyonya Guntur, PhD *(Maine Medical Center Research Institute)*

9:15 AM - 12:00 PM	Using Genetically Engineered Animal Models to Solve Problems in Musculoskeletal Disease: State of the Art and Application Chair: Charles O'Brien, PhD *(University of Arkansas)*
	Validating Cre Driver Models: Where are we Cutting and How Do We Know? Ivo Kalajzic, MD, PhD *(University of Connecticut Health Center)*
	How Can We Improve CRE Driver Models? Charles O'Brien, PhD *(University of Arkansas)*
	Modeling Human Disease in Mice Aris Economides, PhD *(Regeneron Pharmaceuticals, NY)*

4:30 PM – 8:00 PM	Banquet & Symphony	Lodge Terrace

Lessons from Rare Genetic Diseases: From Novel Biology to Drug Discovery

Presenter: Aris N. Economides, PhD

Regeneron Pharmaceuticals

Advances in high-throughput DNA sequencing (exome; whole genome) has revolutionized human genomic discovery, providing the opportunity to identify rare causative variants associated with diseases and related traits. Insights gleaned through these discoveries often offer mechanistic insights that can be leveraged as therapeutic targets for diseases of unmet clinical need. The Regeneron Genetics Center has amassed a portfolio of patient and other populations for this purpose including (i) large patient populations linked to electronic health records (Geisinger Health System DiscovEHR collaboration, UK-Biobank), (ii) focused disease case:control collections for diseases of unmet clinical need, (iii) founder populations which provide opportunities to identify novel drifted disease alleles (Amish, Mennonite, French Canadian, Pima Indian), and (iv) rare families with undiagnosed monogenic diseases. Using this resource, we have made novel discoveries in several disease areas, and for a subset of these diseases we have undertaken the development of therapies. Examples of each will be discussed.

TGFβ regulation of osteocytic perilacunar remodeling is crucial for maintaining bone quality

Neha S. Dole, PhD[1], Courtney M. Mazur, BS[1], Claire Acevedo, PhD[1,2], Justin Lopez, BS[1], David A. Monteiro, MS[1], Bernd Gludovatz, PhD[2,3], Robert O. Ritchie, PhD[2,3], Khalid S. Mohammad, MD, PhD[4], Tamara Alliston, PhD[1]

[1]Department of Orthopaedic Surgery, University of California San Francisco, CA; [2]Materials Science Division, Lawrence Berkeley National Laboratory Berkeley, CA; [3]Department of Materials Science and Engineering, University of California Berkeley, CA; [4]Department of Medicine, Indiana University School of Medicine, Indianapolis, IN

INTRODUCTION: Nearly 50% of atraumatic fractures are bone mass independent, and rather result from impaired bone quality. Bone quality parameters including the material properties and organization of the bone extracellular matrix (ECM), is highly regulated. However, the cellular and molecular mechanisms controlling bone quality are incompletely understood, leaving bone quality as an underutilized therapeutic target for reducing fracture. As an essential regulator of bone homeostasis, transforming growth factor-beta (TGFβ) regulates both bone mass and bone quality [1-3]. Though TGFβ acts on osteoblasts and osteoclasts to control bone mass, the cellular target of TGFβ in the control of bone quality is unknown. This gap in knowledge persists, partly due to our lack of understanding of the function of TGFβ in osteocytes, the most abundant bone cells and master regulators of bone remodeling. Osteocytes are also capable of remodeling the matrix surrounding their intricate lacuno-canalicular network (LCN) through perilacunar remodeling (PLR). We previously implicated PLR, specifically through matrix metalloproteinase 13 (MMP13), in the control of bone quality [4]. Since TGFβ regulates MMP13 expression, *we hypothesize that TGFβ regulates bone quality through osteocyte-mediated PLR*. Here, we test this hypothesis to elucidate the unknown role of TGFβ in osteocytes and the cellular mechanisms controlling bone quality.

METHODS: To evaluate the role of TGFβ in PLR two *in vivo* murine models and *in vitro* studies were used. Using our established model (1), 5-week old mice were administered either vehicle or a TβRI kinase inhibitor (SD208, 60mg/kg, twice daily) for 6 weeks to systemically knock down TGFβ signaling. MicroCT analysis of the bone phenotype and PLR outcomes were conducted in 11-week old mice. To define the osteocyte specific role of TGFβ in PLR, we developed a novel tissue-specific mouse model with ablated TGFβ function only in DMP1-expressing osteocytes, DMP1-Cre$^{+/-}$:TβRII $^{fl/fl}$. MicroCT analysis and PLR outcomes were examined in 8-week old control (DMP1-Cre^{-}:TβRII$^{fl/fl}$) and TβRII$^{ocy-/-}$ (DMP1-Cre^{+}:TβRII $^{fl/fl}$) mice. *In vivo* PLR outcomes analyzed include LCN network through silver staining, PLR gene expression through qPCR, and immunohistochemistry. *In vitro* PLR outcomes were assayed in MLO-Y4 osteocyte-like cells, and include gene expression profiling and measurement of intracellular pH using carboxy-SNARF-AM dye.

To examine the effect of osteocyte specific TGFβ ablation on bone quality, three-point bending tests were conducted on unnotched femora of 8-9-week old TβRII$^{ocy-/-}$ and control mice using a Bose Electroforce 3200 test frame with a displacement rate of 0.01 mm/s. Flexural strength tests measured yield strength and other standard outcomes. For nanoindentation mid-diaphyseal femoral cortical bone surfaces were mounted in a nanoindenter with a Berkovitch tip and subjected to a trapezoidal loading profile with a peak load of 1000 μN and a hold period of 10 seconds. From the resulting load-deformation curves, local elastic modulus was calculated using the Olivier-Pharr method. For fracture toughness tests, one femur per animal was notched on the posterior side to a depth of approximately one third the anterior-posterior diameter. In order to measure crack extension, notched three-point bending was performed using a Gatan Microtest 2-kN stage (Gatan, Abingdon, UK) mounted in a variable pressure scanning electron microscope (Hitachi S-4300SE/N ESEM). Images of the crack extension were obtained in real time in back-scattered electron mode at 25 kV and 35 Pa. Sample size for *in vitro* and *in vivo* approaches was defined as N=3 and N=5-8 respectively. Statistical analysis was performed using ANOVA or Student's t-test. All animal procedures were approved by the Institutional Animal Care and Use Committee (IACUC) at UCSF.

RESULTS: Using the same model in which we evaluated the effect of systemic TβRI-inhibition on osteoclasts and osteoblasts [2], we investigated the unknown role of TGFβ in osteocytes. After verifying the high bone mass phenotype, we found that systemic inhibition of TβRI drove a strong and coordinated repression of several key PLR enzymes, including MMP2, MMP13, MMP14, Cathepsin K (Ctsk) and Tartrate resistant acid phosphatase (Acp5) genes in bone. Immunohistochemistry of cortical femurs revealed a significant decrease in the number of MMP13, MMP14 and Ctsk-expressing osteocytes upon TβRI inhibition. Given that suppression of these genes has been linked to deregulated PLR by osteocytes, we speculated a unique regulatory role of TGFβ in PLR. Therefore, we evaluated hallmarks of PLR, including the osteocyte LCN, in TβRI-inhibitor and vehicle-treated mice. Impeded TGFβ signaling caused a qualitative decline in the

integrity of the osteocyte lacuno-canalicular network (LCN) and canalicular length in the cortical bone. As LCN connectivity is a crucial functional outcome of PLR, our results suggest that TGFβ signaling is an essential regulator of PLR, directly in osteocytes and/or indirectly through interactions with other cells.

To determine if the effect of TGFβ on PLR is osteocyte-intrinsic, we analyzed *in vitro* PLR outcomes in MLO-Y4 cells. TGFβ significantly induced the expression of PLR genes, including MMP13, MMP14 and Ctsk. TGFβ also caused a drop in intracellular pH, a functional measure of osteocyte PLR. This decrease in intracellular pH supports bone resorption by osteocytes engaged in PLR, just as it does for osteoclast-mediated bone resorption. Furthermore, we developed and characterized a novel *in vivo* model of osteocyte-specific ablated TGFβ signaling ($T\beta RII^{ocy-/-}$). Immunohistochemistry demonstrated near complete loss of TβRII in osteocytes, but intact TβRII in osteoblasts and other cell types. Similar to TβRI-I administered bones, $T\beta RII^{ocy-/-}$ bones express dramatically lower levels of MMP2, MMP13, MMP14 and Ctsk mRNA compared to the control mice (Figure 1B). Immunohistochemical staining for MMP13, MMP14 and Ctsk confirmed this finding. Moreover, degeneration in osteocyte LCN connectivity (Figure 1A), canalicular length and area was even more pronounced in the $T\beta RII^{ocy-/-}$ cortical bone than in mice treated systemically with TβRI inhibitors. Together, these findings indicate that TGFβ regulates PLR through osteocyte-intrinsic mechanisms.

To define the role of osteocyte-intrinsic TGFβ signaling in bone quality, we conducted a series of macromechanical and material tests. Using three-point bending, we found that $T\beta RII^{ocy-/-}$ femora exhibited a 26% decline in the bending modulus relative to WT bone, indicating a reduced capacity to resist elastic deformation. Similarly, the yield stress was reduced by 27% in $T\beta RII^{ocy-/-}$ bones. Despite high trabecular bone mass and normal cortical bone mass, $T\beta RII^{ocy-/-}$ bones showed increased fragility, to understand the factors contributing to this fragility we tested material properties of $T\beta RII^{ocy-/-}$ bones. Nanoindentation revealed that the Young's modulus of $T\beta RII^{ocy-/-}$ bone matrix was significantly lower than for WT bone.

To more closely evaluate what toughness mechanisms were compromised in $T\beta RII^{ocy-/-}$ bones we conducted in situ fracture toughness tests. This technique allows the quantitative measurement of crack growth toughness by comparison of crack driving force with crack extension (independent of crack initiation) to form crack-resistance curves (R-curves) and the qualitative observation of the crack growth profile. Overall, $T\beta RII^{ocy-/-}$ bone exhibited a 65% decrease in total work of fracture compared to WT bone (Figure 1D). In addition to these significant quantitative changes in the material behavior of $T\beta RII^{ocy-/-}$ bone, we also observed several qualitative changes in crack growth that reveal loss of extrinsic toughening mechanisms. Specifically, in 100% of WT mice, crack extension was accompanied by crack branching and uncracked ligament bridging. In $T\beta RII^{ocy-/-}$ bones, each of these mechanisms was observed less often, and in some mice was entirely absent (Figure 1C). Collectively these analyses show a defect in the extrinsic toughening mechanisms and overall quality of bone in mice with an osteocyte-intrinsic defect in TGFβ signaling. Together, our results identify a novel function for TGFβ in bone, such that osteocyte-intrinsic TGFβ regulates bone quality through PLR.

DISCUSSION:

Here we report a novel function of TGFβ in osteocyte-mediated PLR and bone quality. Although we previously elucidated the critical function of TGFβ in controlling bone quality, the cellular mechanism was unknown. Using a combination of unique in vivo and in vitro tools, this study demonstrates that osteocyte-intrinsic TGFβ signaling orchestrates the activities of osteoblasts and osteoclasts, while it directly regulates local bone matrix remodeling through PLR. At the molecular level, we find that TGFβ partly relays its effects on PLR through MMP13, the absence of which also impairs LCN integrity and fracture resistance. In conclusion, our results highlight an osteocyte intrinsic-role for TGFβ signaling in dictating bone quality. This discovery will be particularly is critical to treating bone fragility in individuals with normal bone mass and preventing potentially adverse side effects from clinical use of TGFβ inhibitors for cancer and other conditions.

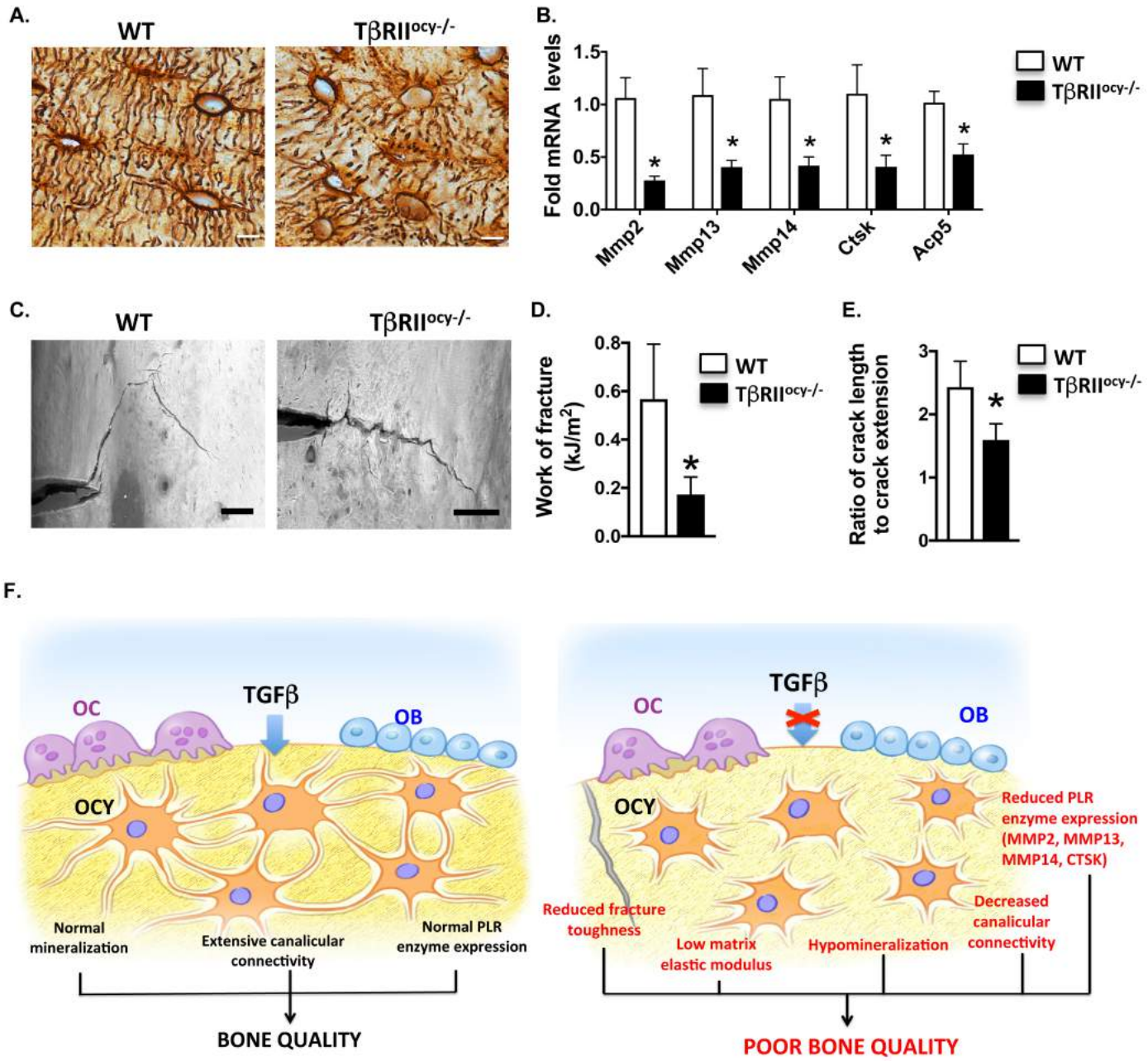

Figure 1: Osteocyte lacuno-canalicular network in the femoral cortical bone of WT and TβRII$^{ocy-/-}$ mice was detected by silver nitrate staining (N=5 mice/group and 4 images/mouse) and representative images of the lacuno-canalicular network is shown (A) (scale bar = 20 µm). Gene expression of Mmp2, Mmp13, Mmp14, Ctsk and Acp5 from the bones of WT and TβRII$^{ocy-/-}$ mice was quantified and normalized to 18s mRNA (B) (N=8-10 mice/group). In situ fracture toughness testing was used to evaluate differences in extrinsic toughening mechanisms of WT and TβRII$^{ocy-/-}$ bones by observing crack propagation. At the end of stable crack growth, differences in the extrinsic toughening mechanism crack deflection are readily seen in two representative samples (C) (scale bar = 100 µm), total work of fracture (WoF) (D) and crack deflection quantified as the ratio of total crack length to crack extension (E) (N=5 mice/group). Schematic figure illustrates the mechanistic role of TGFβ signaling in osteocyte perilacunar remodeling and in maintenance of bone quality (F).

References:

[1] Balooch G et al., PNAS 2005,
[2] Mohammad KS et al., PLoS ONE 2009,
[3] Edwards JR et al., JBMR 2010.
[4] Tang SY et al., JBMR 2012.

Role of Panx1-P2X7R Signaling in Anabolic Bone Response of Type 1 Diabetic Mice

Zeynep Seref-Ferlengez, Albert Einstein College of Medicine, Marcia Urban-Maldonado, Albert Einstein College of Medicine, Mitchell B. Schaffler, City College of New York, Hui B. Sun, Albert Einstein College of Medicine, Sylvia O. Suadicani, Albert Einstein College of Medicine, Mia M. Thi, Albert Einstein College of Medicine

Type 1 diabetes (T1D) manifests at early adolescence and leads to significant skeletal complications and increases risk of osteoporosis and fractures. Our previous studies demonstrated that high glucose levels, which is the major complication of T1D, alter the response of osteocytes to mechanical stimulation. Moreover, we showed that the Panx1-P2X7R signaling complex plays essential roles in osteocyte ATP and Ca2+ mechanosignaling. Given that maintenance of skeletal integrity in response to daily physical activity relies on ability of bone cells to perceive and respond to mechanical loading, and that Panx1-P2X7R complex plays essential roles in bone mechanotransduction, we investigated whether impaired anabolic response to mechanical loading in T1D is associated with altered Panx1-P2X7R signaling. We used the Akita (C57BL/6J-Ins2Akita) mouse model of T1D and Panx1-KO mice. Akita, Panx1-KO and their age-matched wildtype (WT) mice (8 wk old, male, n=6/group) were subjected to mechanical loading by treadmill running (2 or 4 weeks; 5 days/wk, 300 m/day) or to daily cage activities as control. All animals were euthanized immediately after the last running bout. Right Femurs were used for static and dynamic histomorphometry, left hindlimbs were used to study the protein expression of Panx1 and P2X7R by Western blotting (pulverized, osteocyte enriched bones). All experiments were performed under IACUC approval. Histomorphometry studies showed that 4-wk loading caused radial expansion in femur ($p<0.05$; Fig. 1,2) in WT mice compared to cage controls, with a significant increase in periosteal mineralized surface. In contrast, Akita and Panx1-KO mice did not show anabolic response with loading. Basal Panx1 and P2X7R expression levels in Akita bones were significantly lower compared to age-matched WT controls. After 2-wk treadmill exercise, Panx1 and P2X7R were markedly upregulated in WT loaded bone when compared to non-loaded controls (Fig. 2). Protein levels of both Panx1 and P2X7R in 4-wk loaded WT bone were similar to non-loaded controls. This adaptive response was not lost in diabetic bone, but was dysregulated particularly in regard to Panx1 expression, which indicates that diabetic mice are unable to properly adapt to mechanical loading. Our current findings demonstrate that load-induced bone anabolic response is impaired in T1D similar to Panx1-KO mice and is likely related to T1D-induced dysregulation of Panx1-P2X7R, which is essential for proper response to mechanical loading and maintenance of bone health.

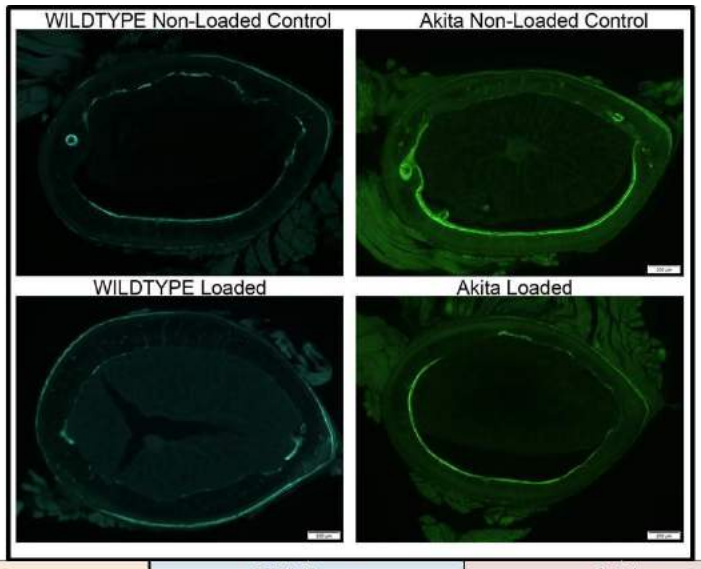

Parameters	Wildtype		Akita	
	non-loaded	loaded	non-loaded	loaded
Ps.MS/Bs (%)	13.7 ± 5	22.5 ± 8 *	11.9 ± 4	8.6 ± 3
Ps.MAR	1.3 ± 0.2	1.4 ± 0.3	1.3 ± 0.2	0.5 ± 0.4 *
En.MS/Bs	27 ± 3	27.4 ± 5	30.7 ± 3	32.3 ± 5
En.MAR	1.4 ± 0.3	0.9 ± 0.4	1.4 ± 0.4	1.0 ± 0.3 *

Figure1. Dynamic histomorphometry study shows that periosteal mineralized surface was significantly increased with loading in WT-Loaded bones. In Akita mice, the anabolic response was impaired.

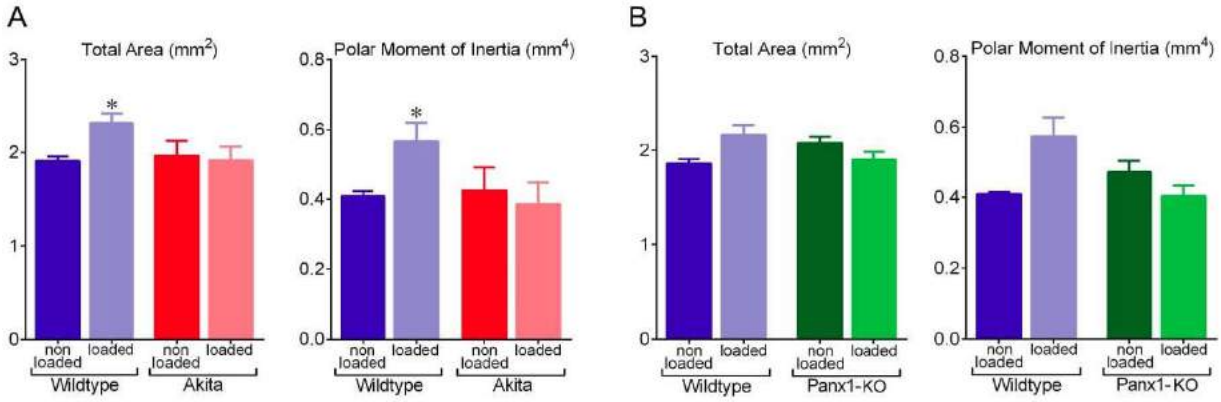

Figure 1. Load-induced anabolic response is impaired in (A) Akita T1D mice and in (B) Panx1-null mice compared to age-matched wildtype. Histological studies showing load-induced changes in Total Bone Area and Polar Moment of Inertia (*J*) in 12-week Akita, Panx1-KO and age-matched wildtype mice. Mechanical loading (treadmill running, 300 meter/day for 5 consecutive days with 2 resting days) was imposed for 4 weeks while the age-matched controls (cage activity). n = 7/group for (A) and n = 4 for (B). Data are presented as the means ± SEM.

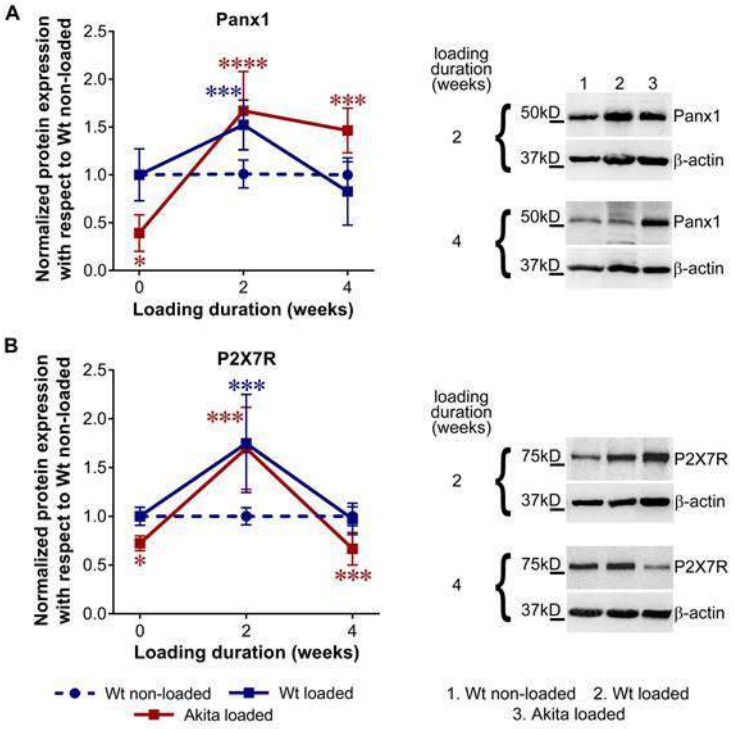

Figure 3. Mechanosignaling complex Panx1-P2X7R responds to mechanical loading differently in WT and Akita mice bones.

Overexpression of MitoNEET in osteoblasts leads to impaired bone mass and energy metabolism in mice

Phuong T Le, Sheila Bornstein Victoria Demambro, Clifford J Rosen and **Anyonya R Guntur**[1 1] Center for Clinical and Translational Research, Maine Medical Center Research Institute,

Scarborough, Maine 04074, USA.

Osteoblasts during *in vitro* differentiation increase glycolytic ATP production rates in response to exogenous glucose supply (glycolysis 67% vs Oxidative phosphorylation 33% . Differentiated osteoblasts also show a profound Crabtree effect to exogenous glucose suggesting a strong preference for glycolytic ATP generation. In contrast adipocytes during differentiation mostly used oxidative phosphorylation to meet ATP demand. To study the role of the two major ATP generating pathways *in vivo* in osteoblasts we overexpressed MitoNEET an outer mitochondrial membrane protein generating a novel osteoblast specific overexpression mouse model. Previous work shows that overexpression of MitoNEET in adipocytes specifically leads to decreased oxidative phosphorylation and a concomitant increase in glycolysis. In our overexpression model, mice containing the tetracycline responsive element (TRE) fused to the MitoNEET open reading frame were crossed to Runx2 reverse-tetracycline trans-activator (rtTA) to generate osteoblast specific overexpression. Two groups of 4 week old male mice were generated and Doxycycline+Saccharin (Dox), and Saccharin (controls) were introduced through drinking water for 12 weeks. Trabecular bone microarchitecture was assessed in the distal femoral metaphysis, whereas cortical bone morphology was assessed at the femoral mid-shaft with μCT analysis at 16 weeks of age. Dox treated male mice had significantly lower trabecular bone mineral density (Tb. BMD, n=8-10, p=0.04) and trabecular thickness (Tb.Th,p=0.0001), along with lower cortical tissue mineral density (Ct.TMD, -0.7%), medullary area (Ma.Ar, -11.8%), total area (Tt.Ar, -10.7%), and minimum moment of inertia (Imin, -22%) compared to controls. Next, we performed indirect calorimetry to obtain energy expenditure (EE) and respiratory quotient (RQ) data. We found a significant increase in day time energy expenditure even though body weight in the Dox group animals was slightly higher compared to controls. Interestingly, 24 hour RQ was significantly lower in the MitoNEET overexpressing animals, suggesting oxidation of fat (n=8-10, p=0.03). There was no difference in food consumption with the Dox group drinking significantly less amount of water (n=8-10, p=0.009). In sum, manipulating MitoNEET expression specifically in the osteoblast impairs bone mass and leads to decreased, energy expenditure and respiratory quotient in male mice potentially affecting whole body energy metabolism.

How can we improve Cre-driver models?

Charles A. O'Brien, PhD, University of Arkansas for Medical Sciences, Little Rock, AR, USA

A powerful and commonly used approach to study protein function in mice is to inactivate the gene encoding the protein of interest in a cell type-specific manner, a process referred to as conditional gene deletion or knockout. The Cre-loxP site-specific recombination system, derived from the P1 acteriophage, is often used for this purpose. Conditional gene deletion has provided us with an abundance of information about the function of specific proteins or pathways in a given tissue or cell type. Yet conclusions based on this technology rely on the cell type specificity of the Cre-driver stains used. To use a common example in our field, if I use a Cre transgene driven by an osteocalcin promoter to delete my gene of interest, I would probably conclude that any phenotype that I observed is due to loss of activity of my gene of interest in osteoblasts. However, as noted by many investigators, most, if not all, Cre driver strains produce recombination in more than one cell type. This limitation is not always crippling, but must be taken into consideration when drawing conclusions about gene function. That said, improvements to the technology, or development of alternatives, is clearly desirable. The goal of this discussion will be to explore two approaches to increase the cell type-specificity of Cre driver stains and to examine the use of CRISPR interference (CRISPRi) as an alternative approach. One of the approaches to improve Cre pecificity is known as intersectional or "split" Cre technology and involves the use of two independent promoters with overlapping expression patterns (1;2). The idea is that only cells that express both promoters will undergo recombination. A second approach that may improve specificity is to use weakened versions of the Cre recombinase. In contrast, CRISPRi involves targeting a transcriptional repressor to the ranscription start-site of the gene of interest (3). Importantly, CRISPRi has the potential to provide an approach to reversibly inactivate a gene of interest, something that is currently not possible using Cre-loxP approaches.

Reference List

1. Hirrlinger,J., Scheller,A., Hirrlinger,P.G., Kellert,B., Tang,W., Wehr,M.C., Goebbels,S., Reichenbach,A., Sprengel,R., Rossner,M.J. et al 2009. Split-cre complementation indicates coincident activity of different genes in vivo. *PLoS. ONE.* 4:e4286

2. Wang,P., Chen,T., Sakurai,K., Han,B.X., He,Z., Feng,G., and Wang,F. 2012. Intersectional Cre driver lines generated using split-intein mediated split-Cre reconstitution. *Sci. Rep.* 2:497.

3. Qi,L.S., Larson,M.H., Gilbert,L.A., Doudna,J.A., Weissman,J.S., Arkin,A.P., and Lim,W.A. 2013. Repurposing CRISPR as an RNA-guided platform for sequence-specific control of gene expression. *Cell* 152:1173-1183

Modeling Human Disease in Mice

Aris N. Economides, PhD[1]
[1]*Regeneron Pharmaceuticals, Tarrytown, NY*

One of the most desired aspects of mouse models is to provide a physiological system for the study of human diseases. To date, the majority of mouse models that have been generated have either been simple 'knockouts' (where the majority or key parts of the transcribed region of a gene are deleted, and usually also replaced by a 'marker', such as LacZ) or conditional versions thereof. These types of alleles – whether unregulated or conditional – are loss-of-function (LOF) alleles and are of great utility in deciphering the function of the target gene. However, an examination of the landscape of the types of genetic variation that drives human disease reveals a much more complex picture. Even if we exclude diseases whose underlying genetic causes cannot be ascribed to variation in a single gene (commonly referred to as polygenic) and we focus on monogenic (Mendelian) disorders, we find that only a subset arises from clear LOF variants; but, in addition to these there are variants that generate neomorphic alleles, and these variants straddle the gamut of 'simple' missense mutations, to splicing-altering mutations, premature truncation variants, and more complex situations such as indels, copy number variation (CNV), inversions, and translocations. Clearly, none of these genetic states and their corresponding biology can be modeled using the traditional knockout and conditional knockout approaches.

In order to address the current technological limitations, we have been developing methodology to model non-LOF variation in the mouse. Clearly, at least missense mutations can now be modeled using Crispr/Cas9, with the limitation that only straight 'knock-ins' can be made efficiently. Though Crispr/Cas9 can facilitate targeting of more complex alleles (those that require a targeting vector), utilizing this method does not obviate the need for design, especially as it relates to the engineering of conditional alleles. As the latter is particularly useful in parsing out the key cell types that participate in the pathophysiology of any given genetic disorder, we have focused on adapting conditional mutagenesis to the study of missense as well as other types of variants. We have mainly relied on two related methods of conditional mutagenesis, FlEx [(1)] and COIN [(2)]. Both of these methods rely on recombinase-mediated inversion rather than deletion of the region of interest to impart conditionality. Typically, we use these inversion-based strategies to hide the missense or splicing variant in the antisense strand and then 'activate it' using a site-specific recombinase, such as Cre. A clear advantage of these methods is that they can utilize the extensive cell type-specific resources that have are available community-wide. In parallel, we have developed methods that allow us to model CNVs, as well as methods for humanizing large regions of the mouse genome. Examples of how these methods have been utilized to model Robinow Syndrome [(3,4)], Spinal Muscular Atrophy [(5)], Fibrodysplasia Ossificans Progressiva [(6,7)], and Hadju-Cheney Syndrome [(8)], to name a few examples.

References

1. Schnutgen F, Doerflinger N, Calleja C, Wendling O, Chambon P, Ghyselinck NB. A directional strategy for monitoring Cre-mediated recombination at the cellular level in the mouse. Nat Biotechnol. May 2003;21(5):562-5.
2. Economides AN, Frendewey D, Yang P, Dominguez MG, Dore AT, Lobov IB, et al. Conditionals by inversion provide a universal method for the generation of conditional alleles. Proc Natl Acad Sci U S A. Aug 20 2013;110(34):E3179-88.

3. Raz R, Stricker S, Gazzerro E, Clor JL, Witte F, Nistala H, et al. The mutation ROR2W749X, linked to human BDB, is a recessive mutation in the mouse, causing brachydactyly, mediating patterning of joints and modeling recessive Robinow syndrome. Development. May 2008;135(9):1713-23.
4. Witte F, Chan D, Economides AN, Mundlos S, Stricker S. Receptor tyrosine kinase-like orphan receptor 2 (ROR2) and Indian hedgehog regulate digit outgrowth mediated by the phalanx-forming region. Proc Natl Acad Sci U S A. Aug 10 2010;107(32):14211-6.
5. Lutz CM, Kariya S, Patruni S, Osborne MA, Liu D, Henderson CE, et al. Postsymptomatic restoration of SMN rescues the disease phenotype in a mouse model of severe spinal muscular atrophy. J Clin Invest. Aug 2011;121(8):3029-41.
6. Hatsell SJ, Idone V, Wolken DM, Huang L, Kim HJ, Wang L, et al. ACVR1R206H receptor mutation causes fibrodysplasia ossificans progressiva by imparting responsiveness to activin A. Science translational medicine. Sep 2 2015;7(303):303ra137.
7. Dey D, Bagarova J, Hatsell SJ, Armstrong KA, Huang L, Ermann J, et al. Two tissue-resident progenitor lineages drive distinct phenotypes of heterotopic ossification. Science translational medicine. 2016;8(366):366ra163-366ra163.
8. Zanotti S, Yu J, Sanjay A, Schilling L, Schoenherr C, Economides AN, et al. Sustained Notch2 signaling in osteoblasts, but not in osteoclasts, is linked to osteopenia in a mouse model of Hajdu-Cheney syndrome. J Biol Chem. Jul 21 2017;292(29):12232-44.

7:00 AM – 8:00 AM	Breakfast & Registration

8:00 AM - 9:00 AM	**ASBMR/Harold M. Frost Young Investigator Award Presentations** Chair: David Burr, PhD *(Indiana University)*
	The Connection Between Fatigue and Fragility Fracture In Bone Claire Acevedo, PhD *(University of California San Francisco)*
	Regulation of Leukemia Inhibitory Factor Receptor (LIFR) in Bone Disseminated Dormant Tumor Cells Rachelle Johnson, PhD *(Vanderbilt University)*
	CKD-MBD in a Model of Targeted FGF23 Deletion Erica Clinkenbeard, PhD *(Indiana University School of Medicine)*

9:15 AM - 12:00 PM	**Problems in Orthopaedics: Degenerative Disk Disease** Chair: James Iatridis, PhD *(Icahn School of Medicine at Mount Sinai)*
	Introduction James Iatridis, PhD *(Icahn School of Medicine at Mount Sinai)*
	Intervertebral Disc Biology: An Enigma Machine Makarand Risbud, PhD *(Thomas Jefferson University)*
	Clinical Perspective of Low Back Pain: Still a Black Box James Kang, MD *(Brigham and Women's Hopsital)*

12:30 PM – 5:00 PM	**Guided Hikes** *Sponsored by*  **Pioneer Cabin** *(rigorous, 8 miles round-trip, led by David Burr)* **TBD Location** *(shorter and easy, led by Sue Bloomfield)* Attendees meet at the back door of the Sun Valley Resort Inn at 12:30 PM

7:30 PM - 9:30 PM	**Next Generation Therapies** Chair: David Burr, PhD *(Indiana University)*
	New Approaches to Anabolic Therapy Ben Leder, MD *(Harvard University)*
	Treatment of Osteoarthritis: New Horizons Nancy Lane, MD *(UC Davis)*
	Novel/Potential Therapies for Age-Related Sarcopenia Roger Fielding, PhD *(Tufts University)*

The connection between fatigue and fragility fracture in bone

Claire Acevedo, PhD[1,2], Vincent A. Stadelmann, PhD[3,6], Dominique P. Pioletti, PhD[4], Robert O. Ritchie, PhD[2,5] and Tamara Alliston, PhD[1]

[1]University of California, San Francisco, [2]Lawrence Berkeley National Laboratory, [3]AO Research Institute Davos, [4]Swiss Federal Institute of Technology Lausanne, [5]University of California, Berkeley, [6]Scanco Switzerland

Prevention of bone fragility fracture in the elderly and population with high risk of fracture has been the clinical quest of the last decade. However, in bone research, the predominant fracture mechanism is still uncertain: are bones more prone to fracture by a fatigue mechanism under cyclic loading, as are 80% of engineering materials, or are they more inclined to break in a quasi-static mode by a single overload, as has been implied in a majority of the scholarly research on bone fragility. Evidence that fatigue-crack growth mechanisms are extensively involved in bone fracture has recently emerged from clinical case studies recognizing that a proportion of fragility fractures might actually be insufficiency fractures (i.e., bone fracture caused by daily cyclic loading on weakened bone) causing the fall, rather than the result of it. Accordingly, our research examines the interactions between cyclic loading, fatigue damage, and repair processes in bone in an attempt to explore the role of fatigue and impact the clinical approach to diagnosis or treatment.

To address these questions, we employed multidisciplinary synchrotron experiments and mechanical testing on mouse and human models with bone fragility associated to age, diabetes, bisphosphonate treatment and irradiation. We gathered evidence that insufficiency fractures might be the result of an imbalance between damage and repair dynamics that are highly sensitive to changes in bone quality, bone quantity, and remodeling with age. Using this multi-scale approach, we have shown that whole-bone quality, and especially fracture toughness, is reduced by excessive non-enzymatic collagen cross-linking at the molecular scale of bones. This will ultimately diminish bone resistance to fatigue by reducing the critical crack size, allowing an incipient fatigue crack to cause complete fracture of fragile bone prematurely. We also brought the experimental proof that fatigue damage can lead to bone failure by identifying characteristic fatigue crack advance. Finally, our investigations indicate osteocyte cells, already known to be involved in the activation of bone resorption and bone formation around microcracks, to be also actors in the local remodeling process. Nonetheless, there are still major gaps in our understanding of the timing of the different stages of the repair process, the activation and the exact role of osteocytes compared to osteoclast resorbing cells, as well the influence of the sequence of fatigue loading (frequency, pause between the loading bout) and the reduced quality of fragile bone on fatigue resistance.

Active investigation using multi-scale approach and *in vivo* mouse loading should lead to new clinical indicators of fracture risk based on bone quality. New therapeutic treatments that stimulate the cellular repair of fatigue damage might emerge to restore bone quality, or prevent its degeneration.

Regulation of leukemia inhibitory factor receptor (LIFR) in bone disseminated dormant tumor cells

Miranda Sowder1, Samuel Dooyema1, Vera Mayhew1, Rachelle W. Johnson, PhD2
1Vanderbilt University, Nashville, TN, 2Vanderbilt University Medical Center, Nashville, TN

Breast cancer cells frequently home to the bone marrow, where they may enter a dormant, or non-proliferative state. The mechanisms that induce tumor cell dormancy and promote the outgrowth of indolent tumor cells remains unclear. We recently published that the leukemia inhibitory factor receptor (LIFR) maintains tumor cells in a dormant state in the bone marrow and that loss of the LIFR enables otherwise dormant tumor cells to become osteolytic and proliferative in the bone. We are therefore interested in both up-stream regulators and down-stream signaling targets of the LIFR as potential therapeutic targets. Our data indicate that hypoxia (low oxygen tensions) down-regulates the LIFR on breast tumor cells, and that this is through epigenetic suppression of the LIFR, since inhibition of histone deacetylases (HDACs) using valproic acid dramatically stimulates LIFR and other pro-dormancy genes on tumor cells in normoxic and hypoxic conditions. This led us to hypothesize that the hypoxic bone microenvironment may drive tumor cells to exit dormancy in the bone marrow through down-regulation of the LIFR. Since HDAC inhibition promotes LIFR expression on tumor cells, we have proposed to use HDAC inhibitors (HDACi) to induce a chronic state of tumor dormancy in breast cancer cells disseminated to the bone marrow. To test this, we treated human MCF7 breast cancer cells with FDA-approved HDACi (romidepsin, panobinostat, vorinostat) or HDACi in phase II clinical trials (entinostat). All HDACi significantly increased LIFR mRNA levels (2.9-6.1-fold, $p<0.05$-0.002) after 6-12 hours of treatment in MCF7 cells and dramatically increased LIFR protein levels in both MCF7 and aggressive MDA-MB-231 bone metastatic cells by 24 hours (12.4-14.4-fold). HDACi also increased mRNA levels of several dormancy-associated genes including AMOT, TGFB2, IGFBP5, and p27 (up to 5.5-fold, $p<0.05$-0.0001), suggesting that HDACi may be effective at inducing tumor cell dormancy. Together, these data indicate that HDACi induce LIFR expression and stimulate a pro-dormancy genotype. Studies to determine whether HDACi can prevent the outgrowth of dormant tumor cell disseminated to the bone *in vivo* and/or revert aggressive breast cancer cells into a dormant state are currently in progress. Importantly, these studies may have clinical implications for the use of HDACi as a means to activate a pro-dormancy program and maintain breast cancer cells in a dormant state in the bone marrow.

CKD-MBD in a model of targeted FGF23 deletion

Erica L. Clinkenbeard[1], Pu Ni[1], Joseph C. Thomas[1], Megan L. Noonan[1], Julia M. Hum[1], Mohammad Aref[2], Matthew R. Allen[2], Kenneth E. White[1]. [1]Department of Medical and Molecular Genetics, Indiana University School of Medicine, Indianapolis, IN, USA. [2]Department of Anatomy and Cell Biology, Indiana University School of Medicine, Indianapolis, IN, USA.

Fibroblast growth factor-23 (FGF23) is a bone-derived hormone central to the regulation of serum phosphate levels. The ability of FGF23 to control phosphate homeostasis is substantially hindered in the common disorder chronic kidney disease (CKD). Additionally, highly elevated levels of FGF23 in patients is associated with increased morbidity and mortality and is found to be associated with left ventricular hypertrophy (LVH). To test the role of FGF23 on CKD phenotypes during early and moderate disease states, a late osteoblast/osteocyte conditional Fgf23 knockout mouse (flox-Fgf23/Dmp1-Cre$^{+/-}$) was placed on an adenine-containing diet to induce CKD. Adenine significantly induced serum intact FGF23 in the Cre- mice over casein fed mice (89-fold at 8 weeks, $p<0.01$), whereas Dmp1-Cre+ mice on adenine diet had a 90% reduction in serum intact and *C*-terminal FGF23 as well as bone Fgf23 mRNA ($p<0.01/0.05$). Serum biochemical analysis showed casein fed Cre+ mice had significantly higher serum phosphate at 8 weeks compared to the casein fed Cre- mice ($p<0.01$), whereas adenine diet fed Cre+ mice had higher serum phosphate versus Cre- mice on the same diet at both 4 and 8 weeks. Serum blood urea nitrogen (BUN), which is inversely related to kidney function, progressively rose in all adenine fed mice, yet the increase in Cre+ mice was significantly greater than Cre- mice at 8 weeks (1.75-fold; $p<0.001$). PTH was significantly elevated in the mice fed adenine diet regardless of genotype. Consistent with this finding, renal Cyp27b1 (vitamin D 1alpha-hydroxylase) was significantly enhanced and midshaft cortical porosity was increased in all adenine fed groups compared to casein fed mice, with no effect of genotype. Echocardiographs of the adenine Cre+ hearts revealed profound calcification of the aortas. Additionally, pronounced LVH was observed in this group compared to adenine Cre- mice. Collectively, our results show that in an animal model of progressive CKD, a marked reduction of FGF23 could not block the hyperparathyroidism or metabolic bone disease, but the elevated FGF23 was sufficient to normalize serum phosphate and impart cardio-protective effects during mild and moderate disease.

Problems in Orthopaedics: Degenerative Disc Disease

James C. Iatridis PhD
Leni & Peter W. May Dept. of Orthopaedics, Icahn School of Medicine at Mount Sinai, NY NY USA

Low back pain is the second most frequent cause of doctor visits and is commonly associated with intervertebral disc (IVD) degeneration. This session will describe biomechanical, biological, and clinical challenges in the diagnosis and treatment of degenerative disc disease. The process of disc degeneration is an aberrant, cell-mediated response to progressive structural failure [1]. A degenerate disc is one with structural failure combined with accelerated or advanced signs of aging. Degenerative disc disease (DDD) should be applied to a degenerate disc that is also painful.

Research on DDD has commonly focused on IVD problems, IVD degeneration is a pathological condition of the whole spine with involvement of all surrounding tissues. Epidemiological studies have determined that modic changes to the vertebral endplate are associated with both IVD degeneration and the presence and severity of back pain [2]. Determinants and association of modic changes in the endplate with disc degeneration and clinical symptoms in the upper versus the lower lumbar spine were different [2], further suggesting biomechanical interactions.

Challenges in treatment of DDD include imprecise phenotypic definitions, a poor healing environment with low cellularity and chronic inflammation, and high biomechanical demands. IVD degeneration and associated spinal changes are commonly considered a single pathology. Improved phenotypic descriptions capable of distinguishing between herniation, endplate defects, and additional spinal disorders can help identify pain producers and target therapies. This is particularly important because the appearance of age-related structural degeneration does not result in painful conditions in all patients. The IVD is the largest avascular structure in the body, producing a hypoxic environment with low cellularity [3]. Presence of chronic pro-inflammatory cytokines in DDD further challenges the healing response [4]. The spine is constantly loaded, and the IVD is subjected to large stresses and high strains so that repair materials have challenging biomechanical design needs [5]. Consequently, attempts to repair IVDs with sutures or biomaterials have been either ineffectual or caused herniation of the biomaterial. The development of novel treatments requires an enhanced understanding of the relationships between injury, inflammation and painful processes. This session will review the literature and to present new data to describe interacting biomechanical, pro-inflammatory, and cellular challenges and opportunities in DDD.

Acknowledgements: This work was funded by NIAMS/NIH Grants (R01 AR057397, and R01 AR064157, and R01 AR069315).

References:

1) Adams MA, Roughley PJ. What is intervertebral disc degeneration, and what causes it? Spine (Phila Pa 1976). 2006 Aug 15;31(18):2151-61.
2) Mok FP, Samartzis D, Karppinen J, Fong DY, Luk KD, Cheung KM. Modic changes of the lumbar spine: prevalence, risk factors, and association with disc degeneration and low back pain in a large-scale population-based cohort. Spine J. 2016 Jan 1;16(1):32-41.
3) Grunhagen T, Shirazi-Adl A, Fairbank JC, Urban JP. Intervertebral disk nutrition: a review of factors influencing concentrations of nutrients and metabolites. Orthop Clin North Am. 2011 Oct;42(4):465-77.
4) Risbud MV, Shapiro IM. Role of cytokines in intervertebral disc degeneration: pain and disc content. Nat Rev Rheumatol. 2014 Jan;10(1):44-56.
5) Iatridis JC, Nicoll SB, Michalek AJ, Walter BA, Gupta MS. Role of biomechanics in intervertebral disc degeneration and regenerative therapies: what needs repairing in the disc and what are promising biomaterials for its repair? Spine J. 2013 Mar;13(3):243-62.

New Approaches to Anabolic Osteoporosis Therapy

Benjamin Z. Leder, MD
Department of Medicine, Harvard Medical School and Endocrine Unit, Massachusetts General Hospital
Boston MA.

Osteoporosis affects over 20 million Americans leading to 1.5 million fragility fractures (including over 300,000 hip fractures) every year. In patients with severe osteoporosis, currently available medications can, at best, decrease hip and non-spine fracture rates by 50% and 30%, respectively. The introduction of teriparatide (a parathyroid hormone (PTH) analog that is administered by daily subcutaneous injection) over a decade ago was an important advance in osteoporosis therapy and until recently was the only approved osteoporosis medication whose mechanism of action involved the stimulation of new osteoblastic bone formation. Teriparatide increases trabecular bone mineral density (BMD) and reduces spine and non-spine fracture risk in postmenopausal women at high fracture risk though its effects on hip fracture risk reduction have not been adequately assessed.[1] Earlier this year abaloparatide (also administered by daily subcutaneous injection) became the second anabolic agent approved for the treatment of postmenopausal osteoporosis. Abaloparatide is a synthetic peptide analog of PTH-related protein (PTHrP) that binds to the PTH/PTHrP receptor with a greater selectivity to the RG conformation than does teriparatide.[2] Like teriparatide, abaloparatide reduces the risk of spine and non-spine fractures in postmenopausal women though its effects on cortical bone may differ somewhat from teriparatide resulting in greater BMD gains at anatomic sites with a significant cortical compartment.[3,4] Another anabolic drug in late stage development is romozosumab, a monoclonal antibody that binds sclerostin, an inhibitor of the Wnt signaling pathway. Romozosumab transiently increases osteoblastic bone formation, inhibits bone resorption in a more sustained manner, and was recently reported in an active-comparator study (versus the bisphosphonate, alendronate) to preferentially reduce vertebral, non-vertebral and hip fractures.[5-7] The results of this comparative-efficacy trial are not yet published, however, and a potential cardiovascular safety signal was identified in this study thus delaying a final decision on FDA approval.

In addition to these new agents, recent studies have demonstrated that the combination of teriparatide and the RANKL inhibitor, denosumab, additively increases BMD, improves bone microarchitecture, and increases bone strength in postmenopausal osteoporotic women.[8-10] These findings contrast with prior studies investigating the effects of combining teriparatide with bisphosphonates in which no additive effects were identified. The reason for the differential effects of these combination approaches may relate to denosumab's ability (unlike bisphosphonates) to fully inhibit PTH's osteoclast activating properties while allowing for continued stimulation of modeling-based bone formation.[11] Moreover, it was also recently reported that the order in which anabolic and antiresorptive drugs are administered has a dramatic effect on cumulative BMD gains and overall efficacy. Specifically, when patients transition from teriparatide to denosumab they experience additional increases in bone mass while those who transition from denosumab to teriparatide experience high-turnover bone loss.[12]

This presentation will highlight the clinical effects of the recently approved PTHrP analog, abaloparatide, the newest findings from studies of romozosumab, as well recent studies demonstrating the effects of combined and sequential anabolic/antiresorptive therapy on bone mass, skeletal microarchitecture and bone strength in postmenopausal osteoporotic women.

References:

1. Neer RM, Arnaud CD, Zanchetta JR, et al. Effect of parathyroid hormone (1-34) on fractures and bone mineral density in postmenopausal women with osteoporosis. N Engl J Med. 2001;344(19):1434-41.
2. Hattersley G, Dean T, Corbin BA, Bahar H, Gardella TJ. Binding Selectivity of Abaloparatide for PTH-Type-1-Receptor Conformations and Effects on Downstream Signaling. Endocrinology. 2016;157(1):141-9.
3. Leder BZ, O'Dea LS, Zanchetta JR, et al. Effects of abaloparatide, a human parathyroid hormone-related peptide analog, on bone mineral density in postmenopausal women with osteoporosis. J Clin Endocrinol Metab. 2015;100(2):697-706.
4. Miller PD, Hattersley G, Riis BJ, et al. Effect of Abaloparatide vs Placebo on New Vertebral Fractures in Postmenopausal Women With Osteoporosis: A Randomized Clinical Trial. JAMA. 2016;316(7):722-33.

5. Genant HK, Engelke K, Bolognese MA, et al. Effects of Romosozumab Compared With Teriparatide on Bone Density and Mass at the Spine and Hip in Postmenopausal Women With Low Bone Mass. J Bone Miner Res. 2017;32(1):181-7.
6. Cosman F, Crittenden DB, Adachi JD, et al. Romosozumab Treatment in Postmenopausal Women with Osteoporosis. N Engl J Med. 2016;375(16):1532-43.
7. McClung MR, Grauer A, Boonen S, et al. Romosozumab in postmenopausal women with low bone mineral density. N Engl J Med. 2014;370(5):412-20.
8. Tsai JN, Uihlein AV, Burnett-Bowie SM, et al. Effects of Two Years of Teriparatide, Denosumab, or Both on Bone Microarchitecture and Strength (DATA-HRpQCT study). J Clin Endocrinol Metab. 2016:jc20161160.
9. Leder BZ, Tsai JN, Uihlein AV, et al. Two years of Denosumab and teriparatide administration in postmenopausal women with osteoporosis (The DATA Extension Study): a randomized controlled trial. J Clin Endocrinol Metab. 2014;99(5):1694-700.
10. Tsai JN, Uihlein AV, Lee H, et al. Teriparatide and denosumab, alone or combined, in women with postmenopausal osteoporosis: the DATA study randomised trial. Lancet. 2013;382(9886):50-6.
11. Tsai JN, Burnett-Bowie SM, Lee H, Leder BZ. Relationship between bone turnover and density with teriparatide, denosumab or both in women in the DATA study. Bone. 2017;95:20-5.
12. Leder BZ, Tsai JN, Uihlein AV, et al. Denosumab and teriparatide transitions in postmenopausal osteoporosis (the DATA-Switch study): extension of a randomised controlled trial. Lancet. 2015;386(9999):1147-55.

Treatment of Osteoarthritis: New Horizons

Nancy E. Lane, MD
Director, Center for Musculoskeletal Health
Endowed Professor of Medicine, Rheumatology and Aging
University of California at Davis and Affiliated Faculty at UCSF

Osteoarthritis (OA) is the most common form of arthritis, and its incidence continues to rise as the elderly population increases worldwide. The most common joints affected with OA include the knee, hip and hand. Knee and hand OA are more common in women, while hip is more common in men. OA is generally referred to as a "degenerative" disease and it involves all the tissues within and surrounding the synovial lined joint including the articular cartilage, subchondral bone, synovium, muscles and ligaments. OA is usually diagnosed by a history of joint pain that increases with joint use and a radiograph or MRI scan will show loss or articular cartilage. OA is similar to other chronic degenerative diseases in that significant joint degeneration is usually present when the patient experiences joint pain. Therefore, treatments that would prevent incident disease are generally not useful. To date, treatment of OA is focused on reduction in joint pain and there are no approved treatments at this time that have been shown to slow or reverse the progression of the disease.

Recently, there has been significant research focused on the chondrocyte, a cell derived from the mesenchymal stem cells, that is located within the cartilage matrix and depending its signals can synthesize the molecules that make up the matrix or degrade the matrix. Recently, work has focused on the WNT/beta-catenin signaling pathway. This signaling pathway appears to be involved with both tissue/organ formation and repair. An allele variant of the wnt signaling antagonist, secreted frizzled related protein, sFRP3, (FRZB gene) has been found to increase the risk of hip OA, and the phenotype of the radiographic hip OA associated with this FRZB allele variant included loss of articular cartilage and proliferation of bone. This is the result of the WNT pathway having opposite effects on the bone and cartilage. Preclinical studies with Frzb KO mice, reported that compared to control mice, the Frzb KO mouse had an increase in chondrocyte MMP enzyme production, and an increase in cortical bone mass. Mixing studies revealed that the addition of the sFRP3 protein could reverse the MMP production in chondrocytes (Lories A and R, Lane A and R). Recently, a compound. SM04690, has been developed that is a small molecule inhibitor of WNT signaling and it is in development as an intra-articular injection into the knee of subjects with OA. In vitro studies with SM04690, have reported that it can reduce MMP production in chondrocytes, and pre-clinical studies in rats with post-traumatic OA have reported some some protection against articular cartilage destruction with SM04690 compared to vehicle treated controls. A phase 1b study of subjects with knee OA, reported a modest reduction in joint pain and improvement in function with SMO4690 compared to placebo controls.

In a subset of individuals with OA, a traumatic injury within the knee joint appears to accelerate the development of knee OA. Therefore, a number of treatments have been developed to try to prevent osteoarthritis after an acute injury (Post-traumatic OA, PTOA) in animal models. In these animal models, the anterior cruciate ligament is transected, then degeneration of the articular cartilage and bone occurs within a few months. A number of treatments to prevent the development of OA have been studied in this model. The injury associated with PTOA results in an increase in vascularity in the joint area and there is the possibility that mesenchymal stem cells delivered to the joint from the vascular invasion (MSCs) might be stimulated to differentiate into chondrocytes. Our research group studied kartogenin, a molecule that can direct MSCs to differentiate into chondrocytes and reported some promising results in preventing the progression of OA. Other research groups have made nanoparticles filled with kartogenin and injected the particle into the OA joint and also reported positive results. Clinical trials are not yet initiated with this compound.

Since MSCs are known to have both anti-inflammatory and regenerative capacities, clinical studies have been initiated to determine the efficacy of MSCs in the treatment of knee OA. Small single center trials report positive results, however well powered randomized placebo controlled trials have not been reported.

Since pain is the main symptom that patients complain of with OA, a major clinical development program is underway on agents that can inhibit Nerve Growth Factor (NGF). NGF is a neurotropin, that is critical to the development of the

nervous system and in the adult it is released from tissues with injury and inflammation and binds to a nociceptive receptor on the neuron ending, TrKA. The NGF/TrkA complex is internalized into the neuron and travels to the dorsal root ganglion and activates pain signals. There is also a minor receptor, p55 that is present on the basophils, hematopoietic derived white blood cells and on the surface of mesenchymal stem cells. Patients with painful knee OA that were treated with an anti-NGF antibody reported a significant and sustained reduction in knee pain. However, in phase 3 clinical studies, a number of subjects treated with higher doses of anti-NGF antibodies alone, or in combination with an NSAID experience rapid progression of OA and/or osteonecrosis. The etiology of these serious adverse events are not yet known, however phase 3.5 studies are now in progress, and includes careful monitoring of multiple joints in the study subjects to try to better understand the relation of this analgesic treatment with progressive OA. Importantly, these adverse events have been reported in both studies with tenazumab and farisumab, which also block NGF signaling.

Also, there have been recent studies reported to determine the effect of weight loss with bariatric surgery on OA progression, and while patients with knee OA have reduced knee pain after weight loss, there is currently no evidence of any cartilage regeneration.

Lastly, the research and breakthrough therapies for OA have lagged behind other chronic diseases. This has been partially the result of the difficulty in imaging the articular cartilage and the subchondral bone. However, there has been significant progress made with MRI imaging in both the ability to quantitate the composition of the articular cartilage (T1rho for proteoglycan and T2 for water), and texture analyses that are almost ready to be utilized in clinical studies. In addition, advances with HRpQCT of the subchrondal bone in subjects with OA has found, that knee OA is characterized by a loss of rods and a thickening of the trabecular plates, which is exactly the opposite to what is observed in subjects with osteoporosis. This alteration in subchondral bone structure may be a biomarker for treatments of knee OA.

In summary, despite the increasing prevalence of OA worldwide, there are currently no treatments to prevent the progression of the disease. Currently studies with a small molecule wnt signaling inhibitor, MSCs, and MSC modulating agents are all being evaluated in clinical trials. In addition, a potent analgesic is also in advanced clinical trials. There is a significant public health need for effective and safe treatments to slow the progression of OA and hope that these agents now in develop are available for our patients with OA very soon.

References for additional information

1.Felson DT. Osteoarthritis as a disease of mechanics.
Osteoarthritis Cartilage. 2013 Jan;21(1):10-5

2. Lane NE1, Lian K, Nevitt MC, Zmuda JM, Lui L, Li J, Wang J, Fontecha M, Umblas N, Rosenbach M, de Leon P, Corr M. Frizzled-related protein variants are risk factors for hip osteoarthritis. Arthritis Rheum. 2006 Apr;54(4):1246-54.

3. Lories RJ, Peeters J, Bakker A, Tylzanowski P, Derese I, Schrooten J, Thomas JT, Luyten FP. Articular cartilage and biomechanical properties of the long bones in Frzb-knockout mice. Lories RJ, Peeters J, Bakker A, Tylzanowski P, Derese I, Schrooten J, Thomas JT, Luyten FP.Arthritis Rheum. 2007 Dec;56(12):4095-103.

4. Yusuf Yazici, Timothy E. McAlindon, Roy Fleischmann, Allan Gibofsky,
Nancy E. Lane, Alan J. Kibitz, Nebo's Skeptic, Eddie Aromas, Christopher J.
Swearingen, Anita DiFrancesco,Jeyanesh R.S. Tambiah, John Hood,Marc C.
Hochberg. A novel Wnt pathway inhibitor, SM04690, for 1 the treatment of moderate to severe osteoarthritis of the knee: Results of a 24-week, randomized, controlled, phase 1
3 study. In press Osteoarthritis and Cartilage Accepted July 1, 2017

5. Lamo-Espinosa JM, Mora G, Blanco JF, Granero-Moltó F, Nuñez-Córdoba JM, Sánchez-Echenique C, Bondía JM, Aquerreta JD, Andreu EJ, Ornilla E, Villarón EM, Valentí-Azcárate A, Sánchez-Guijo F, Del Cañizo MC, Valentí-Nin JR, Prósper F. Intra-articular injection of two different doses of autologous bone marrow mesenchymal stem cells versus hyaluronic acid in the treatment of knee osteoarthritis: multicenter randomized controlled clinical trial (phase I/II).

J Transl Med. 2016 Aug 26;14(1):246

6. Mohan G1,2, Magnitsky S3, Melkus G4, Subburaj K5, Kazakia G3, Burghardt AJ3, Dang A6, Lane NE7, Majumdar S3. Kartogenin treatment prevented joint degeneration in a rodent model of osteoarthritis: A pilot study. J Orthop Res. 2016 Oct;34(10):1780-1789.

7. Seidel MF, Wise BL, Lane NE. Nerve growth factor: an update on the science and therapy. Osteoarthritis Cartilage. 2013 Sep;21(9):1223-8.

8. Lane NE and Corr M. Osteoarthritis in 2016: Anti-NGF treatments for pain - two steps forward, one step back? Nat Rev Rheumatol. 2017 Jan 25;13(2):76-78.

9. Edwards C, Rogers A, Lynch S, Pylawka T, Silvis M, Chinchilli V, Mosher T, Black K. The effects of bariatric surgery weight loss on knee pain in patients with osteoarthritis of the knee. Arthritis. 2012;2012

Novel/Potential Therapies for Age-Related Sarcopenia

Roger A. Fielding, PhD, Senior Scientist and Laboratory Director
Nutrition, Exercise Physiology, and Sarcopenia Laboratory
Jean Mayer USDA Human Nutrition Research Center on Aging
Tufts University, Boston MA

The age-related loss of skeletal muscle mass and function, sarcopenia, is associated with well-characterized functional limitations and physical disability (Fielding, Vellas et al. 2011). The etiology of sarcopenia is similar to many chronic conditions of advancing age with multiple factors and organ systems contributing to this syndrome. Underlying these age-related changes are physiological changes in the force/power generating capacity of skeletal muscle that appear to be driven by changes in skeletal contractile protein function (Larsson, Li et al. 1997, Frontera, Reid et al. 2008), metabolic derangements and alterations in neuromuscular activation (Clark and Fielding 2012) (Reid, Pasha et al. 2014). Underlying the age-related changes in muscle function and metabolic capacity are well-characterized alterations in skeletal muscle protein turnover that are regulated by the interplay between the mTOR protein kinase and the ubiquitin ligase signaling pathways whose activation are necessary for skeletal hypertrophy or atrophy (Bodine, Stitt et al. 2001, Kandarian 2008). Ultimately these biological changes in skeletal muscle structure and performance have impacts on distal outcomes related to physical functioning such as declines in walking speed, deficits in stair climb capacity and ultimately disability (Reid and Fielding 2012) (See Figure 1).

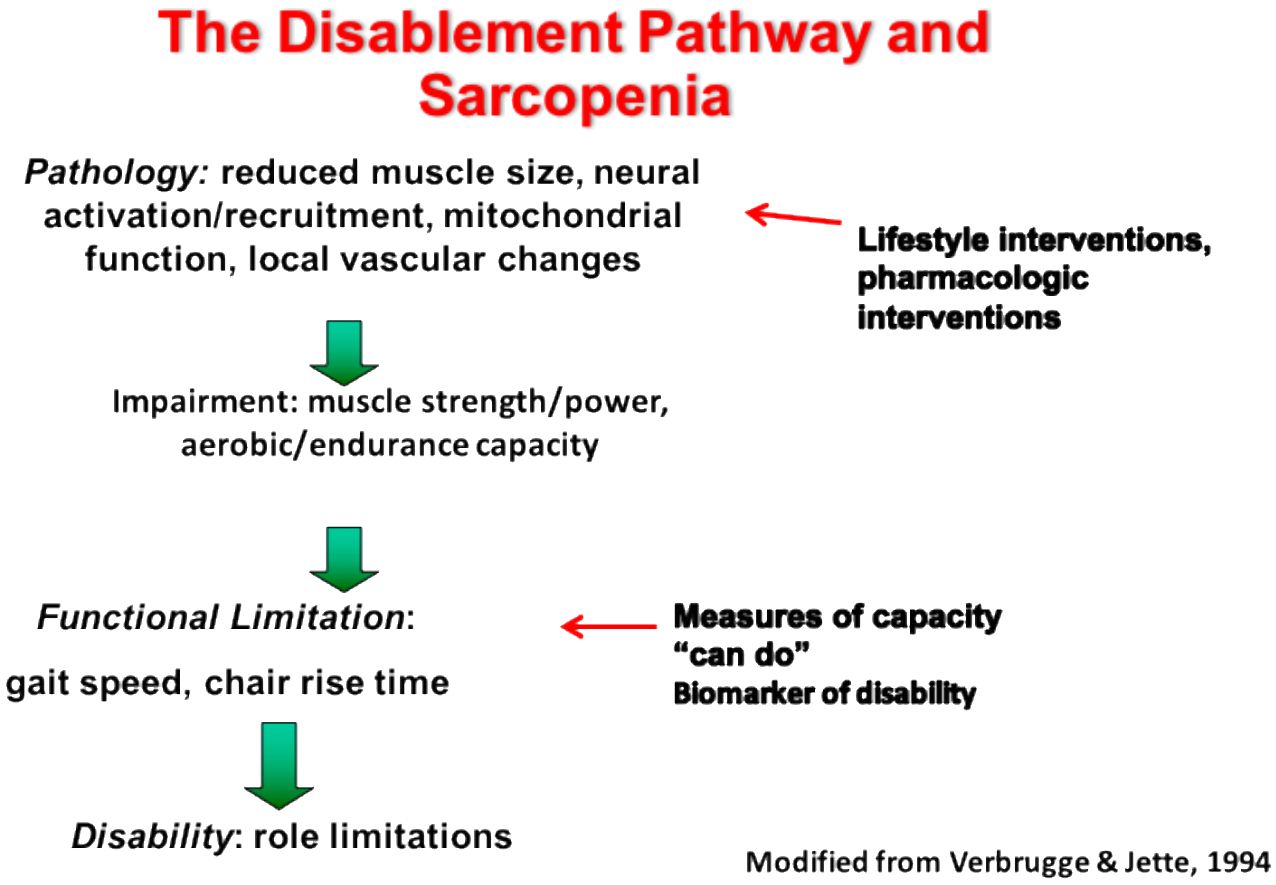

Figure 1. (Verbrugge and Jette 1994)

Data from observational studies suggest that both adequate nutrition and increased physical activity appear to attenuate or reverse several of the age-related changes in skeletal muscle function (Cruz-Jentoft, Landi et al. 2014). However, the data on nutritional and physical activity interventions on muscle function in mobility-limited older adults are more complex. In my presentation, I will review the current literature examining the potential mechanisms by which nutritional supplementation (specifically increased dietary protein and vitamin D) may improve skeletal muscle function and metabolism (Houston, Nicklas et al. 2008, Ceglia, Niramitmahapanya et al. 2013). I will also highlight findings from our recent trials that have addressed the influence of physical activity and nutrition on age-related changes in skeletal

muscle performance and physical functioning/disability in mobility-limited older adults (Pahor, Blair et al. 2006, Fielding, Rejeski et al. 2011, Chale, Cloutier et al. 2012, Pahor, Guralnik et al. 2014).

More recently, underlying molecular targets have been identified that are potentially sites for pharmacologic interventions. In sarcopenia and other disorders of skeletal muscle, two major classes of therapies, selective androgen receptor activation (SARM) and inhibition of myostatin signaling (Anti-myostat), have emerged as potential targets for therapeutic development. In this presentation, I will review the underlying biological mechanisms of SARMs and Anti-myostat. I will summarize the available clinical trials data on these two pathways and discuss the barriers towards regulatory approval for these indications specifically within the context of sarcopenia (Cesari, Fielding et al. 2015).

References:

Bodine, S. C., T. N. Stitt, M. Gonzalez, W. O. Kline, G. L. Stover, R. Bauerlein, E. Zlotchenko, A. Scrimgeour, J. C. Lawrence, D. J. Glass and G. D. Yancopoulos (2001). "Akt/mTOR pathway is a crucial regulator of skeletal muscle hypertrophy and can prevent muscle atrophy *in vivo*." Nat. Cell Biol. **3**: 1014-1019.

Ceglia, L., S. Niramitmahapanya, M. da Silva Morais, D. A. Rivas, S. S. Harris, H. Bischoff-Ferrari, R. A. Fielding and B. Dawson-Hughes (2013). "A randomized study on the effect of vitamin D(3) supplementation on skeletal muscle morphology and vitamin D receptor concentration in older women." J Clin Endocrinol Metab **98**(12): E1927-1935.

Cesari, M., R. Fielding, O. Benichou, R. Bernabei, S. Bhasin, J. M. Guralnik, A. Jette, F. Landi, M. Pahor, L. Rodriguez-Manas, Y. Rolland, R. Roubenoff, A. J. Sinclair, S. Studenski, T. Travison and B. Vellas (2015). "Pharmacological Interventions in Frailty and Sarcopenia: Report by the International Conference on Frailty and Sarcopenia Research Task Force." J Frailty Aging **4**(3): 114-120.

Chale, A., G. J. Cloutier, C. Hau, E. M. Phillips, G. E. Dallal and R. A. Fielding (2012). "Efficacy of Whey Protein Supplementation on Resistance Exercise-Induced Changes in Lean Mass, Muscle Strength, and Physical Function in Mobility-Limited Older Adults." J Gerontol A Biol Sci Med Sci.

Clark, D. J. and R. A. Fielding (2012). "Neuromuscular contributions to age-related weakness." J Gerontol A Biol Sci Med Sci **67**(1): 41-47.

Cruz-Jentoft, A. J., F. Landi, S. M. Schneider, C. Zuniga, H. Arai, Y. Boirie, L. K. Chen, R. A. Fielding, F. C. Martin, J. P. Michel, C. Sieber, J. R. Stout, S. A. Studenski, B. Vellas, J. Woo, M. Zamboni and T. Cederholm (2014). "Prevalence of and interventions for sarcopenia in ageing adults: a systematic review. Report of the International Sarcopenia Initiative (EWGSOP and IWGS)." Age Ageing **43**(6): 748-759.

Fielding, R. A., W. J. Rejeski, S. Blair, T. Church, M. A. Espeland, T. M. Gill, J. M. Guralnik, F. C. Hsu, J. Katula, A. C. King, S. B. Kritchevsky, M. M. McDermott, M. E. Miller, S. Nayfield, A. B. Newman, J. D. Williamson, D. Bonds, S. Romashkan, E. Hadley, M. Pahor and L. R. Group (2011). "The Lifestyle Interventions and Independence for Elders Study: design and methods." J Gerontol A Biol Sci Med Sci **66**(11): 1226-1237.

Fielding, R. A., B. Vellas, W. J. Evans, S. Bhasin, J. E. Morley, A. B. Newman, G. Abellan van Kan, S. Andrieu, J. Bauer, D. Breuille, T. Cederholm, J. Chandler, C. De Meynard, L. Donini, T. Harris, A. Kannt, F. Keime Guibert, G. Onder, D. Papanicolaou, Y. Rolland, D. Rooks, C. Sieber, E. Souhami, S. Verlaan and M. Zamboni (2011). "Sarcopenia: an undiagnosed condition in older adults. Current consensus definition: prevalence, etiology, and consequences. International working group on sarcopenia." J Am Med Dir Assoc **12**(4): 249-256.

Frontera, W. R., K. F. Reid, E. M. Phillips, L. S. Krivickas, V. A. Hughes, R. Roubenoff and R. A. Fielding (2008). "Muscle fiber size and function in elderly humans: a longitudinal study." J Appl Physiol **105**(2): 637-642.

Houston, D. K., B. J. Nicklas, J. Ding, T. B. Harris, F. A. Tylavsky, A. B. Newman, J. S. Lee, N. R. Sahyoun, M. Visser and S. B. Kritchevsky (2008). "Dietary protein intake is associated with lean mass change in older, community-dwelling adults: the Health, Aging, and Body Composition (Health ABC) Study." Am J Clin Nutr **87**(1): 150-155.

Kandarian, S. (2008). "The molecular basis of skeletal muscle atrophy--parallels with osteoporotic signaling." J Musculoskelet Neuronal Interact **8**(4): 340-341.

Larsson, L., X. Li and W. R. Frontera (1997). "Effects of aging on shortening velocity and myosin isoform composition in single human skeletal muscle cells." Am. J. Physiol. **272**: C638-C649.

Pahor, M., S. N. Blair, M. Espeland, R. Fielding, T. M. Gill, J. M. Guralnik, E. C. Hadley, A. C. King, S. B. Kritchevsky, C. Maraldi, M. E. Miller, A. B. Newman, W. J. Rejeski, S. Romashkan and S. Studenski (2006). "Effects of a physical activity intervention on measures of physical performance: Results of the lifestyle interventions and independence for Elders Pilot (LIFE-P) study." J Gerontol A Biol Sci Med Sci **61**(11): 1157-1165.

Pahor, M., J. M. Guralnik, W. T. Ambrosius, S. Blair, D. E. Bonds, T. S. Church, M. A. Espeland, R. A. Fielding, T. M. Gill, E. J. Groessl, A. C. King, S. B. Kritchevsky, T. M. Manini, M. M. McDermott, M. E. Miller, A. B. Newman, W. J. Rejeski, K. M. Sink, J. D. Williamson and L. s. investigators (2014). "Effect of structured physical activity on prevention of major mobility disability in older adults: the LIFE study randomized clinical trial." JAMA **311**(23): 2387-2396.

Reid, K. F. and R. A. Fielding (2012). "Skeletal muscle power: a critical determinant of physical functioning in older adults." Exerc Sport Sci Rev **40**(1): 4-12.

Reid, K. F., E. Pasha, G. Doros, D. J. Clark, C. Patten, E. M. Phillips, W. R. Frontera and R. A. Fielding (2014). "Longitudinal decline of lower extremity muscle power in healthy and mobility-limited older adults: influence of muscle mass, strength, composition, neuromuscular activation and single fiber contractile properties." Eur J Appl Physiol **114**(1): 29-39.

Verbrugge, L. M. and A. M. Jette (1994). "The disablement process." Soc. Sci. Med. **38**: 1-14.